MODELING CLIMATE AND LAND USE CHANGE IMPACTS ON WATER RESOURCES IN THE DANO CATCHMENT (BURKINA FASO, WEST AFRICA)

Dissertation

zur

Erlangung des Doktorgrades (Dr. rer. nat.)

der

Mathematisch-Naturwissenschaftlichen Fakultät

der

Rheinischen Friedrich-Wilhelms-Universität Bonn

vorgelegt von

Yacouba YIRA

aus

Dedougou, Burkina Faso

Bonn, August 2016

Angefertigt mit Genehmigung der Mathematisch-Naturwissenschaftlichen Fakultät der Rheinischen Friedrich-Wilhelms-Universität Bonn

1. Gutachter: Prof. Dr. Bernd Diekkrüger

2. Gutachter: Prof. Dr. Sven Lautenbach

Tag der mündlichen Prüfung: 07.12.2016

Erscheinungsjahr: 2017

Dedicated to my lovely wife *Doris Ariatou Lalongouyé*, and our son *Akim Yannick.*

ACKNOWLEDGEMENTS

This work has been funded by the German Federal Ministry of Education and Research (BMBF) (Grant No. 01LG1202E) through the West African Science Service Centre for Climate Change and Adapted Land Use (WASCAL) project. I'm very grateful to them.

I'm extremely grateful to my supervisor, Prof. Dr. Bernd Diekkrüger, whose guidance, comments, support, solicitude and great humility shaped this work. My gratitude cannot solely be expressed in words, may he find in these lines an idea of this feeling. From him I learnt hydrological science and human values. Many thanks Prof.

I would also like to thank my Tutor, Mr. Gero Steup for his great support and comments. His sense of perspective and persuasiveness has been an invaluable addition to this work. Special thanks also go to his wonderful wife Alex and lovely kids Mattis and Aenne. With you I always felt at home.

My sincere thanks go to all my current and former colleagues & friends of the Hydrology Research Group at the University of Bonn for their wonderful company, especially to Mr. Thomas Jütten for proofreading this work, Dr. A. Y. Bossa, Felix Op de Hipt, Ronja Wolter, Dr. Constanze Leemhuis, Dr. Simone Giertz, Dr. H. Busche, Dr. A. Kebede, Dr. T. Cornelissen, Alexandre-Eudes Danvi, Geofrey Gabiri, Kristian Näschen, Mouhamed Idrissou, Claudia Schepp, Inken Rabbel, Ingrid Althoff, Johannes Rosleff Sörensen and Jonas Götte.

I would like to thank the staff of the WASCAL competence center and executive Management in Ouagadougou and Accra for their support. Thanks go particularly to Dr. B. Barry, Dr. Fonta William, Igor Bado, Dr. Sylvestre Da, Dr. M. Sylla, Dr. B. Ibrahim, Dr. J. Naab, Dr. N. Worou, Dr. S. Sanfo, Aminata Barry, Azéta Ouédraogo, Boukaré Ouédraogo, Symphorin Meda, Marcel Somande, Issa Zongo, Sessouma Moussa. The coordination teams of Dano (Hamadou Barro, Herman Hien, Man Koumbassolo, Salif Somé, Moussa Sidibé, Salia Hebié and Binta Diallo), Benin (Adolph Avocan, Orougoura Doussi, Ezechiel C. Adjakpa, Kiatti D. Yokoue, Alaza Zibrila, Moussa Imorou) and Ghana (Aaron B. Aduna, Samuel Guug, Daid Kwesi Orchard) are acknowledged as well.

I'm grateful to Prof. Dr. K. Borgemeister, Pr. Dr. P. Vlek, Dr. M. Denich, Dr. John Lamers, Dr. G. Manske, Dr. G. Lüchters, Maike Retat-Amin, Dr. D. Wisser, Dr. G. Villamor, Dr. D. Callo-Concha, Dr. P. Sow, Dr. J. Henning, Dr. B. Tishbein, Dr. F. Gatzweiler, Dr. J. Tambo, Dr. V. Kyere, Louis Yameogo, Wenceslas Somda, Adhikari Narayan, Kaderi Boukari, Charles Okyere, Janina Kleeman, HongMi Koo and Kémonou Richard currently or formerly at ZEF for their support. Thanks go to Prof. Dr. M. Becker, Prof. Dr. M. Evers, Dr. T. Gaiser, Dr. H. Webber, Dr. I. Rosendahl, Dr. A. Almoradie and Mr. Ozias Hounkpatin at the University of Bonn for their exhortations.

I express my gratitude to the current and former PhD students of WASCAL graduate research program, namely Eugène W. Yeo, Djigbo F. Badou, Dr. Charlène Gaba, Dr. I. Danso, Jean Hounkpe, Adama Touré, Sambou Djiby, Vincent C. Azuka, Koffi K. Valentin and Ibrahim Moussa, with whom I had very interesting discussions and pleasant moments during their stay here in Bonn.

Many thanks to the inhabitants of Tambiri (Burkina Faso), Ouri-youri (Benin) and Vea (Ghana), as well as to the staff of Dreyer Foundation in Dano for their welcome. Special thanks go to Mr. André Hien in Dano.

ABSTRACT

This study investigated the impacts of climate and land use changes on water resources in the Dano catchment combining hydrological processes understanding, hydrological simulations and climate and land use scenarios application. The catchment covers about 195 km^2 and is located in the Southwest of Burkina Faso in West Africa. The study area is characterized by an annual population growth of about 3% over the past decades.

Based on intensive field investigations on soil hydraulic properties, instrumentation and monitoring of hydro-meteorological variables such as discharge, soil moisture, groundwater level, precipitation, temperature etc. the distributed and physically based hydrological simulation model WaSiM was successfully calibrated and validated for the catchment. Achieved model statistical quality measures (R^2, *NSE* and *KGE*) ranged between 0.6 and 0.9 for total discharge, soil moisture, and groundwater level, indicating a good agreement between observed and simulated variables.

Land use change assessment in the catchment over the period of 1990-2013 exhibited a decrease of natural and semi-natural vegetation at an annual rate of about 2%. Conversely, cropland, and to a lesser extend urban areas, have increased. Land conversion was attributed to population growth, changing in farming practices and environmental conditions.

Four land use maps were used to build land use scenarios corresponding to different levels of land use change in the catchment. Application of the land use scenarios to the calibrated and validated hydrological model indicated that, compared to the land use status in 1990, the current situation leads to an increase in total discharge of about 17% and a decrease of actual evapotranspiration of about 5%. The results of simulations further showed that the increase in total discharge is related to high peak flow, suggesting an alteration of flood risk.

Following field measurements that showed infiltration rates 1.2 times higher under semi-natural vegetation compared to cropland, land use change related effects on soil infiltration rate was integrated in the modeling of LULC change impact assessment. Model results with a refined soil (integrating this additional information) and a classic soil indicated similar trends in water balance components as a result of land use change. However slight differences of 0.5 to 20 mm/year in the water balance component were noticed between the two soil parameterization approaches. The integration of land use related effects on soil properties was suggested to render LULC change scenarios more plausible.

The projected climate change signal in the catchment was analyzed using the representative concentration pathways 4.5 and 8.5 of six datasets of the COordinated Regional climate Downscaling Experiment-project. Compared to the reference period of 1971-2000, the climate models ensemble consistently projects an increased temperature of 0.1 to 2.6°C over the period 2021-2050. However, an agreement was not found among climate models with regards to precipitation change signal as projections for annual rainfall ranged between -13 and +18%.

The application of the climate models ensemble in WaSiM showed future discharge change signals very similar to the projected precipitation change. Individual climate models showed opposite annual discharge change signals ranging from -40 to +50 %. On average, the climate models ensemble suggested a 7 % increase in annual discharge under RCP4.5 and a 2 % decrease under RCP8.5. The analysis of the catchment sensitivity to precipitation and temperature change indicated that discharge is more related to precipitation than to temperature as the environmental system of the catchment is water limited and not energy limited.

ZUSAMMENFASSUNG

Diese Arbeit untersuchte den Einfluss von Klima- und Landnutzungswandel auf Wasserressourcen im Dano-Einzugsgebiet durch eine Kombination von Prozessverständnis und hydrologischen Simulationen sowie durch die Anwendung von Klima- und Landnutzungsszenarien. Das Einzugsgebiet erstreckt sich über 195 km² und befindet sich im Südwesten Burkina Fasos in Westafrika. Das Untersuchungsgebiet wird durch in den vergangen Jahrzehnten geprägt ein starkes jährliches Bevölkerungswachstum von 3%.

Die Untersuchung hydraulischer Bodeneigenschaften, der Aufbau von Messgeräten und die Erfassung von hydro-meteorologischen Messgrößen wie Abfluss, Bodenfeuchte, Grundwasserstand, Niederschlag und Temperatur war die Voraussetzung für die erfolgreich Anwendung des räumlich diskreten, physikalisch basierten hydrologischen Models WaSiM welches für das Einzugsgebiet kalibriert und validiert wurde. Statistische Gütemaße (R^2, *NSE* und *KGE*) zeigten mit Werten zwischen 0.6 und 0.9 für den Gesamtabfluss, die Bodenfeuchte und den Grundwasserstand eine gute Übereinstimmung zwischen beobachteten und simulierten Variablen.

Die Auswertung des Landnutzungswandels im Einzugsgebiet über den Zeitraum von 1990-2013 zeigte eine Abnahme der natürlichen und naturnahen Vegetation mit einer jährlichen Rate von 2%. Im Gegenzug haben Ackerland und, in kleinerem Ausmaß, urbane Flächen zugenommen. Die Flächenumwandlung ist auf das Bevölkerungswachstum sowie, sich ändernde Anbaumethoden und Umweltbedingungen zurückzuführen.

Vier Landnutzungskarten wurden zur Erstellung von Landnutzungsszenarien genutzt, die das Ausmaß des Landnutzungswandels im Einzugsgebiet widerspiegeln. Die Anwendung der Landnutzungsszenarien auf das kalibrierte und validiert hydrologische Model zeigt, dass im Vergleich zum Landnutzungsstatus von 1990 die aktuelle Situation zu einer Zunahme des Gesamtabflusses um ca 17% und einer Abnahme der aktuellen Evapotranspiration um ca 5% geführt hat.

In Anlehnung an Messungen im Feld, die um den Faktor 1.2 höhere Infiltrationsraten unter naturnaher Vegetation im Vergleich zu Ackerland zeigen, wurden Effekte des Landnutzungswandels auf die Infiltrationsrate in die Modellierung des Einflusses von Landnutzungswandel integriert. Modelergebnisse mit den entsprechend geänderten Bodeneigenschaften und die herkömmlich genutzten Bodeneigenschaften zeigten ähnliche Trends in Bezug auf die Komponenten der Wasserbilanz als Ergebnis des Landnutzungswandels. Dennoch wurden kleine Unterschiede der Komponenten des Wasserhaushalts von 0.5 bis 20 mm/Jahr zwischen den zwei Parametrisierungen festgestellt. Es ist davon auszugehen, dass die Integration von Effekten der Landnutzung auf bodenhydrologischen Eig.

Der mögliche Klimawandel wurde für das Einzugsgebiet mit den repräsentativen Emissionspfaden 4.5 und 8.5 von sechs CORDEX-Datensätzen (COordinated Regional climate Downscaling Experiment-project) analysiert. Im Vergleich zur Referenzperiode von 1971-2000 sagt das Ensemble der Klimamodelle durchweg einen Anstieg der Temperatur von 0.1 bis 2.6°C in den Jahren 2021-2050 vorher. Allerdings wurde zwischen den Klimamodellen keine Übereinstimmung im Hinblick auf die Änderung des Niederschlags festgestellt, da die Vorhersagen des jährlichen Niederschlags zwischen -13 und +18% liegen.

Die Anwendung des Ensembles der Klimamodelle auf WaSiM zeigt eine zukünftige Änderung des Abflusses, die der vorhergesagten Änderung des Niederschlags ähnlich ist. Einzelne Klimamodelle zeigen entgegengesetzte Signale der Änderung des jährlichen Abflusses von -40 bis +50%. Im Durchschnitt zeigt das Ensemble der Klimamodelle eine Zunahme des jährlichen Abflusses um 7% unter RCP4.5 und eine Abnahme um 2% unter RCP8.5. Die Analyse der Sensitivität des Einzugsgebiets gegenüber der Änderung von Niederschlag und Temperatur zeigte, dass der Abfluss stark vom Niederschlag abhängt und nicht von der Temperatur da das hydrologische System des Einzugsgebietes sich durch ein begrenztes Wasserangebot und nicht durch ein begrenztes Energieangebot auszeichnet.

RESUME

La présente étude examine l'impact des changements climatiques et d'utilisation des terres sur les ressources en eau du bassin versant de Dano, en combinant compréhension des processus hydrologiques, simulations hydrologiques et application de scenarios de changement climatique et d'utilisation des terres. La bassin versant couvre une superficie de 195 km^2 et est localisé dans le sud-ouest du Burkina Faso, en Afrique de l'Ouest. La zone d'étude se caractérise par son fort taux de croissance démographique qui se situe autour de 3% pour les dernières décennies.

S'appuyant sur des investigations de terrain basées sur les propriétés hydrauliques du sol, l'instrumentation, et la mesure de variables hydrométéorologiques telles que le débit, l'humidité du sol, le niveau de la nappe souterraine etc. le model hydrologique distribué à base physique WaSiM a été calibré et validé pour le bassin de Dano. Les performances du model hydrologique (R^2, *NSE* and *KGE*) varient entre 0.6 et 0.9 pour le débit, l'humidité du sol et la nappe; attestant une bonne concordance entre variables simulées et mesurées.

L'estimation du changement d'affectation des terres dans le bassin, sur la période 1990-2013, indique une perte annuelle en couvert végétal naturel et semi-naturel de l'ordre de 2%. Inversement, les terres agricoles et dans une moindre mesure les zones d'habitation se sont étendues. Cette dynamique de changement d'utilisation des terres est supportée par la croissance démographique, le changement des systèmes de production agricoles ainsi que par les conditions environnementales.

Quatre cartes d'utilisation des terres ont servi à l'élaboration de scenarios correspondant à différents niveaux de changement d'affectation des terres dans le bassin. L'application de ces scenarios au model hydrologique indique que, comparé à l'état de surface de 1990, la situation actuelle conduit à une augmentation de débit annuel de l'ordre 17% et une baisse de l'évapotranspiration effective de l'ordre de 5%. De plus, le résultat des simulations montre que l'augmentation du débit est liée au débit de pointe, suggérant une altération du risque d'inondation.

Les mesures effectuées sur le terrain indiquent en moyenne des taux d'infiltration 1.2 fois plus grands sous les couverts naturels et semi-naturels comparés aux champs. Cet effet de l'utilisation de terres sur le taux d'infiltration a été intégré à la modélisation de l'impact des changements d'utilisation des terres sur les ressources en eau. Les résultats montrent que les simulations faites avec un sol affiné (intégrant cette information supplémentaire) ainsi que celles faites avec un sol classique aboutissent à de similaires tendances en termes de changement du bilan hydrique. Cependant, des différences de l'ordre de 0.5 à 20 mm/an par élément du bilan existent entre les deux approches de paramétrage du sol. Il en résulte que l'intégration des effets de l'utilisation sur les propriétés du sol rend les scenarios futurs de changement d'utilisation des terres plus plausibles.

Deux profils représentatifs d'évolution de concentration en gaz à effet de serre (RCP4.5 et 8.5) dérivés de six produits climatiques du projet COordinated Regional climate Downscaling Experiment ont servi à l'analyse du signal de changement climatique projeté pour le bassin. Comparé à la période de référence 1971-2000, l'ensemble des modèles climatiques projette systématiquement une augmentation de température de l'ordre de 0.1 à 2.6°C sur la période 2021-2050. Par contre, les modèles climatiques montrent des signaux divergents pour les précipitations. Les changements de précipitation annuelles telles que projetés se situe entre -13 et +18%.

L'application des données de l'ensemble de modèles climatiques à WaSiM a montré de futurs débits annuels très semblables aux projections de changement de précipitation. Les divers modèles climatiques ont montré des signaux opposés de changement de débit se situant entre -40 et +50%. En moyenne, l'ensemble des modèles climatiques projette une augmentation de débit de 7% sous RCP4.5 et une baisse de -2% sous RCP8.5. L'analyse de la sensibilité du débit à la variation de température et de pluie indique que le débit est plus dépendant de la pluie que de la température. Les conditions arides au sein du system hydrologique du bassin expliquent la réponse du basin aux variations de ces deux variables.

TABLE OF CONTENTS

LIST OF FIGURES

LIST OF TABLES

ABBREVIATIONS

BMBF	Federal Ministry of Education and Research, Germany
CCLM	COSMO (Consortium for Small-scale Modeling)-Climate Limited-area Modelling
CNRM	Centre National de Recherches Météorologiques
CORDEX	COordinated Regional climate Downscaling Experiment
DEM	Digital Elevation Model
DGM	National Meteorological Service of Burkina Faso
DMI	Danish Meteorological Institute
ESM	Earth System Model
ETa	Actual evapotranspiration
ETp	Potential evapotranspiration
FAO	Food and Agriculture Organization of the United Nations
FAOSTAT	Food and Agriculture Organization Statistics
GCM	General/Global Circulation/climate Model
GWL	Groundwater Level
HIRAM	High Resolution Atmospheric Model
HRU	Hydrologic Response Unit
INSD	National Institute of Statistics and Demography, Burkina Faso
ITCZ	Inter Tropical Convergence Zone
KGE	Kling and Gupta Efficiency
KNMI	Royal Netherlands Meteorological Institute
LAI	Leaf Area Index
LHS	Latin hypercube sampling
LULC	Land Use and Land Cover
MA	Millennium Ecosystem Assessment
MEAHA	Ministry of Water resource, Hydraulic infrastructures and Sanitation
MODIS	Moderate Resolution Image Spectrometer
NorESM	Norwegian Earth System Model
NSE	Nash and Sutcliffe Efficiency
PDIC/D	Communal Development Plan, Dano
PTF	Pedotransfer Function
RACMO	Regional Atmospheric Climate Model
RCM	Regional Circulation/Climate Model
RCP	Representative Concentration Pathway
SCS	Soil Conservation Service
SPI	Standardized Precipitation Index
SRTM	Shuttle Radar Topography Mission
SSA	Sub-Saharan Africa
USGS	United States Geological Survey
WASCAL	West African Science Service Center on Climate and Adapted Land Use
WaSiM	Water flow and balance Simulation Model
WHO	World Health Organization
WWDR	World Water Development Report

1. GENERAL INTRODUCTION

1.1. Problem statement

Water is the “bloodstream” of the biosphere (Falkenmark & Rockström, 2004). It is a key resource for agricultural production and daily life. However, water is a finite resource, unevenly accessible for different world regions and further challenged by global water demand (WWDR, 2015). Although the Millennium Development Goal drinking water target - 88% of the world’s population use improved drinking water sources by 2015- was met since 2010, still one out of nine people worldwide does not have access to safe and clean drinking water and 37% of those people live in Sub-Saharan Africa (SSA) (WHO, 2015).

Besides unmet demand for water infrastructures, WWDR (2015) identifies the management and protection of water resources as a key challenge for sustainable development in SSA. The report highlights increasing population and economic growth as major pressures on ecosystems providing water and water related services. Urbanization, agricultural land expansion, deforestation, pollution etc. are among numerous drivers directly affecting these ecosystems (MA, 2005). Equally significant, climate change and climate variability poses threats to water availability in the region.

Therefore, enabling timely water availability in the region requires an understanding of the hydrological processes involved in water provisioning together with different drivers and factors affecting these processes. A number of studies carried out in West Africa during the past decades represente significant advances in the understanding of hydrological processes (e.g. Bormann et al., 2005; Giertz, 2004; Speth et al., 2010), as well as in the evaluation of hydrological impacts of factors like land use (e.g. Bossa, 2012; Boulain et al., 2009; Hiepe, 2008; Mounirou, 2012; Schmengler, 2011) and climate (e.g. Cappelaere et al., 2009; Karambiri et al., 2011; Kasei, 2009; Mahé et al., 2010).

From the previous studies, insights were gained in the understanding of runoff generation processes: (i) s*urface runoff* is found to be strongly affected by land cover and land management practices, (ii) the stratification of soil horizons (decreasing hydraulic conductivity with depth) proved to be favorable to *interflow* generation, (iii) the abundance of macropores suggests considerable *preferential flow*, (iv) the runoff coefficient decreases with drainage area as a response to the combination of surface heterogeneity, topography-driven ponding and runoff generation process, etc. Knowledge about the role of land use and climate change on the regions hydrology has also been improved: (i) vegetation cover was found to be a key determinant for Hortonian runoff generation, (ii) extension of agricultural land is found to trigger soil erosion, (iii) land use change is known to have a larger impact on terrestrial hydrology compared to climate change in some regions (e.g. Sahel), and (iv) projected discharge change signal was shown to be primarily dependent on precipitation change signal and climate model.

Due to data scarcity in the region, many studies performing land use and climate changes impact assessment on catchment hydrology in the region used simple hydrological models. Although the findings of these previous studies are in general consistent with the methodological approaches used, few hydrological models were set up based on thorough field investigation and processes understanding. Furthermore, the spatial pattern of heterogeneity in soil, vegetation and relief is often ignored or treated in a simplistic way. Consequently, these approaches may be limited for studying the response of hydrological systems to spatially explicit inputs like land use and climate change.

A quantitative analysis of climate and land-use changes impacts on water resources in a hydrological system requires simulation models that adequately represent the system features relevant for the water balance components of interest. Understanding processes within the system is an integral part of the modeling approach. Therefore, the challenge is to model land use and climate change impacts on

hydrological systems, based on processes understanding while preserving the systems spatial organization.

1.2. Research questions

Several research questions arise from the problem stated above:

(i) **how does land use and land cover change affect soil infiltration rate?** This first research question addresses the issue of plot scale impact of LULC change on soil infiltration rate. Soil infiltration rate is a key hydraulic property determining water flow into the soil. Naturally, several factors simultaneously affect infiltration, rendering it a very complex process. Distinguishing the contribution of a specific factor remains challenging and very few field investigations on LULC change effects on soil infiltration rate do exist for West Africa.

(ii) **how does the application of a physically based and spatially distributed hydrological model instead of a conceptual lumped model improve the modeling results?** The added value of the application of a physically based and spatially distributed model represents the second research question of the study. Distributed hydrological models feature the capability to incorporate the spatial pattern of heterogeneity in soil, vegetation and relief. Over the last decades, the tendency in hydrological model development has been to integrate as much understood processes as possible; all which contributed to the emergence of physically based and spatially distributed hydrological models. Undoubtedly, the assessment of the impacts of changing characteristics (e.g. land use) of a catchment is improved with a physically based and distributed model as the catchment characteristics have physical meaning. However, several challenges (data scarcity, effective parameter values at element scale, computer power, etc.) undermine the application of physically based and spatially distributed models.

(iii) **how does LULC change impact water resources in the Dano catchment?** Analyzing the ongoing land use change in the study area and assessing unambiguously its impact on water balance constitutes the focus of the third research question of the study. The relation between LULC change, streamflow and water balance at catchment scale is still under debate, as the net effect of LULC impact on water resources depends on several factors such as local climate, converted LULC class, degree of LULC change etc. Moreover, LULC and climate changes occur simultaneously and differentiating between both effects remain challenging.

(iv) **how does the integration of LULC related effects on saturated hydraulic conductivity affect the modeling result in LULC impact assessment?** The fourth research question of the study addresses the issue of soil parameterization in LULC change impact assessment studies. While several field investigations ascertain significant effects of LULC change on soil physical properties, hydrological modeling exercises usually ignore this relation due to the lack of hydrologic and meteorological observation time series data at a suitable time scale, limited field measurements of soil properties under different LULC classes, and additional model parameterization efforts.

(v) **What is the likely trend in precipitation and temperature for the future period 2021-2050 compared to the historical period 1971-2000 and how is this trend likely to impact water resources in the catchment?** The investigation area is located in a region where global and regional climate models commonly project a temperature increase but a divergent precipitation change signal for the mid-21st century. So far, the available literatures on climate change impact on water resources in the region, do not show a clear trend in future development of water resources while the region is highly exposed to climate change.

1.3. Objectives

The overall objective of the study is to improve the management of water resources in the tropical West African region with a focus on the Dano catchment. It aims to provide information on the potential impact of climate and land use change on water resources in the catchment.

Specifically, and following the research questions, the objectives of the study are to:

(i) improve the understanding of land use change effect on soil infiltration rate;
(ii) set up a robust distributed hydrological simulation model for the catchment;
(iii) assess land use and land cover change impacts on waterflow and water balance components;
(iv) evaluate the model sensitivity to soil parameterization and modeling time scale in land use change impact assessment; and
(v) assess the impact of climate change on the hydrology of the catchment by the middle of the 21st century.

1.4. Structure of the thesis

The thesis is structured into ten chapters starting with this general introduction. Chapter 2 gives a general description of the study area. Chapter 3 covers the description of the hydrological simulation model, its parameterization, the different algorithms and processes. Chapter 4 presents the instrumentation performed in the catchment and the collected secondary data. It also discusses the challenges related to different datasets. Chapter 5 addresses field investigations on soil physical properties. Chapter 6 discusses land use effect on soil infiltration rate at the plot scale by comparing the two dominant land use and land cover classes in the catchment: cropland and savannah/fallow. Chapter 7 examines land use and land cover change in the catchment over the period 1990-2013 and assesses land use change impacts on water resources. Chapter 8 analyzes the relevance of integrating land use change related effects on soil hydraulic conductivity in land use and land cover impact assessment. Chapter 9 focuses on projected climate change signal for the middle 21st century and its potential impact on water resources using an ensemble of CORDEX climate scenarios. Finally, chapter 10 presents the general conclusion of the study.

2. STUDY AREA

2.1. Location

The Dano catchment covers a total area of 195 km^2 in the Ioba province, located in the Southwest of Burkina Faso (Fig. 2-1). In addition to Dassari (Benin) and Vea (Ghana), Dano is one of the WASCAL (www.wascal.org) Core Research Program intervention zones.

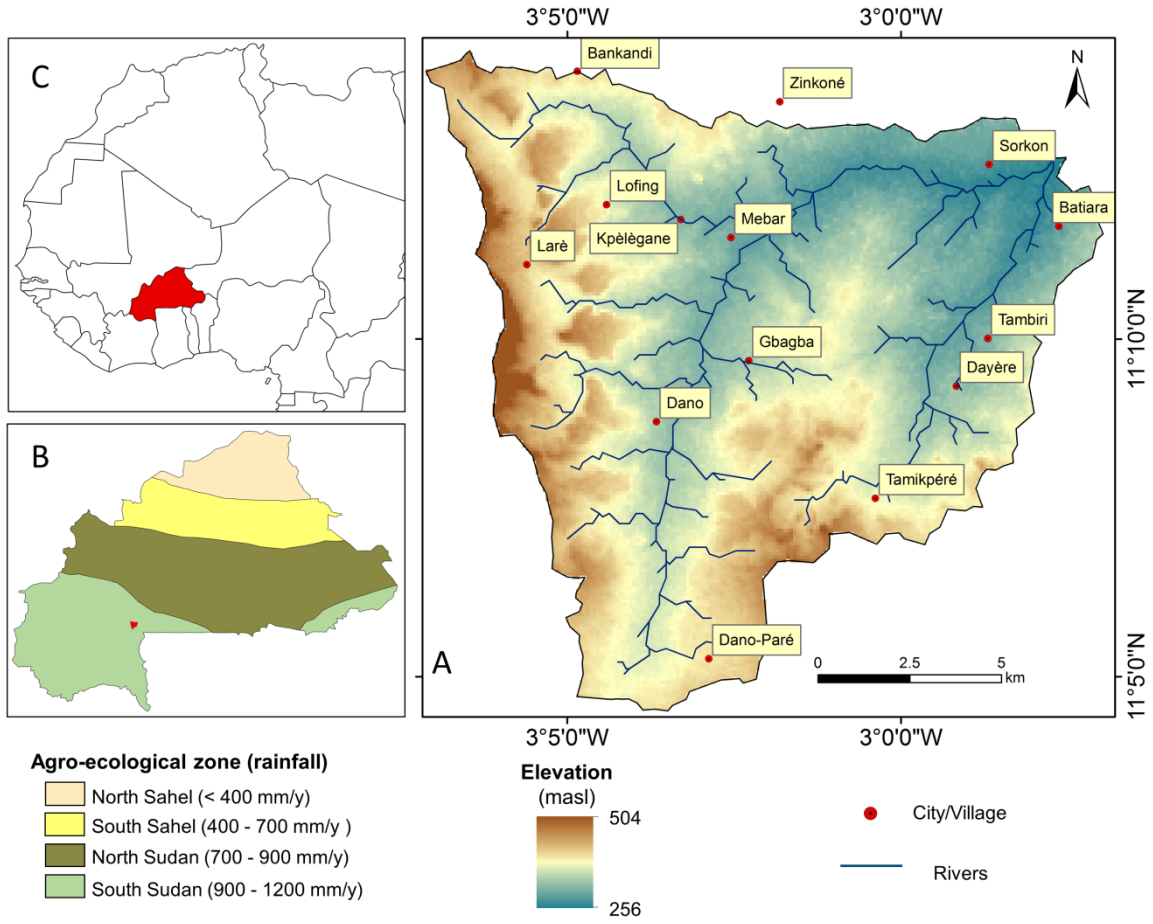

Fig. 2-1 Location map. Part A shows the Dano catchment, part B indicates its position in the agro-ecological zones (Fontès & Guinko, 1995) of Burkina Faso and part C situates Burkina Faso in West Africa.

2.2. Climate

The Dano catchment belongs to the transition zone between the Sudano-Sahelian zone (600-900mm/year) and the Sudanian zone (900-1200mm/year) (Dipama, 2010). The climate over the catchment is characterized by two distinct seasons: a rainy season (May to October) and a dry season (November to April) (Waongo, 2015). The climate regime is regulated by the oscillation of the Intertropical Convergence Zone (ITCZ) front which is driven by the Sahara anticyclone and the Southern Hemisphere anticyclone (Sivakumar & Gnoumou, 1987).

The annual mean temperature in the catchment equals 28°C with monthly mean values varying between 24°C and 32°C (Fig. 2-2). An average +0.31°C/decade and +0.17°C/decade, increase for the minimum and maximum temperature respectively, is reported for the region considering the period of 1960-2010

(Waongo, 2015). The annual precipitation ranged from 800 mm to 1200 mm for the period 1951 to 2005 (Schmengler, 2011). The rainfall statistics computed using climate data of the National Meteorological Service (DGM) show similar ranges. The onset of the rainy season occurs from mid-May to end of June (Diallo, 2001; Sarr et al., 2015) and about 80% of annual rainfall occurs from July to September (Kasei et al., 2009). The climate of the region is also characterized by a considerable inter annual variability as shown by the standardized Precipitation -Evaporation- Index (Fig. 2-3) including moderate to severe drought years that occur with a return period of 9 years (Kasei et al., 2009). Notable drought events in the region are the ones that occurred in the early 1970s, whose impacts (famine and outmigration) were worsened by the weak institutional situation (Callo-Concha et al., 2012).

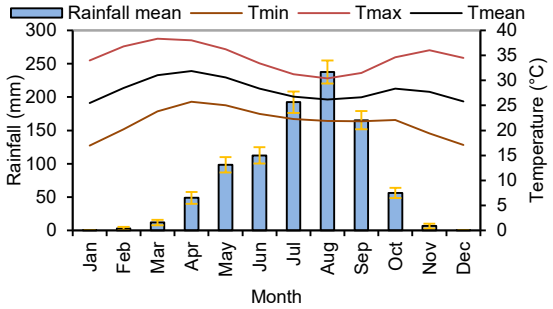

Fig. 2-2 Monthly rainfall and temperature pattern in the Dano catchment for the period of 1990-2014. Error bars refer to standard deviation. Data source: National Meteorological Service (DGM).

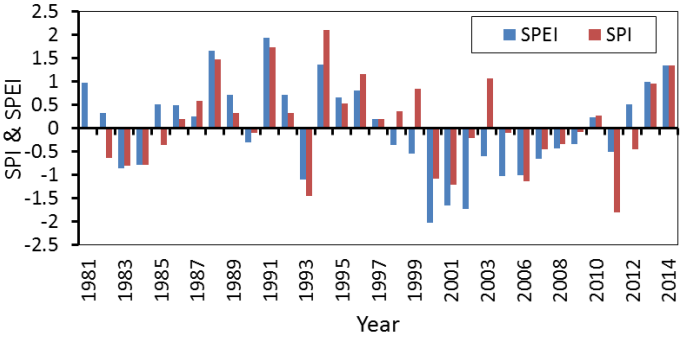

Fig. 2-3 Standardized Precipitation Index (SPI, McKee et al., 1993) and Standardized Precipitation Evaporation Index (SPEI, Vicente-Serrano et al., 2009) in the Dano catchment. Period of 1981-2014).

2.3. Vegetation

The catchment is part of the Sudanian phytogeographic domain, which is the savannah and forest patches zone (Boussim, 2010). Natural vegetation of this sector is characterized by:

- tree species, dominated by *Faidherbia albida, Lannea microcarpa*, *Parkia biglobosa*, *Tamarindus indica*, *Vitellaria paradoxa, Acacia erythrocalyx, Anogeissus leiocarpa, Celtis integrifolia, Diospyros mespiliformis, Pterocarpus erinaceus* etc.;
- herbaceous stratum, composed of *Andropogon pseudapricus, Elionurus elegans, Loudetia togoensis, Pennisetum pedicellatum, Schizachyrium exile, Aristida adsenscionis, Cenchrus biflorus, Ctenium elegans, Cymbopogon schoenanthus, Schoenefeldia gracilis* etc.

As investigated in more details in chapter 7, the major part of the primary vegetation has been converted to agriculture and long-term fallowing during the past decades. The dominant crops are: *Sorghum bicolor* (sorghum), *Gossypium hirsutum* (cotton), *Zea mays* (maize), *Pennisetum glaucum* (millet), *Oryza sativa & Oryza glaberrima* (rice, produced in inland valleys), *Vigna unguiculata* (cowpeas, often associated to sorghum), *Arachis hypogaea* (groundnut) and *Sesamum indicum* (sesame).

A particular feature of Dano (and the south-western part of the country) is the intensive use of firewood to produce the local beer "*dolo*". About 6 442 tons of wood are used annually for the production of *dolo* (Blin & Sidibe, 2012). This constitutes an additional driver to the degradation of the natural vegetation.

2.4. Geology and geomorphology

The craton of the region consists of paleoproterozoic or Precambrian basement (Sandwidi, 2007; Villeneuve & Cornée, 1994). The rocks form the West African craton which covers major parts of the country as the Man or Leo shield (Debat et al., 2003; Ouédraogo et al., 2003). This shield is made of

volcanic sedimentary rocks and granitoids known as Birrimian rocks (Sandwidi, 2007). Granitoids are the main components of the basement rocks and comprise migmatites, granodiorites and migmatic granites in combination with volcanic sedimentary rocks, mainly amphibolites. The basement rocks are often covered by sediments ranging from Neoproterozoic to the present time (Ouédraogo et al., 2003; Villeneuve & Cornée, 1994).

The landscape of the catchment is predominantly flat with an average slope of 2.9%, an elevation range from 256 to 504 m above sea level (masl) and a mean elevation of 295 masl. The relief of the catchment is notably characterized by the Ioba hills which border the southern part of the catchment.

2.5. Hydrology

The catchment is drained by several streams which dry up in the dry season. Rivers regime is governed by the ITCZ front. Storm events during the rainy season induce runoff (for the period of June-October). Groundwater occurrence in the region is reported to be associated with the development of secondary porosity such as from joints, fractures, shears and fissures (Amisigo, 2005). Therefore the aquifer systems in the catchment are reported to be highly discontinuous with individual compartments in which isolated groundwater circulation occurs (Amisigo, 2005).

2.6. Population

The city of Dano and surrounding villages had about 46 550 inhabitants in 2010 (PDIC/D, 2010). Over the decades 1985-1996 and 1996-2006, the population has been growing at an annual rate of 2.7% and 3.1% respectively (INSD, 2006). Population density consequently increased from 24.9 persons per Km^2 in 1985 to 51.8 persons per Km^2 in 2006. Like the country's economy, land use in Dano is essentially agricultural. The sector employs about 86% of the population. Agriculture is mostly rainfed with poor technology and investments (Callo-Concha et al., 2012). An average area of 1.5-5 ha is used by agricultural household (PDIC/D, 2010). Besides agricultural activities, women are especially active in fruit and firewood gathering, petty trade, artisanship and foodstuff trading (Callo-Concha et al., 2012).
The rate of access to safe drinking water in the rural areas is about 63% (MEAHA, 2013). Therefore, a very large part of the population relies on surface water as source of supply.

3. MODELING APPROACH -WASIM

3.1. Principles and main features

The Water flow and balance Simulation Model (WaSiM) is a deterministic and spatially distributed model, which uses mainly physically based approaches to simulate the water cycle above and below the land surface (Schulla, 2014). The model was originally developed to analyze the impact of climate and land use change on water resources in alpine regions (Schulla, 1997). Since then, it has been continuously improved and successfully applied to quantify changes in all major water balance components and to estimate change trends in several studies in different climate regions (e.g. Kassa, 2013; Kasei, 2009; Korck et al., 2012; Leemhuis, 2006; Logemann et al., 2013; Ott et al., 2013). Version 9.05.04 of the model (Schulla, 2014; Schulla, 2015), based on Richards-equation to represent the soil water flow and coupled to a 2-D groundwater module, is applied in this study. Fig. 3-1 illustrates the main features of the model.

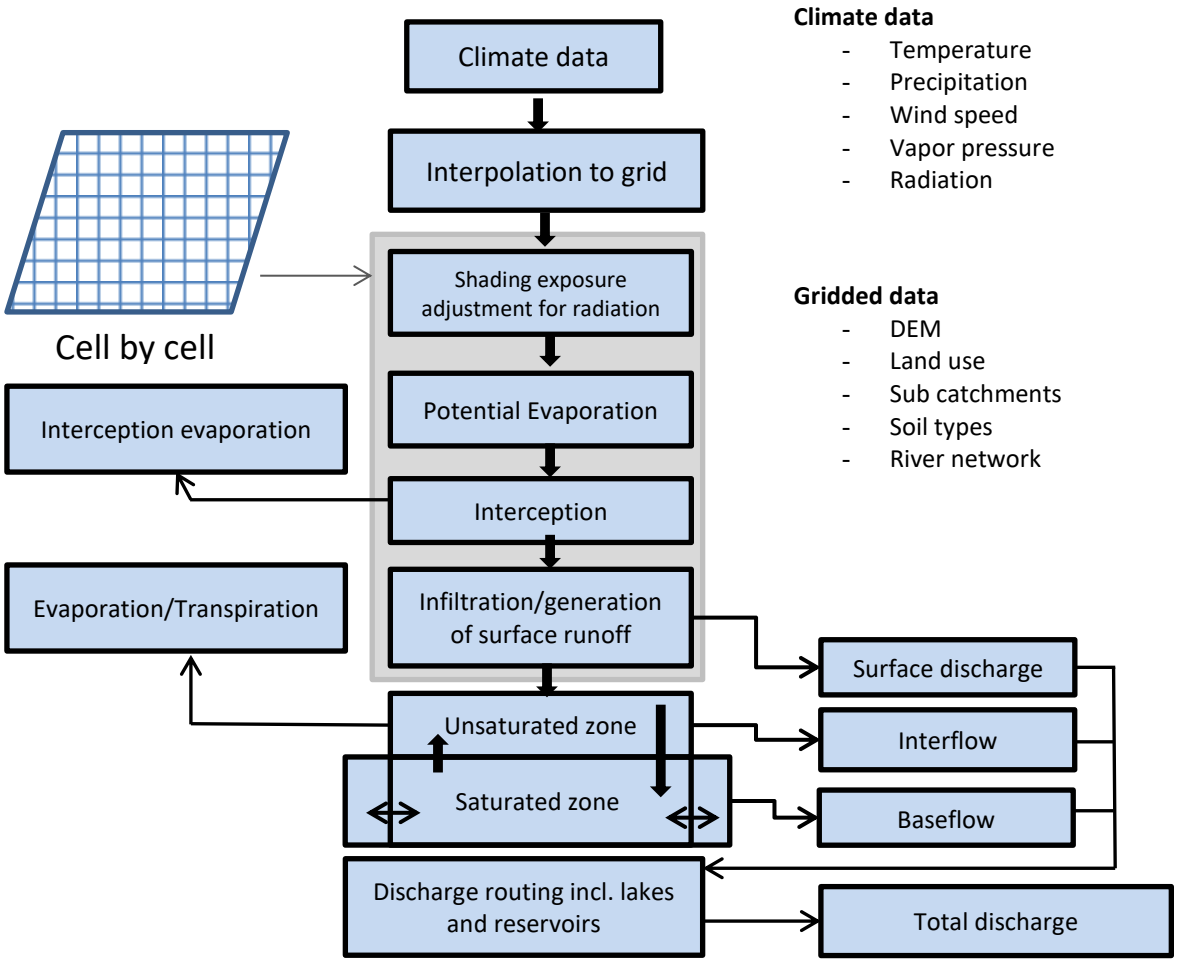

Fig. 3-1 WaSiM structure (Adapted from Schulla, 2014).

3.2. Data requirement

Depending on the aim of the application and on the available input data, various model configurations (modules) can be used to set up WaSiM. The model can also be run in various spatial (few meters to 5

km grid) and temporal (1minute to 1 day) discretizations depending on the catchment size and the available computing power.

3.2.1. Spatially gridded data

Spatial distributed data is required for the model application. This includes soil types, land use classes and digital elevation model (DEM) of the catchment. Spatial data is required in a raster data set with identical resolution and extension and data must be provided either in binary or in ASCII-format. The topography analysis program TANALYS (Schulla, 2014), provided along with the model, is used as preprocessing tool to perform DEM analysis and generates a number of terrain attributes like local slope, aspect and curvature. Important hydrologic information such as flow directions, flow accumulations, stream network, sub-catchment area etc. is also generated using TANALYS. The required gridded data set can similarly be provided using any GIS program assuring the specific extension for each required grid.

3.2.2. Temporal data and Interpolation

An optimum configuration of the model requires time series data of precipitation (mm/time step), air temperature (°C), relative humidity (%), wind speed ($m.s^{-1}$), global radiation ($Wh.m^{-2}$) and relative sun shine duration (h) as meteorological data. Specific discharge data (mm or m^3/time step) for each sub-basin is also required for model calibration and validation. The temporal resolution of time series data however depends on the research objectives (e.g. hourly time step for flood simulation and daily for long term water balance simulation). Meteorological data are provided as time series of climate stations (identified by point coordinates and elevation). The model allows various (12) methods to interpolate input data with a sparse spatial resolution to the model grid resolution. These methods encompass Inverse Distance Interpolation (IDW), Thiessen Polygons, Elevation Dependent Regression etc.

3.3. Processes simulation

3.3.1. Evapotranspiration

Transpiration and evaporation of a reference crop under no limited water availability is denoted as potential evapotranspiration (*ETp*) (Katul & Parlange, 1992). It includes all processes of water transfer as vapour from the Earth's land and water bodies' surfaces to the atmosphere.

The potential transpiration from plant leaves, the evaporation from bare soil and the evaporation from interception surfaces and water bodies are calculated in WaSiM after Penman-Monteith (Monteith, 1975; Brutsaert, 1982) as shown by Eq. 3-1. However, the model allows the calculation of *ETp* following Wendling (1975) and Hamon (based on Federer and Lash, 1983).

$$\lambda \mathrm{E} = \frac{3.6\,\frac{\Delta}{\gamma_p}.(RN - G) + \frac{\rho.c_p}{\gamma.r_a}.(e_s - e\,)}{\frac{\Delta}{\gamma_p} + 1 + \frac{r_s}{r_a}}\,t_i \qquad \text{Eq. 3-1}$$

Where	λ	latent vaporization heat, λ = (2500.8 - 2.372**T*)	[$kJ.kg^{-1}$]
	T	temperature in	[°C]
	E	latent heat flux	[$mm.m^{-2}$]
	Δ	tangent of the saturated vapor pressure curve	[$hPa.K^{-1}$]
	RN	net radiation	[$Wh.m^{-2}$]
	G	soil heat flux (here: 0.1.RN)	[$Wh.m^{-2}$]

ρ	density of dry air	[kg.m^{-3}]
c_p	specific heat capacity of dry air at constant pressure	[kJ.(kg.K)$^{-1}$]
e_s	saturation vapor pressure at the temperature *T*	[hPa]
e	actual vapor pressure (observed)	[hPa]
t_i	number of seconds within a time step	[-]
γ_p	psychrometric constant	[hPa.K^{-1}]
r_s	bulk-surface (canopy) resistance	[s.m^{-1}]
r_a	the bulk-aerodynamic resistance	[s.m^{-1}]

Actual evapotranspiration (*ETa*) is computed based on the relation between soil water content, actual capillary pressure and land use parameters. A mechanism of reducing *ETa* due to oxygen stress under saturated soil condition is also implemented in the model based on Feddes et al. (1978). The concept is presented in Fig. 3-2. Two parameters regulate this mechanism: the relative soil water value for beginning water stress for crops which depend on an aeral zone (*TReduWet*), and the maximum reduction of transpiration due to oxygen stress (*LimitReduWet*). However, open water evaporates with the maximum evaporation rate. Land use parameters for water are consequently set at specific values for this purpose. *ETa* is computed in the model based on Eq. 3-2.

$$
\begin{aligned}
ETa_i &= 0 && for \quad \theta(\psi) < \theta_{wp} \\
ETa_i &= ETP_i . \frac{\left(\theta(\psi_i) - \theta_{wp}\right)}{\theta_{\psi_g} - \theta_{wp}} && for \quad \theta_{wp} \leq \theta(\psi) \leq \theta_{\psi_g} \\
ETa_i &= ETP_i && for \quad \theta_{\psi_g} \leq \eta . \theta_{sat} \\
ETa_i &= ETP_i . \frac{\theta_{sat} - \theta(\psi_i)}{(\theta_{sat} - \eta . \theta_{sat})} && for \quad \eta . \theta_{sat} \leq \theta(\psi) \leq \theta_{sat}
\end{aligned}
$$

Eq. 3-2

Where	*i*	index of the soil layer	[-]
	ETa	actual evapotranspiration	[mm]
	ETp	potential evapotranspiration	[mm]
	$\theta(\psi)$	actual relative soil water content	[-]
	ψ	actual suction	[m]
	η	content at *TReduWet* (Fig. 3-2 below)	[-]
	θ_{sat}	saturated water content	[-]
	θ_{ψ_g}	soil water content at a given suction ψ_g	[-]
	θ_{wp}	soil water content at wilting point	[-]

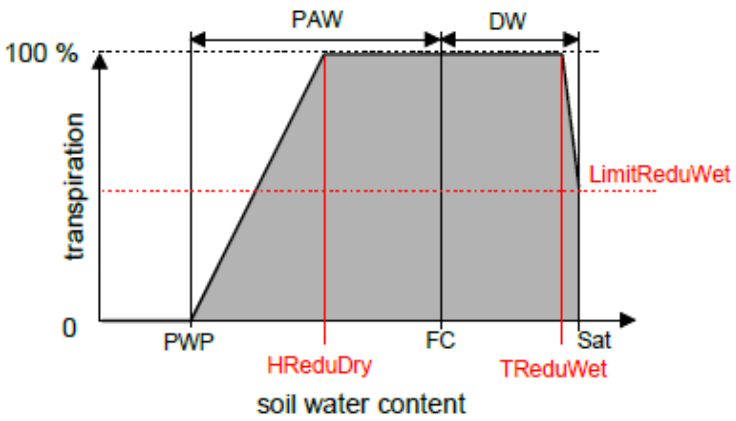

Fig. 3-2 Reduction of actual evapotranspiration with water stress (after Schulla, 2014). *PWP* is permanent wilting point, *FC* is field capacity, *HReduDry* is threshold value for starting dryness stress, *PAW* is plant available water and *DW* is drainage water.

3.3.2. Interception

Interception refers to the storage of precipitation in the leaves and branches of plants (canopy). In WaSiM a simple bucket approach depending on the leaf area index (*LAI*), the vegetation coverage fraction, and the maximum height of water at the leaves is used (Eq. 3-3). Water intercepted by the canopy is evaporated at potential rate (*ETp*). Once the interception storage is filled, further precipitation is defined as throughfall and is handled by the soil model.

$$SI_{max} = vfc.LAI.h_{SI} \qquad \text{Eq. 3-3}$$

Where	SI_{max}	maximum interception storage capacity	[mm]
	vfc	vegetation covered fraction	[$m^2.m^{-2}$]
	LAI	leaf area index (crop specific annual course)	[$m^2.m^{-2}$]
	h_{SI}	maximum height of water at the leaf surfaces	[mm]

3.3.3. Infiltration

Infiltration is calculated based on the fillable porosity of the uppermost numerical soil layer and the precipitation amount per time step. For precipitation amount (*P*) lower than fillable porosity of the uppermost numerical soil layer, all precipitation infiltrates. For *P* higher than the fillable porosity of the uppermost numerical soil layer, rainwater infiltrates until the upper soil layer is fully saturated and the excess rainfall is converted to surface runoff.

3.3.4. Unsaturated zone

Water flow in the unsaturated zone is based on Richard's equation (Eq. 3-4). The modeling is done one-dimensional in the vertical direction using a soil with several numeric layers of same thickness.

$$\frac{\partial \Theta}{\partial t} = \frac{\partial q}{\partial z} = \frac{\partial}{\partial z}\left(-k(\Theta)\frac{\partial \psi(\Theta)}{\partial z}\right) \qquad \text{Eq. 3-4}$$

Where	Θ	water content	[m^3/m^3]
	t	time	[s]
	ψ	hydraulic head (Σ suction ψ and geodetic altitude *h*)	[m]

	q	specific flux	[m/s]
	z	vertical coordinate	[m]

The parameterization of the soil hydraulic properties for unsaturated flow was carried out by applying the soil water retention after van Genuchten (1980) (Eq. 3-5). The empirical parameters α, n and the saturated hydraulic conductivity are used for the calculation of the unsaturated conductivity function $k(\psi)$.

$$\theta(\psi) = \theta_r + \frac{\theta_s - \theta_r}{(1 + (\alpha/\psi)^n)^m} \quad \text{Eq. 3-5}$$

Where	θ	actual water content	[m^3/m^3]
	ψ	suction	[hPa]
	θ_r	residual water content at k(θ) = 0	[m^3/m^3]
	θ_s	saturated water content	[m^3/m^3]
	α, n	empirical parameters (m=1-1/n)	[-]

3.3.5. Interflow

Interflow is generated between soil layers of different hydraulic conductivities or porosities. However, the soil layer suction (ψ) should be lower than 3.45 m and there must be a sufficient slope else waterlogging will be the result. Interflow (q_{ifl}) is a result of conductivity, river density and hydraulic gradient as given by Eq. 3-6.

$$q_{ifl} = K_s(\theta_m).\Delta_z.d_r.tan\beta \quad \text{Eq. 3-6}$$

Where	*Ks*	saturated hydraulic conductivity	[m/s]
	θ_m	water content in the actual layer m	[-]
	d_r	drainage density	[-]
	β	local slope angle	[°]
	Δ_z	layer thickness	[m]

3.3.6. Groundwater table elevation

A two-dimensional Darcy based groundwater module is coupled with the one-dimensional unsaturated zone module to simulate lateral fluxes in the saturated zone. The groundwater table elevation results from the balance of inflows and outflows of soil layers containing the groundwater. While deep percolation and lateral inflow increase groundwater level; baseflow, lateral outflow of and (evapo) transpiration from groundwater reduce the groundwater level.

Changes of the groundwater table for a given cell calculated by the groundwater module are converted into vertical fluxes: positive for a falling groundwater table, and negative for a rising groundwater table. This boundary flux and the amounts of infiltration, exfiltration, precipitation and fluxes between the unsaturated layers are considered to estimate the groundwater table. After each time step, groundwater level (h_{GW}) is interpolated based on the water content a layer must have if being in a hydrostatic equilibrium with the groundwater using Eq. 3-7.

$$h_{GW} = h_{geo,m} + d_m(\theta_{m,i} - \theta_{GW,min})(\theta_s - \theta_{GW,min}) \quad \text{Eq. 3-7}$$

Where $\theta_{GW,min}$ is water content for hydrostatic equilibrium ($GW = \theta_r + (\theta_s - \theta_r)\left(\frac{1}{1+(0.5.d_m\alpha)^n}\right)^m$),

$h_{geo,m}$	geodetic altitude of the lower limit of the layer *m*	[m]
d_m	thickness of layer *m*	[m]
$\Theta_{m,i}$	actual water content of layer *m* at time step *i*	[-]
Θ_s	saturated water content	[-]
Θ_r	residual water content of layer m	[-]
α, n, m	*van Genuchten* parameters	[-]

3.3.7. Baseflow

Baseflow is generated as exfiltration from the groundwater into the surface river system. Thus it is generated only at grid cells which are marked as river cells (stream network). Baseflow is calculated in two steps. During the first step, exfiltration is calculated using the hydraulic gradient and the exfiltration resistance at the river bed following Eq. 3-8.

$$q_{exf,pot} = l_k . \Delta H . \frac{b_{rb}}{cs} \qquad \text{Eq. 3-8}$$

In the second step, $q_{exf,pot}$ is partitioned to all affected soil layers and water can be extracted from layers only until the predefined suction of 3.45 m is reached (suction ψ < 3.45 m) according to Eq. 3-9.

$$q_{exf,m} = (\Theta_m - \Theta_{\psi\_3.45}) . \frac{\Delta z_e}{\Delta t} \qquad \text{Eq. 3-9}$$

Where			
	$q_{exf,pot}$	maximum possible baseflow	[m.s^{-1}]
	$q_{exf,m}$	maximum possible exfiltration from layer *m*	[m/s]
	l_k	leakage factor (colmation resistance)	[s^{-1}]
	ΔH	difference between groundwater table and river bed	[masl]
	b_{rb}	width of the river bed	[m]
	cs	grid cell size	[m]
	m	layer index	[-]
	Θ_m	water content in layer *m*	[-]
	$\Theta_{\psi\_3.45}$	water content at suction ψ = 3.45 m	[-]
	Δz_e	effective layer thickness	[m]

3.4. Sensitivity, Calibration and Uncertainty

Sensitivity analysis aims to understand the quantitative sources of uncertainty in model calculations and to identify those sources that contribute the largest amount of uncertainty in a given outcome of interest (van der Sluijs et al., 2004). The inputs considered in the sensitivity analysis are those having a large possible value range either difficult to be observed or are empirical parameters. There are however complexities in assessing the sensitivity of parameters for distributed models notably because of the large number of parameters involved and the possibilities for parameters interactions. This remains a challenge as parameter calibration is improved if efforts are concentrated on parameters to which the model simulation results are most sensible (Beven, 2003).

Model parameters reported sensitive from previous WaSiM applications differ depending on whether one is interested in the modeled discharge, the groundwater table fluctuation or soil moisture dynamic. The current study investigates each of these 3 model outputs, suggesting *a priori* considering all empirical parameters as well as observed parameters with large range of possible values. Only parameters that are

derivable with certain degree of consistency and showing little or no variability (e.g. saturated and residual water content, *van Genuchten* parameters) were excluded from the calibration. The investigated parameters are namely: drainage density (*dr*), saturated hydraulic conductivity (*Ks*), recession constant of *Ks* with depth (K_{rec}), groundwater hydraulic conductivity (*Kx_y*), river colmation resistance (*Kol_factor*), soil surface resistance (*Rse*), leaf surface resistances (*Rsc,)*, surface storage coefficient K_D and interflow storage coefficient K_H.

As a first step, the model was "set up" using graphical and numerical calibration based on the coefficient of determination (r^2), and the Nash Sutcliffe Efficiency (NSE) using river discharge at the outlet. Trial and error "optimization" of these model efficiency criteria was performed by tuning the considered parameters and this model delivering acceptable simulations was used as starting point for the sensitivity analysis. A first feeling of the parameters sensitivity was gained; this step also supported the effectiveness of the parameters reported to be sensitive in previous studies. Using a pre-calibrated model is also reported to protects global sensitivity analysis to a reasonable extent from numerical instability (Christiaens & Feyen, 2002).

With regard to the number of potentially sensitive parameters, the Latin Hypercube Sampling (*LHS*) was adopted for its higher efficiency. The method ensures that each of the considered parameters is represented in a fully stratified manner (physically meaningful parameter distributions are assigned to each parameter) no matter which components might turn out to be important (McKay et al., 1979), thus making minimal assumptions about the shape of the model response surface (Beven, 2003). A Latin Hypercube Sampling is an extension of stratified sampling. Conversely to a standard stratified sampling where the range space of a parameter is arbitrarily partitioned, in a *LHS* the partitions are constructed in a specific manner using partitions of the ranges of each of the parameters. Richter et al. (1996) describe in more details the method. The method can be summarized in the following three steps (Christiaens & Feyen, 2002; Janssen et al., 1994):

1. Equi-probable subdivision of the distribution function of each considered parameter (or input) into *r* ranges with a probability of occurrence equal 1/*r*;
2. Single value sampling within each interval (stratified sampling);
3. Random pairing: *r* data sets of *p* parameters are generated with *r* > 4/3 *p* (Janssen et al., 1994).

Using the data set of the *p* parameters, *r* runs of the model are performed and various statistics are employed to quantify the sensitivity and uncertainty contribution of each parameter to the model outputs.

Statistics used to quantify sensitivity and uncertainty contribution of each *p* parameter following the *LHS* are mostly based on regression and correlation analysis of the ensemble model outputs (Christiaens & Feyen, 2002; Janssen et al., 1994). In this sense, a regression "metamodel" $\hat{y}(r)$ (Christiaens & Feyen, 2002) that fit a linear combination of varying *p* parameters to simulated discharge was constructed following Eq. 3-10:

$$y_v(r) = \hat{\beta}_{0,v} + \sum_{i=1}^{p} \hat{\beta}_{i,v} \, . \, x_i(r) + \hat{e}_v(r) \approx \hat{y}_v(r) + \hat{e}_v(r) \qquad \text{Eq. 3-10}$$

Where r is number of model run (1…r),
v is the studied objective function (*SSE* using discharge);
$\hat{\beta}_{0.v}$ & $\hat{\beta}_{i,v}$ are regression coefficients,

$\hat{e}_v$ is regression residual.

Using the regression model $\hat{y}(r)$, different measures are calculated:

(a) The correlation coefficient (R^2) of the regression model, measuring the validity of the regression model. R^2 denotes which fraction of *the objective function's* variance is explained by the regression model ($\hat{y}_v$). R^2 varies between 0 and 1, and perfect fit gives a R^2= 1. σ^2 in Eq. 3-11 refers to the sample variance.

$$R^2 = 1 - \frac{\sigma_{\hat{e}}^2}{\sigma_y^2} \quad \text{Eq. 3-11}$$

(b) The absolute sensitivity measures $\hat{\beta}_{i,v}$ (or ordinary regression coefficient *ORC*) approximates the absolute change-Δy_v of y_v, if x_i changes with amount Δx_i, while others parameters remain constant. The *ORC* however doesn't allow ranking the importance of the *p* parameters as it depends on the scale and dimension of x_i. To detect the most sensitive parameter, the standardized regression coefficient (*SRC*) is calculated.

(c) The *SRC* quantifies the fraction of uncertainty in y_v which is contributed by x_i. It measures how much y_v will change relative to its standard deviation σ_{y_v}, when x_i changes with it standard deviation σ_{x_i} (Eq. 3-12). Since the *SRC* uses real variation in its calculation it can also be an uncertainty measure (Christiaens & Feyen, 2002). The limitation of the SRC is that it does not consider the correlation among *p* parameters. As none the *p* parameters of this study was found to be correlated, such a shortcoming was excluded.

$$SRC = \beta_{i,v} \frac{\sigma_{x_i}}{\sigma_y} \quad \text{Eq. 3-12}$$

3.5. Model performance criteria

Schemes of metrics focusing on several aspects of a system are needed for a comprehensive evaluation of models, as a single performance criterion generally measures only specific aspects of a model's performance and may lead to results favoring models that do not reproduce important features of a system (Bennett et al., 2013; Kling et al., 2012). Multiple performance approaches were used to assess the model performance and the "optimal" calibrated parameter values. The following section presents a brief view of selected criterion.

(i) Sum of Squared Errors (*SSE*), measures the deviation of simulated from observed values of data. It is the sum of the squares of residuals; it thus avoids positive and negative errors to cancel each other. *ESS* ranges between 0 and +∞ and it is commonly accepted that the lower the *SSE* is, the better the model performs (Moriasi et al., 2007).

$$SSE = \sum_{i=1}^{n} (Y_i^{obs} - Y_i^{sim})^2 \quad \text{Eq. 3-13}$$

Where Y_i^{obs} and Y_i^{sim} are observed and simulated variables respectively.

(ii) Pearson product moment correlation (*r*) and coefficient of determination (r^2). *r* ranges from -1 to 1 and describes the degree of linear relation between observed and simulated data. A value equals zero indicates no relation. For r equals 1 (-1) a perfect positive (negative) relation exists. r^2 is the squared of r, with the same interpretation of results, but ranges from 0 to 1 (Bennett et al., 2013). In addition to the linearity assumption, r and r^2 are over sensitive

to high extreme values and can return an ideal result for a model with constant offset (Bennett et al., 2013; Moriasi et al., 2007).

$$\boldsymbol{r} = \frac{\sum_{i=1}^{n}(Y_i^{obs} - \hat{Y}_i^{obs})(Y_i^{sim} - \hat{Y}_i^{sim})}{\sqrt{\sum_{i=1}^{n}(Y_i^{obs} - \hat{Y}_i^{obs})^2}\sqrt{\sum_{i=1}^{n}(Y_i^{sim} - \hat{Y}_i^{sim})^2}} \quad \text{Eq. 3-14}$$

Where $\hat{Y}_i^{obs}$ and $\hat{Y}_i^{\mathrm{sim}}$ are respectively the means of observed and simulated data

(iii) Nash-Sutcliffe coefficient-*NSE* (Nash & Sutcliffe, 1970). *NSE* is also commonly referred to as the coefficient of determination in hydrological modelling (Bennett et al., 2013) although they are slightly different (Węglarczyk, 1998) indicating how well the model explains the variance in the observation. *NSE* ranges from -∞ to 1 with the optimum at unity and is known to give a good explanation of how well observed variable peaks are captured by the simulations. *NSE* is a combination of observed and simulated data R^2, means and standard deviations (Gupta et al., 2009a). Eq. 3-15 presents the decomposition of *NSE* after Murphy (1988) in which the first term measures the strength of the linear relation between observed and simulated data, the second term represents the conditional bias, and the third term the unconditional Bias (Gupta et al., 2009). Gupta et al. (2009) highlighted a trend toward the underestimation of the variability in the flows by the NSE due to the interplay between the first two terms.

$$NSE = [r]^2 - \left[r - (\sigma_{Y^{sim}}/\sigma_{Y^{obs}})\right]^2 - \left[(\hat{Y}_i^{sim}/\hat{Y}_i^{obs})/\sigma_{Y^{obs})}\right]^2 \quad \text{Eq. 3-15}$$

Where $\sigma_{Y^{sim}}$ and $\sigma_{Y^{obs}}$ stand for the standard deviation of simulated and observed data respectively.

(iv) Kling-Gupta Efficiency, *KGE* (Gupta et al., 2009; Kling et al., 2012). The KGE is another way of combining observed and simulated data's r^2, means and standard deviations that conversely to the *NSE* presents the bias component explicitly. The *KGE* (Eq. 3-16) is an interesting criterion because it reproduces the temporal dynamics (measured by r) as well as preserving the distribution of flows (summarized by β and γ) (Kling et al., 2012). KGE ranges from -∞ to 1 with the optimum at the unity.

$$KGE = 1 - \sqrt{(r-1)^2 + (\beta - 1)^2 + (\gamma - 1)^2} \quad \text{Eq. 3-16}$$

With $\beta = \hat{Y}_i^{sim}/\hat{Y}_i^{obs}$ and $\gamma = (\frac{\sigma_{Y^{sim}}}{\hat{Y}_i^{sim}})/(\frac{\sigma_{Y^{obs}}}{\hat{Y}_i^{obs}})$

4. INSTRUMENTATION AND DATA AVAILABILITY

4.1. Introduction

Process based hydrological modeling implies the availability of both spatial and temporal data. Multiple data types further permit constraining the uncertainties in predicted variables (Pappenberger & Beven, 2006), thus increasing the confidence in the modeling outcome. Knowledge of hydrological processes and the influencing factors is also a prerequisite to physically based hydrological modeling (Giertz & Diekkrüger, 2003). Datasets initially available for the Dano catchment include topographic, soil, geology, land use, socioeconomy and climate (Table 4-1).

Table 4-1 Initial data sets available for the Dano catchment

Data set	Resolution	Source
Topography	90m	SRTM
Soil	1:500 000 to 1:300 000	Kaloga et al. (1973)
Land use	5 to 250 m	Landmann et al. (2007), Forkuor et al. (2014) and Cord et al. (2010)
Climate (observation)	Daily	DGM
Climate (simulation)	Daily	CORDEX-Africa project (http://www.cordex.org/)
Socioeconomy	Local	PDIC/D (2010)
Geology	1:1 000 000	Hottin & Ouédraogo (1992)

In order to gather the required data for setting up the hydrological model (WaSiM), to gain insights and understanding of the hydrological processes, an instrumentation concept was designed and implemented. An observation network composed of climate, groundwater (piezometer) and discharge stations was implemented within the catchment. Tambiri (see Fig. 4-7) was chosen as super test site for continuous soil moisture monitoring and hydrological processes analysis at a finer scale. Furthermore, point measurements of soil hydraulic properties were performed throughout the catchment in order to capture not only soil type variation but also soil hydrological properties change with land use. This chapter presents the instrumentation work, and gathered data.

4.2. Materials and methods

4.2.1. Climate data

A network of four automatic climate stations (CR.200, CR800 and CR1000 CAMPBELL SCIENTIFIC, INC) was used in the study. The recorded variables include rainfall, temperature, solar radiation, relative humidity as well as wind speed and direction (Fig. 4-1). The locations of the climate stations were selected following recommendations after the World Meteorological Organization (WMO). This implies considering the distribution of stations at a range of different elevations, the “representativeness” of locations, the morphology and nature of the surroundings, and the safety of places (WMO, 1993). As the entire catchment presents a patchy land use (cropland, fallow, savannah and settlements), the topography, the areal distribution and the safety criteria (closeness to a village) drove the choice of final locations.

Additionally to the instrumentation performed in the study area, climate data was also collected from the national meteorological service (DGM, see Fig. 4-7). This constitutes the sole source of ground historical climate data for the Dano catchment.

Simulated climate data was also retrieved for six regional climate models-global climate models (RCMs-GCMs) for the purpose of performing climate change impacts assessment in the catchment. Two periods and two greenhouse gas emission scenarios were considered.

Fig. 4-1 Climate station (Yabogane site) recording rainfall [mm], air temperature [°C], relative humidity [%],wind speed [m s^{-1}] & direction [°], solar radiation (incoming short wave) [W/ m^2], storage interval: 5 min.

Fig. 4-2 Gauging station (Dano-Paré site)**.** Recording water level [mm], storage interval: 10 min.

4.2.2. River discharge

A first location of gauging stations was determined during the instrumentation design phase based on the stream network hierarchy and the physiography of the catchment. During the implementation phase, the final location of each gauging station was then selected to get the most suitable locally available conditions for stage and discharge measurement (WMO, 2010). The suitability of a location was defined following the WMO (2010) guidelines, which includes among others the straightness course of the stream, a channel free of vegetation and readily accessible for ease in installation.

Once a site is selected, a measurement device (EcoLog 500, OTT Hydromet GmbH) was installed to continuously record the water pressure (Fig. 4-2). To establish the relationship between stage and discharge, several instantaneous discharge measurements were performed at various stages using a digital acoustic current meter (ADC, OTT Hydromet GmbH) consistently with the recommendations after ISO 1100-2 (2010).

4.2.3. Groundwater data

Due to it spatial coarseness, the available geological map of the catchment does not exhibit distinct units in the catchment, therefore the areal distribution and the topography were the main criteria used to identify the location of the piezometers. The implementation approach combined both shallow and deep groundwater monitoring.

The shallow groundwater probes were installed in boreholes drilled on the super test site. Three sets of piezometers were installed at different topographic positions following a transect line. The installation is designed to record the dynamic of groundwater level on the one hand and on the other hand to test whether *petroplinthic* layer reacts as impervious or not (Fig. 4-3). Deep groundwater level recording devices (DL/N 70, Ecotech) were installed in existing local boreholes (Fig. 4-4).

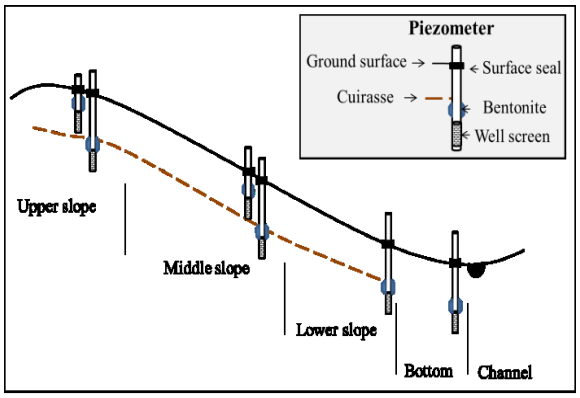

Fig. 4-3 Cross sectional profile of shallow groundwater monitoring experiment at Tambiri (see Fig. 4-7 for the location). Cuirasse refers to a hardened *petroplinthite*.

Fig. 4-4 Installation of a deep groundwater piezometer in a local pump at Gninkpière (see Fig. 4-7 for the location).

4.2.4. Soil water dynamic

The first field investigations on land use and land use dynamic in the catchment showed a trend toward the expansion of cropped areas and the reduction of semi-natural/fallow areas. Therefore, the instrumentation for soil moisture measurement integrated the land use factor. Topography and soil type were further associated to the instrumentation design.

Four hydrological response units (HRU, entities having a common soil type, topography and land use) were identified on the super test site by combining the dominant soil (*Plinthosol*), the dominant land use types (crop & Fallow/savannah) and two topographic positions (upper slope & lower slope). Soil water content and soil water tension were then recorded continuously under these *HRU* using two Soil-Water-Stations (Fig. 4-5 A).

The dominant soil type (*Plinthosol*) in the catchment generally presents a *petroplinthic* layer (Bt) at a shallow depth (< 50 cm), leaving the possibility for soil moisture monitoring only in the first two soil horizons with respect to the available equipment. Three frequency domain reflectometry probes (FDR, EcoTech Umwelt-Meßsysteme GmbH) and three soil tension probes (pF-Meters, EcoTech Umwelt-Meßsysteme GmbH) were installed per soil horizon at each observation profile (Fig. 4-5 B).

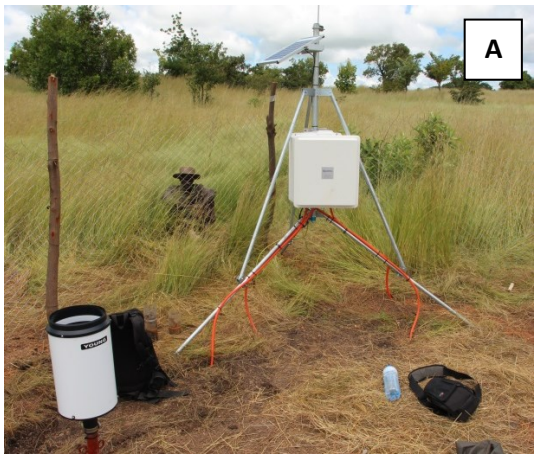

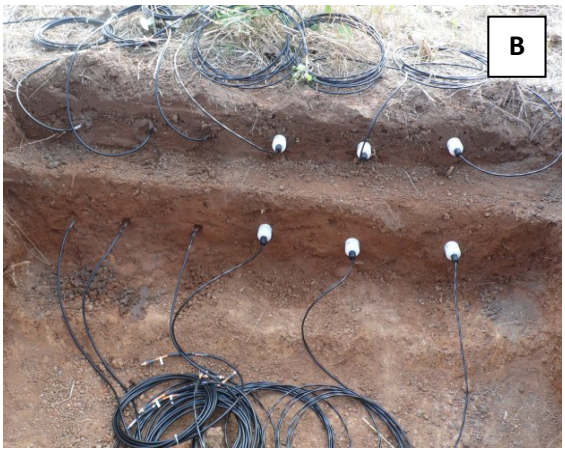

Fig. 4-5 Soil water station. Part A shows an external view of the station and part B shows one of the two profiles of the station. For each profile 3 FRD probes and 3 pF-meters are installed per soil horizon (A-horizon and B_1-horizon, see Fig. 4-10 for profile description).

4.2.5. Soil data

The initial soil map available for the catchment (after Kaloga et al., 1973) proved to be too coarse for the modeling exercise. Indeed, the variability of soil groups along hillslopes as well as hydromorphic soils groups (*Gleysols*) in inland valleys were not shown in this map. Therefore, a new soil map of the catchment was produced by the *Soil Science and Soil Ecology* working group of the University of Bonn, following the Soil and Terrain Digital Database (SOTER) approach. The mapping methodology follows a stepwise approach for differentiating, first between major landforms, which are further divided into regional landforms and later into terrain components. Finally, the soil components within the terrain component are identified (Igué et al., 2004).

In conjunction with the soil mapping which implies collecting soil samples for laboratory analysis additional soil samples were collected for soil hydraulic measurement. This joint approach allows for establishing the related attributes for texture, organic carbon content, pH, saturated hydraulic conductivity, saturated/residual water content, Bulk density etc. for each soil group and soil component

4.2.6. Land use data

Five local land use maps were available for the catchment. These land use maps correspond to land use and land cover (LULC) for the years: 1990,2000, 2007 (after Landmann et al., 2007), 2006 (after Cord et al., 2010), and 2013 (after Forkuor et al., 2014). Four of them are used in the study (Fig. 4-6). The LULC map of 2006 was excluded from the study due to its temporal proximity with the LULC of 2007.

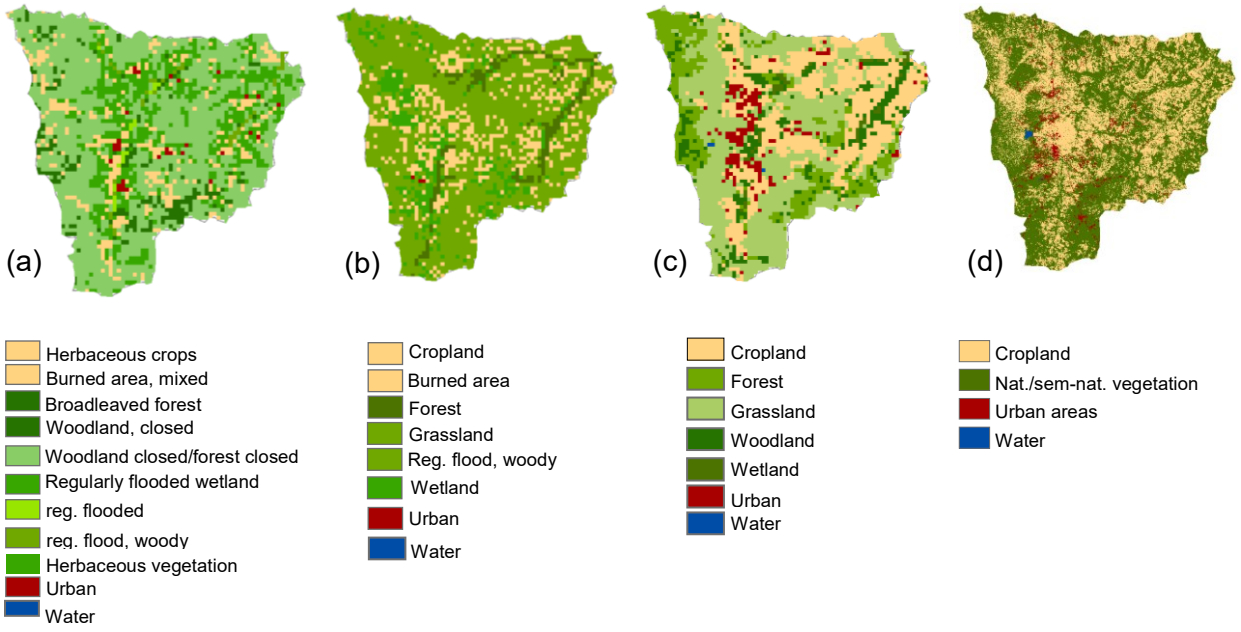

Fig. 4-6 Land use in the catchment: *(a)* year 1990, *(b)* year 2000, *(c)* year 2007, and *(d)* year 2013. Sources: (*a)*, (*b)* and (*c)* are after Landmann et al. (2007) and (*d)* is after Forkuor et al. (2014).

4.3. Results and discussion

An overview of the catchment instrumentation as used in the study is shown in Fig. 4-7. A number of instruments (climate stations and piezometers) are outside of the modeling domain. This is because the instrumentation is done for a catchment that is larger than the modeling domain defined in this study.

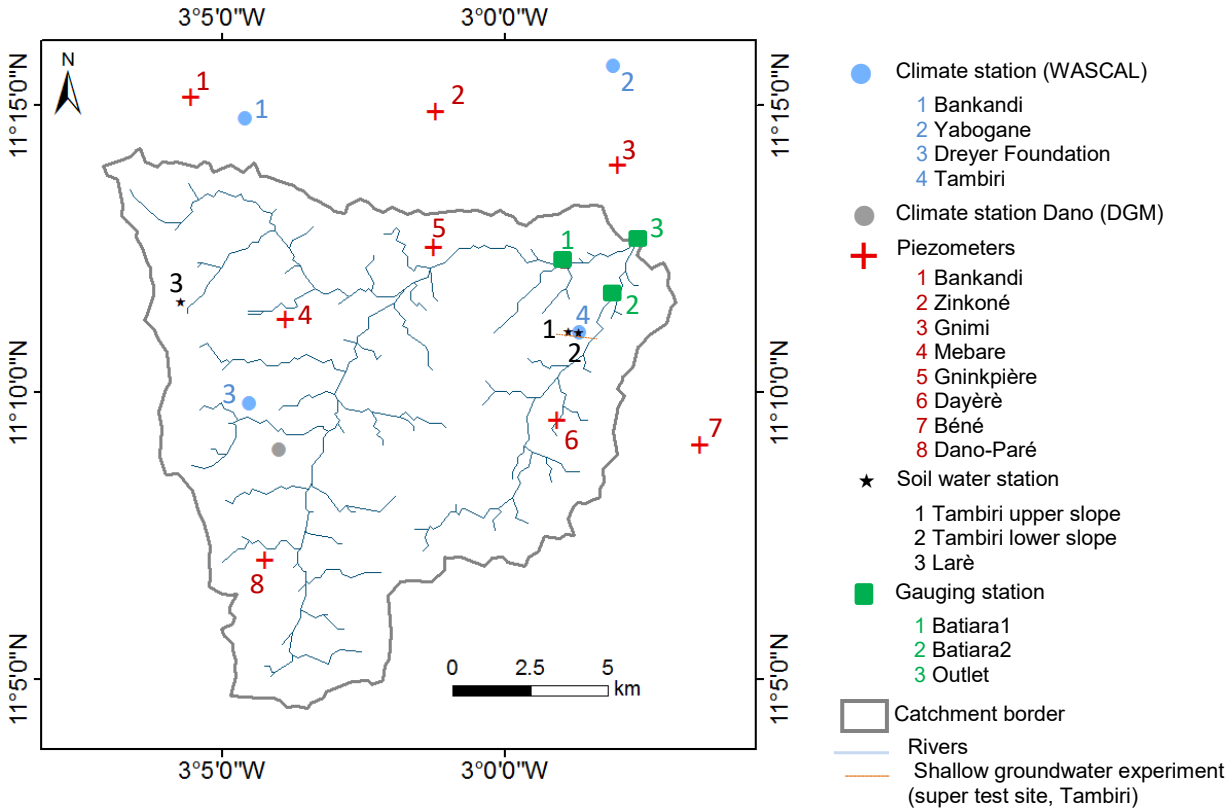

Fig. 4-7 Instrumentation of the Dano catchment as used in this study.

4.3.1. Climate data

Climate data gathered from the instrumentation were recorded at 10 minute intervals. These data were aggregated stepwise from 10 minutes to 1, 8, 12, 24 and 48 hours for different modeling purposes. For instance, in land use impact assessment as addressed in chapter 7, a daily time step data was used as a complement of the historical (24 hours) time series data initially available for the catchment.

Simulated daily precipitation and temperature climate data were retrieved from the CORDEX-Africa project (www.cordex.org). These data cover two time windows: (i) the historical period of 1971 to 2000, also used as the reference period in climate change impact assessment; and (ii) the future period of 2021 to 2050. Two representative concentration pathways-*RCP* (Moss et al., 2010) are considered for the projected period: RCP4.5 and RCP8.5. As discussed in more detail in chapter 9, compared to observation, simulated data show some biases which require corrections to be undertaken.

4.3.2. Groundwater data

Groundwater data was recorded at one-hour time intervals. As deep groundwater piezometers were installed in local boreholes used for drinking water supply, the water table was subject to fluctuation due to water pumping (Fig. 4-8 A). Water pumping usually takes place during the day, leaving the water level to rise in the night. Therefore, a given daily groundwater level was inferred from hourly time step data using the highest water table level within the 24 hours of that day (Fig. 4-8 B).

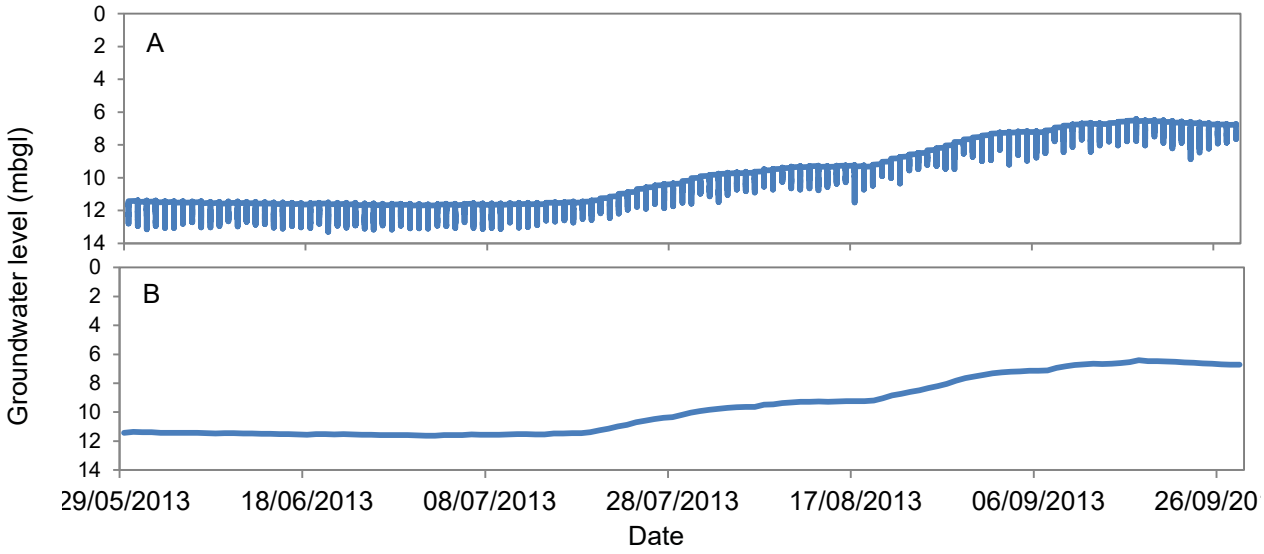

Fig. 4-8 Sample of groundwater level data at Bankandi (see Fig. 4-7 for the location). Part *A* shows the data as recorded at hourly time step and part *B* shows the same data at daily time step, processed as indicated above.

4.3.3. Discharge data

The yearly stage-discharge rating curves of the gauging stations, derived (using a power-law equation) from measured discharge and recorded stream water level, are shown in Fig. 4-9.

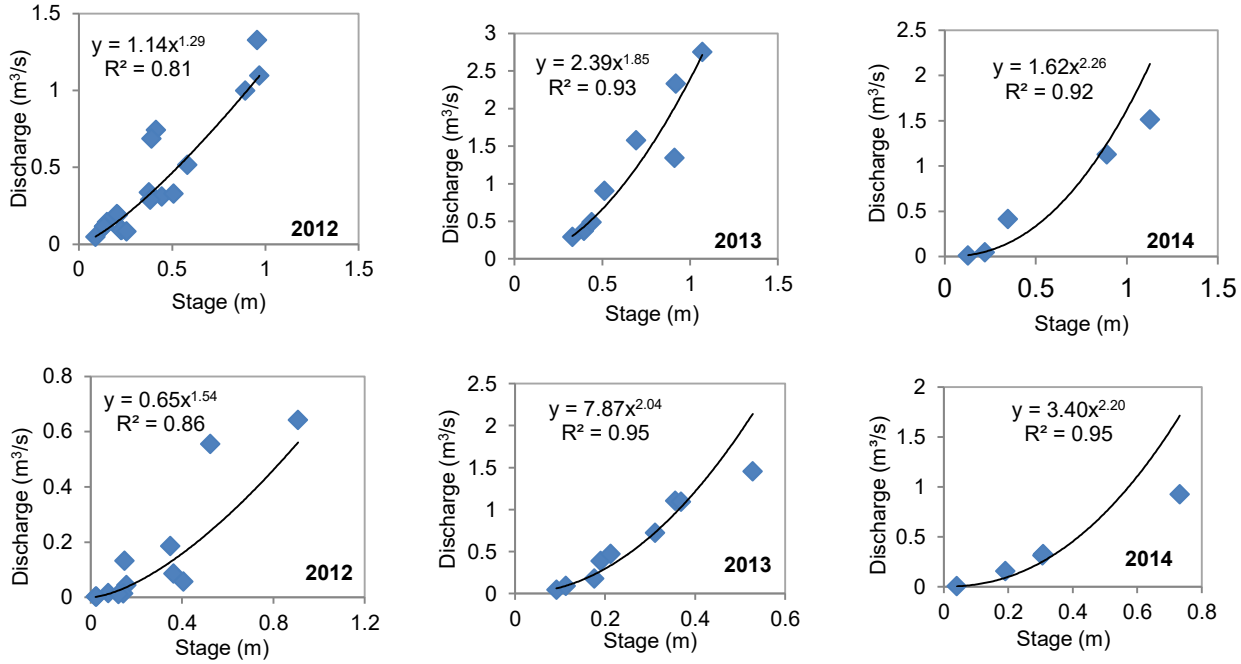

Fig. 4-9 Rating curves. First row refers to Batiara1 gauging station and second row indicates Batiara2 (see Fig. 4-7 for the location).

High correlation coefficients (>0.8) are achieved for the entire rating curves. However, one can notice that the stage-discharge relation slightly changes from one year to another, partly due the channel conditions. As the channels are natural, they are often affected by vegetation growth which changes their friction

properties. Other sources like operator' errors, sediment deposit in the channel and alteration of downstream channel control such as fallen trees have to be considered.

Overbank flow was observed at all gauging stations following heavy rainfall events. Discharge measurement for those events and high flow periods was not possible mainly for safety reasons. Consequently, extrapolation of the rating curve beyond the highest measurement was done. It is generally acknowledged that the part of the rating curve that is extrapolated beyond limits of measured discharged is less reliable than the measured range (Leonard et al., 2000; Tomkins, 2014). An extrapolation of 1.5 times the highest measured discharge is generally recommended (ISO 1100-2, 2010). However, this value reached 2 for some specific events. These extrapolation errors of high discharge events constitute a major source of uncertainty in the observed discharge.

4.3.4. Soil water dynamic

Fig. 4-10 illustrates a sample of recorded soil moisture data for the year 2013 at the two topographic positions (Upper & lower slope positions, Tambiri). It can be noticed that the topsoil horizon is responsive to rain events immediately at the beginning of the rainy season, whereas the *B*-horizon requires more events to get responsive. Water retention in the first horizon and the time required for the wetting front to descend through soil profile explain this difference of response time. However, the *B-horizon* remains wetter compared to the *A-horizon* during the dry season. For both topographic positions, soil moisture shows slight differences between cropland and fallow suggesting difference in rainfall interception and/or soil water uptake by evapotranspiration. A difference in soil properties between soil profiles is also observed.

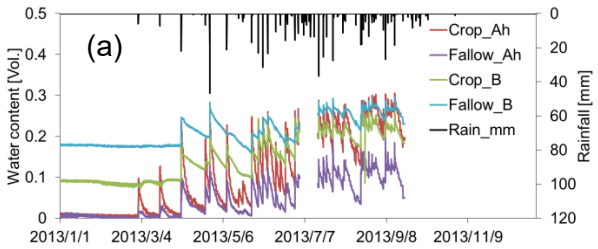

	Ah-horizon		*B*-horizon	
	Crop	Fallow	Crop	Fallow
Depth (cm):	0-8	0-12	8-32	12-18
Sand (%):	26.5	30	28.2	29.4
Silt (%):	73.4	65.1	56.3	54.9
Clay (%):	2.7	8.8	17.9	18
Bulk density (g/cm^3)	1.53	1.5	1.41	1.7
Corg (%):	2.43	2.46	0.52	0.61
pH (water):	6.23	6.31	6.42	6.31

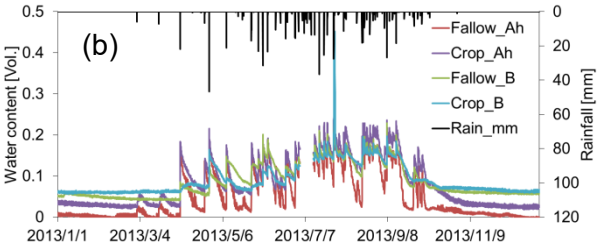

	Ah-horizon		*B*-horizon	
	Crop	Fallow	Crop	Fallow
Depth (cm):	0-10	0-10	10-17	10-15
Sand (%):	40.4	12.6	30	40.4
Silt (%):	54.0	38	54	41
Clay (%):	7.9	50.5	15.4	21.1
Bulk density (g/cm^3):	1.52	1.52	1.58	1.56
Corg (%):	0.82	0.56	1.19	1.03
pH (water):	6.27	6.26	6.08	6.33

Fig. 4-10 Sample of soil moisture data for the year 2013, and the related horizons' properties. *(a)* refers to upper slope position and *(b)* to lower slope position. *Ah* and *B* refer to the first and second horizons respectively (See Fig. 4-7 for plots location).

4.3.5. Soil data

The new soil map of the Dano catchment presents 21 soil components (prefix qualifiers added to the name reference soil group) (Fig. 5-1a) which can be grouped into 6 main reference soil groups (WRB, 2006) (Fig. 5-1b): *Leptosols, Cambisols, Plinthosols, Lixisols, Stagnosols and Gleysols*. The distribution and hydraulic properties of each soil group and soil component are addressed in detail in chapter 5.

4.3.6. Land use data

Having multi-temporal LULC maps for about 25 years (1990-2013) permits to analyze LULC change within the catchment. It further allows assessing the impacts of LULC change on the catchment hydrology (as addressed in chapter 7). However, several challenges are associated with the available land use data sets:

- **LULC classes**. The maps do not show the same number of land use classes (10, 7, 7 and 4 classes for the years 1990, 2000, 2007 and 2013 respectively). However, the variation in LULC class's number is not a result of complete conversion of a given LULC class; it is rather related to use of different LULC class grouping options for the maps;
- **small inconsistencies** in land use maps are observed at the local scale when comparing the four LULC maps. These inconsistencies include among others, changes from urban to cropland and back to urban or reduction in urban areas from 2007 to 2013;
- **spatial resolution**. Out of the four LULC maps, three present a spatial resolution of 250m whereas the fourth is available at a 5 m resolution;
- **imagery products**. The maps are derived from different imagery products: Landsat TM, MODIS and RapidEye.

Throughout the study, the initial LULC classes are grouped into four standardized units (Savannah, cropland, water and urban areas) and the spatial resolution is harmonized at 90 m for the four LULC maps. The modeling exercise, LULC dynamic and LULC change impact assessment are performed using this harmonized spatial resolution and LULC units.

4.4. Conclusion

Starting from an initial scarce data situation, the instrumentation work combined to data mining from different sources permitted establishing a considerable dataset. These data are not exempt from limitations as often observed throughout this chapter; however, none of these limitations is prohibitive to the use of the hydrological model WaSiM. Rather, the instrumentation, besides reinforcing the hydrological and meteorological observation network of the region, allows performing a wide set of hydrological investigations including those addressed in the following chapters.

5. SOIL PHYSICAL PROPERTIES

5.1. Introduction

Soil information is a basic input in environmental analysis. In hydrological modeling, soil parametrization is a key element for processes simulation. Considering spatial patterns in hydrological modeling further requires spatially referenced soil information. However, soil information data are not available for the great majority of catchments in developing countries (Young et al., 1999).

A comprehensive ground investigation on soil hydraulic properties is generally challenged by the effort and time required to collect and process soil samples or to perform *in situ* measurements of soil properties. Therefore, pedotransfer functions (PTFs) are often applied using basic soil information to derive sufficient information. As PTFs are developed for various regions, a common practice is to test them against measured data (Bossa et al., 2012; Wang et al., 2013) and/or to consider an ensemble of PTFs and estimate a range of plausible parameter values (e.g. Gwenzi et al., 2011; Minasny and Hartemink, 2011; Young et al., 1999).

A major constraint to the application of a physically based hydrological model in the Dano catchment was the lack of quantitative soil data. To address the issue, several field investigations were carried out in the catchment in order to collect and analyze soil physical and chemical properties necessary for soil parametrization in WaSiM. The current chapter presents the approach used and the achieved results. Insights with regard to how these soil properties influence the dynamic of water fluxes are also addressed.

5.2. Materials and Methods

5.2.1. Investigation area and sampling

A soil map of the catchment was produced by the *Soil Science and Soil Ecology* working group of the university of Bonn (www.boden.uni-bonn.de), following the Soil and Terrain Digital Database (SOTER) approach (Van Engelen & Wen, 1995). 21 soil components, referred to as “second level” of classification in the WRB (2006), were identified within the catchment (Fig. 5-1a). Overall, the catchment is dominated by *Haplic Plinthosols* (43.75 %), followed by *Epipetric Plinthosols* (15.20 %), *Haplic Gleysol* (10.77 %), *Lixic Plinthosols* (10.10 %), *Haplic Cambisols* (5.78 %), *Endopetric Plinthosols* (3.31 %). *Haplic Lixisols*, *Plinthic Lixisols*, *Haplic Leptopsols*, *Haplic Stagnosols* and *Plinthic Gleysols* occupy between 1.24 % and 2.36 % of the land. None of the remaining soil groups (*Stagnic Lixisols, Lixic Stagnosols, Plinthic Cambisols, Gleyic Cambisols, Plinthic Stagnosols, Stagnic Cambisols, Lixic Gleysols and Gleyic Plinthosols*) represents more than 1 % of the catchment.

For every soil component, one or more profiles of 1 m depth (where possible) (Fig. 5-1b), were described according to the WRB (2006). Texture and soil organic carbon (*SOC*) content were provided by the *Soil Science and Soil Ecology* working group along with the description of the profiles. The core of the additional investigations outlined in this chapter consisted of gathering hydrological properties for every soil component. For consistency, the soil hydrological properties were determined on soil samples collected at the same location as did the *Soil Science and Soil Ecology* working group. Further properties were derived from the provided soil texture and *SOC* content using PTFs.

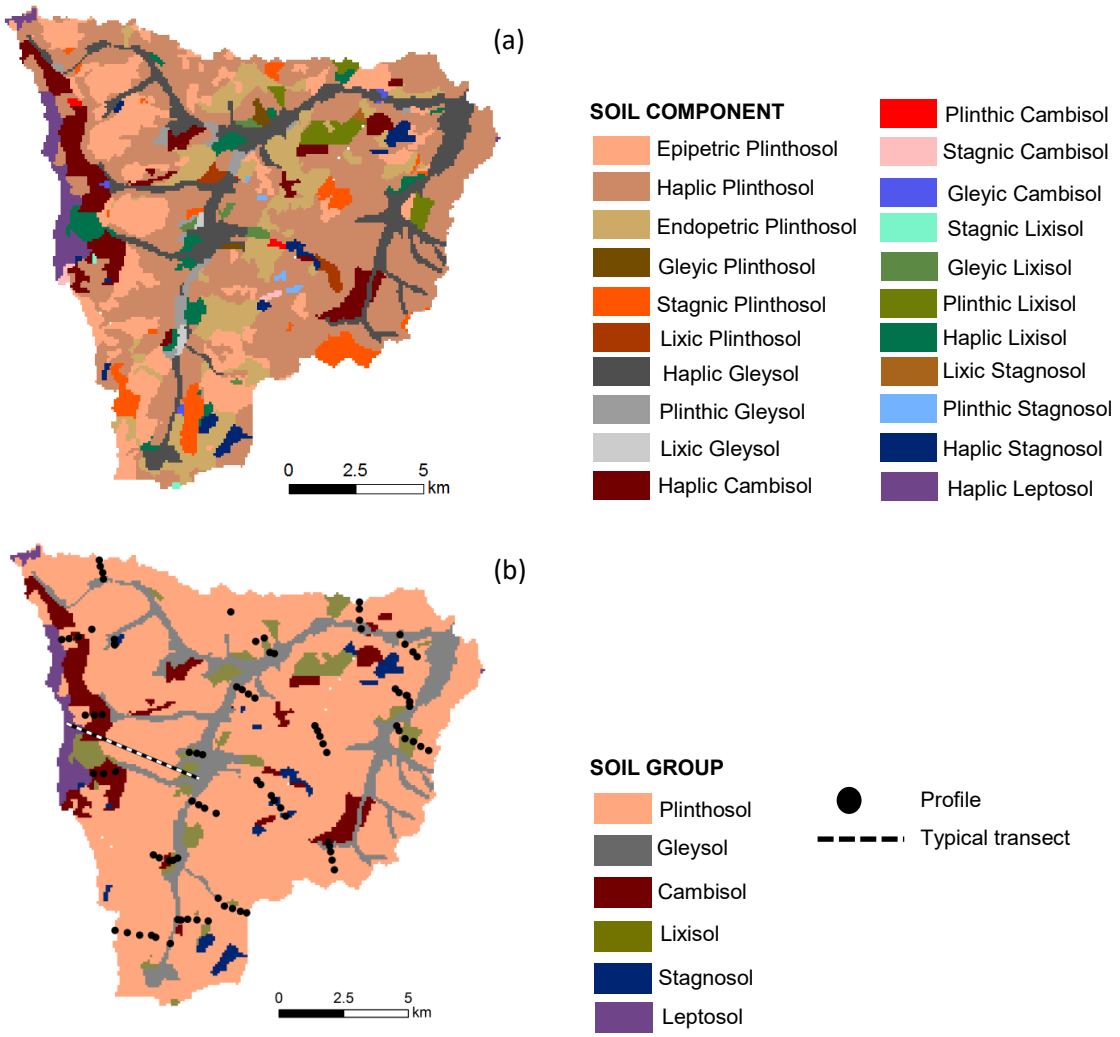

Fig. 5-1 Soil map of the Dano catchment. Part (a) shows soil components. Soil components are merged per soil groups in part (b). Part (b) further indicates the location of soil profiles used in the study as well as a transect line used to describe a typical soil catena within the catchment.

5.2.2. Saturated hydraulic conductivity (*Ks*)

Undisturbed soil samples were taken using stainless steel sample rings and the drop hammer method on leveled soil horizons of the soil profiles mentioned above. Three samples (repetitions) were collected per soil horizon. The core cylinders were 250cm^3 volume, i.e. 4 cm and 5cm in radius and height, respectively. After leveling the core ends, samples were gradually saturated from top to bottom for a period of 24 hours. To minimize air encapsulation during saturation, the water level inside the saturation tank was progressive increased up to near the upper edge of the cylinders. A constant-head laboratory permeameter method was then used to measure K_s. After establishing a constant flow rate, percolated water volume per time unit was recorded and *Ks* was calculated following Darcy's equation for saturated conditions (Eq. 5-1):

$$Ks = \frac{Q\ L}{h\ A} \qquad \text{Eq. 5-1}$$

Where K_s refers to the saturated hydraulic conductivity (cm/d); *Q* the volume of water flowing through the sample per unit of time (cm^3/d); *L* length of the soil sample (cm); h water level difference inside and outside the ring holder (cm) and *A* the cross section surface of the sample (cm^2).

Additionally to laboratory measurement, the saturated hydraulic conductivity was estimated based on soil texture, bulk density and organic carbon content using five PTFs: Saxton & Rawls (2006), Saxton et al. (1986), Schaap et al. (2001), Vereecken et al. (1990) and Cosby et al. (1984) (Table 5-1).

Table 5-1 Required input for *Ks* determination by the selected PTFs.

PTF	Input variables
Cosby et al. (1984)	Clay (< 2 µm), sand (50-2000 µm)
Saxton & Rawls (2006)	Clay (< 2 µm), sand (50-2000 µm), organic matter, gravel content
Saxton et al. (1986)	Clay (< 2 µm), sand (50-2000 µm)
Schaap et al. (2001)	Clay (< 2 µm), Silt (2-50 µm), sand (50-2000 µm), bulk density
Vereecken et al. (1990)	Clay (< 2 µm), sand (50-2000 µm), bulk density, organic matter

5.2.3. Saturated water content (θ_s)

After 24 hours of saturation, the saturation water content was determined following a classic laboratory determination of the water (moisture) content of a soil specimen by oven-drying (ISO 17892, 2014). The saturated sample was weighted and afterwards placed in a drying oven maintained at 105 °C and dried to a constant mass (for 24 hours). The mass of the oven-dried sample was then determined. The saturated water content of the soil was calculated according to Eq. 5-2:

$$\theta_s = \frac{(m_w - m_d)\,\rho}{V} * 100 \qquad \text{Eq. 5-2}$$

Where θ_s (Vol.%) refers to the saturated water content ; m_w (g) is the weight of the saturated sample; m_d (g) is the weight of dried sample; ρ (g/cm^3) represents the density of water and *V* (cm^3) the volume of the cylinder.

5.2.4. Bulk density (*BD*)

The core method was used for dry bulk density determination (ISO 11272, 1998). This involves drying and weighing a soil sample of known volume. Following the same procedure adopted in the previous section (saturated water content), the weight of the dried sample m_d (g) is obtained and knowing the sample's volume *V* (cm^3), the bulk density (g/cm^3) was calculated as:

$$BD = \frac{m_d}{V} \qquad \text{Eq. 5-3}$$

5.2.5. van Genuchten parameters

The van Genuchten parameters, the inverse of the air entry suction (*α)* and the pore size distribution (*n)* as well as the residual water content were derived from soil texture, bulk density and coarse particles content following van Genuchten (1980).

5.3. Results

21 soil components were identified in the study area as mentioned in section 5.2.1. However, for reasons of clarity and concision, the results are presented per soil reference group (first level of classification of the WRB, 2006) (Fig. 5-1b); nevertheless, details of the soil hydraulic properties for each soil component are provided in Appendix 1, Appendix 2 and Appendix 3. Fig. 5-2 shows the typical distribution of the major soil groups following a catena in the catchment and soil properties are shown in Fig. 5-3.

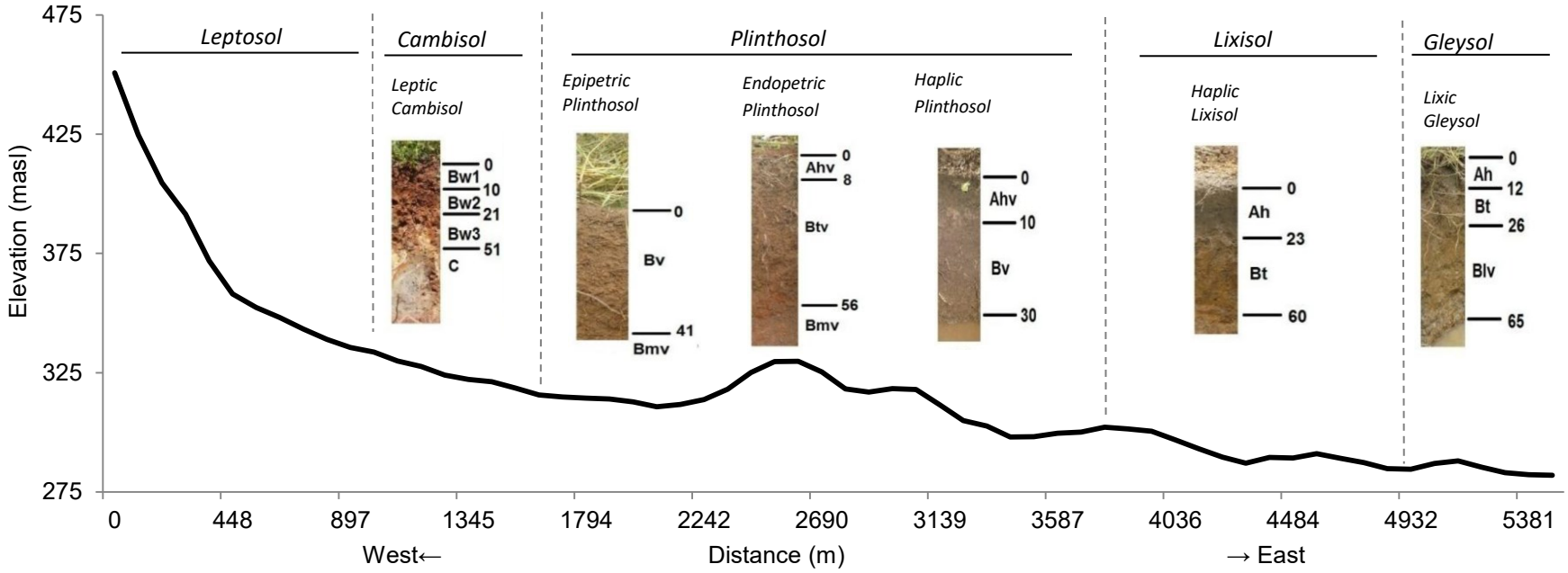

Fig. 5-2 Typical distribution of main soil groups following a catena in the Dano catchment. Profile description after Op de Hipt (2013).

Table 5-2 PTF based saturated hydraulic conductivity per soil group and horizon.

	Saturated hydraulic conductivity (cm/d)																			
	Saxton & Rawls (2006)				**Saxton et al. (1986)**				**Schaap et al. (2001)**				**Vereecken et al.(1990)**				**Cosby et al. (1984)**			
Soil group	A	B1	B2	B3	A	B1	B2	B3	A	B1	B2	B3	A	B1	B2	B3	A	B1	B2	B3
Plinthosols	11.3	2.97	1.7	0.75	19.8	8.5	6.11	6	14.3	12.7	14.2	24.1	10.5	8.9	8.5	5.4	29.9	17.7	14.2	14
Gleysols	16.3	5.2	2.9	-	25.3	11.1	5.9	-	17.8	12.1	13.2	-	32.1	20.9	81	-	23.3	16.1	13.5	-
Cambisols	8.13	5.7	7.1	9.3	10.3	9.33	12.4	30.8	12	11.3	12.9	12.5	90.6	111	48.4	1513	20.4	19.7	17.9	14.5
Lixisols	10.8	5.13	5.1	-	21.1	10.7	8.8	-	12.3	12.3	12.5	-	59.4	108	148	-	28.2	13.6	13.8	-
Leptosols	12.6	-	-	-	20.9	-	-	-	14.3	-	-	-	26	-	-	-	20.4	-	-	-
Stagnosols	13.6	4.06	4	-	17.5	6.8	6	-	13	12.5	10.2	-	37.1	12.5	2.16	-	31.5	16.6	19.7	-

5.3.1. Plinthosols

The catchment is dominated by *plinthosols* (about 73%), which are soils characterized by a *plinthite, petroplinthite* or *pisoliths* layer in the upper first meter of the soil profile. Except at the lower valley position, *plinthosols* occur all over the catchment. Both e*pipetric* and *endopetric* (having a *petroplinthic* layer in the 0-50 cm depth or the 50-100cm depth respectively) *plinthosols* are abundant in the catchment, which makes soil depth highly dependent on the depth of *petroplinthite* formation. *Petroplinthite* is often found at the soil surface, as a result of soil erosion.

Fig. 5-3 (*Plinthosol*) shows mean values of soil properties for a hypothetical *plinthosol* profile (computed using all investigated *plinthosols*). Consistent analysis on *petroplinthic* horizon could not be performed due to the difficulty in digging the profile and proper sample collection. Therefore, horizons 3 and 4, as presented in Fig. 5-3 (*Plinthosols*), could not be investigated for *epipetric plinthosols.* Similarly, horizons 4 could not be investigated for *endopetric plinthosols*. *Petroplinthites* found at the soil surface could not be analyzed either.

Soil texture of the A-horizon for *plinthosols* is in general loamy, with abundant coarse particle as are the deeper horizons. The texture turns to clay-loam for the B_1-horizon and clay for B_2 and B_3-horizons as a result of decreasing sand and increasing silt and clay contents with depth. The increase in clay content with depth is also reflected in measured *Ks*, as *Ks* decreases with depth. The organic carbon content decreases with depth conversely to the bulk density (BD). Changes in saturated and residual water contents do not show a clear trend when moving from A-horizon to deeper horizons (B_1, B_2, etc.).

5.3.2. Gleysols

Gleysols are the second most important soil group in the catchment (12%), and typically occur along rivers (toe slope). They denote soils characterized by a *gleyic* color pattern in 25% or more of the soil volume (WRB, 2006). Average soil properties of *gleysols* are shown in Fig. 5-3 (*Gleysols*). Due to the long period of saturated conditions, undisturbed soil samples could be collected only for the upper 70 cm.

The soil texture is silty loam for the A-horizon and silty-clay-loam for the B-horizons. The saturated hydraulic conductivity and saturated water content decrease with soil depth. Similar to *plinthosols*, *BD* increases with soil depth. However, measured *Ks* values for *gleysols* are lower for the same horizon compared to *plinthosols*.

5.3.3. Cambisols

Cambisols cover about 6% of the catchment. They occur at the upper slope position (shoulder) along the hills located at the southern part of the catchment. According to the WRB (2006), *Cambisols* are characterized by “moderate weathering of parent material and by absence of appreciable quantities of illuviated clay, organic matter, Al and/or Fe compounds”. *Cambisols* are moderately developed soils; therefore the horizon differentiation is weak. Although up to four horizons have been described in some profiles, the distinction between horizons was difficult to establish. The weak differentiation in soil horizons is reflected by the texture and *SOC* which do not show any clear organization with depth. Measured *Ks* and saturated/residual water contents however show a decrease with soil depth, contrary to the *BD*. The texture is clay-loam for the first two upper layers and silty-loam for horizon 3 and 4. Measured *Ks* values are comparable for *cambisols* and *plinthosols*.

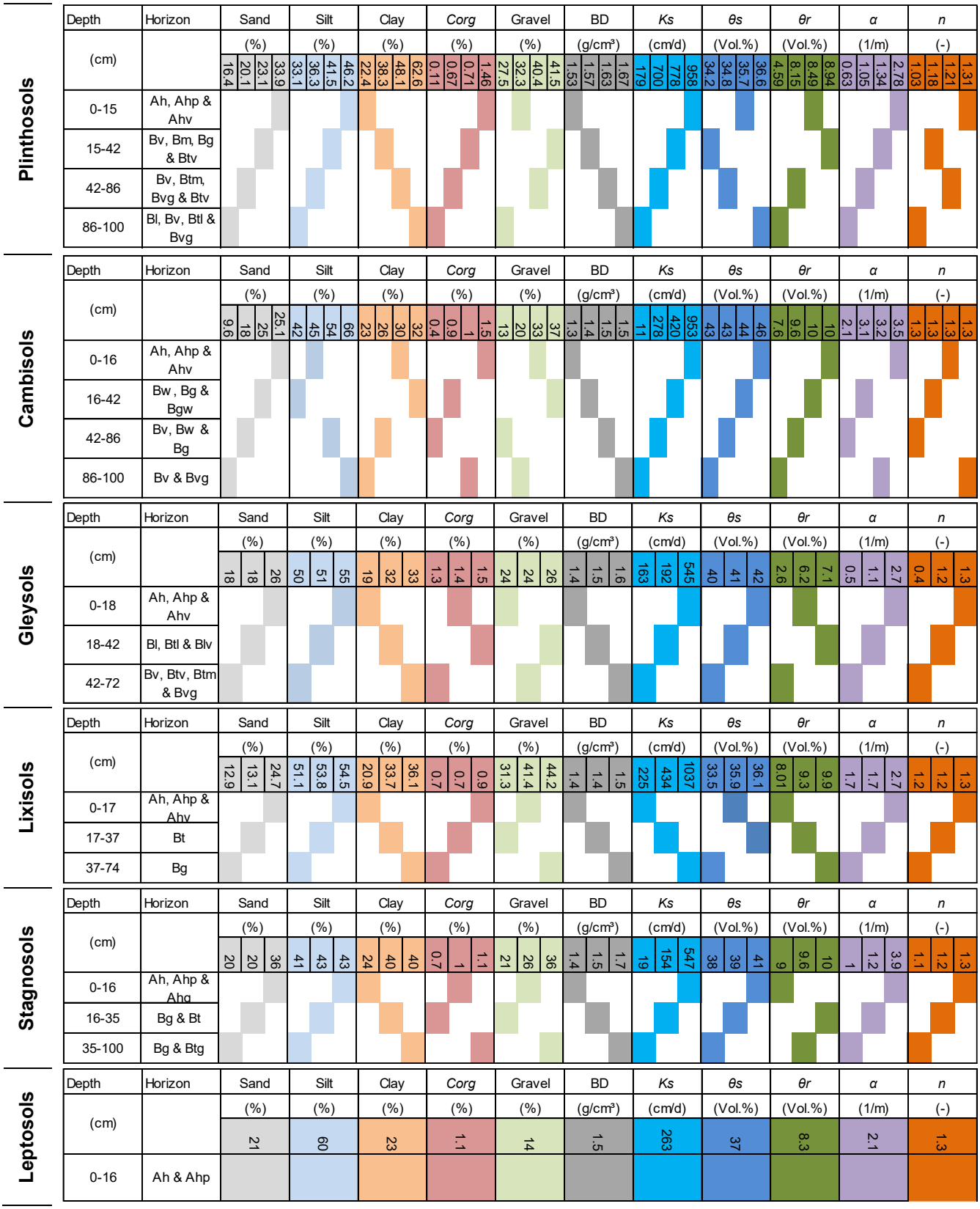

Fig. 5-3 Mean soil groups properties. *Ks* values are measured.

5.3.4. Lixisols

Lixisols are soils having a higher clay content in the subsoil compared to the topsoil as a result of pedogenetic processes leading to an *argic* subsoil horizon (WRB, 2006). They occupy about 4.5% of the catchment and mainly occur at the lower slope. The texture is silty-loam for the A-horizon, but turns to silty-clay-loam with the accumulation of clay in the B-horizons (B_t and B_g). Saturated hydraulic conductivity, organic carbon and residual water contents decrease with soil depth, whereas bulk density shows an opposite trend.

5.3.5. Leptosols

Leptosols are soils characterized by a very shallow depth over continuous rock or extremely graveled and/or stony soils. They are found at the crest and upper slope positions of the Ioba hill (southern part of the catchment) and cover about 2% of the catchment area. Investigations showed that soil depth is in general lower than 30 cm. The texture is silty loam.

5.3.6. Stagnosols

About 2% of the catchment is covered by *stagnosols*. The spatial distribution of *stagnosols* is determined by the occurrence of a perched water table creating stagnating water. Field investigations did not show any clear pattern in their spatial distribution. The texture is loam and silty-clay for A-horizon and B-horizons respectively. Contrary to bulk density, saturated hydraulic conductivity and saturated water content decrease with soil depth. They are characterized by low *Ks* values in the third horizon (Bg & Btg).

5.4. Discussion

5.4.1. Texture

Various soil textural classes are observed in the catchment. These textures vary between soil groups and from one horizon to another. However, in general, a trend towards increasing clay and decreasing sand contents with soil depth can be noticed for all soil groups (except leptosols, as this soil group presents a single horizon). Studies have explained the variation of *Ks* by soil texture (e.g. Cosby et al., 1984). *Ks* is known to be negatively correlated with the clay fraction and positively correlated with sand fraction (Cosby et al., 1984; Zhao et al., 2016). This feature of the soil texture suggests a decrease of saturated hydraulic conductivity with soil depth.

5.4.2. Soil organic carbon

The primary soil hydraulic properties affected by *SOC* are porosity, soil water retention and hydraulic conductivity (Kusumandari & Nugroho, 2015; Rawls et al., 2004), but reports about the relation between soil water retention and *SOC* are often contradictory (Rawls et al., 2003). In some regions the *SOC* is observed to be strongly related to the clay+silt fraction (Zinn et al., 2005); this relationship is particularly strong for non-agricultural soils (Jobbágy & Jackson, 2000). Organic carbon content in the soils of the Dano catchment is very low (<1.5%, mineral soils according to Huang et al., 2009). *SOC* further decreases with depth in the catchment (contrary to the clay+silt fraction) and the soils are cultivated or are under fallow of differing durations. Therefore, how the measured *SOC* affects soil hydraulic properties depends on both proportions of textural components and amount of *SOC* (Rawls et al., 2003).

5.4.3. Coarse particles

Soil content in gravel and other constituents > 2 mm was found to be very high in the catchment, reaching up to 80% (mass) in many samples. The coarse particle content is known to affect the available porosity and the saturated hydraulic conductivity (Rawls & Brakensiek, 1989). Chow et al. (2007) showed that soil

moisture (from saturation to –103.3 kPa matrix potential) decreases with increasing percentage of coarse fragments. Therefore, the Brakensiek & Rawls (1994) method allowing an adjustment for the amount of coarse particles content was applied in the computation of the van Genuchten parameters. The high coarse particles content also resulted in a variable level of soil disturbance during core extraction, which strongly affected measured saturated hydraulic conductivity.

5.4.4. Bulk density

Irrespective of the soil group, bulk density shows a clear trend towards an increase with depth. As the sand fraction decreases with depth, the reduction of *SOC* and change in soil structure with depth can explain the stratification observed for the *BD*.

5.4.5. Saturated hydraulic conductivity

Measured saturated hydraulic conductivity varies with soil depth and from one soil group to another. Irrespective of the soil group, measured *Ks* is higher than 500 cm/d for the A-horizon, placing the top horizon in the high *Ks* class (SCS, 1993). Measured *Ks* for the B-horizons range from low to moderately high classes, depending on the soil group. For all soil groups, *Ks* for the A-horizon is higher than *Ks* for B-horizons. High *Ks* values for both A and B-horizons suggest the predominance of vertical flow. However, the reduction of *Ks* with depth for all soil type indicates soil stratification favorable to lateral flow (interflow) generation between horizons.

The abundance of (*epipetric* and *endopetric*) *plinthosols* suggests the hydraulic properties of *petroplinthic* horizons to be a major factor controlling soil water fluxes. Although consistent analysis could not be performed on *petroplinthite*, field observation and profile description suggest variable *Ks* for *petroplinthic* horizons depending on the level of cementation and the presence of macropores:

- soil surface *petroplinthite* generally show strong cementation with few to no visible macropores. They constitute areas leading to important overland flow;
- subsurface *petroplinthite* with few or no macropores. They characterize the areas leading to perched subsurface flow and are also favorable to the formation of *stagnosols*;
- subsurface *petroplinthite* with abundant macropores and fragmentations. They suggest high *Ks* and important vertical water movement.

Compared to measured *Ks* values available in West Africa for the same soil groups (Agyare, 2004; Azuka et al., 2015; Giertz & Diekkrüger, 2003), the obtained values are extremely high. PTFs derived *Ks* (Table 5-2) also suggest that measured *Ks* is considerably high. Indeed, the maximum PTF derived *Ks* is 111 cm/d whereas up to 1050 cm/d is observed for measured *Ks*. PTFs derived *Ks* place the saturated hydraulic conductivity for all soil groups in the moderately high and moderately low classes for A-horizon and B-horizons respectively. Difference between measured and PTFs derived *Ks* stems notably by the fact that the applied PTFs are mainly texture driven (see Table 5-1) and do not consider biopores. Consequently, PTFs derived *Ks* are low, as biopores that have a considerable effect on the saturated hydraulic conductivity are ignored. However, conversely to measurement, the PTFs derived values are in accordance with those reported by the studies mentioned above (Agyare, 2004; Azuka et al., 2015; Giertz & Diekkrüger, 2003).

Nevertheless, PTF derived *Ks* show stratification consistent with measured *Ks* that is a decrease with depth. This suggests that both *Ks* determination methods (measured or derived) similarly represent the interflow generation process. However, vertical water flow is likely to be strongly influenced by the *Ks* determination method, as with PTFs derived *Ks* the likelihood of infiltration excess overland flow increases considerably, whereas with measured *Ks* surface runoff is likely not to occur with regards to the observed

rainfall intensities in the catchment. Field observations support the abundance of surface runoff in the catchment.

This difference between derived and measured *Ks* values can be attributed to several factors, including the high coarse particle content and the measurement method. Reported to affect the porosity and the saturated hydraulic conductivity, the high coarse particle content has led to a high “sidewall leakage” effect (Kanitpong et al., 2001; Mohanty et al., 1994). This sidewall effect, inherent to the laboratory permeameter method, was further aggravated by the small volume of the core sample that can easily be perturbed by coarse fragments. Efforts and care put in core sample collection, handling and analysis seem to have not sufficed to avoid these effects.

5.4.6. Soil water retention

The saturated water contents range from 35 to 46 Vol.% (average values for sandy and silt soil), while residual water content ranges between 5 and 10 vol.% which are the average values for silt and clay soil respectively. These values are all in accordance with the observed soil texture. Pore-size distribution parameter (*n*) and inverse of the air entry suction (α) are all consistent with the average values for the observed soil texture as well.

5.5. Conclusion

Combining field investigation and laboratory measurements to the soil map and basic soil information (texture and *SOC*) provided by the *Soil Science and Soil Ecology* working group of the University of Bonn permitted to gather sufficient information for soil parameterization in the hydrological model (WaSiM). The results showed that *plinthosols* are the dominant soil group in the catchment, covering more than 70% of the total area and occurring all over the catchment except at the toe slope which is occupied by *gleysols*. *Leptosols* occur exclusively at the crest and upper slope position of the Ioba hill. *Cambisols* and *lixisols* are found at the middle slope and lower slope position respectively. No clear spatial pattern is observed for stagnosols, which are governed by the presence of a perched water table.

Due to the abundance of both *epipetric* and *endopetric plinthosols*, the hydraulic properties of *petroplinthic* horizons appear to be a major factor controlling soil water movement. As core samples could not be collected for the *petroplinthite*, the analysis was mainly based on field observations which highlighted plausible wide range for *Ks* since crust as well as weakly cemented with abundant macropores were observed for different *petroplinthite*. Therefore, *petroplinthite* are potentially areas for infiltration excess overland flow, interflow and groundwater recharge.

Soil texture of the first horizon (A-horizon) is in general silt-clay or clay-loam for all soil groups with a trend towards clay and silt enrichment with depth. This results in a decrease of saturated hydraulic conductivity with depth, irrespective of the *Ks* determination method. While PTF based *Ks* values are similar to those commonly reported for the region, the measured ones show a strong positive deviation. These high *Ks* were attributed to the high coarse particles content and the small volume of core samples which aggravated the sidewall leakage during *Ks* measurement. Field observations of abundant surface runoff during rain events seem to support an overestimation of *Ks* by laboratory measurements. Finally, soil physical properties were found to be highly variable for the same soil group.

6. LAND USE INFLUENCE ON SOIL INFILTRATION RATE

6.1. Introduction

Hydraulic conductivity (*Ks*) is a key hydraulic property determining water flow in the soil. It is an essential input for hydrological process analysis and simulation, as well as for crop models. *Ks* is potentially influenced by several factors like topography, soil type and parent material, vegetation, land use and seasonal change (Bormann et al., 2005; Bormann and Klaassen, 2008; Giertz and Diekkrüger, 2003; Pirastru et al., 2013; Rienzner and Gandolfi, 2014; Wang et al., 2013). The combination of these factors makes *Ks* a highly variable soil physical property and measured values may considerably vary for a particular soil (SCS, 1993). A clear understanding of *Ks* variability and the contribution of influencing factors thus remain challenging. This understanding, however, is a prerequisite to comprehend any hydrological system behavior, improve infiltration process representation in different applications, and to develop management strategies within hydrological systems.

Many studies have increased the understanding of *Ks* variation due to: (i) soil texture (Rawls & Brakensiek, 1989; Tietje & Hennings, 1996; Vereecken et al., 1990; Wang et al., 2013; Schulze-Makuch et al., 1999), (ii) land use and land cover change (Shabtai et al., 2014; Giertz & Diekkrüger, 2003; Bormann et al., 2005), (iii) soil type (Zeng et al., 2013; Novák et al., 2011), (iv) agricultural practices (Green et al., 2003; Moret & Arrúe, 2007) etc. Whereas the function of many *Ks* influencing factors is known to some degree, insights gained from agricultural practices (tillage, crop pattern, fallow duration) induced *Ks* variation have proved to be context specific. This is consistent with a literature review by Strudley et al., (2008) concerning the effects of agricultural practices on soil hydraulic proprieties which reached the conclusion that the results of the reviewed studies are so contradictory that hardly a general rule can be drawn when comparing the effects of agricultural practices on soil hydraulic properties. Due to its high natural spatial and temporal variability, *Ks* may be a poor indicator of soil hydraulic response to management practices, because this natural variability may overshadow management practices effects (Strudley et al., 2008; Green et al., 2003). Strudley et al. (2008) suggested that research to determine the impact of agricultural management options on the hydraulic conductivity, should consequently be designed in a manner to consider the effect of dominant factors affecting soil hydraulic properties such us soil type, soil local heterogeneity, topography, etc.

To be able to consider effects of land use conversion on runoff generating processes, Hölzel & Diekkrüger (2010) compared field measurements of *Ks* on cut pasture and a neighboring pasture. They found that saturated hydraulic conductivity was on average five times smaller under cut pasture compared to neighboring pasture. To exclusively quantify the differences in the soil hydraulic conductivity caused by forest conversion to spontaneous grass, Pirastru et al. (2013) followed an approach based on the comparison of adjacent forest-grass fields. This way, they excluded (minimized) the potentially confounding factors in order to interpret differences in soil hydraulic conductivity as a function of land use alone. To rule out other influencing factors and assess the influence of land use change on soil hydraulic proprieties, Zimmermann et al. (2006) compared native forest, pasture and trees plantation located on homogenous soil units. Although findings achieved by these authors and many others (Scheffler et al., 2011; Schwartz et al., 2003) differ, they underline the importance of considering homogenous soil units to overcome the influence of dominant factors (e.g. soil type, topography) affecting *Ks* while assessing the impact of land use and land cover change.

Various procedures -*in situ* and laboratory- are used to determine the hydraulic conductivity, each involving a wide range of instruments and solutions. Many studies (Fodor et al., 2011; Reynolds et al., 2000; Wang et al., 1998; Mohanty et al., 1994) highlighted the dependency of *Ks* value on the determination method. The laboratory methods are conducted in a more controlled environment and are generally considered very reliable though sample taking and transportation might introduce an error factor.

Field method also applies approximation, assumption or simplification causing some bias in the *Ks* value (Fodor et al., 2011). *In situ* measurement of *Ks* in the unsaturated zone for instance leads to air bubbles entrapped in the soil due to the advancing wetting front and results in a field hydraulic conductivity that may be underestimated. As air entrapment is observed in most natural infiltration processes, field measurements methods are generally considered to be more representative of soil-water conditions (Rienzner & Gandolfi, 2014; Ramos et al., 2006; SCS, 1993).

All studies mentioned above consistently show that land use change potentially alters the soil hydraulic conductivity. They underline the changes in soil hydraulic conductivity related to land use change to depend on the local context (crop types, management practices etc.). Ultimately, they highlight the influence of land use on soil water movement. Very few field investigations concerning hydrological processes were made in the tropical African sub-humid zones. A very limited number has performed comparative investigations between land use types. Croplands have progressively replaced natural vegetation and fallow areas in the Dano catchment during the past decades. The influence of such a land use dynamic on soil hydraulic conductivity has not yet been investigated. It is hypothesized that cropping and fallowing/natural vegetation differently influence soil hydraulic conductivity, and that a decrease of natural vegetation and fallow for the benefit of cropland might modify soil water dynamic and consequently change the hydrological behavior of the catchment. The objectives of this chapter are: (i) to determine -at plot level- the infiltration rate under fallow/natural vegetation and cropland, and (iii) to gain insights regarding surface runoff generation processes as affected by land use change in the catchment.

6.2. Materials and Methods

6.2.1. Sampling design

The investigations were carried out in the Dano catchment. Infiltration tests were performed on adjacent plots, one in a cropland and the other in a fallow area following transect lines. In collaboration with the *Soil Science and Soil Ecology* working group of the university of Bonn, transect lines were defined ensuring an even coverage of the study area. Infiltration plots were then located on these transect lines (Fig. 6-1). To account for local soil heterogeneity, crop-fallow adjacent plots were chosen as close as possible and three infiltration tests were carried out per plot. The procedure of adjacent plot selection was repeated forty-two times throughout the catchment, yielding to a set of 42 plots in croplands and related 42 in fallow areas. The infiltration test thus compares a paired sample of the two land use types. The test was carried out in the period of August to October 2012, corresponding to the crop development and mid-season stages, i.e. 6 to 8 weeks after ploughing during the rainy season.

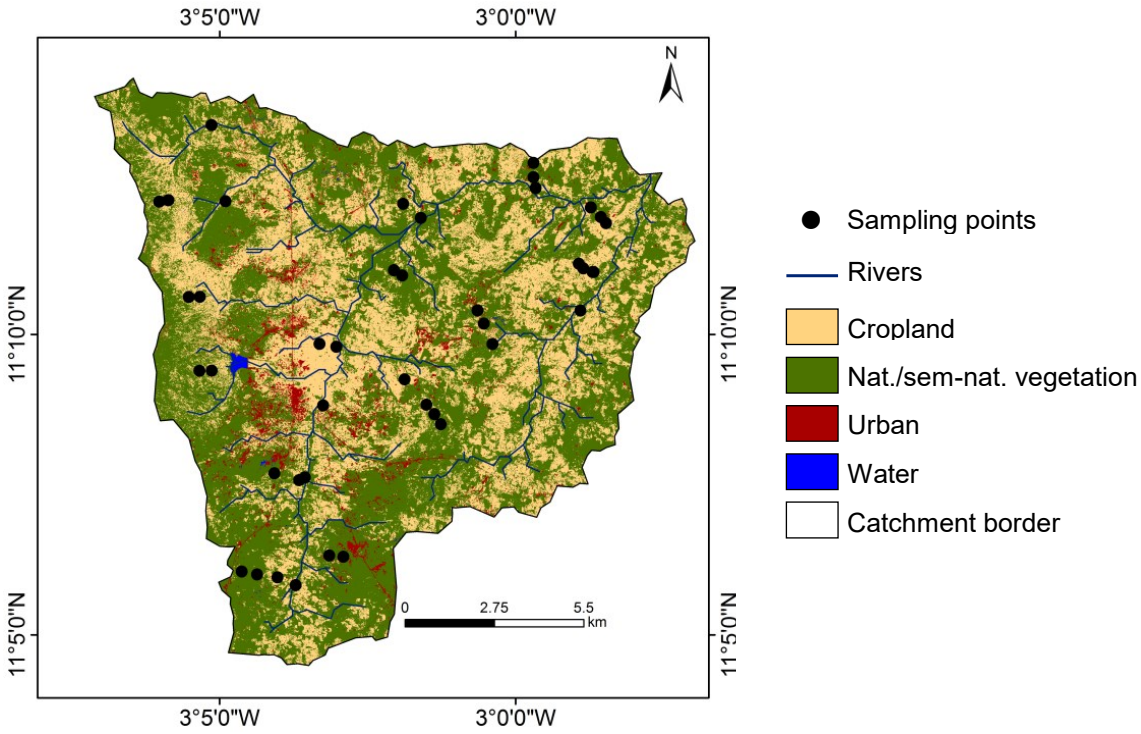

Fig. 6-1 Location of sampling points within the catchment. Each sampling point refers to two adjacent crop and fallow (or savannah) plots. Land use map after Forkour (2014).

6.2.2. Measuring methods

A Hood infiltrometer (Schwärzel & Punzel, 2007; Vogeler et al., 2009; Scheffler et al., 2011) was used for the purposes of this study (Fig. 6-2). The Hood infiltrometer is a tension infiltrometer for measuring both soil surface near saturated (*Ks*) and unsaturated hydraulic conductivity (*Kh*). Among the advantages of the method are: the *in situ* measurement of soil hydraulic conductivity, the minimizing of soil disturbance, and the possibility to observe the air entry points during the measurement. The air entry point depicts the existence and distribution of macropores at the measurement point. Infiltration with the Hood infiltrometer starts from a closed hood about three-quarters filled with water and standing on the ground. The control of the hydraulic pressure head in the water volume under the hood is made by adjusting the intake pipe immersion depth in the bubble tower. The difference of height at the U-tube manometer and the water level in the standpipe indicates the applied hydraulic head under the hood. During a measurement, the hydraulic head is progressively increased starting from value zero up to the air entry point.

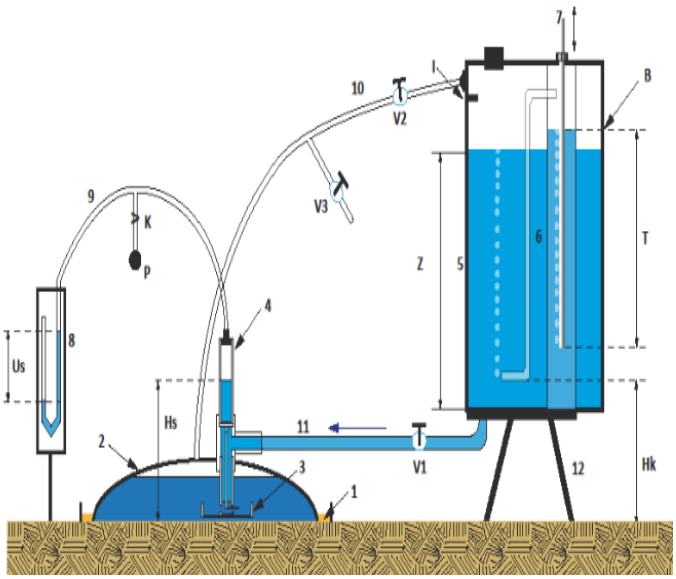

1 Fine sand sealing
2 Plastic hood
3 Buffer vessel
4 Standpipe
5 Infiltration reservoir
6 Bubble Tower
7 Air intake pipe
8 U-tube manometer
9 Hose connection 1
10 Vent pipe
11 Hose connection 2
12 Stand

B Filling level of the bubble tower
Hk Distance between soil surface and air outlet
Hs Water level in the standpipe
I Maximum filling level of the infiltration reservoir
K Valve for cutting off the pipette ball
P Pipette ball
T Immersion depth of the air intake pipe
Us height difference at the U-tube manometer
V1 Valve for separating the water volumes
V2 Valve for separating the air volumes
V3 Valve for pressure adjustment
Z Filling height of the infiltration reservoir

Fig. 6-2 Schematic setup of the Hood Infiltrometer (UGT, 2012).

Several procedures are available for calculating the hydraulic conductivity from the measured raw data (Fodor et al., 2011). However, it is recommended to calculate the hydraulic conductivity from the steady-state infiltration according to Wooding (1968) respectively to the Instructions Manual coming along with the Hood infiltrometer (UGT, 2012). The theoretical principle underling the Hood Infiltrometer is as follows.

Hydraulic conductivity *Ks* is a function of water tension *h* in the soils (Gardner, 1958):

$$K(h) = Ks\ \exp(\alpha^* h) \qquad \text{Eq. 6-1}$$

Where *Ks* (L T^{-1}) is the saturated hydraulic conductivity, *h* (L^{-1}) is hydraulic pressure head and *α* is an empirical fitting parameter.

Under steady-state, and based on Eq. 6-1, Wooding (1968) found the following approximate solution for the infiltration rate from a shallow circular pond of radius r:

$$Q(h_o) = \pi r^2 Ks\ \exp(\alpha h_o)\left(1 + \frac{4}{\pi r \alpha}\right) \qquad \text{Eq. 6-2}$$

Where $Q(h_o)$ is the steady flow rate (L^3T^{-1}) under a given supply potential h_o (L).

Ks and α are the only unknowns from Eq. 6-2. They can be either solved by making measurements at a fixed water tension with multiple disc radii, or inversely making measurements with a fixed disk radius at multiple water tensions. The latter was applied in this study.

The application of Eq. 6-2, for neighboring values of water tensions (h_1, h_2) gives:

$$\frac{Q_1}{\pi r^2} = Ks \exp(\alpha h_1)(1 + \frac{4}{\pi r \alpha})$$

$$\frac{Q_2}{\pi r^2} = Ks \exp(\alpha h_2)(1 + \frac{4}{\pi r \alpha})$$

And by the way of division, α can be derived:

$$\alpha = \frac{\ln(\frac{Q_1}{Q_2})}{h_1 - h_2} \quad \text{Eq. 6-3}$$

Finally, the hydraulic conductivity for $h_1$is given by Eq. 6-4:

$$K(h_1) = \frac{\frac{Q_1}{\pi r^2}}{1 + (\frac{4}{\pi \alpha r})} \quad \text{Eq. 6-4}$$

6.2.3. Soil physical and chemical properties

Alongside with the infiltration measurement, undisturbed topsoil (1-10 cm) core samples and composite topsoil samples were collected for laboratory analyses. The samples were collected on 50 % of the infiltration test plots, i.e. 21 composite samples and 21 undisturbed soil cores for each land use type. The bulk density was determined by dividing the oven-dry mass of the core soil by its volume, and the coarse particles content was determined by passing the sample through a 2mm diameter sieve. The texture analysis was carried out by a combination of wet sieving (sand fractions) and sedimentation (silt and clay fraction) (ISO 11277, 2002) and *Corg* content was determined by elemental analysis (ISO 10694, 1995; ISO 13878, 1998).

6.2.4. Statistical analysis of the collected data

Soil hydraulic conductivity is generally reported to be a *Log* normally distributed property (Helsel et al., 1993; SCS, 1993), thus needs to be transformed in order to be normal distributed. The Shapiro–Wilk test for normality was performed to determine whether or not the infiltration data where normally distributed, for the purpose of a transformation in order to conduct variance analysis. A paired two tailed student's *t-test* was performed on the normal distributed data set to test the statistical difference of *Ks* and other variables between cropland and fallow.

6.2.5. Rainfall records

Twelve tipping bucket rain gauges (M. 52203, Young company) connected to Campbell loggers recorded 10-min rainfall intensity values at the starting of the infiltration test period. From the 10-min intensities records (I 10), hourly intensity (I 60) were computed. Both I 10 and I 60 were compared to the infiltration rate under cropland and fallow using sample means and cumulative probability functions. For clarity reason, infiltration rate and rainfall intensities are presented in cm per day (cm/d). Others descriptive statistic tests performed on the data set include the mean, median, minimum, maximum, standard deviation and coefficient of variation and the quartile range.

6.3. Results and discussion

6.3.1. Infiltration rate under different land use

The Shapiro-Wilk test indicated a non-normal distribution of saturated hydraulic conductivity values. The same result is reported by several authors (e.g. Schwen et al., 2011; Alletto & Coquet, 2009; Diekkrüger, 2003). Therefore, the non-normally distributed data were then *Log* –base 10- transformed, and the resultant *Log Ks* shows a normal distribution (Table 6-1and Fig.6-3).

The infiltration rate ranged from 17.27 to 2048 cm/d under cropland, and between 69.29 and 2445.9 cm/d under fallow. The mean, median and standard deviation are all higher under fallow than under cropland. The coefficient of variation (*CV*) of *Ks* were relatively high under both fallow (94.15%) and cropland (116 %) confirming the non-normal distribution. $Log_{10}Ks$ however shows a relatively low *CV*, 13.65 and 24.17 for fallow and cropland respectively, indicating uniformity in the distribution of $Log_{10}Ks$. The mean value of *Ks* for both cropland and fallow indicates a high infiltration rate under saturated condition (this class after SCS (1993) ranges from 86.4 to 864 cm/d). However, both land use types presented single *Ks* values ranging from very low to very high class.

Table 6-1 Descriptive statistics for Ks and $Log_{10}Ks$ for cropland and fallow (n=42)

Variable	Land use	Mean (cm/d)	Median (cm/d)	SD	CV %	Min (cm/d)	Max (cm/d)	SWilk p-value
Ks	Cropland	433.660	214.52	506.1133	116.70	17.27	2048	< 0.001
	Fallow	568.774	375.61	535.5539	94.15	69.29	2445.9	< 0.001
$Log_{10}Ks$	Cropland	2.327	2.331468	0.562	24.177	1.237	3.31133	0.307
	Fallow	2.607	2.574711	0.356	13.654	1.840	3.3884	0.399

SD: standard deviation; *CV*: coefficient of variation; *SWilk p-value*: Shapiro & Wilk skewness significance test p-value; *n*: sample size.

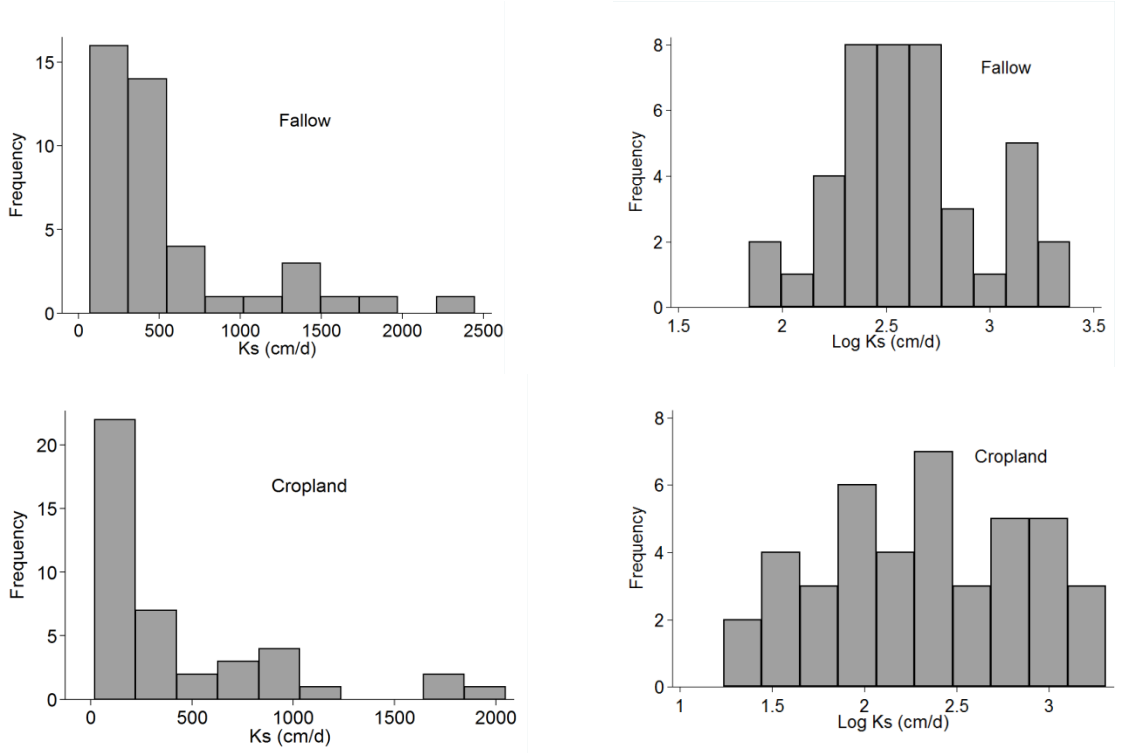

Fig.6-3 Histograms of saturated hydraulic conductivity *Ks* and the resultant Log_{10} transformed Log *Ks* under cropland and fallow (n=42).

Beyond the effect of factors like topography and soil type that affect *Ks* under both land use types, other specific factors may underline the high dispersion of *Ks* under fallow:

(i) the difference in the age of the fallow areas under investigation (between1 and 5 years). Miranda et al. (2009) highlighted the increase in both total porosity and macro-porosity with the extension of the fallowing period, leading to an increase in hydraulic conductivity; and

(ii) the fallowing practice. Bush-fallow or natural regrowth, as commonly done in the catchment, leads to the development of a diversity of plants species on the fallow areas.

Different fallowing periods associated to herbaceous plants of different species may have led to the wide variation of Ks within the fallow sample.

The variation of *Ks* under cropland can specifically be attributed to:

(i) the difference of crop species. The investigated croplands were mainly composed of sorghum, cotton, maize, cowpea and groundnut, each with a specific cropping calendar. The difference in the cropping calendar implies different crop development stages. Alletto & Coquet (2009) highlighted the root development stage as a *Ks* temporal variation factor under cropland.

(ii) the ploughing of the croplands. All investigated fields were tilled. Tillage is known to have a transient effect on *Ks*. The saturated hydraulic conductivity generally increases immediately after tillage due to an increase in water-conducting meso and macropores, but decreases afterward due to settlement and consolidation of the soil (Schwen et al., 2011; Moret & Arrúe, 2007). Osunbitan et al., (2005) noticed that, eight weeks after tillage, *Ks* under cropland could decrease to a rate lower than *Ks* under land use without tillage.

As the cropland sample involved several ploughed fields with several crop types and development stages, the finding of these authors may explain the observed high dispersion of *Ks* under cropland.

Fig. 6-4 suggests a saturated hydraulic conductivity, in general higher under fallow compared to cropland. The paired two tailed student's *t-test* shows that there is a difference between *Log Ks* under cropland and *Log Ks* under fallow at a probability of 0.05 (*p-value* = 0.007).

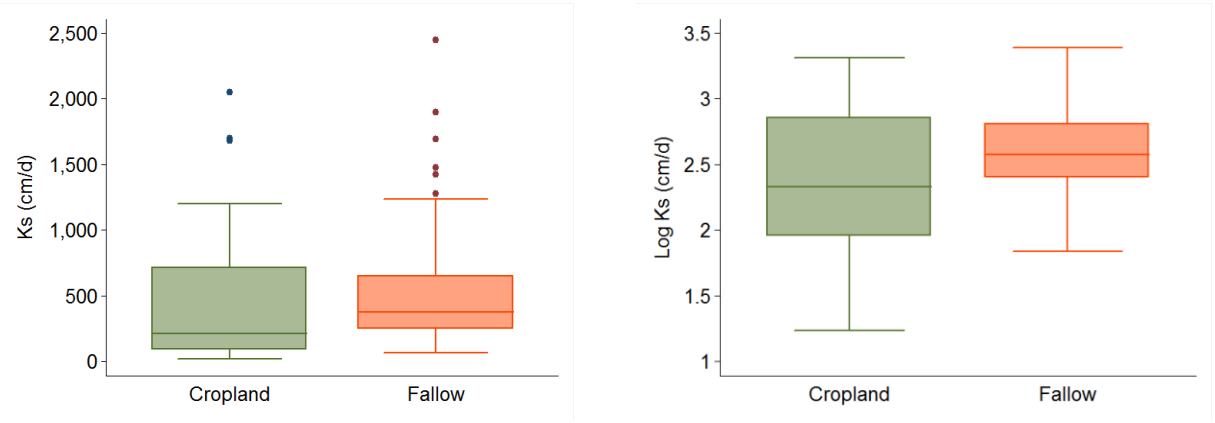

Fig. 6-4 Boxplot comparison of saturated hydraulic conductivity (Ks and Log Ks) on cropland and fallow

These results are in line with the conclusion of several studies addressing the topic of land use and land cover change impact on the saturated hydraulic conductivity (e.g. Neris et al., 2012; Zimmermann et al., 2006), describing hydraulic conductivity with increasing land use intensity.

90% of the sampling points were located on *plinthosols*, but the sample size was too small to differentiate between crop species, fallowing period or soil type. Nevertheless, the results evidence that *Ks* is significantly higher under fallow than cropland, suggesting a difference in the soil porosity under the two land use types.

As already mentioned in section 5.4.5, macropores have a larger influence on the hydraulic conductivity at saturation than mesopores even though they generally occupy a much smaller fraction of total soil porosity (Holden, 2009; Moret & Arrúe, 2007; Cameira et al., 2003). Macropores under fallow and natural

vegetation are primarily formed by biological activity of earthworms, ants, termites (Giertz & Diekkrüger, 2003) and roots (Cameira et al., 2003; Benjamin, 1993). Under tillage, macropores are formed by the rearrangement of the solid phase by the tillage tool, the roots and to a lesser extent by earthworms (Benjamin, 1993). Benjamin (1993) reported macroporosity to be reduced under tillage as compared to no tillage, fallow and other natural vegetation types due to earthworm and termite populations abundance under the latter compared to cropland. Tillage is furthermore a punctual operation with a transient effect on porosity increment; however tillage-induced disturbance is reported to have a detrimental impact on preexisting macropores as well as earthworm and termite population abundance (Hauser et al., 2012; Peigné et al., 2009; EriKsen-Hamel et al., 2009; Sileshi & Mafongoya, 2003). Against this trend of increasing infiltration with increasing biological activity, Jouquet et al. (2012) reported that termite sheetings break-down generate structural crusts which reduces the infiltration rate under fallow. Mettrop et al. (2013) also report a reduction of the infiltration rate due to termite activity in northern Burkina Faso.

Field observations during the infiltration test attested a root density much higher under fallow compared to cropland. The decomposition of roots and subsequent formation of root channels may contribute to the higher macroporosity under fallow. No comparative investigation on the earthworm, termite, ant etc. population density was carried out, however the quasi systematic annual ploughing of cropland suggests that the fauna activity might be lower under cropland compared to fallow areas.

6.3.2. Unsaturated hydraulic conductivity

Unsaturated hydraulic conductivity was derived from the infiltration rate measurements. At supplied tension heads (h) below -2 cm, unsaturated hydraulic conductivity under cropland and fallow were tested statistically not different at the probability of 0.05. As the supplied tension decreases up to the saturation state, the hydraulic conductivity under fallow becomes significantly higher compared to cropland (Table 6-2). This ascertains that differences of *Ks* between fallow and cropland become greater towards saturation as reported by Kelishadi et al. (2014) (Fig.6-5). The result supports the idea that the difference in the hydraulic conductivity under fallow and cropland is indeed associated to the difference of macroporosity as suggested in section 6.3.1. Under high water tension, whilst water predominantly flows through the soil matrix no difference between land use types is noted. This ascertains that matrix conductivity is quite similar under the different land use types. However, toward saturation, when water starts flowing into soil macropores, significant differences are observed between the land use types, signifying a predominant function of soil macropores.

Table 6-2 Summary of statistics for the Log_{10} of unsaturated hydraulic conductivity with increasing water tension (n=42).

Water tension (cm)	$Log_{10}K(h)$ under cropland			$Log_{10}K(h)$ under fallow			Cropland vs. *fallow t-test p-value*
	Mean	95% C.I		Mean	95% C.I		
-0.1	2.29	2.11	2.46	2.57	2.46	2.68	0.0078
-0.5	2.16	1.98	2.34	2.43	2.32	2.54	0.0096
-1	2.00	1.81	2.18	2.26	2.14	2.37	0.0186
-1.5	1.83	1.63	2.04	2.09	1.95	2.22	0.0417
-2	1.67	1.44	1.90	1.91	1.75	2.07	**0.0853**
-2.5	1.51	1.25	1.77	1.74	1.55	1.93	0.1482
-3	1.34	1.05	1.64	1.57	1.34	1.79	0.2229
-5	0.69	0.26	1.13	0.88	0.51	1.25	0.511
-10	-0.93	-1.76	-0.10	-0.84	-1.58	-0.09	0.8674

C.I: confidence interval, *n*: sample size

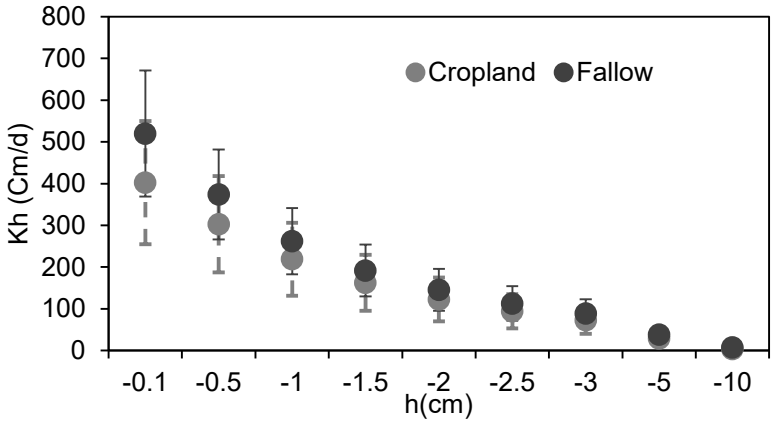

Fig.6-5 Mean and 95% Confidence interval of unsaturated hydraulic conductivity K(h) estimated from field measurement with increasing water tension under cropland and fallow.

6.3.3. Soil properties and the hydraulic conductivity

The *t-test* shows no significant difference between the textures of different land use types and denotes that the observed difference of hydrological conductivity was caused by land use and not pre-existing difference in texture (Table 6-3). The comparison of bulk density and soil carbon content under the two land uses shows a similar trend. These results suggest that the difference of *Ks* between cropland and fallow are unlikely to be attributable to the initial arrangement and size in soil pore. The fact that the lands of the Dano catchment have been cultivated for some decades, and the shortening of fallowing periods, do not allow a consequent organic matter accumulation in the topsoil even under fallowing. The rapid rotation between cropland and fallow tends to even the soil texture and organic matter content in the catchment.

Table 6-3 Soil texture, coarse particles, bulk density under cropland and fallow at the investigated plots.

	Cropland					Fallow					Cropland vs Fallow t-test
Variable	Mean	SD	Min	Max	n	Mean	SD	Min	Max	n	*p-value*
Sand (%)	37.75	8.83	21.05	53.47	21	35.59	10.38	14.69	51.26	21	0.4709
Clay(%)	20.58	9.31	4.69	37.34	21	22.08	7.12	13.77	34.86	21	0.5622
Bulk Density (g/cm^3)	1.43	0.12	1.24	1.75	21	1.42	0.14	1.14	1.60	21	0.9042
Coarse particles (%)	43.21	27.73	0.88	84.96	21	53.21	29.38	0.00	89.70	21	0.2636
C(%)	1.39	0.63	0.33	3.39	21	1.47	0.64	0.18	2.75	21	0.6795

6.3.4. Rainfall intensities and *Hortonian* overland flow

From the period September 2012 to December 2013, the rain gauges recorded 10207 and 3439 precipitation values on 10 minutes (I 10) and 60 minutes interval (I 60) basis respectively (Table 6-4).The distribution of recorded intensity values (Fig.6-6) shows that regardless of the aggregation interval, more than 80% of the intensities are lower than 20cm/d, which is the lowest infiltration rate measured during the infiltration test. However, I 60 presents a remarkably lower maximum compared to I 10. Furthermore, very high rainfall intensities (> 100cm/d) are observed within the catchment.

Table 6-4 Statistics of rainfall for period September 2012 to December 2013. I 10 refers to intensities of rainfall recorded at 10 minutes interval and I 60 represents intensities of rainfall calculated at 1 hour interval.

Time step	Number of records	Minimum	Mean	Maximum
I 10(cm/d)	10207	0.432	15.552	335.52
I 60 (cm/d)	3439	0.216	7.704	137.76

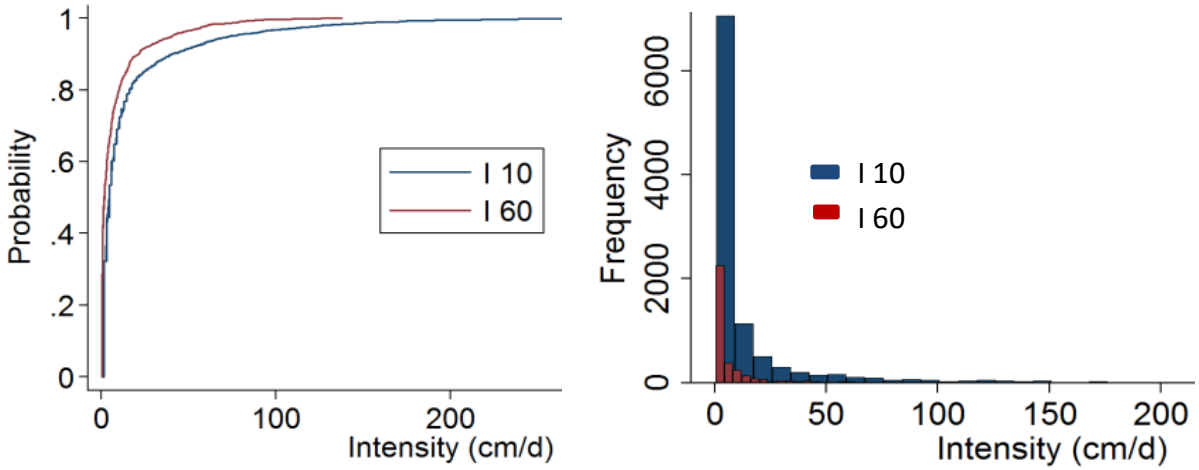

Fig.6-6 Histograms and cumulative distribution of **I 10** and **I 60** for the period September 2012 to December 2013 for the catchment.

As reported in Section 6.3.1, the infiltration rate presents a wide variation under the same land use type. However, by comparing the infiltration rate under cropland and fallow to I 10 and I 60 (Fig.6-7) one can infer the following regarding the *Hortonian* overland flow generation:

- about 20% of rainfall records present intensities higher than the minimum soil infiltration rate under cropland and fallow. Thus both land use types are exposed to *Hortonian* over land flow.
- rainfall events with intensities higher than 69 cm/d (minimum *Ks* under fallow) have the potential to generate infiltration excess overland flow within the catchment regardless of the land use type. This threshold is further reduced to 17 cm/d for croplands. Therefore, cropland is on average more prone to *Hortonian* overland flow than fallow.
- under I 10, the max rainfall intensity (335 cm/d) is likely to generate infiltration excess runoff over 61% of croplands and 45% of fallow area. Under I 60 max, these proportions are respectively 42% and 7%. Therefore, aggregating rainfall records to larger time step leads to an underestimation of the *Hortonian* overland flow.

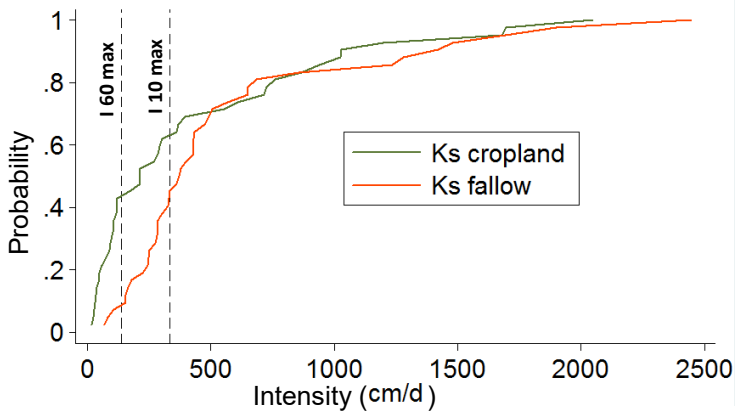

Fig.6-7 Cumulative distribution functions of the infiltration rate under cropland and fallow and maximum rainfall intensities (I 10; I 60) for the period September 2012 to December 2013.

6.4. Conclusion

The investigations exhibited that for the same land use type, the infiltration rate is a highly variable parameter in the catchment. However, the adjacent plots comparison approach as performed in the study reveals significant differences of *Ks* between cropland and fallow. This difference was associated to abundant macropores under fallow. Soil macroporosity appears to be reduced under cropland. Therefore, ploughing and other farming activities are likely to negatively affect soil pore size and arrangement.

Results further indicate that a decrease in soil infiltration following a conversion from fallow to cropland, does not systematically implies an increase in infiltration excess overland flow generation as many recorded rainfall intensities were lower than the minimum infiltration rate measured under cropland. However, the exposure to infiltration excess overland flow increases with land conversion from fallowing to cropping. The threshold for rainfall intensity to generate overland flow was higher under fallow compared to cropland (69cm/d and 17 cm/d respectively). The time step used for recording rainfall is determinant in surface runoff generation process.

Land conversion from fallow and savannah to cropland in the Dano catchment showed -at the plot scale- a potential to exacerbate surface runoff generation. However, infiltration excess overland flow also depends on antecedent soil moisture conditions and vegetation canopy interception capacity (which is dynamic throughout plant development period and even for two consecutive rain events). Considering such a complexity in the understanding of runoff generation processes implies the use of simulation models able to handle this complexity and will be addressed in the following chapters.

7. MODELING LAND USE CHANGE IMPACTS ON WATER RESOURCES[1]

Abstract

This chapter investigates the impacts of land use change on water resources in the Dano catchment, Burkina Faso, using a physically based hydrological simulation model and land use scenarios. Land use dynamic in the catchment was assessed through the analysis of four land use maps corresponding to the land use status in 1990, 2000, 2007, and 2013. A reclassification procedure levels out differences between the classification schemes of the four maps. The land use maps were used to build five land use scenarios corresponding to different levels of land use change in the catchment. The water balance was simulated by applying the Water flow and balance Simulation Model (WaSiM) using observed discharge, soil moisture, and groundwater level for model calibration and validation. Model statistical quality measures (R^2, *NSE* and *KGE*) achieved during calibration and validation ranged between 0.6 and 0.9 for total discharge, soil moisture, and groundwater level, indicating a good agreement between observed and simulated variables. After a successful multivariate validation, the model was applied to the land use scenarios.

The land use assessment exhibited a decrease of savannah at an annual rate of 2% since 1990. Conversely, cropland and urban areas have increased. Since urban areas occupy only 3% of the catchment it can be assumed that savannah was mainly converted to cropland. The conversion rate of savannah was lower than the annual population growth of 3%.

A clear increase in total discharge (+17%) and decrease in evapotranspiration (-5%) was observed following land use change in the catchment. A strong relationship was established between savannah degradation, cropland expansion, discharge increase and reduction of evapotranspiration. The increase in total discharge is related to high peak flow, suggesting (i) an increase in water resources that are not available for plant growth and human consumption and (ii) an alteration of flood risk for both the population within and downstream of the catchment.

Keywords: land use change; land use scenarios; WaSiM; multivariate evaluation; water resources.

7.1. Introduction

Socio-economic development drives land use and land cover (LULC) changes, which have potentially large impacts on water resources (Wagner et al., 2013). Changes in LULC affect the partitioning of precipitation through the vegetation and soil into the main water balance components of interception, infiltration, evapotranspiration, surface runoff and groundwater recharge (Falkenmark et al., 1999; Warburton et al., 2012). In regions with limited available water or flood and erosion prone areas, LULC changes can result in an increase of water shortage, flood risk and erosion rate and thus contribute to the deterioration of living conditions. Understanding the impacts of LULC change on water resources is therefore of decisive importance when addressing the issue of human well-being in a changing environment.

In order to assess LULC change impacts on water resources, it is essential that the hydrological functions of different LULC classes are understood. Previous investigations in West Africa have contributed to improve the knowledge of LULC change impacts on water resources at local and regional scales (e.g. (Bossa et al., 2012; Descroix et al., 2009; Diekkrüger et al., 2010; Mahé et al., 2010, 2005).

[1]Published as: Yira, Y., Diekkrüger, B., Steup, G., Bossa, A.Y., 2016. Modeling land use change impacts on water resources in a tropical West African catchment (Dano, Burkina Faso). J. Hydrol. doi:10.1016/j.jhydrol.2016.03.052

Table 7-1 Selected relevant studies of land use and land cover change impacts on hydrology in tropical regions. The three components of the "Key results" column refer to: (1) assess land use and land cover change; (2) assess hydrological model suitability and performance; and (3) assess land use and land cover change impact on hydrology. Not all studies evaluate these three components, as indicated by N/A representing "not applicable".

Study	Data/model used	Location/Climate/study size	Key results
1- Mahé et al. (2010)	Landsat, gauge data/No model used	Nakambé Basin, West Africa/ Sahel/ 21 000 km²	(1) 50% of natural vegetation replaced by cropping in 40 years (2) N/A (3) Increased flood occurrence and surface discharge related to LULC change
2- Descroix et al. (2009)	SPOT images, gauge data/No model used	West Africa/Sudanian and Sahelian region	(1) Percentage of natural vegetation passed from 50% to 0% in 50 years due to cropland expansion (2) N/A (3) Streamflows are increasing in the Sahelian regions in spite of the reduced rainfall whereas streamflows are reducing in the Sudanian areas
3- Diekkrüger et al. (2010)	Field measurements of infiltration rate, gauge data, SRTM 90 m/SIMULAT-H, UHP-HRU, SWAT	Ouémé Catchment, Benin/sub-humid region/From local to large scale	(1) N/A (2) Successful model validation using discharge (and sediment for SWAT). Good model performances achieved (3) High correlation between land use/cover and runoff coefficient
4- Cornelissen et al. (2013)	Gauge data, Landsat data, SRTM 90 m, /WaSiM, SWAT, UHP-HRU, GR4J	Térou Catchment, Benin/sub-humid region/2 344 km²	(1) N/A (2) Good performance achieved by all model using observed discharge (3) Increase in the fraction of agricultural land causes an increase in discharge
5- Awotwi et al. (2015)	Landsat data, gauge data, SRTM 90 m/SWAT	White Volta Basin, Burkina Faso and Ghana/semiarid and sub humid zone/	(1) Decrease in savannah attributed to the increase in farming activities (2) Good model performance (using discharge) even though there are data limitations associated with the model application (3) Surface runoff and groundwater decreased with savannah and grassland conversion to crop land
6- Beck et al. (2013)	Landsat data, gauge data/HBV-light	12 catchments, Puerto Rico/tropical maritime climate/24-177 km²	(1) In all catchments forest and urban areas increased markedly between 1951 and 2000 at the expense of pasture and agricultural areas (2) Good model performance achieved using observed discharge (3) At large scale, changes in discharge characteristics could not be (strongly) related to changes in urban or forest area.
7- Giertz et al. (2006)	Field measurements of soil hydraulic properties, gauge data, /SIMULAT-H	3 catchments, Benin/Tropical sub-humid/3-16 km²	(1) N/A (2) Successful multi-variate validation achieved using soil moisture and discharge (3) Land use proved to be a major factor in runoff generation process
8- Leemhuis et al. (2007)	Landsat data, LULC scenarios, gauge data/WaSiM-ETH	Gumbasa River catchment, Indonesia/ Tropical humid region/1 275 km²	(1) Increase of grassland and shrub land by 18% and 48% respectively due to forest degradation (2) Model validated using discharge (3) An increase of about 0.2 to 1.8% in total discharge related to LULC change
9- Zimmermann et al. (2006)	Infiltration and saturated hydraulic conductivity measurements/ No model used	Rancho Grande, Brazil/Tropical humid/ N/A	(1) N/A (2) N/A (3) Infiltration rate decreases from forest to bananas and from banana to pasture but this decrease did not affect flowpath pattern.
10- Wagner et al. (2013)	Landsat data, ASTER 30 m, FAO soil database/ SWAT	Mula and the Mutha Rivers Catchment, India/ tropical wet and dry region /2036km²	(1) Natural vegetation decreased from 79 % in1990 to 70 % in 2010 (2) Model validated using discharge (3) At the catchment scale no LULC change impact was observed, but at sub-catchment scale up to 7% increase in total discharge was simulated.
11- Current study	SRTM 90 m, LANDSAT and RapidEye derived maps, gauge data(Climate, discharge, soil moisture, groundwater), National climate dataset, field measurements of soil hydraulic properties/ WaSiM	Dano catchment, Burkina Faso/tropical sub-humid/ 195 km²	(1) Decrease of savannah at an annual rate of 2% since 1990 (2) Successful multi-variate model validation using Soil moisture, groundwater level and discharge (3) Strong relation between LULC and discharge is established, up to 5% increase is discharge was observed following land use/cover change

A decrease of soil hydraulic conductivity with land conversion from savannah and forest to crop, mainly due to the reduction of macropores that are linked to the soil fauna activity, is highlighted by those studies. However the relation between LULC change, streamflow and water balance at catchment scale is still under debate in the tropics (Table 7 1).The net effect of LULC impact on water resources is reported to be dependent on the investigation scale (Giertz et al., 2006; Wagner et al., 2013; Zimmermann et al., 2006) as well as the local climate (Descroix et al., 2009) and the LULC type (Beck et al., 2013; Leemhuis et al., 2007).

The application of hydrological models is a typical approach used to assess LULC change impacts on water resources. Numerous studies have proven the suitability of hydrological models in LULC change impact assessments on water resources of the tropical West African climate (e.g. Cornelissen et al., 2013; Giertz et al., 2006). However, models differ in terms of their perceptual, conceptual, and procedural concepts (Beven, 2012), and therefore their application in impact assessment studies may lead to different outcomes. In LULC impact assessments, physically based hydrological models are generally preferred to conceptual models as they represent the underlying hydrologic and land surface processes in greater detail (Beven, 2012). WaSiM (Schulla, 2014) has been successfully applied in several hydrologic impact studies worldwide, and in the West African region as well (e.g. Bormann et al., 2009; Cornelissen et al., 2013). The model has proven to be suitable in LULC impact studies under conditions of limited data availability.

Dano is a headwater catchment of the Volta river basin (400,000 km^2). A limited number of investigations of LULC change and its impacts have been carried out in this large scale catchment. The investigations have revealed a trend toward the reduction of forest and savannah covers (Landmann et al., 2007) and the expansion of agricultural lands as a result of population increase and the subsequent need for more natural resources (Codjoe, 2004). Impacts of LULC change on the water resource assessments in the Volta river basin include both changes in the water balance components and the alteration of water quality (Awotwi et al., 2015; Mounirou, 2012). As mentioned before, additional investigations are required to consolidate these achievements. Moreover, due to a large variability of socioecological systems within the Volta basin, the results and conclusions achieved by those studies may hide important discrepancies at the local scale. This sets limits to their integration into water resources planning for specific cases.

The Dano catchment experiences a rapid population growth (roughly 3% per year) that has induced an important LULC change over the recent decades. For a catchment with seasonally limited water availability, social development could be significantly compromised by any driver altering the hydrological cycle. The purpose of this study is to improve the understanding of the dynamics between land use and hydrology in order to assist water resources management in the catchment. Accordingly, it has the following three objectives:

(i) to assess LULC change in the Dano catchment over the past 25 years;
(ii) to set up a robust hydrological model of the catchment suitable for LULC impact assessment; and
(iii) to analyze LULC change impacts on waterflow and water balance components in the catchment.

7.2. Study area and materials

7.2.1. Study area

The Dano catchment covers a total area of 195 km^2 in the Ioba province, located in the Southwest of Burkina Faso (Fig. 7-1). LULC in the catchment is characterized by shifting cultivation over one third of the catchment area. In the context of unplanned development, the annual population growth of about 3% results in an increasing demand for arable lands leading to the extension of cropped areas.

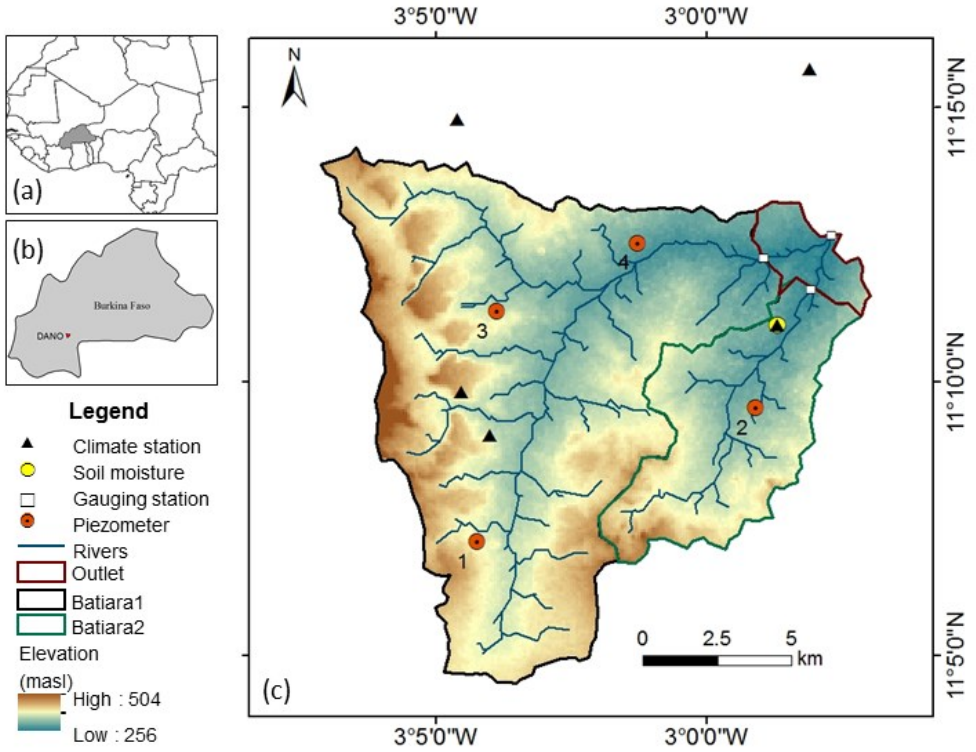

Fig. 7-1 Location map. Part (a) shows the location of Burkina Faso in West Africa, (b) provides the location of the Dano catchment in Burkina Faso, and (c) shows the study area and sub-catchments in the Dano catchment.

The natural vegetation of the catchment is part of the Sudanian region with wooded, arboraceous or shrubby savannah and abundant annual grasses. However, a major part of this primary vegetation has been converted to agricultural land and long-term fallowing. In this study it is not differentiated between savannah and fallow; both land use types are in the following summarized under the term *savannah*. The predominant crops in the catchment are sorghum (*Sorghum bicolor*), millet (*Pennisetum glaucum*), cotton (*Gossypium hirsutum*), maize (*Zea mays*), cowpeas (*Vigna unguiculata*) and groundnut (*Arachidis hypogaea*).

The landscape is predominantly flat with an average slope of 2.9%, an elevation range from 256 to 504 m above sea level (masl) and a mean elevation of 295 masl. The annual mean temperature equals 28.6°C and the annual precipitation ranged from 800 mm to 1200 mm for the period 1951 to 2005 (Schmengler, 2011). The annual rainfall pattern is marked by a dry season covering the period of November to April. Around 80% of annual rainfall occurs from July to September and the catchment experiences monsoonal rains. This rainfall pattern limits water availability during the dry season as the population in the catchment heavily relies on surface water.

The predominant soil type in the catchment according to the World Reference Base for soil resources (WRB, 2006) is *plinthosol* (73.1% of the area), characterized by a *plinthite* subsurface layer in the upper first meter of the soil profile. The remaining soil types are *gleysol*, *cambisol*, *lixisol*, *leptosol* and *stagnosol*.

7.2.2. Data sources

Confidence in the hydrologic modeling effort depends to a large extent on the availability of high quality hydrological and hydro-meteorological data (Miller et al., 2002). Multiple data types further permit constraining the uncertainties in the predicted variables (Pappenberger and Beven, 2006b), leading to more accurate model results. Table 7-2 shows the type and source of applied datasets and the required parameters used in the modeling exercise.

Table 7-2 Applied datasets and required inputs for WaSiM.

Data set	Resolution/ scale	Source	Required parameters
Topography	90 m	SRTM (Jarvis et al., 2008)	Slope, aspect, curvature, sub-basin, channel etc.
Soil	1:25 000	Soil survey Pedotransfer function	Θ_{sat}, *BD*, texture, Soil carbon, gravel. *van Genuchten* parameters, K_S, Θ_{res}
Land use map	5 to 250 m	Forkour (2014); Landmann et al. (2007)	Soil units
Land use characteristic		Literature	LAI, albedo, ET resistance, veg. height, root depth & distribution, oxygen stress threshold, dryness stress threshold
Climate	Hourly, Daily	Instrumentation WASCAL, DGM*	Rainfall, temperature, humidity, solar radiation, wind speed
Discharge	10 minutes	Instrumentation WASCAL	Discharge, electric conductivity
Soil moisture	30 minutes	Instrumentation WASCAL	Soil water content
Groundwater level	Daily	Instrumentation WASCAL	Groundwater depth
Aquifer		Literature, soil survey	Specific yield, thickness, saturated conductivity; boundary

*Direction Générale de la Météorologie

In order to complement the existent dataset for the Dano catchment and gather the data required to set up the model, an instrumentation concept was designed and implemented in mid-2012. The observation network used in the current study consists of: (i) four automatic climate stations, (ii) four piezometers, (iii) a soil moisture station using three FDR-probes per soil horizon, and three discharge stations (Fig. 7-1).
In conjunction with the instrumentation, soil samples were collected throughout the catchment to analyze physical and chemical properties necessary for soil parametrization. For the simulation period prior to the instrumentation date, the Dano climate station (located within the catchment) of the national meteorological service (DGM) was used.

7.3. Methods

7.3.1. Land use and land cover change

Four multi-temporal LULC maps of the Dano catchment were used to assess LULC change, three maps corresponding to LULC status for the years1990, 2000 and 2007 (Landmann et al., 2007) and one map of the year 2013 (Forkour, 2014). The land cover data sets after (Landmann et al. (2007) were derived from Landsat TM (http://glovis.usgs.gov/) and MODIS (https://mrtweb.cr.usgs.gov/) data and are available at 250 m resolution. The map after Forkour (2014) was derived from Landsat TM and RapidEye (http://blackbridge.com/rapideye/), and is available at 5 m resolution. The four maps use the Land Cover Classification System (LCCS) legend from the Food and Agricultural Organization (FAO) for land cover descriptors. LULC classes are, however, differently grouped (Table 7-3).

Table 7-3 Initial land use and land cover classes provided in the land use datasets and standardized land use and land cover classes applied in this study. Initial datasets do not use the same LULC classes, "--" refers to a class not used in a given dataset.

Initial land use/cover class	Proportional area (%) per year				Land use/cover applied in the study
	1990	2000	2007	2013	
Regularly flooded, woody, closed to open	2.4	33.3	--	--	Tree and shrub savannah
Broadleaved forest, closed, evergreen (>=65%)	1.5	--	--	--	Tree and shrub savannah
Woodland, closed	63.3	--	9.8	--	Tree and shrub savannah
Burned area	3.7	1.6	--	--	Cropland
Bare soil, scattered vegetation	1.0	--	--	--	Urban area
Herbaceous crops	7.3	--	--	--	Cropland
Herbaceous vegetation, closed (>=65%)	20.4	--	--	--	Tree and shrub savannah
Forest	--	5.2	14.9	--	Tree and shrub savannah
Grassland	--	31.3	40.3	--	Tree and shrub savannah
Cropland	--	17.1	28.6	37.7	Cropland
Wetland	--	10.9	1.6	--	Tree and shrub savannah
Urban Area	0.08	0.08	4.3	3.6	Urban area
Water	0.2	0.2	0.2	0.2	Water
Natural/semi-natural vegetation	--	--	--	58.2	Tree and shrub savannah

In order to obtain a single LULC classification structure applicable to the four maps, a combination process was undertaken to group the initial LULC classes into four standardized units. The maps of years 1990, 2000 and 2007 which had each more than seven classes, were grouped to fit the four LULC classes of the year 2013 (Table 7-3). The rules used to combine the initial LULC classes into four LULC units were driven by the seasonality of the vegetation cover and the hydrological properties of the classes. The units forest, *woodland*, and *regularly flooded* areas are characterized by a partial cover of perennial plants and were combined into the unit *Tree and shrub savannah.* The units *bare soil* and *settlements* constitute areas partially or totally impervious to rainfall, and are therefore grouped into the *Urban area* unit. The *cropland* unit represents areas dominated by seasonal crop species. *Water* refers to free surface water bodies (allowing an evaporation rate equal to the potential evapotranspiration). LULC change was then assessed based on the change in the proportion of these four classes throughout the period of 1990-2013 within the catchment.

7.3.2.Hydrological modeling

7.3.2.1. Model description

In this study the grid based version 9.05.04 of the Water flow and balance Simulation Model (WaSiM) (Schulla, 1997) was applied. Originally developed to evaluate the influence of climate change on hydrology in alpine regions, WaSiM has been continuously improved and successfully applied in various contexts and regions (Schulla, 2014). Successful applications of the model in the West African region include groundwater modeling (e.g. Martin, 2005), and assessment of LULC and climate change impact studies (e.g. Cornelissen et al., 2013; Kasei, 2009; Leemhuis et al., 2009). WaSiM is a deterministic and spatially distributed model, which uses mainly physically based approaches to describe hydrological processes. A brief description of the main processes used in the model is presented in this section, further details of model structures and various processes involved are given in chapter 3, and an extended description is provided in the Model Description Manual (Schulla, 2014).

- ***Potential evapotranspiration*** (ETp). The potential transpiration from plant leaves, the evaporation from bare soil and the evaporation from interception surfaces and water bodies are calculated following the Penman-Monteith equation (John Lennox Monteith, 1975).

- ***Actual evapotranspiration*** (ETa) is computed based on the relation between soil water content, actual capillary pressure and land use parameters. A mechanism of reducing transpiration due to oxygen stress under saturated soil condition is implemented in the model following Feddes et al. (1978).

- ***Interception*** is calculated using a bucket approach depending on the leaf area index (*LAI*), the vegetation covered fraction (*VCF*), and the maximum height of water on leaves.

- ***Infiltration*** is computed after Schulla (2015).

- **Water flow in the unsaturated zone** is based on Richard's equation.

- ***Interflow*** is a result of conductivity, drainage density and hydraulic gradient. Interflow occurs between soil layers of different hydraulic conductivities or porosities and under sufficient slope.

- ***Baseflow*** is generated at river grid cells as exfiltration from the groundwater into the surface river system.

- ***Groundwater*** system as used in this study is represented by a two-dimensional Darcy based groundwater module coupled with the unsaturated zone module to simulate lateral fluxes in the saturated zone.

7.3.2.2. Land use parametrization

It is essential that the LULC properties relevant for water resources assessment are well characterized by the model parameters relating to LULC. In WaSiM a (non-layered) LULC class is characterized by fifteen (constant and plant development stage dependent) parameters (Table 7-4). Therefore, changes in LULC classes are described by these parameters and changes in the spatial distribution of land use classes are accounted for using different land use maps.

Quantitative data of vegetation characteristics for the LULC types in the catchment is rare. Therefore, land use parameters were mainly derived from literature. Details of LULC parameterization for the savannah, settlements and cropland were taken from Cornelissen et al. (2013) and Kasei (2009). Water bodies were parameterized after Schulla (2014).

Table 7-4 Soil and land use and land cover characterization in WaSiM.

	Parameter	Description	Unit
Land use/cover	*Constant*		
	RootDistr	Root distribution	-
	TReduWet	Threshold value for starting oxygen stress due to nearly water saturated based on Feddes et al. (1978)	%
	LimitReduWet	Maximum reduction of transpiration due to oxygen stress based on Feddes et al. (1978)	%
	HReduDry	Threshold value for starting dryness	m
	IntercepCap	Specific thickness of the water layer on the leaf	mm
	Variable in time		
	DoY	Plant development phases	days
	Albedo	Albedo	-
	Rsc	Leaf surface resistance	s/m
	Rs_interception	Interception surface resistance	s/m
	Rse	Soil surface resistance (for evaporation)	s/m
	LAI	Leaf area index	-
	Z0	Aerodynamic roughness length	m
	VCF	Vegetation covered fraction	%
	RootDepth	Root depth	m
	AltDep	Shift in temporal vegetation development per meter elevation	masl
Soil	**θ_s**	Saturated water content	(Vol.%)
	θ_r	Residual water content	(Vol.%)
	K_s	Saturated hydraulic conductivity	cm/day
	K_{rec}	Recession of K_s with depth	-
	α	van Genuchten empirical parameter	1/m
	n	van Genuchten empirical parameter	-
	Horizon	Number of horizon per soil unit	-
	Layer	Number of numerical layer per soil unit	-
	d_m	Thickness of soil layer	m

7.3.2.3. Soil parametrization

The modeling is done one-dimensional in the vertical direction using a soil with several numerical layers. The parameterization of soil hydraulic properties applies the method after van Genuchten (1976) (Table 7-4). Besides the empirical parameters α and n, a third parameter k_{rec} has to be specified for each soil type for describing the recession of the saturated conductivity with depth. Saturated water content for each soil was directly measured in the laboratory. Residual water content, α and n were derived from

laboratory soil texture and organic matter content measurements using van Genuchten (1980). Using soil texture and organic matter content, the saturated hydraulic conductivity was estimated for each soil type and horizon after Saxton and Rawls (2006).

7.3.2.4. Spatial discretization

As WaSiM is a grid based model, spatial data is required in a raster format with identical resolution and extension. Meteorological data are given as time series of climate stations (point data). The model allows various methods to interpolate input data with a sparse spatial resolution to the model grid resolution. The inverse weight distance method was used for climate data interpolation. Based on the digital elevation model of the study area, terrain attributes were generated using the topography analysis program TANALYS (Schulla, 2014). This information includes, among others, slope, flow direction, flow accumulation, and stream network. Additional parameters related to the catchment discretization are the interflow drainage density (d_r), the storage coefficient for surface runoff (k_D) and the storage coefficient for interflow (K_H).

7.3.2.5. Model calibration and validation

Due to the process-based model character of WaSiM, the number of effective parameters that need to be calibrated is limited (Schulla, 2014). However, some parameters must still be calibrated by comparing simulated and measured variables. In WaSiM, this applies particularly to *Rsc*, *Rse*, K_{rec}, d_r, K_D, K_H, specific yield and hydraulic conductivity for the groundwater module.

With regard to the set of parameters to be calibrated, the Latin Hypercube Sampling (*LHS*) was adopted for its high efficiency. The method ensures that each of the considered parameters is represented in a fully stratified manner no matter which components might turn out to be important (McKay et al., 1979).Thus it makes minimal assumptions about the shape of the model response surface. A dataset of the parameters (p) to be optimized was generated and used to perform (r) model runs. The approaches used to optimize each parameter following the *LHS* included graphical and numerical analysis of the ensemble model outputs. A multivariate regression was performed to analyze the relation between the objective function and the calibrated (p) parameters:

$$y(r) = \hat{\beta}_o + \sum_{i=1}^{p} \hat{\beta}_i . x_i(r) + \hat{e}(r) \qquad \text{Eq. 7-1}$$

Where y is the regression model, r is the number of simulation; $\hat{\beta}_o$ and $\hat{\beta}_i$ are ordinary regression coefficients, $\hat{e}(r)$ is the regression residual, p refers to the number of calibrated parameter, x is the parameter value.

The standardized regression coefficient (*SRC*) was then computed to identify and optimize the calibrated parameters (Christiaens & Feyen, 2002; Janssen et al., 1994):

$$SRC_i = \hat{\beta}_i \frac{\sigma_{x_i}}{\sigma_y} \qquad \text{Eq. 7-2}$$

Where SRC is the standardized regression coefficient, σ_{x_i} is the standard deviation of the i^{th} calibrated parameter, and σ_y is the standard deviation of the regression model.

The Sum of Squared Error (*SS*) was set as an objective function for calibration. The simulated discharges at the three gauging stations were simultaneously calibrated; the area of each sub-catchment was used as weight to the objective function (based on Abbaspour, 2009) as follows:

$$SS = \left[A.w \sum_{i=1}^{n} (Q_m - Q_s)^2 \right]_{sub1} + \left[A.w \sum_{i=1}^{n} (Q_m - Q_s)^2 \right]_{sub2} + \left[A.w \sum_{i=1}^{n} (Q_m - Q_s)^2 \right]_{sub3} \quad \text{Eq. 7-3}$$

Where SS is the sum of squared error, $w = \frac{1}{\sigma^2}$, σ^2 is the variance of the measured discharge, $A = \frac{a_p}{a_t}$, a_t is the Dano catchment total area, a_p is the sub-catchment area, $sub1 .. 3$ are the sub-catchments, Q represents the discharge, m and s stand for measured and simulated.

A multiple-variate approach including observed discharges at the three gauging stations, soil moisture under the dominating soil type and groundwater level recorded by four piezometers was used to validate the hydrological model. The model performance was assessed through the Pearson product-moment-correlation-coefficient (R^2), the Nash Sutcliffe Efficiency (NSE) (Nash & Sutcliffe, 1970) and the Kling-Gupta Efficiency (KGE) (Gupta et al., 2009; Kling et al., 2012). For the calibration and validation of the model, as well as the LULC impacts assessment period, a uniform raster-cell size of 90 m and a daily time step were chosen as a compromise of calculation effort, detail of input data and certainty of model results.

7.3.3. Land use scenarios

After validation, the hydrological simulation model WaSiM was used to assess the impacts of LULC changes on water resources over the period of 1990-2014. For the analysis of LULC change impacts on the water balance components, five model runs or scenarios (M1, M2,…M5) are performed with measured weather data from 1990 to 2014 using five distinct land use parameterizations as follows and outlined in Table 7-5. The scenario M1, considered as baseline, is performed using the LULC map of the year 1990 for the entire simulation period (1990 to 2014). The scenario M2, M3 and M4 are performed with the LULC maps status of 2000, 2007 and 2013 respectively. The scenario M5 reflects the chronology of LULC change as it occurred in the catchment. The four LULC maps (1990, 2000, 2007 and 2013) are successively (and continuously) used for the periods 1990-1996, 1997-2003, 2004-2010 and 2011-2014.

Table 7-5 Modeling periods and applied land use maps for the different modeling scenarios.

Scenario	Simulation period			
	Warm-up period	Evaluation period		
	1990-1996	1997-2003	2004-2010	2011-2014
M1	LULC_1990	LULC _1990		
M2	LULC_1990	LULC_2000		
M3	LULC_1990	LULC_2007		
M4	LULC_1990	LULC_2013		
M5	LULC_1990	LULC_2000	LULC_2007	LULC_2013

The period 1990-1996 of each scenario is used as a model warm-up phase. Thus, analysis of water resources was carried out for the period 1997-2014 by comparing average water balance components using the model results of the 5 modeling scenarios. It is important to note that inputs and boundary conditions are kept unchanged for the five scenarios. Thus the comparison approach exhibits the main

changes on the hydrologic components due to LULC changes (Ghaffari et al., 2010; Miller et al., 2002; Wagner et al., 2013).
Mean water balance components of the five scenarios were calculated for each sub-catchment considering the periods 1997-2003, 2004-2010 and 2011-2014. The percentages of different LULC classes for these periods were also derived from the LULC maps of 2000, 2007 and 2013. The percentages of the major LULC classes (savannah and cropland) were then fitted to the corresponding simulated total discharge and actual evapotranspiration.

Kruskal-Wallis hypothesis tests were conducted to determine if the water balance components were significantly different for the five scenarios. The test showed that there were statistically significant differences for both actual evapotranspiration ETa (mm/month) and total discharge (mm/month) between the five scenarios, with $\chi^2(4) = 64.8$, $p<0.001$ and $\chi^2(4) = 5382.8$, $p<0.001$ respectively. Pairwise comparisons of the five scenarios were then conducted using Mann-Whitney *U* tests at a probability of 0.005 (0.05/10) (Marascuilo & McSweeney, 1977). Histograms in section 7.4.3 are grouped according to these tests.

7.4. Results

7.4.1. Land use and land cover change

The major LULC changes during the period 1990-2013 as shown in Fig. 7-2 are conversions from savannah to cropland and, in a lesser extent, to urban areas. The area of savannah has continuously decreased from 87.9 % in 1990 to 58.7% in 2013 (82.7% in 2000 and 66.9% in 2007). Conversely, the cropped area has increased from 11.6% in 1990 to 37.7% in 2013 (17.1 % in 2000 and 28.6% in 2007). Permanent water area remained relatively unchanged with 0.2% throughout the assessment period. As no additional facilities for permanent surface water storage has been built since 1990, the Mountouri reservoir remains the major permanent surface water in the catchment. Urbanization has led to an increase of built-up area from 0.09% in 1990 to 3.6% in 2013.

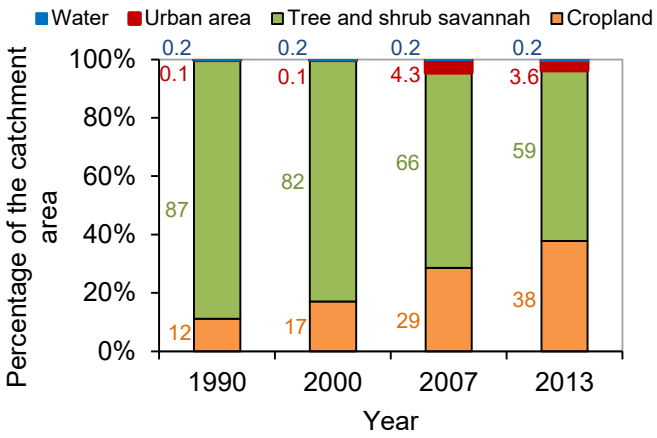

Fig. 7-2 Percentage of the catchment area per land use/cover classes between 1990 and 2013. Numbers at the left of each bar indicate the percentage values of the land use classes.

Similar figures of savannah conversion due to expanding population and expansion of agricultural land in the region are shown by many authors (Mahé et al., 2005; Stephenne and Lambin, 2001; Thiombiano & Kampmann, 2010). The increase in cropland areas is also in accordance with several aerial image studies in the region (e.g. Gray, 1999; Paré et al., 2008; Zoungrana et al., 2015), as well as with official statistics of cropped areas.

7.4.2. Hydrological modeling

Calibrated parameters having a standardized regression coefficient significantly different from zero (at 95% significance level), include the interflow drainage density (d_r), the surface flow storage constant (k_D) and interflow storage constant (k_H) (Table 7-6). The ranges of these parameters considering the 10% best simulations of the *LHS*, based on the sum of R^2, *NSE* and *KGE* indicate that several model parametrizations lead to good (or similar) model quality measures (equifinality as defined by Beven & Freer, 2001). Out of the parameter sets used in the *LHS*, the one scoring the highest sum of R^2, *NSE* and *KGE* (equally weighted) was used for LULC impact assessment.

Table 7-6 Statistics of the most sensitive parameters obtained after calibration (using total discharge as variable).

Sub-catchment	Parameter	Standardized regression coefficient	Parameter range for the best 10 % Simulations		Fitted Value
			Min	Max	
Batiara1 (145 km^2)	*dr*	-0.33	15	27	23
	k_D	0.28	57	70	70
	k_H	-0.11	35	51	49
Batiara2 (42 km^2)	d_r	-0.15	15	29	25
	k_D	-0.09	35	49	35
	k_H	-0.07	29	42	29
Outlet (8 km^2)	k_D	0.11	41	60	60
	d_r	-0.16	17	34	29

dr: interflow drainage density; k_D :surface flow storage constant; K_H *:* interflow storage constant.

Water balance and model performances were compared for the calibration and validation periods (Table 7-7). The total rainfall shows that the model was calibrated and validated during periods of relatively similar rainfall patterns. The Standardized Precipitation Index (SPI) (McKee et al., 1993) of the catchment for the period 1990-2014 (Fig. 7-3) further indicates that both calibration and validation periods are near normal (*SPI* < 1), and are thus comparable and also reflect the annual rainfall pattern in the catchment for the period 1990-2014. Water balance components are also similar for both periods.

Table 7-7 Water balance and model performance for the calibration and validation periods using the fitted values from Table 7-6 (Batiara1, Batiara2 and Outlet are shown in Fig. 7-1).

	Batiara1	Batiara2	Outlet	Batiara1	Batiara2	Outlet
	Calibration (2011-2013)			Validation (2014)		
Rainfall (mm)	964	946	966	958	949	949
Eta (mm)	807	778	821	800	785	803
Total discharge (mm)	157	168	145	158	164	145
Surface Runoff (mm)	74.418	83.496	60.465	61.778	62.156	48.575
Interflow (mm)	71.121	80.304	76.85	80.58	91.512	86.275
Baseflow (mm)	11.461	4.368	7.685	16.748	6.56	10.73
R^2	0.9	0.8	0.9	0.9	0.7	0.9
NSE	0.9	0.8	0.9	0.9	0.6	0.9
KGE	0.8	0.7	0.8	0.6	0.8	0.7

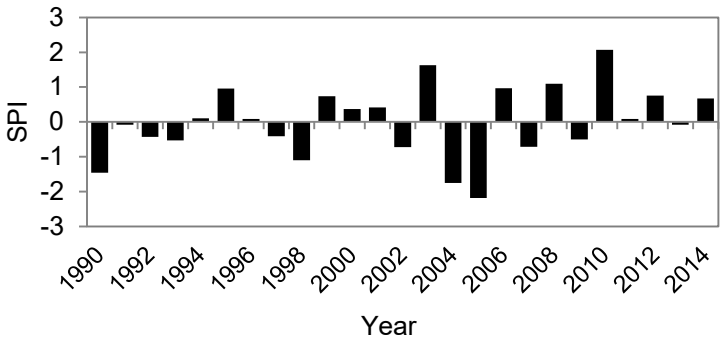

Fig. 7-3 Standardized precipitation index (SPI) in the Dano catchment (1990-2014).

Fig. 7-4 compares the simulated and observed discharges for the years 2013 and 2014 at the outlet. Similar figures are also obtained for Batiara1 and Batiara2. The figure shows a good accordance between observed and simulated discharge although some peaks are underestimated by the model. Measurement errors during high discharge events can be an explanation for the misrepresentation of peak flow as overbank flow was often observed at the gauging stations.

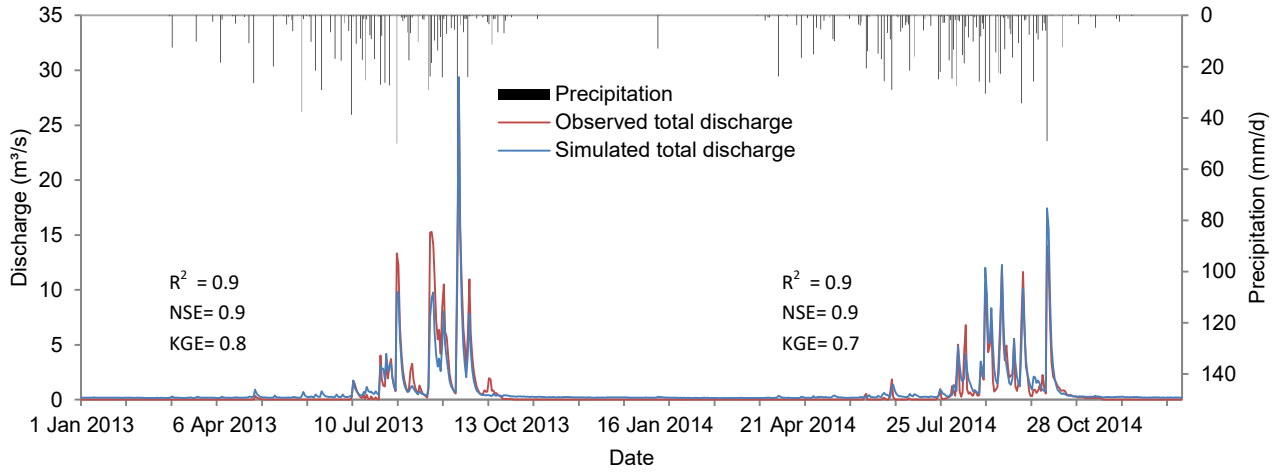

Fig. 7-4 Observed and simulated discharges for the calibration period (2013) and validation period (2014) at the outlet. R^2, NSE and KGE refer to Pearson product-moment-correlation-coefficient, Nash Sutcliffe Efficiency and Kling-Gupta Efficiency respectively.

Soil moisture and groundwater level were additionally used to validate the model. No calibration was performed for these variables as the soil water retention parameters were derived from laboratory analysis. Simulated and observed soil moisture was compared at two different soil depths (7 and 16 cm) for a *plinthosol* under savannah, and the simulated groundwater level was compared to the observations of the 4 piezometers (Fig. 7-5c). Fair to good model quality measures with regard to the simulated soil moisture and groundwater level were achieved.

Short term and long term soil wetting-drying dynamics are well simulated by the model. The comparison of simulated and observed soil moistures for the first horizon (7 cm depth) shows a good agreement (Fig.

7-5 a). An over-estimation of the soil moisture by the model can be observed particularly for the year 2013. However, it is important to note that the maxima in the observed soil moisture in 2013 are lower than the ones in 2014. The comparison of simulated and observed soil moisture for the second horizon (Fig. 7-5 b) shows that the long term soil moisture dynamic is also well captured by the model. A good agreement between simulated and observed groundwater levels is also highlighted by Fig. 7-5(c).

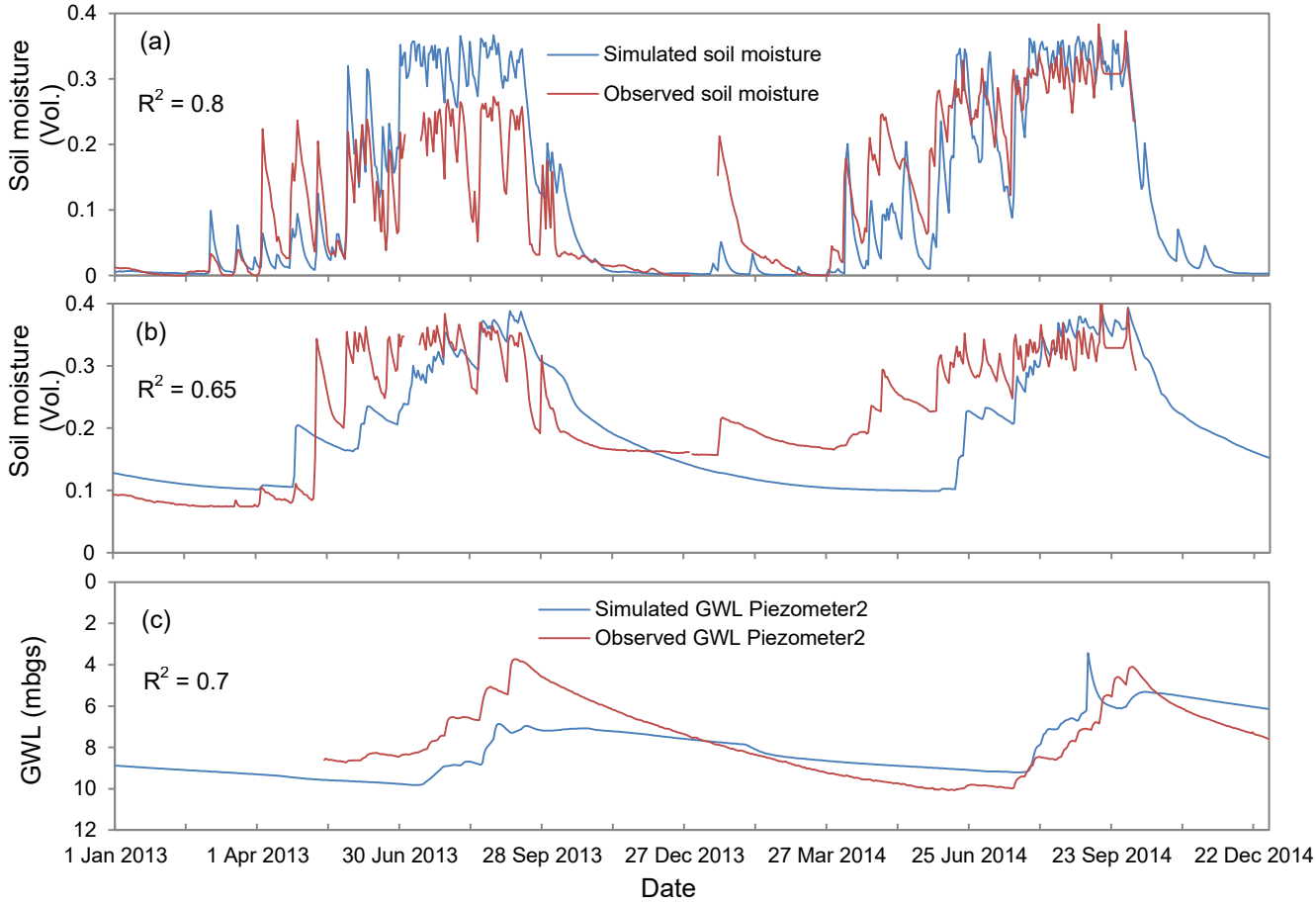

Fig. 7-5 Comparison of simulated and observed soil moisture and groundwater depth at a daily time step. (a) shows soil moisture of the first horizon at 7 cm depth, (b) indicates soil moisture of the second horizon at 16 cm depth, and (c) shows groundwater level (GWL) for piezometer2. R^2 refers to Pearson product-moment-correlation-coefficient.

7.4.3. Land use scenarios

Changes in annual discharge and actual evapotranspiration per sub-catchment resulting from the land use scenarios are shown in Fig. 7-6. An increase of total discharge between scenarios is readily observable for all sub-catchment following the order M1, M2, M5, M3 and M4. A decrease of ETa is also exhibited in the same order. As described in section (3.3), LULC change was characterized by a continuous conversion from savannah to cropland from 1990 to 2013. The LULC scenarios M1, M2, M3 and M4 follow this chronology of LULC change. The assessment of savannah and cropland areas ranks the scenario M5 between M2 and M3, with 22-32% of cropland and 65-75% of savannah per sub-

catchment. Thus the observed order between scenarios in term of changes in total discharge and ETa suggests the percentages of savannah and cropland of the scenarios to be the major driver.

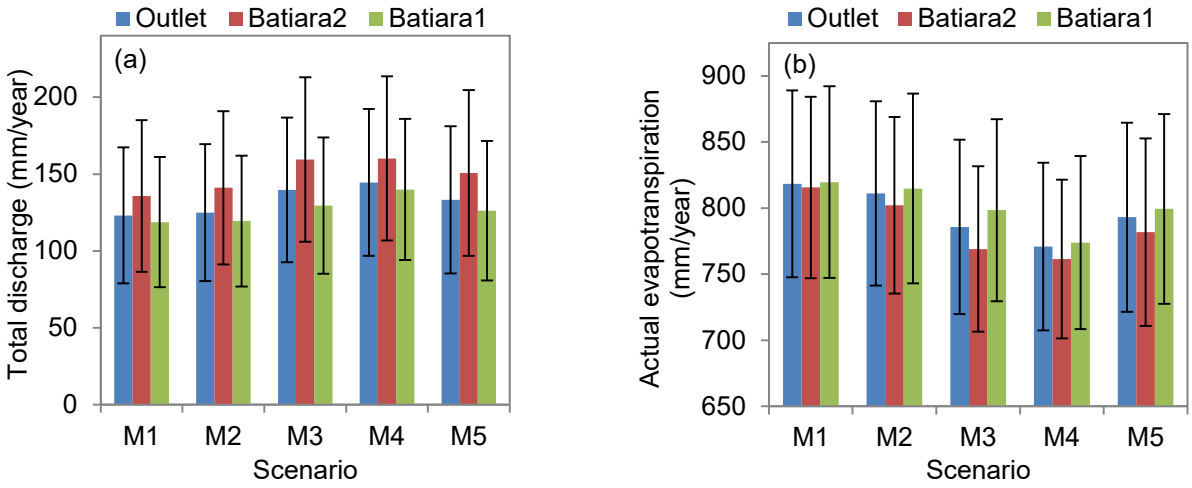

Fig. 7-6 Mean annual total discharge and actual evapotranspiration per sub-catchment and land use scenario. (a) scenarios are all statistically different. (b) scenarios M3, M4 and M5 were tested statistically different from the reference scenario M1. P-level =0.005. Error bars indicate the standard deviation.

The maximum percentage change in the total discharge approximates +17% for all three sub-catchments and is obtained by comparing the scenarios M1 and M4. The comparison of the same scenarios gives a change in ETa equaling -5%. The change in mean monthly discharge is used to assess the influence of LULC change on discharge dynamics. Fig. 7-7 suggests that the conversion from savannah to cropland has a higher impact towards the month of high precipitation (August). Hence, peak flows and high discharges increase with savannah degradation.

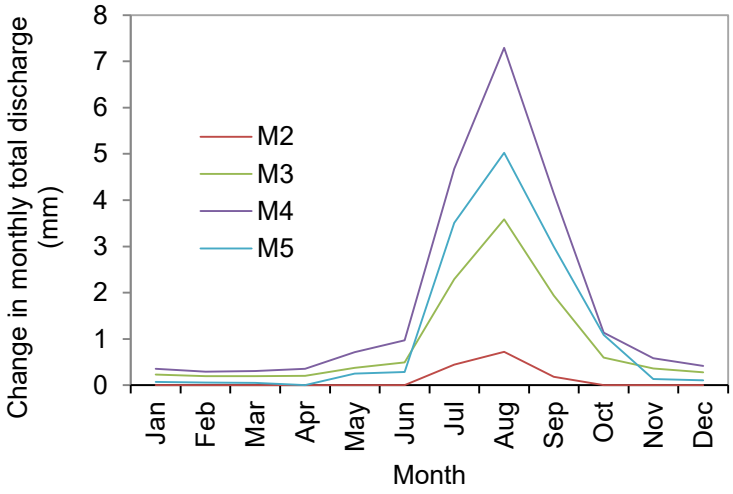

Fig. 7-7 Change in monthly total discharge for land use and land cover change scenarios M2, M3, M4 and M5 compared to the reference scenario M1 for the sub-catchment Batiara1. Values shown are computed using the average monthly values of the evaluation period (1997-2014).

Fitting the percentage of LULC classes to the corresponding simulated discharge through a linear regression (correlation coefficient R^2 = 0.7 and regression significance *p-value*<0.001), indicates that changes in the total discharge can be attributed to the changes of savannah and cropland areas (Fig. 7-8). Fig. 7-8 (b) shows that total discharge and percentage of savannah areas are negatively correlated and Fig. 7-8 (d) indicates that total discharge and cropland areas are positively correlated. Savannah was mainly converted to cropland; therefore increases in total discharge can be explained by the interplay between savannah depletion and cropland expansion.

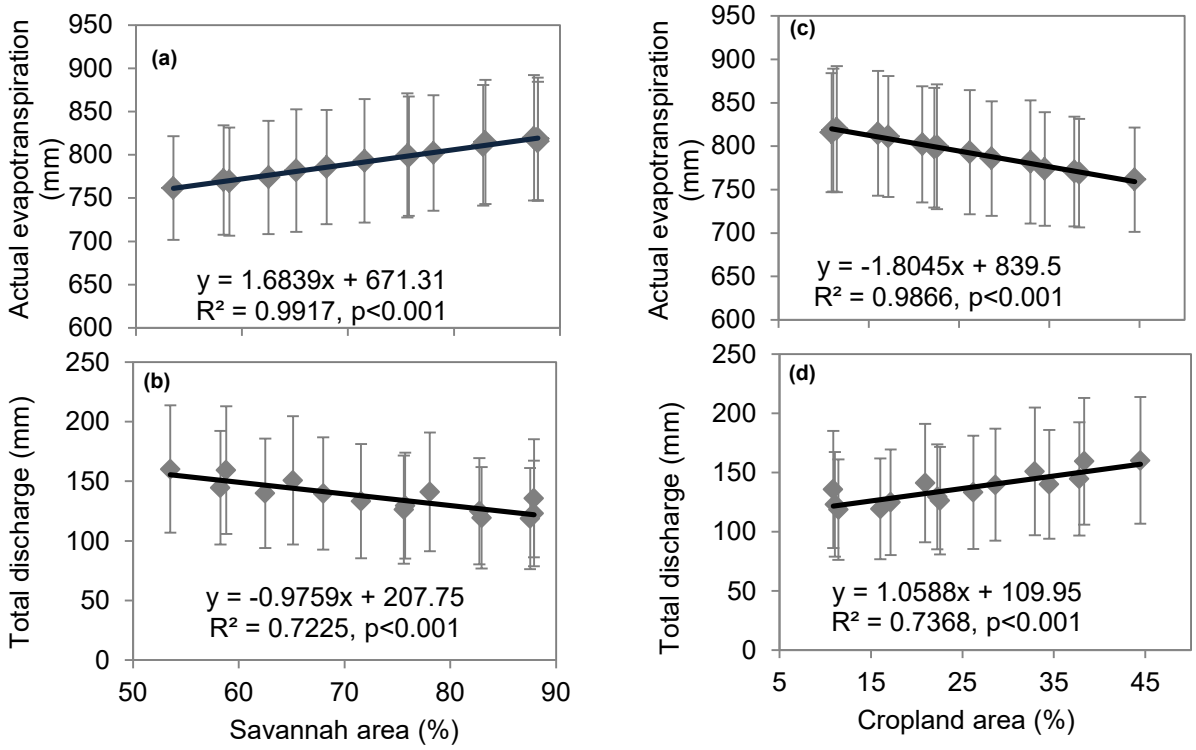

Fig. 7-8 Change in actual evapotranspiration and total discharge explained by the percentage of savannah and cropland areas. Error bars indicate the standard deviation.

Changes in the mean annual ETa can also be attributed to the conversion from savannah to cropland Fig. 7-8 (a & c) shows significant (*p-value*< 0.001) and strong correlations (R^2> 0.9) between savannah areas and ETa, and between cropland areas and ETa.
The increase of total discharge and decrease in evapotranspiration due to expansion of agricultural land is confirmed in several LULC impacts studies in the region (e.g. Awotwi et al., 2015; Cornelissen et al., 2013; Mahé et al., 2005).

7.5. Discussion

7.5.1. Land use and land cover change

The conversion rate of savannah to cropland for the investigated period in the Dano catchment equals 2% per year on average. This trend agrees with previous studies in the region (Descroix et al., 2009; Mahé et al., 2010; Zoungrana et al., 2015). However, this conversion rate is slightly lower than the results of 3.7% obtained by Paré et al. (2008) in the Sissili and Ziro provinces (≈100 km from Dano). They found

that the conversion rate from natural vegetation to cropland for the period 1986-2002 was highly correlated with the population growth (3.3% per year). The results achieved in the current study (a conversion rate of 2% per year for an annual population growth of 3%) are similar to their findings.

The farming system, which is characterized by subsistence farming (mainly in the form of shifting cultivation) and cash crop farming are also reported to be an important driver of land conversion. In the region, farm sizes for subsistence farming are reported to be consistently correlated with the population size (and thus with population growth), whereas cash crop farms do not follow this pattern (Paré et al., 2008). Cotton is the main cash crop in the Dano catchment and throughout the country. The production of cotton in Burkina Faso has increased by 370% from1990 to 2012 (FAOSTAT, 2015) and the catchment has experienced a similar expansion. The expansion of cotton areas did not only affect farm size but also farming practices with a notable increase in the use of fertilizers. Results of earlier studies (e.g. Lendres et al., 1992) highlighted the increase of maize yields in a cotton-maize rotation system due to the residual effects of the fertilizers used on cotton. This effect, which is well-known by the local farmers, has led to the expansion of cotton-maize rotation systems in the region. Ouattara et al. (2007) exhibited a loss in soil fertility in such a rotation system under intensive farming due to the depletion of soil organic carbon, wish lead to the reduction of soil productivity. Descroix et al. (2009) underline this reduction in soil productivity and land yields as an important factor of degradation of vegetation cover in West Africa.

A thorough analysis of the social and ecological system of the catchment is therefore required to understand the forces driving the degradation of savannah. An increase in crop yield, as it has been observed in the region during the last decades, buffers the expansion of cropland areas induced by population growth, whilst recent activities like gold mining increase the degradation rate of savannah. Descroix et al. (2009) highlighted the occurrence of droughts as an additional factor (resulting in the death of trees) that potentially drives LULC change. Moreover, the spatial pattern of savannah conversion (Fig. 7-9) implies that the whole catchment area is affected. This suggests an increasing pressure on marginal lands (like hillsides) and ecosystems.

The procedure of combining the initial individual LULC classes into a unique LULC classification permits to identify the major land use changes in the study area. However, some unlikely LULC changes have been noticed. This applies in particular to the conversion of urban areas and permanent water bodies to cropland or savannah. These may stem from (a) a misclassification of urban areas and water bodies in the initial maps, (b) the initial resolutions of the LULC map (250m resolution for instance discriminates scattered settlements of smaller size) and (c) different seasons (dry, wet) of the satellite images used in the initial LULC maps (Cord et al., 2010; Wagner et al., 2013).

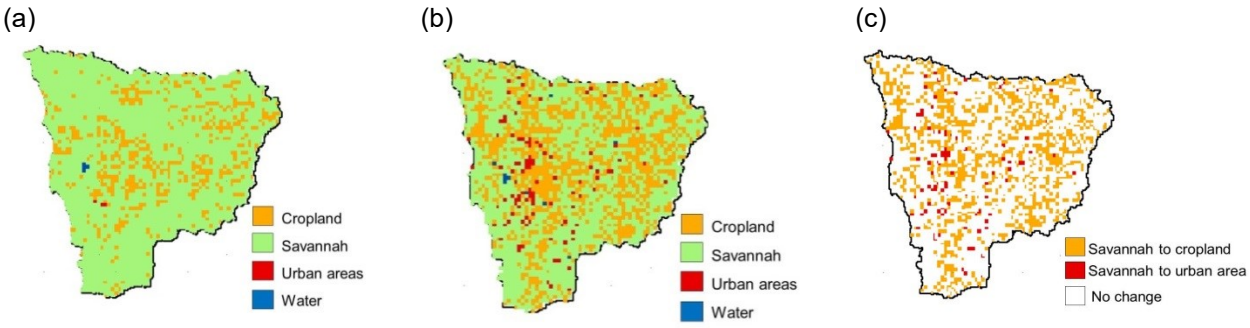

Fig. 7-9 Spatial pattern of land use and land cover (LULC) change: (a) LULC for the year 1990, (b) LULC for the year 2013, (c) LULC conversion between 1990 and 2013.

7.5.2. Hydrological modeling

Achieved model statistical quality measures are fair to good for the calibration and validation periods, indicating a good agreement between simulated and observed discharges for the three sub-catchments. However, the sub-catchment Batiara2 exhibits relatively low quality measures compared to Batiara1 and Outlet. The characteristic north/south gradient and the spatial variability of the rainfall in the catchment can partly explain this difference.

The agreement between simulated and observed groundwater level at piezometer3 appeared relatively low (R^2 equals 0.54, 0.66, 0.71 and 0.73 for Piezometers 3, 1, 2 and 4 respectively). Observed groundwater levels indicate that piezometer3 has a faster response time than the three other piezometers, suggesting a different hydraulic conductivity for the piezometer3 area. As the groundwater module was evenly parameterized for the entire catchment, the model did not properly capture the particular behavior of Piezomzter3.

Beside model imperfection, the discrepancy between observation scale (point) and modeling scale (spatial discretization of 90*90 m) has to be considered. Knowledge about soil properties at the local scale in the catchment is very limited, and although a macropore module is available in WaSiM, it could not be implemented due to data scarcity and limited knowledge. As the sensors (FDR-probes) used in the study measured soil moisture at the point scale, the measurements might be affected by local soil heterogeneity which is not considered in the modeling.

Several studies report the model to be sensitive to the interflow drainage density d_r and the storage coefficients K_D and K_H with respect to the modeled discharges (e.g. Cullmann et al., 2011, 2006; Reusser & Zehe, 2011; Singh et al., 2012). In WaSiM, the interflow drainage density d_r is a scaling parameter used to consider river density for the unsaturated zone. It linearly affects the amount of interflow (Schulla, 2014). Parameters k_D and k_H are storage coefficients and apply respectively to the surface flow and the interflow recession slope. Increase or decrease of these coefficients improves simulated peak flow discharges and recession periods.

7.5.3. Land use scenarios

The increase in water yield following the conversion of savannah to cropland is generally attributed to the increase of the *Hortonian* surface runoff. Giertz et al. (2005) observed that an increase in the fraction of agricultural land causes an increase in discharge. By comparing infiltration rates under savannah and cropland they found that the infiltration rate was significantly higher under savannah than under cropland and that a catchment dominated by cropland yields much higher discharge than a catchment dominated by savannah.

The observed increase in the total discharge in this study is also related to surface runoff. Surface runoff as well as interflow and baseflow increase with the degradation of savannah (Table 7-8). However, no infiltration rate dependent parameter was considered in the modeling approach and thus the infiltration rate cannot explain differences of total discharge or surface runoff observed between the five scenarios. The increase in surface runoff can rather be attributed to vegetation characteristics (*LAI*, vegetation cover fraction, stomata resistance, root depth etc.), which determine rainfall interception and evaporation capacity of a given LULC class. Donohue et al. (2007) demonstrated the important explanatory function of vegetation in catchment hydrology. They showed how dynamics of *LAI* and rooting depth of vegetation affect vegetation water use and therefore waterflow and water balance for catchments experiencing net vegetation change. The reduction of the interception capacity also explains the increase in interflow and baseflow as throughfall increases. Several studies (e.g. Beck et al., 2013; Leemhuis et al., 2007) support such an argument and attribute the increase of total discharge resulting from agricultural land expansion to a decline of *LAI*, root depth, vegetation height and stomata conductance. As a consequence, less

water is evaporated by interception, through fall increases and more water can infiltrate into the soil or flow as infiltration excess runoff. Moreover, the reduction of evapotranspiration leads to higher soil moisture contents and makes soils more responsive to rainfall.

Niehoff et al. (2002) showed that the influence of LULC conditions on surface runoff and high discharges depends greatly on the rainfall event characteristics and the related spatial scale. They highlighted that the influence of LULC is much more relevant for storm events with high precipitation intensities than long-lasting events with low precipitation intensities because of canopy interception. Moreover, high intensity rainfall events restricted to a small area have minor relevance for the formation of high discharges at a larger scale. This underlines the uncertainty in precipitation data as reported by Beck et al. (2013) to be a potential factor affecting the relation between LULC change and streamflow. Historical climate data time series for the Dano catchment were only available on a daily basis at the Dano climate station. Hence rainfall events were already averaged to daily scale, and the small scale spatial variability in rainfall was not observable due to a limited density of rainfall stations. Daily aggregation of rainfall reduces the maxima of rainfall intensities and leads to an underestimation of infiltration excess overland flow as this process mainly depends on rainfall intensity and soil infiltration rate. Therefore, the simulated surface runoff for all scenarios might have been underestimated due to the time step used in the study.

Table 7-8 Mean annual water balance per sub-catchment for the five land use scenarios.

	M1	M2	M3	M4	M5
Outlet					
Rainfall (mm)	943.7	943.7	943.7	943.7	943.7
Potential evapotranspiration (mm)	2108	2092	2044	2013	2054
ETa (mm)	818.4	811.1	785.8	773.9	793.1
Total discharge (mm)	123.1	130.4	155.7	167.6	148.4
Surface Runoff (mm)	58.4	62.3	72.9	78.9	70.2
Interflow (mm)	62.3	66.6	73.3	78.9	73.2
Baseflow (mm)	2.3	1.5	9.4	9.8	6.0
Runoff coefficient (%)	13.0	13.8	16.5	17.8	15.7
Batiara2					
Rainfall (mm)	951.4	951.4	951.4	951.4	951.4
Potential evapotranspiration (mm)	2109	2077	2008	1996	2031
ETa (mm)	815.6	806.8	769.1	761.5	781.8
Total discharge (mm)	135.7	141.1	159.4	160.2	150.8
Surface Runoff (mm)	72.3	75.1	84.2	84.8	79.7
Interflow (mm)	62.8	65.7	69.8	71.1	68.6
Baseflow (mm)	2.1	1.3	6.9	6.5	4.6
Runoff coefficient (%)	14.3	14.8	16.8	16.8	15.8
Batiara1					
Rainfall (mm)	952.8	952.8	952.8	952.8	952.8
Potential evapotranspiration (mm)	2060	2084	1997	2023	2036
ETa (mm)	819.7	802.1	798.4	770.8	799.4
Total discharge (mm)	118.7	119.4	129.5	140.0	126.2
Surface Runoff (mm)	52.3	53.0	56.9	61.5	55.7
Interflow (mm)	63.1	64.3	64.9	68.2	65.7
Baseflow (mm)	1.8	1.1	5.6	5.7	3.8
Runoff coefficient (%)	12.5	12.5	13.6	14.7	13.2

7.6. Conclusion

This study evaluated the impacts of ongoing land use and land cover change on water resources in the Dano catchment using hydrological simulations and land use scenarios. The investigations showed that:

(i) the main LULC change in the catchment was conversion of savannah to cropland and settlements. This result is consistent with previous studies carried out in the region. A degradation rate of 2% per year was found for the savannah. The observed agricultural land expansion did not exhibit a clear spatial pattern as the newly cropped areas are scattered over the entire catchment area. Such a trend suggests that marginal lands like hillslopes, which until now were only partially influenced by the conversion process, will undergo important changes. The aggregation of LULC classes from different products was an important source of uncertainty in land use change assessment, and requires future works to consider maps derived from comparable products;
(ii) overall, good representations of total discharge, soil moisture and groundwater dynamics were achieved by the model. The multivariate validation approach used in the study increases the confidence in the model results. Shortcomings were limited data of the soil moisture dynamic for the deep horizons and some peak flows that could not be well captured by the model due to limited knowledge about soil properties and limitations in discharge measurement techniques;
(iii) an increase in total discharge following the degradation of savannah was found. The discharge dynamic and discharge components analysis further indicate that the increase of total discharge is related to high flows. Therefore, the catchment is likely to experience important changes in flood frequency. Changes in transport of sediments and nutrients from land to streams can also be expected.

Soil physical alterations due to LULC change were not included in this study; therefore it is most likely that the hydrological model underestimates the increase of total discharge and surface runoff due to LULC change. Moreover, it has to be noted that part of the increase of the water yield as well as surface runoff was caused by the expansion of urban areas. Settlements cover only 3% of the catchment, which does not permit to clearly identify impacts on the water balance.

Further investigations should integrate the alteration of soil properties in the modeling exercise. This requires not only field investigations with regard to LULC impacts on soil properties, but also the availability of observed climate and hydrological variables at a suitable spatial and temporal scale for a better representation of the hydrological processes. Moreover, climate and LULC change occurs simultaneously and investigations towards a clear distinction of their respective impacts still need to be carried out.

8. SENSITIVITY TO SOIL PARAMETERIZATION AND MODELING TIME STEP IN LAND USE CHANGE IMPACT ASSESSMENT

8.1. Introduction

Land use and land cover (LULC) change impact on water resources was analyzed in chapter 7 using four land use maps corresponding to different levels of savannah degradation in the Dano catchment. The results indicated that the replacement of savannah by cropland influences actual evapotranspiration, annual discharge and discharge components. Greater water yield under the most degraded land use status (year 2013) was attributed to decreased vegetation coverage, leaf area index, root depth, vegetation height and stomata conductance, resulting from the degradation of the savannah. The increase in water yield represented about 17% compared to the baseline period (years 1990).

The lack of long term hydrologic and meteorological observation time series data at a finer time scale than daily supported the parameterization of the model at a 24 hour time step. Accordingly, the results achieved in chapter 7 underlined a potential underestimation of surface runoff, specifically the *Hortonian* overland flow as a consequence of the misrepresentation of rainfall intensities. To further evaluate this result, investigations with observed climate and hydrological variables at a finer spatial and temporal scale were suggested; hypothesizing that the use of high temporal data leads to better model results (Andréassian et al., 2001; Finnerty et al., 1997; Foufoula-Georgiou & Georgakakos, 1991).

Soil infiltration rate was considered to be independent of land use in the hydrological modeling exercise as performed in chapter 7. As shown in chapter 6, soil infiltration rate *(Ks*) is significantly higher under fallow and savannah compared to cropland. Changes in soil infiltration rate potentially affect rain water partitioning at the soil surface. Therefore, integrating the influence of land use on soil infiltration rate into the assessment of land use change impacts on water resources can potentially cause a shift in the terms of water balance and discharge components (Bormann et al., 2007). The direction and magnitude of the shift involve both environmental components (such as rainfall intensity and duration) and modeling scale issues (Krajewski et al., 1991). As hydrological processes operate at different time (and spatial) scales - from very fast response for *Hortonian* overland flow to slower responses for saturation overland flow, subsurface flow, groundwater-controlled flow etc. (Blöschl & Sivapalan, 1995) -, a shift in modeling time scale is generally assumed to potentially affect processes representation and therefore influence modeling outcomes.

The availability of climate and hydrologic variables at an hourly time scale for the period 2013-2014 and field evidences of land use impacts on soil infiltration rate provide the opportunity to assess the importance of considering land use dependent soil properties in the hydrological modeling, while integrating time scale effects on the result. A modeling exercise incorporating knowledge gained from field investigations with regards to land use impacts on soil infiltration rate may require additional parameterization effort, but the method has proven to improve hydrological processes representation (Hölzel & Diekkrüger, 2010).

The current chapter addresses the importance of integrating the influence of land use on soil infiltration rate into land use change impact assessment. It aims to analyze how soil parameterization and modeling time step could affect the results achieved in land use change impact assessment (chapter 7). It has the following specific objectives: (i) assess the sensitivity of the hydrological simulation model to land use related effect on soil infiltration rate, (ii) assess the consequences of integrating land use related effect on soil infiltration rate in LULC impact assessment, and (iii) to evaluate whether the importance of integrating land use related effect on soil infiltration rate in the modeling exercise depend on the modeling time step.

8.2. Methods

8.2.1. Field investigations

A hood infiltrometer (Schwärzel & Punzel, 2007) was used for soil infiltration rate measurements (chapter 6). The Infiltration tests were performed on adjacent cropland-savannah plots following transect lines. Measurements showed an on average (1.16-fold) higher *Ks* under savannah compared to cropland, with a wide variation of *Ks* under both land use types (Table 8-1). Alongside with the infiltration measurement, undisturbed topsoil (1-10 cm) core samples and composite topsoil samples were collected to analyze the physical and chemical properties. Contrary to infiltration rate, no significant difference between cropland and savannah could be observed for soil texture, bulk density (*BD*), organic carbon (*Corg*) and coarse particles content (Table 8-1).

Table 8-1 Statistics of soil properties under cropland and savannah.

Variable	Cropland					Savannah					Cropland vs Savannah
	Mean	SD	Min	Max	n	Mean	SD	Min	Max	n	t-test p-value
Ks (cm/d)	433	506	17	2048	42	568	535	69	2445	42	NA
Log_{10} *Ks* (cm/d)	2.3	0.5	1.2	3.3	42	2.6	0.3	1.8	3.3	42	**0.007**
Sand (%)	37.7	8.83	21.05	53.47	21	35.59	10.38	14.69	51.26	21	0.4
Clay (%)	20.5	9.3	4.69	37.3	21	22.08	7.12	13.77	34.86	21	0.5
Bulk density (g/cm^3)	1.4	0.12	1.2	1.75	21	1.4	0.14	1.14	1.60	21	0.9
Coarse particles (%)	43.2	27.7	0.8	84.96	21	53.21	29.38	0.0	89.70	21	0.2
Corg (%)	1.3	0.6	0.3	3.3	21	1.4	0.6	0.1	2.7	21	0.6

NA: not applicable due to skewness, *SD*: standard deviation, n: sample size.

8.2.2. Land use change

The land use and land cover (LULC) maps after Forkour (2014) and Landmann et al. (2007) corresponding to LULC status for the years 2013 and 1990 respectively, were used for LULC change impact assessment. The reclassified version of both maps was used, and the year 1990 was considered as baseline. Differences in land classes between the two LULC maps are summarized in Table 8-2 and the difference in interception is addressed in section 8.3.3.

Table 8-2 Percentage of the catchment area per land use class in 1990 and 2013

Land use class	**years**	
	1990	**2013**
Cropland (%)	11.6	38
Savannah (%)	87	58
Water (%)	0.05	0.05
Urban area (%)	1	3

8.2.3. Soil map refinement

The soil infiltration rate is parameterized in WaSiM through the soil map and soil classes' characteristics, while no infiltration rate dependent parameter is associated with this parameterization. Following the results of field investigation that revealed significant difference between *Ks* under cropland and savannah (section 8.2.1), it becomes possible to integrate this additional knowledge in the modeling exercise. The method applied by Hölzel & Diekkrüger (2010) was adopted to address this issue. The method can be summarized in the following three steps:

- cropland and savannah areas were separated from the land use maps of the investigation area;
- *ArcMap combination* function was used to overlap the cropland and savannah units on the classic soil map (CS). The result is a refined soil map (RS) exhibiting the original soil classes with additional qualifier for cropland and savannah;

- a ratio of the measured infiltration rates under cropland and savannah was applied to the parameterization of soil units under each land use type. A refined $K_{s_{x_i}}^{ref}$ for each land use type is calculated fallowing Eq. 8-1.

$$K_{s_{x_i}}^{ref} = K_{sat}{}^{map} * \frac{\widehat{K}_{s_{x_i}}^{meas}}{\widehat{K}_{s_x}^{meas}} \quad \text{Eq. 8-1}$$

Where $\widehat{K_s}$ is the mean of the infiltration rate, x refers to all samples, x_i is the samples of the specific area (cropland or savannah), ref refers the refined values, $meas$ refers to measured values, and map indicates the initial values given by the classic soil map (as used in chapter 7).

The reference basis for *Ks* was provided by the *Ks* values from the classic soil map (CS), which were derived from laboratory measurements for each soil type and different soil horizons following Saxton & Rawls (2006). However, the refinement was performed solely to the top first soil horizon as the hood infiltration applies only to the topsoil. As two distinct land use maps (1990 & 2013) were used in this study (see next section), the refinement procedure was applied using both.

8.2.4. Modeling approach and simulation experiment

Version 9.05.04 of WaSiM, calibrated and validated at a daily time step using a classic soil parameterization and the LULC map of 2013 (more details in chapter 7) is used as the initial model in this chapter.
Simulation experiments were performed considering three factors:

- ***land use change***. The LULC maps of years 1990 (***LU1990***) and 2013 (***LU2013***) are used as land use change scenarios,

- ***soil parameterization.*** The soil parameterization integrating LULC dependent soil infiltration rate (Refined soil-***RS***), and the classic soil-***CS*** parameterization are used,

- ***modeling time step.*** The available climate and hydrologic data sets of sub hourly resolution were averaged stepwise to higher temporal resolution of ***8***, ***12***, ***24*** and ***48 hours***. These aggregated temporal data were used.

Overall, 16 models were set up combining these three factors (Table 8-3). The fitted calibrated parameters of the initial model were kept constant for all the simulations experiments. A change of model statistical quality measures due to time scale and soil parameterization changes was preferred to a multiple calibration approach which would not provide common basis for the different simulations experiments. Average water balance components (ETa, total discharge, surface runoff, interflow, baseflow,) were compared between different model set ups.

Table 8-3 Combined land use scenarios, soil parameterizations and time scales experiments.

	Classic soil (***CS***)				Refined soil (***RS***)			
Land use status 2013 (***LU2013***)	CS_LU2013_8h	CS_LU2013_12h	CS_LU2013_24h	CS_LU2013_48h	RS_LU2013_8h	RS_LU2013_12h	RS_LU2013_24h	RS_LU2013_48h
Land use status 1990 (***LU1990***)	CS_LU1990_8h	CS_LU1990_12h	CS_LU1990_24h	CS_LU1990_48h	RS_LU1990_8h	RS_LU1990_12h	RS_LU1990_24h	RS_LU1990_48h
	8	***12***	***24***	***48***	***8***	***12***	***24***	***48***
	Time scale (hours)				Time scale (hours)			

8.2.5. Comparison of land use and soil parameterization effects

The "signal-to-noise-ratio" (*SNR*) (Bormann, 2005; Bormann et al., 2009) was adapted to compare LULC change effects with soil parameterizations effects (Eq. 8-2). In this study, the "noise" is represented by soil parameterization effect, and "signal" is represented by land use change effect. The *SNR* indices were also interpreted after Bormann et al. (2009): *positive* SNR values indicate that the land use change effects are larger than soil parameterization effects. Values larger than 1 are called *high* SNR values and are deemed to indicate a sufficient suitability of a model for a given case study (soil parameterization effect negligible). *Negative SNR* values imply in this study, that soil parameterization effect is larger than land use change effect.

$$SNR = \left[\frac{\left|X_{CS\_LU1990} - X_{CS\_LU2013}\right|}{\left|X_{CS\_LU1990} - X_{RS\_LU1990}\right|}\right] - 1 \qquad \text{Eq. 8-2}$$

Where SNR is the "signal-to-noise-ratio", X is the simulated variable (discharge, ETa, etc.).

8.3. Results and discussion

8.3.1. Soil Maps

The initial soil map (*CS,* Fig. 8-1 A) of the study area had 21 soil components. Soil refinement has yielded in 60 and 63 refined components for “combined initial soil map+LULC1990” and “combined initial soil map+LULC2013” respectively (Fig. 8-1 B & C). The units *Lixic Gleysol, Lixic Stagnosol* and *Plinthic Cambisol* are only found in Fig. 8-1 B, while these units are associated to either cropland or savannah in Fig. 8-1 C. Inversely, *Endopetric plinthosol, Gleyic plinthosol, Stagnic Cambisol and Stagnic cambisol* units are found only in Fig. 8-1 C, and are associated to cropland or savannah in Fig. 8-1 B. These differences between Fig. 8-1 B & C exclusively stem from the difference in the spatial pattern of cropland and savannah between LULC2013 and LULC1990.

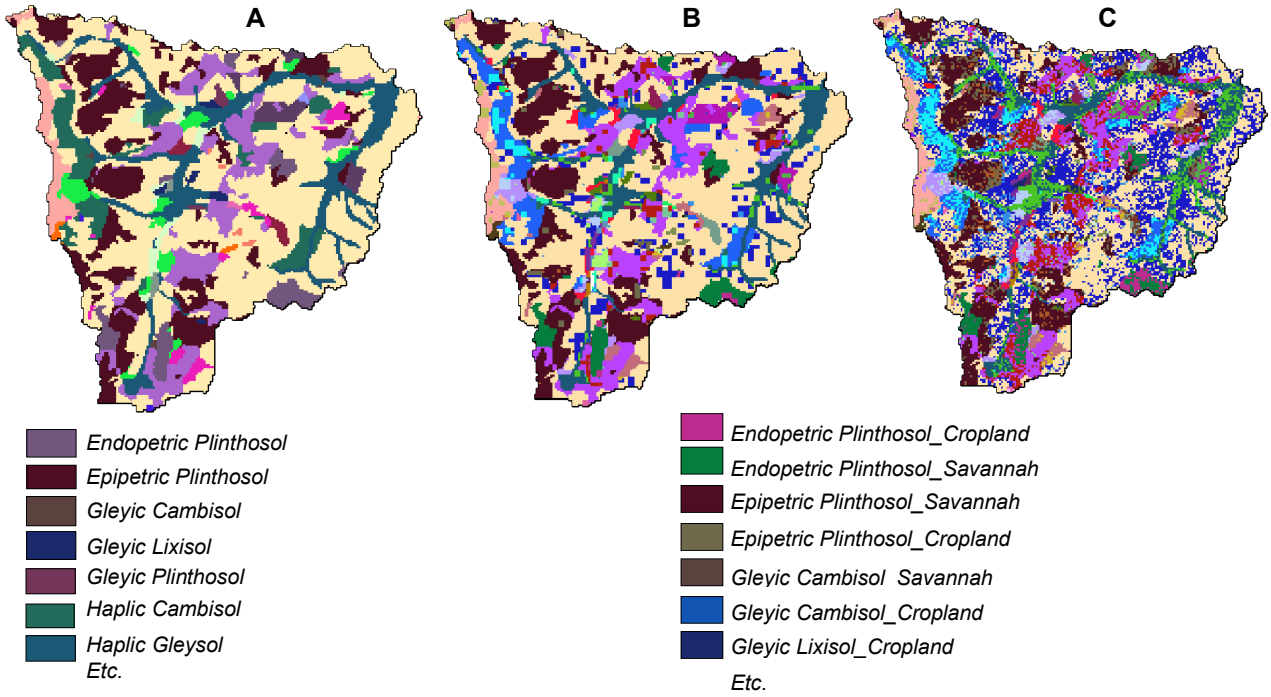

Fig. 8-1 Soil maps used in the modeling exercise: A) Classic soil map (*CS*), B) Refined soil map using the LULC map of 1990 (*RS*) and C) Refined soil map using the LULC map of 2013 (*RS*).

8.3.2. Modeling time step and model performance

The initial model, calibrated and validated at a daily time step using a classic soil parameterization and the LULC of 2013 (CS_LULC2013_24h), and the other seven model set ups using the same LULC map but different soil parameterizations and time steps (see Table 8-3) are compared to observed discharge in order to relate change in model performance to soil parameterization and time step (Fig. 8-2). The annual variation of discharge appears well reproduced by each model set up, although difference in simulated peak discharges can be noticed (Fig. 8-3). Good model quality measures are achieved as well, although slight differences from one model set up to another can be noticed. However, these differences do not systematically imply a deterioration of model performance as shown by simulations performed at a 48 hour time step which in general outscore the initial model (CS_LULC2013_24h). A readily observable difference between model set ups is a decreasing total discharge and peak flow with increasing modeling time step.

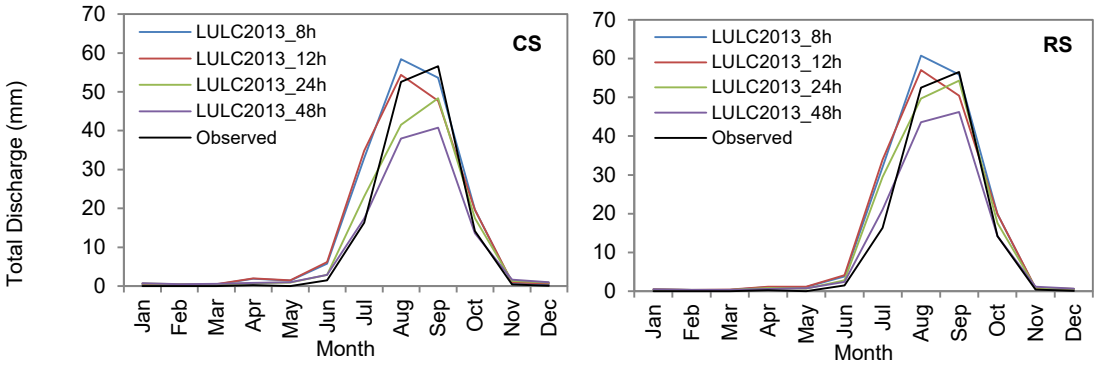

	CS				RS			
	8h	12h	24h	48h	8h	12h	24h	48h
R^2	0.90	0.83	0.94	0.98	0.92	0.87	0.93	0.97
NSE	0.92	0.90	0.95	0.90	0.93	0.91	0.96	0.96
KGE	0.69	0.69	0.82	0.76	0.71	0.72	0.82	0.86

Fig. 8-2 Model performance using different modeling time steps and soil parameterization approaches. Period of Jan-2013 to Dec-2014. Performance is calculated using mean monthly discharges.

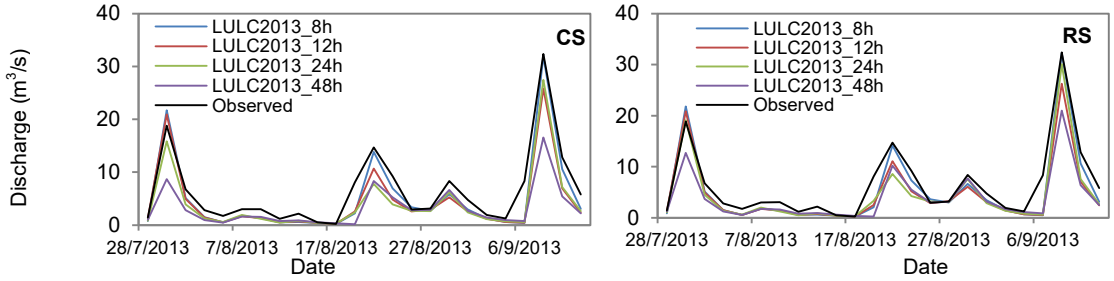

Fig. 8-3 Peak discharge simulation by different modeling time steps and soil parameterizations.

Soil refinement appears beneficial to all simulations performed at 8, 12 and 48 hour time steps irrespective of the considered model statistical quality measure; this may suggest that refined *Ks* is more *effective* than classic *Ks*. However, at the 24 hour time step, classic soil (CS) outscores refined soil (RS) for Pearson product-moment-correlation-coefficient. Notwithstanding a general increased model statistical quality measures with increased modeling time step, increasing the modeling time step cannot be interpreted as an approach towards model quality improvement. This mainly stems from the fact that the calibration strategy followed to set up the initial model (CS_LULC2013_24h) was driven by the modeling time step (24 hours). Calibrated parameters are likely to be different when other modeling time steps are chosen. Importantly, comparison between models reassures that each model set up irrespective of time step and soil parameterization performs well despite using parameter set calibrated for 24 hours time step and the classic soil map.

8.3.3. Modeling time step and water balance

Results of modeling of the time step effect on water balance components are shown in Fig. 8-4. Trend in water balance components with increasing modeling time step under land use status of 2013 and 1990 are very similar: (i) an increase of actual evapotranspiration, (ii) a decrease in total discharge, (iii) a decrease in surface runoff, (iv) an increase in baseflow, (v) a decrease in interception, and (vi) an increase followed by a decrease for interflow. The comparison of red and green histograms for the same time step shows the effect of soil parameterization on discharge components. For all simulation time steps, total discharge and discharge components clearly appear sensitive to soil parameterization.

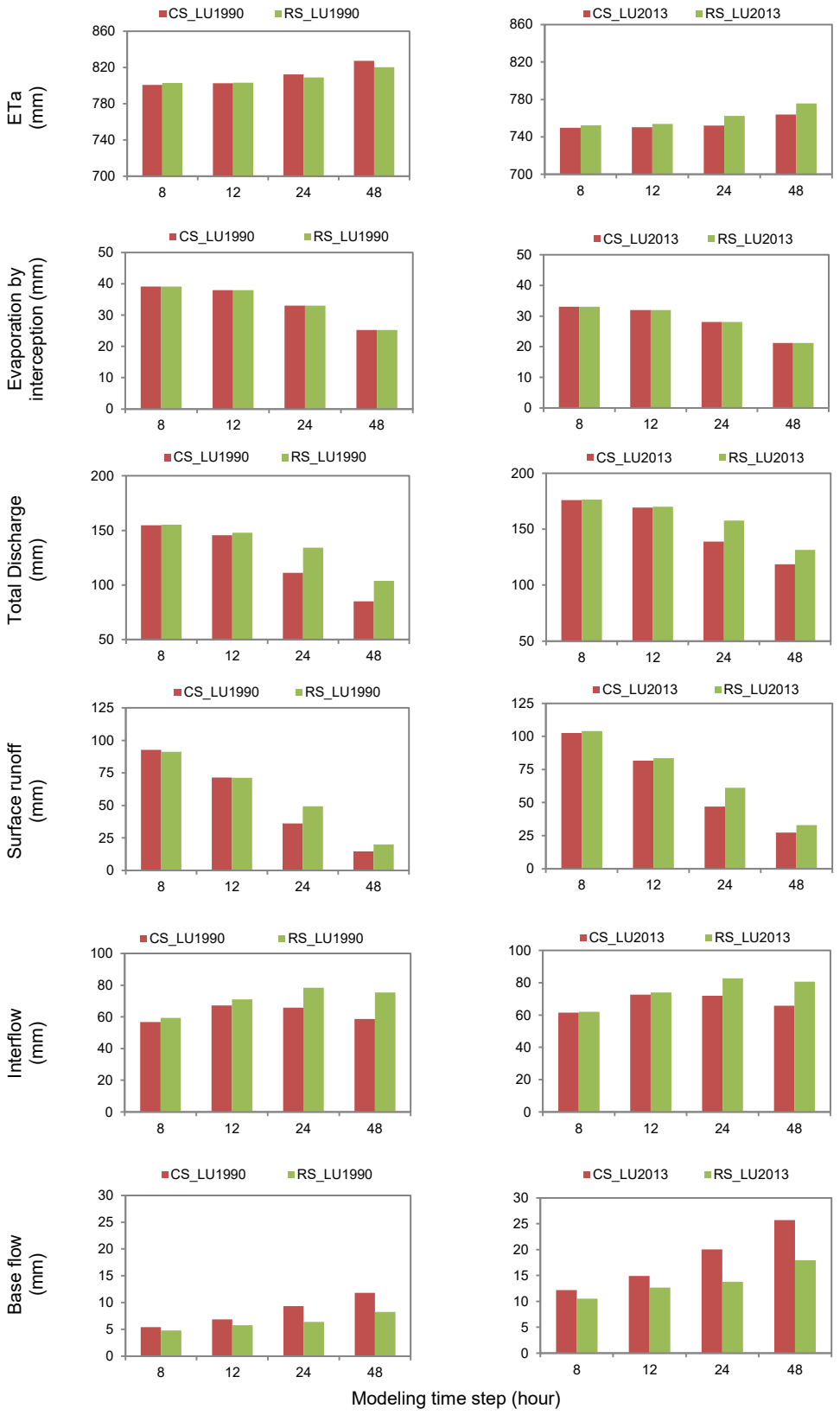

Fig. 8-4 Annual water balance components for different modeling time steps and soil parameterization approaches for the period of Jan-2013 to Dec-2014.

Difference in water balance due to LULC change (between 1990 and 2013) has been largely discussed in chapter 7. Consequences of LULC conversion from year 1990 to year 2013 are the reduction of *LAI*, vegetation cover fraction, root depth etc. which leads to the increase of throughfall and the reduction of water that is evaporated by interception. Therefore, more water can infiltrate into the soil or flow as infiltration excess runoff. Interflow and baseflow increase with throughfall.

Chapter 7 also suggested the difference in water balance with modeling time step to be potentially related to the aggregation of rainfall data from sub-daily to daily time step as maximum rainfall intensities decrease with an increment of rainfall aggregation time step (Bruneau et al., 1995). In WaSiM, surface runoff generation only depends on rainfall amount (per time step) and the upper most soil layer moisture deficit. However, drainage of the upper layer influences soil moisture deficit and this depends on *Ks*. While sub-daily high precipitation are likely to exceed the drainage rate of the upper layer and therefore generate more surface runoff, aggregation of precipitation to daily time step leads to drainage amount higher than precipitation.

Change in the water balance between classic soil and refined soil parameterization has to be interpreted solely by the difference in hydraulic conductivity at the soil surface, as this is the only difference between CS and RS. Change in hydraulic conductivity at the uppermost numerical soil layer due to soil refinement leads CS and RS to partition throughfall differently which affects surface runoff generation and water balance. As mentioned above, this is done indirectly through the drainage rate of the upper most soil layer.

Conversely to the infiltration, while decreasing the modeling time step, the model favors the interception as shown by the amount of precipitation evaporated by interception (Fig. 8-4) leading to a decrease of net precipitation. A simple bucket approach is used to simulate interception and the extraction of water out of the interception storage by evaporation is done at the potential rate (*ETp*). Sub daily time step rainfall events are repeatedly intercepted for a simulation done at a sub daily time step, whereas a daily time step simulation leads two events occurring the same day to be intercepted once.

8.3.4. Soil refinement and land use change impact

Fig. 8-5 presents the change in the water balance components due to LULC change (LULC of 1990 compared to LULC of 2013) following a classic soil parameterization (Fig. 8-5 a) and a refined soil parameterization (Fig. 8-5 b). A very comparable decrease in actual evapotranspiration and an increase in discharge (all components) characterize LULC change impacts for both soil parameterization approaches. However, differences in the water balance components between soil parameterization approaches can be noticed as shown by Fig. 8-5 c. These differences vary with the modeling time step and water balance component. A LULC change impact assessment performed with a classic soil leads to a higher decrease in *ETa* compared to an assessment performed with a refined soil; this difference appears to further increase with the modeling time step. Increase in surface runoff following LULC change is higher with the RS than the CS. Furthermore, the difference in surface runoff between RS and CS decreases with the modeling time step. Simulated change in total discharge, baseflow and interflow following LULC change are lower with the refined soil compared to the classic soil.

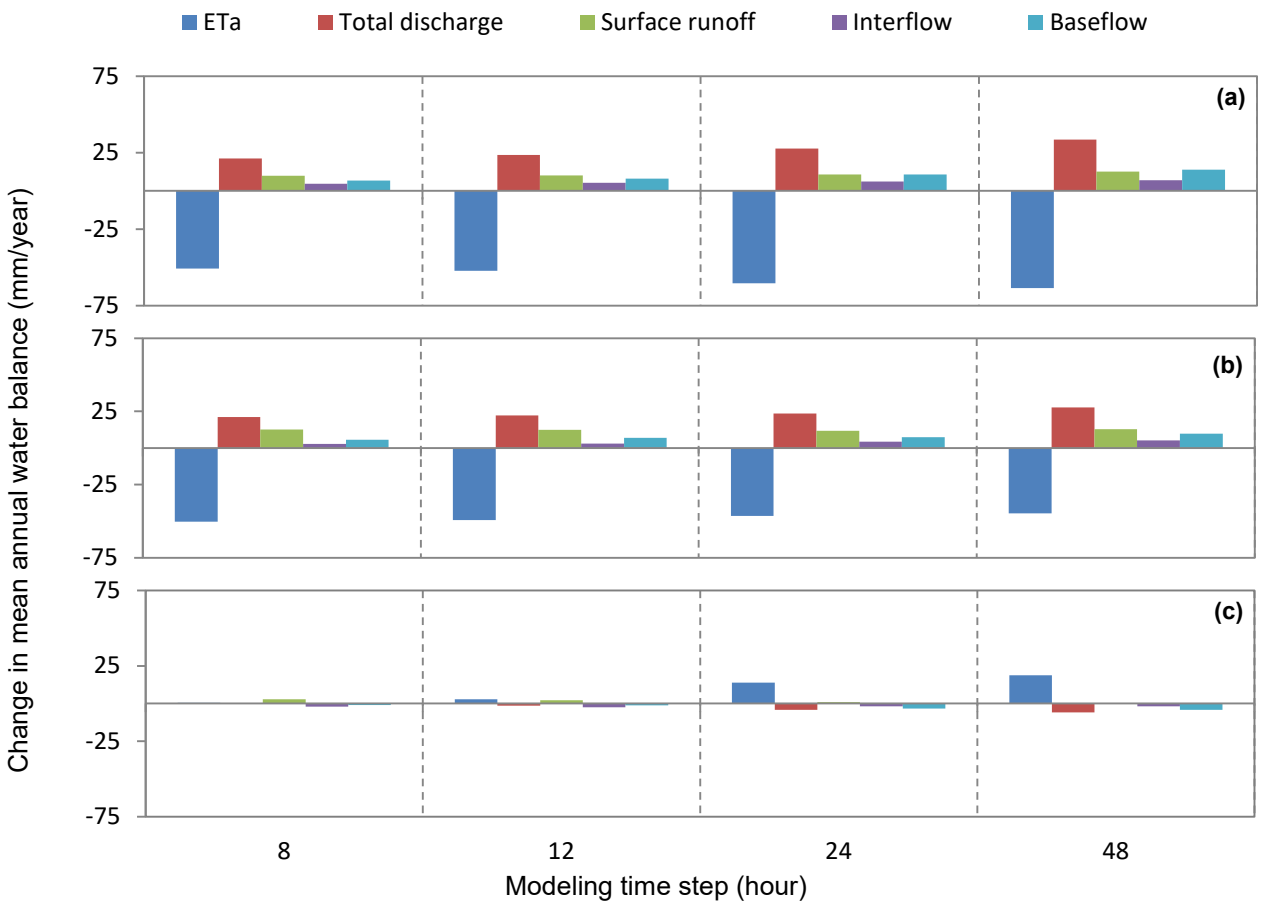

Fig. 8-5 Change in water balance as a result of LULC change, modeling time step and soil parameterization. Part *(a)* compares LULC1990 to LULC2013 using a classic soil-CS, part *(b)* compares LULC1990 to LULC2013 using a refined soil-RS, and *(c)* shows the difference between soil parametrization approaches (*b*-*a*).

It can be deduced from Fig. 8-5 (c) that irrespective of modeling time step, a LULC change impact assessments performed with a refined and classic soil parameterization do not yield in the same water balance. Differences range from 0.2 to 18 mm/year depending on water balance components. As soil properties change associated with LULC change are supported by field evidences, it is worth considering this additional information since it makes LULC change scenarios more plausible (Bormann et al., 2007). Fig. 8-5 further indicates that simulated changes in water balance due to LULC change are larger than the change due to soil parameterization, suggesting that soil refinement might have a marginal impact in LULC impact assessment.

The signal-to-noise-ratio (*SNR*) is calculated to test whether the LULC change effect is significantly larger than the soil refinement effect. Table 8-4 shows both positive and negative *SNR*. Except interflow, all water balance components show positive *SNR*, indicating that LULC change impact is larger than soil refinement, meaning the noise created by soil refinement does not affect LULC change signal. In other words, results achieved in LULC impact assessment with both soil parameterizations (CS and RS) are very comparable except for interflow. Noise is larger than signal only for simulations performed at 24 and 48 hours, even though this noise is low. Therefore, an LULC impact assessment focusing on discharge components is necessary using a refined soil as omitting this information produced an effect higher than LULC scenario effect.

Table 8-4 Signal-to-noise ratio for different modeling time steps. Signal refers to LULC change effect, and noise is soil refinement effect.

	Signal to noise ratio				
Modeling time step (hour)	Actual evapotranspiration	Total discharge	Surface runoff	Interflow	Base flow
8	22.91	39.83	5.94	0.82	9.61
12	69.76	9.35	27.51	0.42	6.20
24	17.18	0.20	0.07	-0.52	2.63
48	8.13	0.81	1.34	-0.58	2.86

8.4. Conclusion

In this chapter land use change related effects on soil infiltration rate was integrated in the modeling of LULC change impact on the Dano catchment hydrology. Field investigation showed that soil surface hydraulic conductivity was significantly affected by land use. This additional information was integrated in the modeling as refined soil (RS), and was compared to a simulation ignoring this information (CS). Modeling time step was further considered as a potential factor affecting the model outputs. Several models were then set up combining soil parameterization, modeling time step, and LULC change.

Although WaSiM was initially calibrated for *24 h* time step simulations using a classic soil, the different model set ups (with no additional calibration) show good performance for all simulation time steps (*8* to *48 h*) and soil parameterizations. Therefore the sensitivity of the model to modeling time step and soil parameterization was carried out using model set ups potentially applicable for LULC impact assessment.

Trends in water balance and discharge component change following LULC change was similar for classic and refined soil parameterization irrespective of the modeling time step. However, slight differences in model results could be observed between soil parameterization approaches, indicating that the model is sensitive to the integration of LULC related effects on soil hydraulic conductivity. This supports the idea that integrated land use related effects on soil properties renders LULC change scenarios more plausible.

However, effects of LULC change appear larger than soil refinement effects for the water balance, as confirmed by positive *SNR* indices. Exceptionally, for interflow the soil refinement effect was larger than the LULC effect for some modeling time steps, implying that a consistent assessment of LULC change impact on interflow (and consequently, on discharge components) should integrate LULC related effects on soil properties.

Finally, it is worth noting that the primary aim of this chapter was to evaluate whether integrated LULC related effects on soil hydraulic conductivity in the modeling would yield in results different from those achieved in chapter 7 (*24h* time step, and classic soil). One can conclude that the reported trends in water balance would be the same, but water balance and discharge components values would show differences ranging from 0.9 to 19 mm/year. However, these differences are modeling time step dependent. Reducing the modeling time step from 48h to 8h leads to an increasing positive bias of simulated discharge as the model was calibrated for 24h time step simulation. Due to this bias, the minimum simulation time step was kept to 8h. As 8h modeling time step is larger than the infiltration process time scale, different results might by achieved with experiments performed at a finer time scale. Lastly, spatial resolution was kept constant in this exercise, as it is an additional factor influencing WaSiM sensitivity to LULC change (Bormann et al., 2009), one may expect this to affect the general results.

9. IMPACT OF CLIMATE CHANGE ON WATER RESOURCES[1]

Abstract

This chapter evaluates climate change impacts on water resources using an ensemble of six Regional Climate Models (RCMs)-Global Climate Models (GCMs) in the Dano catchment (Burkina Faso). The applied climate datasets were performed in the framework of the COordinated Regional climate Downscaling Experiment (CORDEX-Africa) project.
After evaluation of the historical runs of the climate models ensemble, a statistical bias correction (*Empirical Quantile Mapping*) was applied to daily precipitation. Temperature and bias corrected precipitation data from the ensemble of RCMs-GCMs was then used as input for the Water flow and balance Simulation Model (WaSiM) to simulate water balance components.
The mean hydrological and climate variables for two periods (1971-2000 and 2021-2050) were compared to assess the potential impact of climate change on water resources up to the middle of the twenty-first century under two greenhouse gas concentration scenarios, the Representative Concentration Pathways (RCPs) 4.5 and 8.5. The results indicate: (i) a clear signal of temperature increase of about 0.1 to 2.6 °C for all members of the RCMs-GCMs ensemble; (ii) high uncertainty about how the catchment precipitation will evolve over the period 2021-2050; (iii) individual climate models show opposite discharge change signals; (iv) the RCMs-GCMs ensemble average suggests a +7 % increase in annual discharge under RCP4.5 and a -2 % decrease under RCP8.5; (v) the applied bias correction method only affected the magnitude of climate change signal. Therefore, potential increase and decrease of future discharge has to be considered in climate change adaptation strategies in the catchment. The results further underline on the one hand the need for a larger ensemble of projections to properly estimate the impacts of climate change on water resources in the catchment and on the other hand the high uncertainty associated with climate projections for the West African region. An ecohydrological analysis provides further insight into the behavior of the catchment.

Keywords: Hydrological modeling, RCP, bias correction, West Africa, Ecohydrological analysis, WaSiM.

9.1. Introduction

Development of adaptation strategies to deal with potential impacts of climate change on hydrological systems is a considerable challenge for water resources management (Muerth et al., 2013; Piani et al., 2010). Besides being highly exposed to climate change, the West African region presents a low adaptive capacity (IPCC, 2014). Projections for the late 21st century suggest severe consequences of climate change on water resources for the region. This includes an increased risk of water stress and flood (Sylla et al., 2015; Oyerinde et al., 2014), and a significant change in river discharge regimes (Aich et al., 2014; Ardoin-Bardin et al., 2009; Mbaye et al., 2015).

Rising temperatures, commonly acknowledged by regional climate models (RCMs) and global climate models (GCMs), are expected to intensify the hydrological cycle due to an increased water holding capacity of the atmosphere, leading to an increased amount of renewable fresh water resources (Piani et al., 2010). Another consequence of temperature increase ascertained by Piani et al., (2010) for some regions, is the decrease in precipitation associated with the intensification of the seasonal cycle and the frequency of extreme events. These opposite trends imply that high uncertainties are associated with predicted rising temperatures' impact on the hydrological cycle for some regions (Salack et al., 2015).

[1]Published as: Yira, Y., Diekkrüger, B., Steup, G., and Bossa, A. Y.: Impact of climate change on water resources in a tropical West African catchment using an ensemble of climate simulations, Hydrol. Earth Syst. Sci. Discuss., doi:10.5194/hess-2016-387, in review, 2016.

Confidence in RCMs and GCMs over West Africa relies on their ability to simulate the West African monsoon (WAM) precipitation (Klein et al., 2015). However, simulating the WAM remains challenging for both RCMs and GCMs (Cook, 2008; Druyan et al., 2009; Paeth et al., 2011; Ruti et al., 2011), as each RCM and GCM produces a version of the WAM, but with some distortion of structure and/or timing. Some GCMs do not generate the WAM at all (Cook & Vizy, 2006). Part of this divergence is related to: (i) imperfect characterization of tropical precipitation systems; (ii) uncertain future greenhouse gas forcing; (iii) scarcity of observations over West Africa; and (iv) natural climate variability (Cook & Vizy, 2006; Foley, 2010).The hydrological climate change signal is therefore unclear for the region. Several authors (Kasei, 2009; Paeth et al., 2011; Salack et al., 2015) observed diverging precipitation signals among models. Moreover, several models fail to accurately reproduce the historical rainfall onset, maxima, pattern, and amount of the region (Nikulin et al., 2012; Ardoin-Bardin et al., 2009).

Despite significant advances, outputs of GCMs and RCMs are still characterized by biases that challenge their direct use in climate change impact assessment (Ehret et al., 2012) Indeed, unless the precipitation from climate models are bias corrected, results from hydrological simulations are unrealistic and may lead to incorrect impact assessments (Johnson & Sharma, 2015; Teutschbein & Seibert, 2012; Ahmed et al., 2013). However, correction of climate model based simulation results does not ensure physical consistency (Muerth et al., 2013) and may affect the signal of climate change for specific regions as reported by Hagemann et al. (2011). Consequently, simulated hydrological variables using bias corrected data need to be explored in climate change impact assessment.

There is essential consensus on the necessity of performing multi (climate)-model assessments to estimate the response of the West African climate to global change (Sylla et al., 2015). Accordingly, several studies (e.g. Chen et al., 2013; Zhang et al., 2011) emphasize the importance of using multiple climate models to account for uncertainty when assessing climate change impacts on water resources. Taking advantage of the results of the COordinated Regional climate Downscaling Experiment (CORDEX-Africa) project, this study evaluates potential climate change impacts on water resources using an ensemble of six RCMs-GCMs in the Dano catchment in Burkina Faso. The catchment experiences seasonally limited water availability, and like other catchments of the region, it has experienced the severe droughts of the 1970s (Kasei et al., 2009) which resulted in a decline of water flow in many West African catchments.

A few studies have already investigated the impacts of projected climate change on water resources in West Africa. Most of these studies have used an approach based on hydrological models driven by a single RCM or GCM data set (e.g. Mbaye et al., 2015; Cornelissen et al., 2013; Bossa et al., 2014; Bossa et al., 2012). Therefore, uncertainty related to the choice of the climate model was not explicitly evaluated. However, a limited number of studies have used multi-climate model data sets (Kasei, 2009; Ruelland et al., 2012); most of these studies have resulted in a diverging projected hydrological change signal. Climate model outputs have often been bias corrected to fit the historical climate variables and then used as input for hydrological models but few have investigated the necessity of performing such corrections in detecting the signal of future climate change impacts on water resources.

The current chapter aims to investigate the future climate change impacts on the hydrology of the Dano catchment in Burkina Faso, thus contributing to the management of water resources in the region. Besides the small scale of the catchment that implies some scaling issues, the novelty of the study includes the use of an ensemble of climate simulations and an ecohydrological analysis. Specifically, it has the following objectives: (i) evaluate the historical runs of six RCMs-GCMs at the catchment scale; (ii) analyze the climate change signal for the future period of 2021-2050 compared to the reference period of 1971-2000; (iii) assess the impacts of climate change on the hydrology of the catchment by the middle of

the 21st century; (iv) evaluate the uncertainty related to the projected hydrological change signal; and (v) investigate the effect and necessity of bias correction on the detected signal.

9.2. Materials and methods

9.2.1. Climate data

Observed mean daily temperature and daily precipitation used in the study were collected from the national meteorological service of Burkina Faso (DGM). The dataset covers the reference period of 1971-2000. Although the national observation network includes several rainfall gauges and synoptic stations, solely the data of the Dano station were used as it is located in the study area.

An ensemble of six RCM-GCM datasets is exploited in the study (Table 9-1). The RCM-GCM simulations were performed in the framework of the CORDEX-Africa project. The datasets were produced by three RCM groups (CCLM: Climate Limited-area Modelling Community, Germany; RACMO22: Royal Netherlands Meteorological Institute, Netherlands; HIRHAM5: Alfred Wegener Institute, Germany) using the boundary conditions of four GCMs (CNRM-CM5, EC-EARTH, ESM-LR, NorESM-M). Each dataset consists of historical runs and projections based on the emission scenarios RCP4.5 and RCP8.5 (Moss et al., 2010). The retrieved data (precipitation and temperature) range form 1971-2000 for the historical runs and 2021-2050 for the RCPs. An extent of 20 nodes of the African CORDEX domain, surrounding the catchment, was delineated to simulate the catchment's climate and consider climate variability in the catchment region (Fig. 9-1 B).

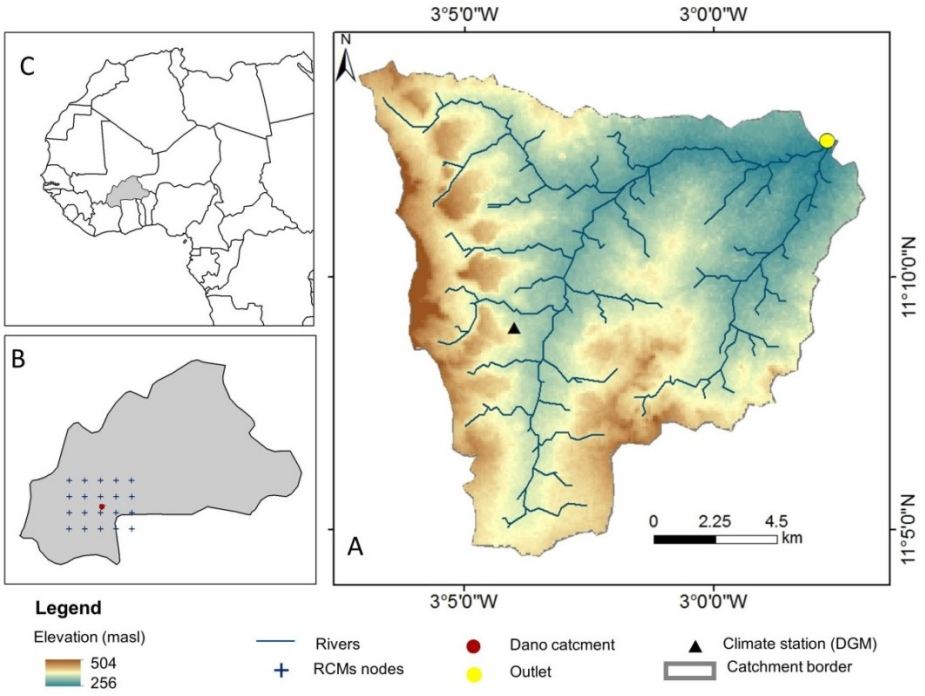

Fig. 9-1 Location map: (A) Dano catchment, (B) its location in Burkina Faso and (C) in West Africa. (B) RCMs domain used in the study.

Due to the discrepancy between the RCM-GCM data resolution (0.44°, about 50 * 50 km^2) and the hydrological modeling domain (about 18 * 11 km^2) the data of each node were separately used as climate input for the hydrological simulation model. Therefore, for each period (historical and projected scenarios) 20 simulations corresponding to the 20 nodes are performed per RCM-GCM. Monthly water balance for each RCM-GCM is then calculated as arithmetic mean.

Table 9-1 RCM-GCM products and corresponding label used in the study

RCM	Driving GCM	RCM Centre/Institute	Label used in the study
CCLM48	CNRM-CM5	CCLMcom	CCLM-CNRM
CCLM48	EC-EARTH	CCLMcom	CCLM-EARTH
CCLM48	ESM-LR	CCLMcom	CCLM-ESM
HIRHAM5	NorESM1-M	DMI	HIRHAM-NorESM
HIRHAM5	EC-EARTH	DMI	HIRHAM-EARTH
RACMO22	EC-EARTH	KNMI	RAMCO-EARTH

9.2.2. Bias correction of precipitation data

The RCMs-GCMs ensemble was evaluated to get an estimate of the historical simulated variables for the catchment by comparing RCMs-GCMs based simulations of historical climate variables to the observations provided by the National Meteorological Service (DGM). As presented in section 9.3.1, whereas temperature simulated by the models ensemble enveloped the observed temperature with moderate deviation, precipitation simulated by individual RCM-GCM exhibited biases such as overestimation of annual precipitation as well as misrepresentation of the timing of the rainy season. A precipitation bias correction was therefore applied to the six RCMs-GCMs following the non-parametric quantile mapping using the empirical quantiles method (Gudmundsson et al.; 2012). For each member, a transfer function was derived using observed and modeled precipitation for the period of 1971-2000; afterwards the transfer function was applied to the projected climate scenarios (period 2021-2050).

9.2.3. Hydrological modeling

Observed and RCMs-GCMs based (historical runs and projections) data were used as climate input for version 9.05.04 of the Water flow and balance Simulation Model (WaSiM) (Schulla, 2014). WaSiM is a deterministic and spatially distributed model, which uses mainly physically based approaches to describe hydrological processes. The model configuration as applied in this study is shown in Table 9-2. Further details of model structures and various processes involved are given in the Model Description Manual (Schulla, 2014).

The suitability of WaSiM to model the hydrology of the Dano catchment was confirmed in chapter 7. Details of the model setup and parameterization are available in that chapter. Briefly summarized, the model was calibrated and validated using discharge, soil moisture and groundwater depth for the period of 2011-2014. Daily time steps and a regular raster-cell size of 90 m were used. Minimum values of 0.7 for Pearson product-moment-correlation-coefficient, Nash Sutcliffe Efficiency (Nash & Sutcliffe, 1970) and Kling-Gupta Efficiency (Gupta et al., 2009; Kling et al., 2012) were achieved during the calibration and validation using observed discharge. Good representations of soil moisture and groundwater dynamics were also achieved by the model (R^2 >0.6). Therefore, no further model calibration was done in the current study.

No hydrologic observations (discharge, soil moisture and groundwater level) are available for the reference period (1971-2000) in the catchment. The expected climate change for an RCM-GCM is therefore expressed as the relative difference between simulated hydrological variables under reference period (1971-2000) and future period (2021-2050).

Nevertheless, discharge simulated with RCM-GCM historical runs (bias corrected and not bias corrected) were compared to the discharge obtained with observed historical climate data. RCM-GCM based simulations able to reproduce the runoff regime of the past were used for climate change impact assessment. These comparison runs (performed with CCLM-ESM) showed that bias correction was necessary for RCMs-GCMs based simulations to reproduce the historical discharge regime. Hydrological

variables simulated under historical (1971-2000) and projected (2021-2050) climate conditions were therefore compared with bias corrected RCMs-GCMs data. To integrate the potential effect of bias correction on climate change signal as raised by different authors (e.g. Muerth et al., 2013; Ehret et al., 2012; Hagemann et al., 2011), the hydrological model was also run with not bias corrected future climate for CCLM-ESM (which was randomly selected among the 6 RCMs-GCMs).

Table 9-2 Selected sub models and algorithms of WaSiM.

Sub model	Algorithm
Potential evapotranspiration	Hamon (based on Federer and Lash, 1983)
Actual evapotranspiration (ET)	Suction depended reduction according to Feddes et al. (1978)
Interception	Leaf area index dependent (bucket approach)
Infiltration	Based on saturated hydraulic conductivity, soil water content and rainfall (Schulla, 2015)
Unsaturated soil zone	Richard's equation parameterized based on van Genuchten (1980) parameterization of the water retention curve
Discharge routing	Kinematic-wave using Manning-Strickler equation

9.2.4. Ecohydrologic analysis

A concept of water-energy budget (Tomer & Schilling, 2009; Milne et al., 2002) was applied to estimate the effectiveness of water and energy use by the catchment as it undergoes climate change. While experiencing climate change, a trend towards the optimization of total unused water-P_{ex} Eq. 9-1) and energy-E_{ex} Eq. 9-2) existing in the environment is usually observed. Plotting P_{ex} against E_{ex} allows for determining the ecohydrologic status of the catchment. The climate change signal can therefore be detected by the shift of this status. The direction of the shift indicates whether the catchment experienced water stress or increased humidity. The approach was used to test its validity in analyzing the interplay between temperature increase and precipitation change as projected by the RCMs-GCMs ensemble.

$$P_{ex} = (P - ET_a)/P \quad \text{Eq. 9-1}$$

$$E_{ex} = (ET_p - ET_a)/ET_p \quad \text{Eq. 9-2}$$

Where P is precipitation, ET_a and ET_p refer to actual and potential evapotranspiration respectively.

9.2.5. Assessment criteria

A set of evaluation measures was used to analyze the RCMs-GCMs historical runs, to assess model performance and to estimate the effects of different climate scenarios on hydrological variables:

(i) *P-Factor*, measures the percentage of observed climate data covered by the RCMs-GCMs ensemble historical runs;

(ii) the *R-factor*, indicates for an observation series, how wide the range between minimum RCM-GCM and maximum RCM-GCM for precipitation and temperature is, compared to the observation:

$$R - factor\ (Var) = \frac{1}{n\sigma_{Var_{obs}}} \sum_{l=1}^{n} (Var_{Si_{max}} - Var_{Si_{min}}) \quad \text{Eq. 9-3}$$

Where *Var* is the climate variable (e.g. precipitation), *n* refers to the observations data points; σ is the standard deviation, *obs* refers to observation, and Si_{max} and Si_{min} are respectively the maximum and minimum values of the RCMs-GCMs ensemble.

(iii) the normalized root-mean-square deviation (NRMSD), expresses the deviation of each RCM-GCM based precipitation and temperature from the observations;

(iv) the Pearson product-moment-correlation-coefficient (R^2), the Nash Sutcliffe Efficiency (NSE) (Nash & Sutcliffe, 1970) and the Kling-Gupta Efficiency (KGE) (Gupta et al., 2009; Kling et al., 2012) assess the RCM-GCM based discharge simulations ability to reproduce discharge computed using observed climate data;

(v) change signal (Δ) in climate and hydrological variables (precipitation, temperature and discharge) expresses the difference between projected and historical values Eq. 9-4); and

$$\Delta Var = \frac{\left(Var_{Proj} - Var_{Ref}\right) \times 100}{Var_{Ref}} \quad \text{Eq. 9-4}$$

Where Var is the evaluated variable (e.g. discharge), *Proj* = the projected period (2021-2050 under RCP4.5 and RCP8.5) and *Ref* = Reference or historical period (1971-2000).

(vi) the Wilcoxon (1945) rank-sum test was used to compare discharge change signal with bias corrected and not bias corrected precipitation data (for CCLM-ESM) following Muerth et al. (2013). The test evaluated the null hypothesis: “discharge change signal under bias corrected CCLM-ESM data equals discharge change signal under not bias corrected CCLM-ESM data”. The rejection of the test at 5 % implies that future discharge change under bias correction and no bias correction are significantly different. If the test is not rejected, both discharge change under bias correction and change under not bias correction yield the same result, and thus bias correction do not alter the climate change signal on projected discharge.

9.3. Results

9.3.1. Historical runs analysis

The comparison between RCM-GCM historical runs and observations for temperature and precipitation is done for the reference period of 1971-2000 for average monthly values. The correlation coefficient is plotted against the *NRMSD* (Fig. 9-2) for a cross-comparison between RCMs-GCMs in order to assess the relative ability of each RCM-GCM to represent historical climate conditions in the catchment. The correlation coefficient for the RCM-GCM ensemble is in general higher than 0.7 for both precipitation and temperature. The highest coefficients (0.96) are scored by CCLM-ESM for temperature and HIRAM-NorESM for precipitation. The RCMs-GCMs ensemble mean outscores five members of the RCMs-GCMs ensemble with regard to temperature and precipitation (Fig. 9-2).

The RCMs-GCMs ensemble shows a clear deviation from observed precipitation compared to temperature (Fig. 9-2). HIRAM-EARTH and CCLM-EARTH present the lowest deviation for temperature and precipitation respectively. The RCMs-GCMs ensemble mean outscores four out of six RCMs-GCMs for temperature and precipitation with regards to the deviation from observed data.

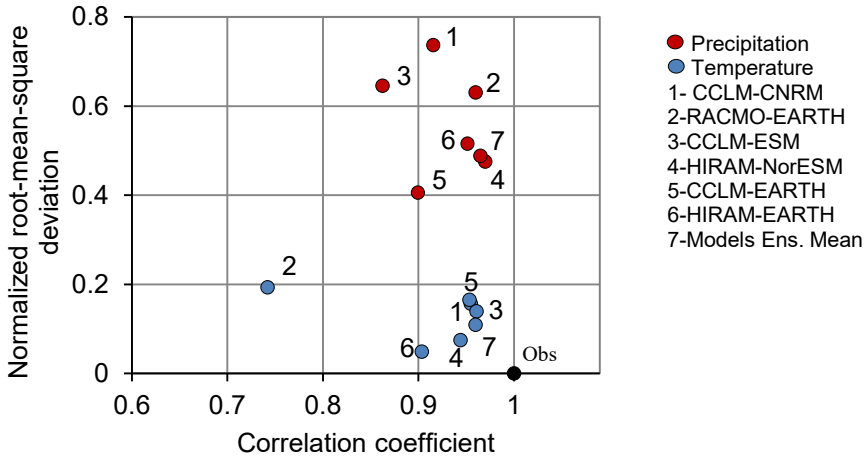

Fig. 9-2 Statistics of RCM-GCM based precipitation and temperature compared to observations (Obs) for the reference period (1971-2000). Climate model data are not bias corrected. Statistics are computed based on average monthly values.

Fig. 9-3 shows a trend towards an overestimation of annual precipitation throughout the reference period for the RCMs-GCMs ensemble when precipitation data are not bias corrected (UC). Although the RCMs-GCMs ensemble presents a large dispersion (*R-factor* = 4.3) only 50 % (*P-factor* = 0.5) of observed precipitation is covered by the RCMs-GCMs ensemble. After bias correction (BC), the RCMs-GCMs ensemble agrees in general with the observed precipitation (P-factor = 0.8), moreover the dispersion of climate models based precipitation decreases (*R-factor* = 3.2).

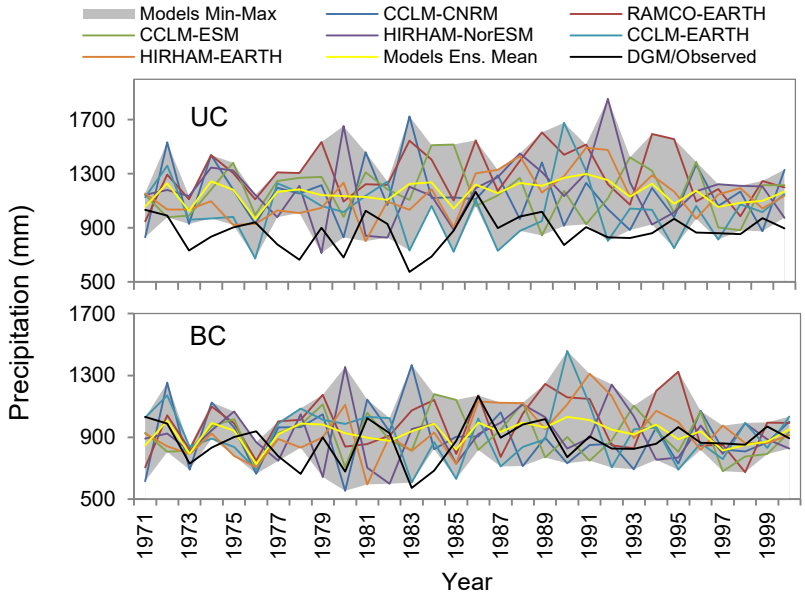

Fig. 9-3 Historical annual precipitation. *UC* refers to not bias correct, *BC* is bias corrected. *P-factor* equals 50 % and 80 % for *UC* and *BC* respectively. *R-factor* equals 4.3 for *UC* and 3.2 for *BC*.

The mean annual precipitation pattern is in general well captured by all RCMs-GCMs (Fig. 9-4). However, the climate models ensemble, when not bias corrected, covers only 50 % of monthly precipitation despite a large dispersion (Fig. 9-4 UC). After bias correction, the agreement between RCMs-GCMs based precipitation and observation is considerably improved (Fig. 9-4 BC); and the uncertainty band of the climate model is considerably reduced (*R-factor* = 0.1). However, a slight positive bias is still presented by the climate models ensemble.

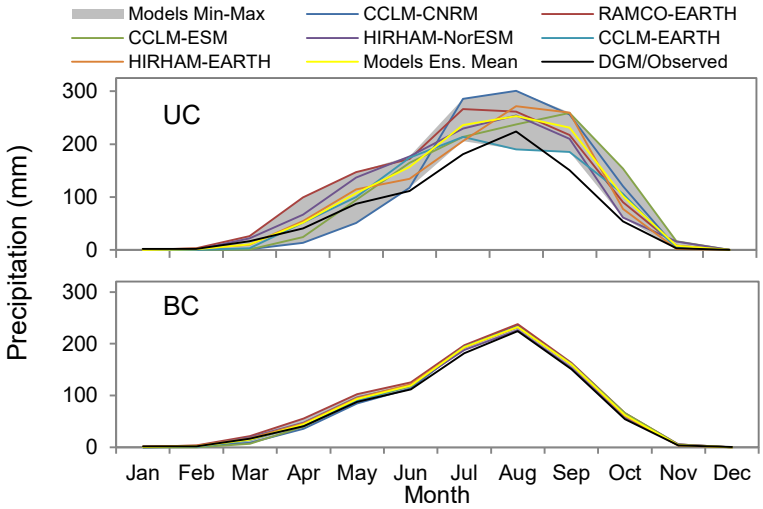

Fig. 9-4 Mean monthly precipitation derived from climate models and observations for the reference period (1971-2000): *UC* refers to not bias corrected and *BC* is bias corrected. *P-factor* equals 50% for both *UC* and *BC*. *R-factor* equals 0.68 for *UC* and 0.11 for *BC*.

Fig. 9-5 shows that the RCMs-GCMs ensemble fully captures the annual temperature pattern (*P-factor*= 100 %). However, a gap of up to -4 °C between some climate models and observations is noted. This translates into an *R-factor* reaching 8.2. On average, RACMO-EARTH shows an underestimation of temperatures throughout the year, whereas HIRAM-NorESM indicates an opposite trend.

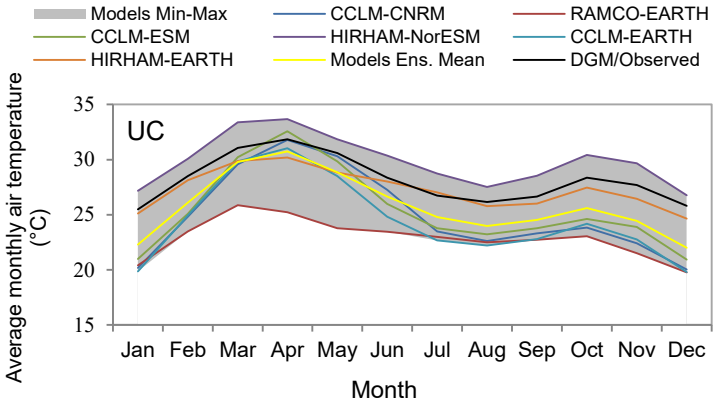

Fig. 9-5 Monthly air temperature derived from climate models and observations for the reference period (1971-2000). Data are not bias corrected. *P-factor*= 100% and *R-factor*= 8.2.

9.3.2. Climate change signal

The RCMs-GCMs ensemble exhibits a mixed annual precipitation change signal between reference period (1971-2000) and future period (2021-2050) (Table 9-3). CCLM-CNRM, RAMCO-EARTH and HIRHAM-NorESM project a precipitation increase of about 2.5 to 21 % whereas CCLM-ESM and CCLM-EARTH indicate a decrease of 3 to 11 %. Bias correction has a minor impact on these signals, as the magnitude of projected precipitation increase ranges from 1 to 18 % and the decrease is around 5-13 % after bias correction.

Table 9-3 Projected rainfall change between reference (1971-2000) and future (2021-2050) period with bias corrected and not bias corrected RCM-GCM based simulations.

	Not bias corrected			Bias corrected		
RCM-GCM	Historical Precipitation	Precipitation change RCP4.5	Precipitation change RCP8.5	Historical precipitation	Precipitation change RCP4.5	Precipitation change RCP8.5
	(mm)	(%)	(%)	(mm)	(%)	(%)
CCLM-CNRM	1150.4	+11.0	+21.2	900.3	+8.6	+18.1
CCLM-EARTH	1027.5	-11.7	-7.5	917.7	-9.1	-7.5
CCLM-ESM	1165.2	-3.2	-9.0	911.4	-5.7	-8.1
HIRHAM-NorESM	1173.3	+2.8	+11.7	911.6	+1.4	+5.3
HIRHAM-EARTH	1135.0	+12.1	-13.0	933.5	+15.1	-13.5
RAMCO-EARTH	1292.2	+5.4	+13.2	977.9	+6.2	+16.2
Models Ens. Mean	1157.3	+3.0	+3.2	925.4	+2.8	+1.8

A much more complex intra-annual precipitation change signal is projected by the climate models ensemble (Fig. 9-6). CCLM-CNRM and HIRHAM-NorESM, which projected an increased annual precipitation, are characterized by an increased rainfall from May to June followed by a decreased rainfall in August. RAMCO-EARTH shows an increased rainfall throughout the season except in July. The decrease in annual precipitation projected by CCLM-ESM and CCLM-EARTH is consistent throughout the entire season. The climate model ensemble consistently projects mean monthly temperature increase of about 0.1 to 2.3 °C under RCP4.5 and 0.6 to 2.5 °C under RCP8.5 leading to an increase of potential evapotranspiration for the climate models ensemble.

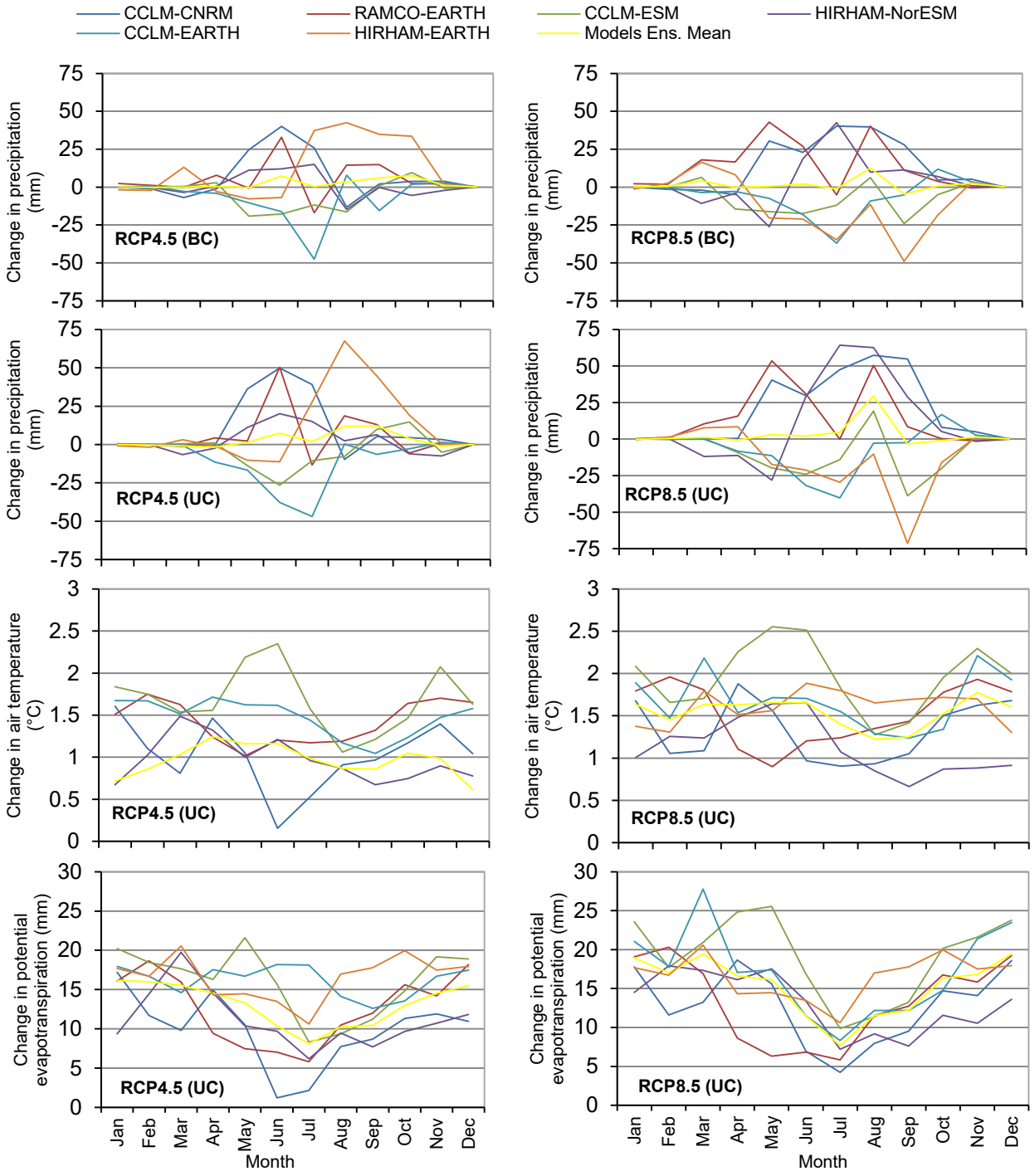

Fig. 9-6 Climate change signal of precipitation, air temperature and evapotranspiration between the reference (1971-2000) and the future (2021-20150) periods under emission scenarios RCP4.5 and RCP8.5. BC is bias corrected and UC refers to not bias corrected.

9.3.3. Historical discharge

RCMs-GCMs ensemble based discharges are compared to discharge simulated using observed climate data to evaluate the climate models ability to reproduce the historical discharge regime over the reference

period (Fig. 9-7). Accordingly, performances (R^2, *NSE* and *KGE*) achieved by the climate models are presented in Table 9-4. Fig. 9-7 (a) shows good agreement between (bias corrected) climate models based discharge and observation based discharge, with a trend towards discharge overestimation for some climate models (RACMO-EARTH, CCLM-EARTH and HIRAM-EARTH). All climate models show good statistical quality measures after bias correction. Bias correction impact on simulated historical discharge is shown in Fig. 9-7 (b) for CCLM-ESM. As an example, simulated discharge for CCLM-ESM with not bias corrected data leads to a misrepresentation of the discharge regime, as peak flow is shifted from August to September and discharge is highly overestimated. Moreover, poor quality measures are achieved by CCLM-ESM with not bias corrected data (Table 9-4).

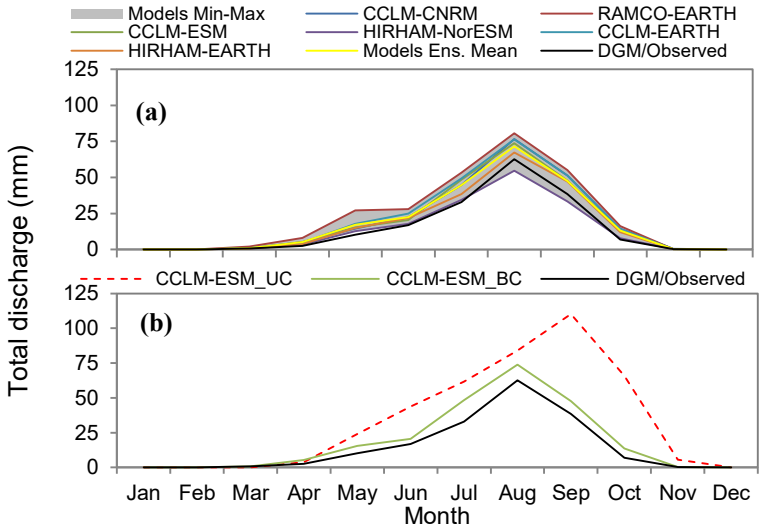

Fig. 9-7 Historical RCMs-GCMs based discharge simulations and observation based discharge: (a) all RCM rainfall are bias corrected, (b) simulated discharge with bias corrected and not bias corrected rainfall data are compared for CCLM-ESM.

Table 9-4 Performance of RCMs-GCMs based discharge compared to observation based discharge. Performance is calculated using mean monthly discharges for the period 1971-2000.

Climate model	R^2	NSE	KGE
CCLM-CNRM	0.99	0.92	0.65
CCLM-EARTH	0.97	0.89	0.59
CCLM-ESM	0.97	0.92	0.68
CCLM-ESM_UC*	0.51	-0.51	-0.36
HIRHAM-EARTH	0.98	0.97	0.78
HIRHAM-NorESM	0.98	0.99	0.92
RAMCO-EARTH	0.94	0.78	0.40
Models Ens. Mean	0.98	0.94	0.69

* Simulation performed with not bias corrected rainfall data.

9.3.4. Discharge change

Projected change in annual discharge for the period of 2021-2050 compared to the reference period is presented in Table 9-5. Alike for precipitation, a mixed annual discharge change signal is projected by the climate model ensemble. It projects: (i) more than 15 % decrease in annual discharge, which is a consequence of relative decrease in precipitation and a consistent increase in potential evapotranspiration for CCLM-ESM, CCLM-EARTH and HIRHAM-EARTH (RCP8.5); (ii) about 5 % decreased in annual discharge for the RCMs-GCMs ensemble mean under RCP8.5 which is the

consequence of a slight increase in precipitation counterbalanced by a high increase in potential evapotranspiration; (iii) low to very high (3 to 50 %) increase in total discharge due to increased precipitation not counterbalanced by the evapotranspiration for CCLM-CNRM, RAMCO-EARTH, HIRHAM-NorESM, HIRHAM-EARTH (RCP4.5) and the RCMs ensemble mean (RCP4.5). The intra-annual change in discharge appears strongly determined by the precipitation change signal (Fig. 9-8). The divergence between climate models is reflected through a large amount of uncertainty associated with the projected annual discharge (Fig. 9-9).

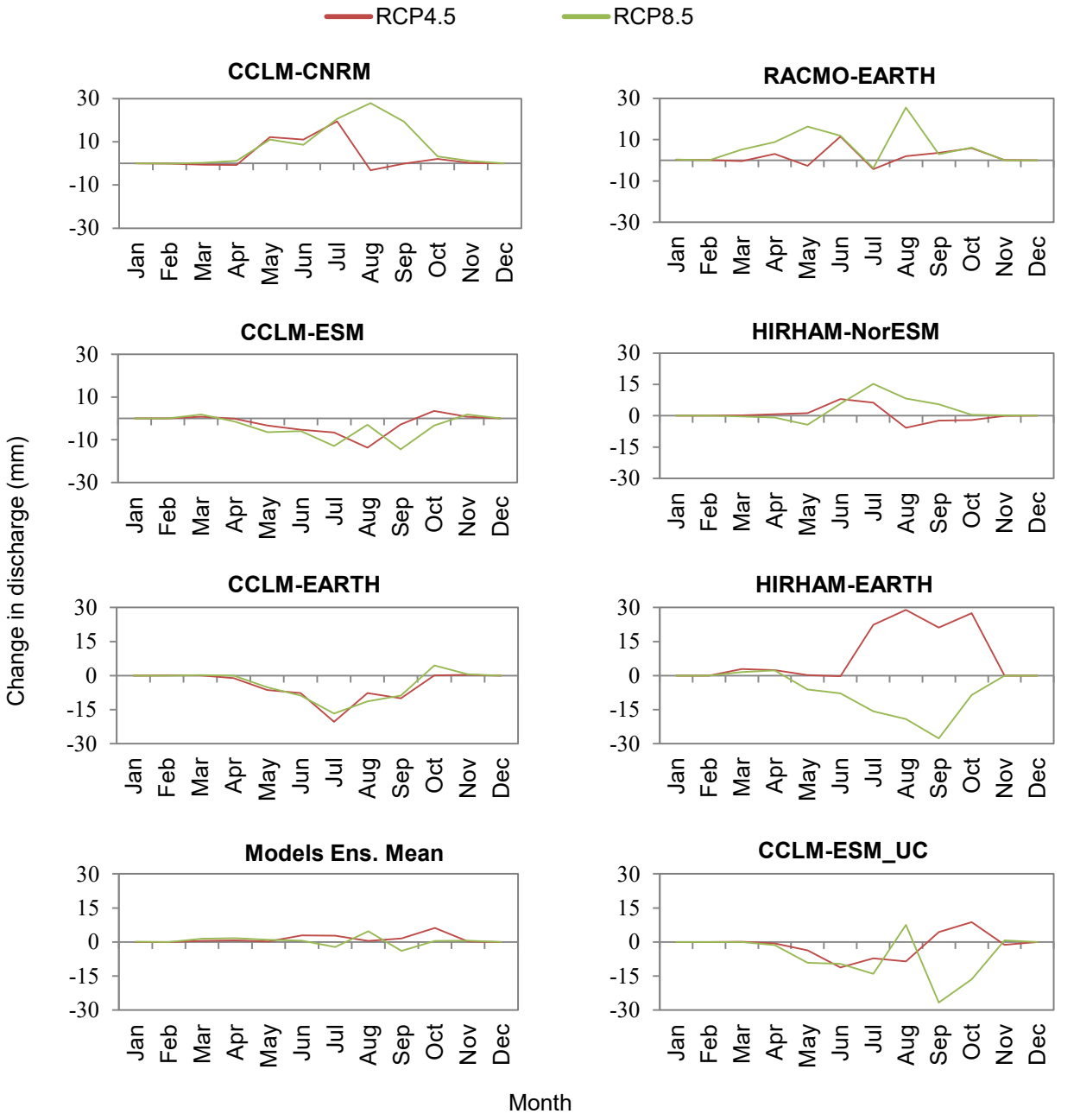

Fig. 9-8 Monthly discharge change between the reference period (1971-2000) and the future period (2021-20150) under emission scenarios RCP4.5 and RCP8.5. *UC* refers to not bias corrected.

Table 9-5 Mean annual discharge change projected by the RCMs-GCMs ensemble for the period 2021-2050 compared to the reference period 1971-2000.

Climate model	Reference discharge	Discharge change RCP4.5	Discharge change RCP8.5
	(mm)	(%)	(%)
CCLM-CNRM	230.6	+17.4	+40.4
CCLM-EARTH	240.1	-21.9	-18.9
CCLM-ESM	226.0	-11.9	-19.5
CCLM-ESM_UC*	407.1	-4.7	-17.0
HIRHAM-NorESM	194.9	+3.7	+18.1
HIRHAM-EARTH	206.6	+52.0	-39.3
RAMCO-EARTH	271.4	+7.2	+27.1
Models Ens. Mean	223.3	+7.0	-2.0

* Simulation performed with not bias corrected rainfall data.

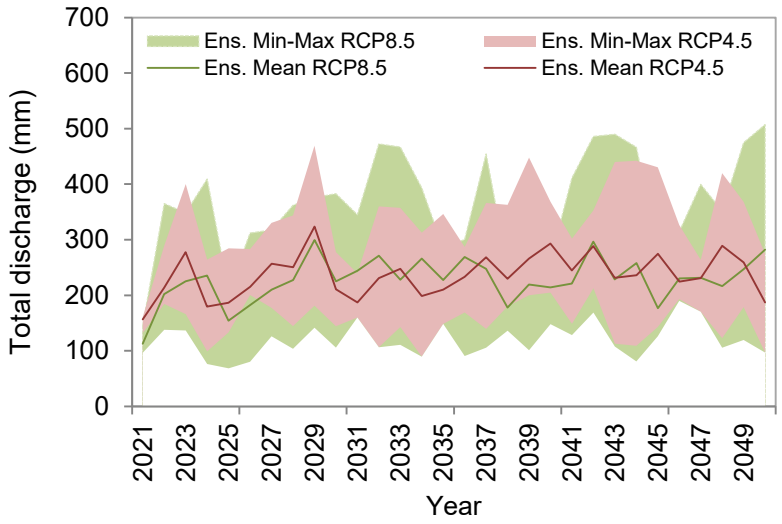

Fig. 9-9 Projected annual discharge for the climate models ensemble. Simulations are performed with bias corrected precipitation data.

Under RCP4.5, the discharge change signal for CCLM-ESM is more pronounced with bias corrected precipitation data compared to not bias corrected. Indeed, the projected annual discharge equals -12 % and -5 % with and without bias correction respectively (Table 9-5). Under RCP8.5, bias correction impact is relatively low. The Wilcoxon (1945) rank-sum, testing the significance of the difference between bias corrected and not bias corrected discharge change signal, indicates that the two signals are not different at *p-level* equals 0.05. A *p-value* of the Wilcoxon rank-sum test equals 0.51 and 0.7 is required under RCP4.5 and RCP8.5 respectively to reject the null hypothesis (H_0: discharge change with bias corrected CCLM-ESM data = discharge change with not bias corrected CCLM-ESM data). Hence, the bias correction impact on discharge change signal alteration can be considered negligible.

The sensitivity of the catchment discharge to precipitation and temperature change is tested by plotting, for each member of the climate models ensemble, predicted precipitation and temperature change against predicted discharge change. The result shows that change in total discharge cannot be strongly related to change in potential evapotranspiration (Fig. 9-10 a). However, a high sensitivity of river discharge to precipitation change (Fig. 9-10 b) is observed. Under scenario RCP4.5, an increase of +5 % in precipitation leads to an increase of discharge of about +12.5 %, whereas a decreased precipitation of the same order leads to a decrease of discharge of -13 %. The same simulations under RCP8.5 yield in a

+8.3 % discharge increase and a -14.7 % discharge decrease. Interestingly, under RCP8.5 and assuming comparable precipitation between reference and future periods, a discharge decrease of about -3.2 % should be expected (Fig. 9-10 b).

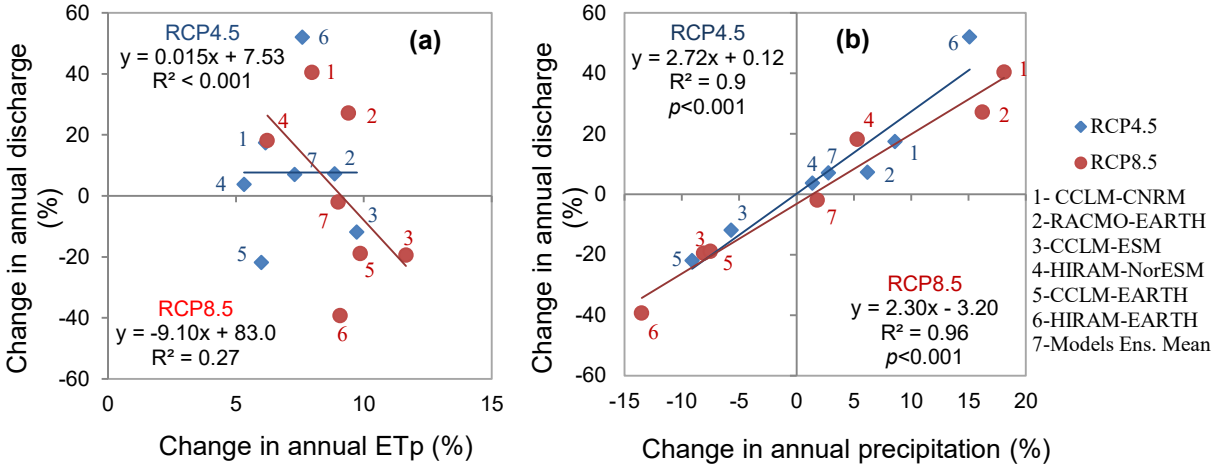

Fig. 9-10 Change in the annual discharge as a response to potential evapotranspiration (a) and precipitation (b) change under emission scenarios RCP4.5 and RCP8.5. Projected precipitation, potential evapotranspiration and discharge changes are calculated comparing period 1971-2000 to period 2021-2050.

9.3.5. Ecohydrologic status

The Eco-hydrologic status of the catchment for the reference period and future scenarios RCP4.5 and RCP8.5 is shown in Fig. 9-11 to illustrate the use of energy and water by the catchment while undergoing temperature increase and precipitation change. Moving left to right along "*Excess water-P_{ex}*" axis indicates that the environmental conditions in the catchment lead to an increase in discharge (CCLM-CNRM, RAMCO-EARTH and HIRHAM-NorESM). Reduction of discharge is experienced when moving the other way round (CCLM-ESM and CCLM-EARTH).

Moving upwards along "*Excess evaporative demand-E_{ex}"* implies drier environmental conditions due to an increase in evaporative demand and soil water deficit. Except for HIRAM-EARTH, all the climate models project drier conditions (increase in *Excess evaporative demand*) under RCP4.5 as a result of an increased temperature not compensated by the amount and/or timing of precipitation. Increased evaporative demand, with marginally aggravated drier conditions, is shown by CCLM-ESM, HIRAM-NorESM, CCLM-EARTH and RCMs-GCMs ensemble mean under RCP8.5.

The ecohydrologic status of the catchment, irrespective of climate model and emission scenario, projects a shift for the period of 2021-2050 compared to the reference period. Therefore, differences in climate conditions between the two periods influence the hydrology (discharge, evapotranspiration, precipitation) of the catchment.

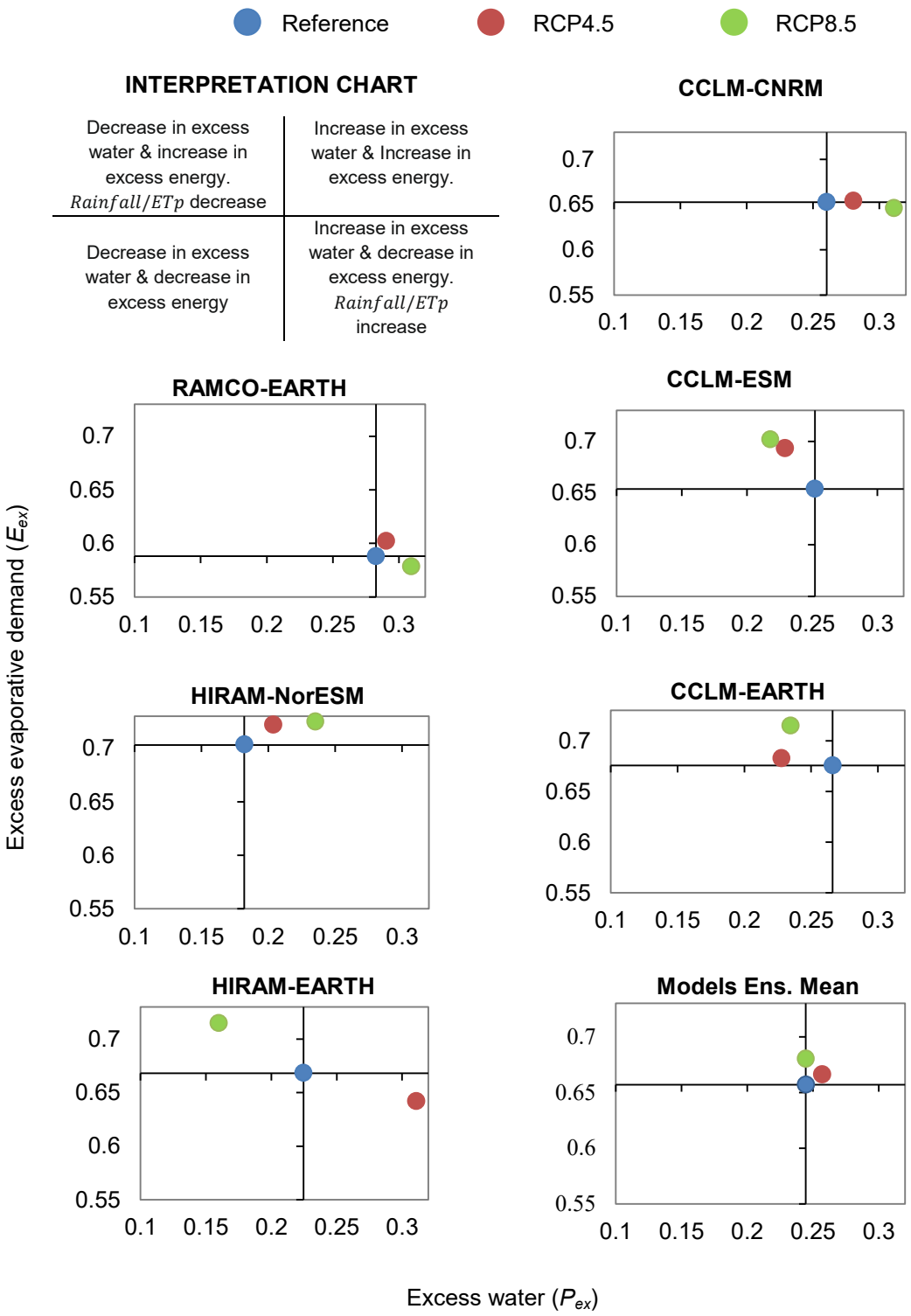

Fig. 9-11 Plot of excess precipitation (P_{ex}) versus evaporative demand (E_{ex}) for the reference period (1979-2000) and the emission scenarios RCP4.5 and RCP8.5 (2021-2050) for the RCMs-GCMs ensemble. The shift of RCP dots compared to the reference period's dot indicates the effects of climate change on the catchment hydrology. P_{ex} and E_{ex} for each period are calculated from the annual average rainfall, potential evapotranspiration and actual evapotranspiration.

9.4. Discussion

9.4.1. Historical runs analysis

All GCMs and RCMs applied in this study have proved in previous works to fairly reproduce the climatology of West Africa (Cook & Vizy, 2006; Dosio et al., 2015; Gbobaniyi et al., 2014; Paeth et al., 2011). The RCMs-GCMs ensemble reasonably captures the annual cycle of temperatures, and following several authors (e.g. Buontempo et al., 2014; Waongo et al., 2015) no bias correction was performed for this climate variable. The systematic positive bias and large deviation from observed precipitation exhibited by the climate models ensemble in this study is also reported by several authors (Nikulin et al., 2012; Paeth et al., 2011) for the southern Sahel Zone. This deviation motivated the bias correction of precipitation. After correction, the positive bias is significantly reduced for all individual climate models and the improvement is clearly visible.

In general, the RCMs-GCMs ensemble mean outperforms individual climate models for both temperature and precipitation. This is due to the fact that individual model errors of opposite sign cancel each other out (Nikulin et al., 2012; Paeth et al., 2011). However, the climate models ensemble mean should not be considered as an expected outcome (Nikulin et al., 2012). Rather considering a large ensemble of climate models should be seen as necessary to properly perform future climate impact studies in the catchment (Gbobaniyi et al., 2014) and to assess the range of potential future hydrological status required for adaptation and management strategies.

9.4.2. Climate change signal

Compared to the period of 1971-2000, a clear temperature increase signal is projected for 2021-2050 by the six members of the RCMs-GCMs ensemble in the catchment. This feature is common to all multi-model ensemble studies performed in the region (IPCC, 2014). However, the climate models ensemble does not agree on the projected precipitation change signal as wetter (RAMCO-EARTH), drier (CCLM-ESM and CCLM-EARTH) as well as mixed (CCLM-CNRM, HIRHAM-NorESM and HIRAM-EARTH) trends are shown by the individual model. It is worth noting that the Dano catchment is located in a region where the "*Coupled Model Intercomparison Project Phase 5 (CMIP5)*" models showed divergent precipitation change for the mid-21st century (IPCC, 2014).

The precipitation change projected by CCLM-CNRM and HIRHAM-NorESM, wetter conditions associated with drought during specific months, is consistent with the change reported by Patricola & Cook (2009) for the West African region. They highlighted an increase in precipitation in general, but also noted drier June and July months. A similar result is achieved by Kunstmann et al. (2008) in the Volta Basin, albeit with a decrease in precipitation at the beginning of rainy season in April.

Precipitation change projected by CCLM-ESM and CCLM-EARTH is consistent with the decrease in June-July-August season noted by Buontempo et al. (2014). A reduction in precipitation during the rainy season is also achieved with RegCM3, driven by ECHAM5 in the Niger River Basin (Oguntunde & Abiodun, 2012). Up to 20.3 % reduction of precipitation in some months is projected, but an increased precipitation during the dry season is also expected.

A critical analysis of CCLM (by Dosio et al., 2015) showed that the model is significantly influenced by the driving GCM (including EC-Earth, ESM-LR, and CNRM-CM). Such an analysis was not found for RACMO and HIRAM. Overestimation of precipitation is a common feature to the RCMs-GCMs ensemble applied in this study, which could suggest that the RCMs inherit the bias from the GCM (Dosio et al., 2015). Consistently with Paeth et al. (2011), the relation between RCM trend and driving GCM cannot be observed in the current study as CCLM-EARTH and RACMO-EARTH clearly show opposite trends

although both are driven by EC-EARTH. Differences in projected trends are also highlighted by individual RCMs driven by different GCMs (e.g. CCLM-EARTH and CCLM-CNRM).

9.4.3. Historical discharge

Compared to the observation based simulation, not bias corrected RCMs-GCMs based discharge is characterized by an overestimation of annual discharge. This misrepresentation results from the positive precipitation bias presented by the climate models ensemble. The bias correction significantly improves the ability of all members of the climate models ensemble to reproduce the historical discharge regime. By comparing simulated discharge for CCLM-ESM with bias corrected and not bias corrected precipitation data, it clearly appears that the bias correction methodology is effective with regards to both discharge regime and total discharge. However, a trend towards discharge overestimation was noticed after bias correction of precipitation. This could be related to:

(i) the relative long period used for the bias correction (1971-2000). As noticed by Piani et al. (2010), fragmenting the correction period to decade and deriving several transfer functions can improve the bias correction result and further contribute to capture the decadal rainfall change that characterizes the West African climate; and

(ii) the fact that temperature was not bias corrected. This led to *ETp* values that vary from one RCM-GCM to another (Table 9-7) since *ETp* after *Hamon* is computed based on temperature values only. As a result, a relatively large range of potential evapotranspiration is observed for the climate models ensemble (Table 9-7).

In view of the general good simulation of historical discharge for the climate models ensemble, it is worth noting that running the hydrological model with simulated climate data of one node at a time (section 9.2.1) has reasonably bridged the discrepancy between RCMs-GCMs data resolution and hydrological modeling domain. Therefore, the approach can be seen as eligible for climate change impact assessment for small scale catchments. However, besides regional specificities, it reliability might rely on the extent of the RCM-domain used to simulate a given catchment climate, which in the case of this study was set at 0.44°*4 over 0.44°*5 in order to account for climate spatial variability.

9.4.4. Discharge change

A mixed annual discharge change signal is projected by the climate models ensemble for the period of 2021-2050. These trends agree with several studies in the region (Table 9-6), although all were carried out at the mesoscale and macroscale:

- ***Negative trend*** (CCLM-ESM and CCLM-EARTH). A discharge decrease of 30 to 46 % is reported by Ruelland et al. (2012) using MadCM3 and MPI-M in the Bani catchment. A similar trend, resulting from a combination of temperature increase and precipitation decrease was reached by Mbaye et al. (2015) using the climate model REMO in the Upper Senegal Basin; as did Cornelissen et al. (2013) and Bossa et al. (2014) in the Térou and the Ouémé catchment respectively.
- ***Positive trend*** (CCLM-CNRM, RAMCO-EARTH and HIRHAM-NorESM)***.*** An increase of 38 % in annual discharge in the region is reported by Ardoin-Bardin et al. (2009) for the Sassandra catchment (South of the Dano catchment) using climate projections of HadCM3-A2. This results from a 11 % increase in precipitation not counterbalanced by the 4.5 % increase of potential evapotranspiration.
- ***Mixed trend*** *(*HIRHAM-EARTH and RCMs-GCMs ensemble). A mixed discharge change signal for the future period is the common signal projected by multi-climate models studies performed in the West African region. In the Niger basin, Aich et al. (2014) simulated change in annual

discharge ranging from an increase of up to 50 % to a decrease of up to 50 % using an ensemble of five climate models. Similar signals are reported by Kasei (2009) who applied two climate models (MM5 and REMO) in the Volta basin.

Table 9-6 Selected studies of climate impact on water resources in the West African Region

Study	Location/seize	GCM/RCM	Scenario	Reference period	Future period	Precipitation change (%)	Discharge change (%)
Ruelland et al. (2012)	Bani catchment, Mali/100 000Km²	MadCM3 and MPI-M	A2	1961-1990	2041-2070	-2 to -10	-30 to -46
Mbaye et al. (2015)	Upper Senegal Basin, Senegal-Mali-Mauritania/218000 Km²	REMO-MPI-ESM-LR	RCP4.5 and RCP8.5	1971-2000	2071-2100	negative trend	up to -80
Aich et al. (2014)	Niger Basin/ 2156000 Km²	HadGEM2-ES, IPSL-5 CM5A-LR, MIROC-ESM-CHEM, GFDL-ESM2M, NorESM1-M	RCP8.5	1970-1999	2070-2099	mixed trend	-50 to +50
Ardoin-Bardin et al. (2009)	Sassandra, Ivory Coast/ 62173 Km²	HadCM3-A2	-	1971-1995	2036-2065	11.4	38
Bossa et al. (2014)	Ouémé catchment, Benin/ 49256 Km²	REMO-ECHAM5/MPI-OM	A1B	2000-2009	2010-2029	-10	-18
Cornelissen et al. (2013)	Térou Catchment, Benin/2344 km²	REMO-ECHAM5/MPI-OM	B1	2001-2010	2031-2049	-11	-11
Kasei (2009)	Volta Basin/400000 km²	MM5 and REMO	B1	1991-2000 and 1961-2000	2030-2039 and 2001-2050	+12 and -6	+40 and -5

This mixed hydrological change signal is the result of high uncertainties associated to the precipitation change projected by climate models for the catchment (IPCC, 2014). The Wilcoxon rank-sum test further indicated that bias correction did not significantly alter these discharge change signals. Due to the high sensitivity and nonlinear response of the catchment discharge to precipitation, any change in precipitation will have a strong impact on the discharge; the impact will further be pronounced under RCP8.5 compared to RCP4.5. Irrespective of emission scenario, change in potential evapotranspiration alone failed to strongly explain change in annual discharge (Fig. 9-10 a); this is partly explained by the fact that the hydrological system of the catchment is water limited and not energy limited.

The water limited environment of the catchment might also explain the performance of the hydrological model for the climate models ensemble despite the non-bias correction of temperature data (up to 4°C gaps between observed and simulated temperature were noticed for some months, section 9.3.1). The annual evaporative demand for the climate models ensemble, including RACMO-EARTH which underestimated observed temperature for the reference period, exceeds (almost double) precipitation (Table 9-7). In such a system, also characterized by an extended periods with little to no precipitation (November-May) actual evapotranspiration is strongly controlled by precipitation (Guswa, 2005; Schenk & Jackson, 2002). Therefore, an increase in *ETp* is not necessarily translated in an increase in *ETa* as limitation in precipitation (soil moisture) dictates water fluxes (Newman et al., 2006) (e.g. CCLM-EARTH and CCLM-ESM in Table 9-7).

Table 9-7 Mean annual water components per RCM-GCM for the historical (1971-2000) and projected (2021-2050) period.

	CCLM-CNRM			RACMO-EARTH			CCLM-ESM			HIRAM-NorESM			CCLM-EARTH			HIRAM-EARTH			OBSERVED
Water balance components	Historical	RCP4.5	RCP8.5	Historical	RCP4.5	RCP8.5	Historical	RCP4.5	RCP8.5	Historical	RCP4.5	RCP8.5	Historical	RCP4.5	RCP8.5	Historical	RCP4.5	RCP8.5	Historical
Precipitation (mm/y)	900	978	1063	978	1038	1136	911	859	837	912	924	960	917	834	849	934	1074	807	898
Potential ET (mm/y)	1992	2110	2145	1703	1853	1863	1979	2170	2208	2216	2349	2372	1918	2112	2132	2053	2251	2253	2070
Actual ET (mm/y)	666	704	732	701	737	785	682	663	655	746	753	765	673	644	650	724	741	678	703
Total discharge (mm/y)	231	270	324	271	291	345	226	199	182	194	201	229	240	187	195	207	314	126	198
Surface runoff (mm/y)	103	141	170	135	153	195	100	90	76	80	84	104	111	78	83	88	174	47	92.9
Interflow (mm/y)	116	118	141	123	125	135	114	98.7	95.2	104	76.9	81.1	117	98	101	107	128	69	98.0
Baseflow (mm/y)	11.0	11.0	11.1	12.6	12.5	14.2	10.8	9.9	9.9	10.3	9.9	9.5	11.5	10.4	10.4	10.8	10.7	9.6	8.9

9.4.5. Ecohydrologic status

The E_{ex}-P_{ex} plot (Fig. 9-11) allows accurately displaying climate change impact on the catchment hydrology, as main water balance components (precipitation, discharge and evapotranspiration) are presented in an integrated manner. The overall ecohydrologic effect of climate change in the catchment, as shown by the plots, is a trend towards drier environmental conditions due to increased evaporative demand-E_{ex}. This denotes an increase in potential evapotranspiration higher than the increase in actual evapotranspiration. By contrast, change in the proportion of precipitation converted to discharge-P_{ex} appears specific to each climate model, with a marginal trend towards discharge increase for the models ensemble under RCP4.5 and discharge decrease under RCP8.5.

The climate models ensemble mean projects a precipitation increase of about 1.5 % under RCP8.5 with a resulting discharge decrease of 2%. This indicates that the catchment ecosystem is able to optimize the use of water and energy available in the environment, thus reducing unused water (P_{ex}) with temperature increase(Caylor et al., 2009). Such an optimization, although not investigated in this study, may lead plants to change the allocation of fixed carbon to various tissues and organs (Collins & Bras, 2007; Milne et al., 2002). The suitability of the catchment area for the current plant species could also be affected (McClean et al., 2005) by the projected climate change.

In chapter 7, land use in the catchment was found to be characterized by conversion from savannah to cropland implying the reduction of the vegetation covered fraction, root depth, leaf area index etc. Such a land use and land cover change strongly affects the ecohydrologic status of a catchment. Tomer & Schilling (2009) highlighted that removal of perennial vegetation leads to an increase of both *Excess Water*-P_{ex} and *Excess evaporative demand*-E_{ex}. Combining this land use change to climate change impact would therefore on the one hand aggravate water stress for plants in the catchment and on the other hand increase the unused water in the catchment.

9.5. Conclusion

An ensemble of six RCMs-GCMs data, all produced in the frame of the CORDEX-Africa project, were used as input to a hydrological simulation model to investigate climate change impact on water resources in the Dano catchment by the mid-21st century. The ability of the RCMs-GCMs ensemble to simulate historical climate and discharge was evaluated prior to future climate change impact assessment.

The six climate models fairly reproduce the observed temperature. By contrast, bias correction was necessary for all climate models to accurately reproduce observed precipitation and historical discharge. The applied bias correction method further proved not to alter the discharge change signal. However, projected discharge change signal with and without bias corrected data were tested very comparable. This result indicates that it is safe to perform bias correction; it also points out the “non-necessity” of performing bias correction in order to detect future discharge change signal in the catchment.

A temperature increase is consistently projected by the models ensemble. This reinforces the commonly acknowledged warming signal for the region. However, the lack of agreement among models with regard to the projected precipitation change signal creates a considerable uncertainty about how the catchment discharge will evolve by 2050. As discharge in the catchment is strongly determined by precipitation, no clear trend in future development of water resources can be concluded due to the high variability of the different climate models and scenarios. Therefore, potential increase and decrease of future discharge have to be considered in climate change adaptation strategies in the region.

The ecohydrological concept as applied in this study proved to fully capture climate change impact on the catchment hydrology as both discharge change signal, precipitation and actual/potential evapotranspiration change signal are consistently displayed by the E_{ex}-P_{ex} plot. The approach appears suitable to display the results of climate change impact on catchment hydrology; it further brings insights about the catchment environmental conditions, which can assist in development of climate change adaptation strategies.

The results further underline on the one hand the need for a larger ensemble of projections to properly estimate the impacts of climate change on water resources in the catchment and on the other hand the high uncertainty associated with climate projections for the West African region. Therefore, assessing future climate change impact on water resources for the region needs to be continuously updated with the improvement of climate projections.

10. GENERAL CONCLUSION

Climate and land use/cover change, which are two major challenges for water resources management in West Africa, have been addressed in this study throughout investigations performed in the Dano catchment. The study falls in line with previous works carried out in the region during the past decades, which have constituted significant advances in LULC and climate change impact assessment on water resources. Consistently with the previous works, the general approach of this study combines field investigations, hydrological modeling and application of climate and LULC scenarios.

However, besides the achieved results, the methodological approach followed by the study differs from the existing works in several noteworthy ways: (i) it was carried out at local scale in a data scarce region, which implied instrumentation work and data mining from different sources, (ii) it investigates *in situ* surface runoff generation processes as influenced by land use and land cover change, (iii) it quantifies land use change in the investigation area, (iv) it assesses how the ongoing LULC change affects the hydrology of the study area, (v) it investigates the importance of integrating land use change related effect on soil properties into LULC change impact assessment, (vi) it uses a multi-climate models approach in climate change impact assessment, which addresses the issue of the choice of a climate model in climate change impact assessment, (vii) it uses regional climate models, (viii) it tackles the bias correction issue of climate models outputs, and (ix) proposes an ecohydrological approach to climate change impact assessment in the study area.

The study first established a hydro-meteorological observation network and determined soil physical properties, which allowed overcoming the issue of data scarcity in the investigation area. Afterwards i*n situ* soil infiltration rate measurements were performed. Based on the gathered data, the hydrological simulation model WaSiM was calibrated and validated for the catchment. Four LULC maps of the study area were analysed to quantify land used change. Finally, the LULC maps and an ensemble of future climate projection were applied as LULC and climate change scenarios.

The achieved results allow answering the research questions formulated in the general introduction as follows:

(i) **how does land use and land cover change affect soil infiltration rate ?**
The effect of LULC change on soil infiltration rate was assessed through the comparison of adjacent savannah and cropland plots. It was shown that infiltration rate was significantly higher under savannah compared to cropland. As high rainfall intensities are observed in the investigated area, it was concluded that land conversion from savannah to cropland increases the exposure to *Hortonian* overland flow. The results further showed that the difference of infiltration rates under savannah and cropland is driven by biopores and not by soil texture which was found to be similar under both land use classes. However, the infiltration rate was found to be highly variable under the same land use class. Beside local soil heterogeneity, this implies that differentiating between factors influencing infiltration rate like soil types, crop species and fallowing duration in the comparison of adjacent LULC classes could increase the understanding of LULC effect on soil infiltration rate;

(ii) **how does the application of a physically based and spatially distributed hydrological model instead of a conceptual lumped model improve the modeling results?**
The physically based and spatially distributed model WaSiM was successfully calibrated and validated for the catchment using river discharge. While delivering good simulations for discharge, the model was able to satisfactory simulate soil moisture and groundwater dynamic which is not possible using conceptual lumped models. Such a multivariate validation approach increases the confidence in the model results. Some model parameters were optimized without undermining the physical meaning of both land use and climate related parameters. Therefore, a more reliable land use change impact assessment can be performed with the model by adjusting the changing characteristics of the

catchment. Similarly, climate change scenarios can be provided as climate variables. Increased confidence in model results (through a multivariate validation) and the ability to represent changes in the catchment characteristics on a physical basis are the added value provided by the modeling approach;

(iii) **how does LULC change impact water resources in the Dano catchment?**
Land use and land cover dynamic in the catchment over the past decades was first assessed based on four existing multi-temporal LULC maps. The results indicated that, since the year 1990, LULC change in the catchment was characterized by a continuous conversion from semi-natural vegetation (fallow and savannah) to cropland. Settlements and water areas remain negligible in the catchment. To assess LULC change impact in the catchment, the four LULC maps were used to build five LULC change scenarios that were used as input for WaSiM. As the LULC change scenarios used the same parameterization and boundary conditions, the differences in hydrologic components following scenarios application were solely related to LULC changes. The hydrological impact of cropland expansion and degradation of savannah was found to be a significant reduction of actual evapotranspiration and increase of all discharge components. It was concluded that flood and erosion risk is likely to increase in the catchment;

(iv) **how does the integration of LULC related effects on saturated hydraulic conductivity influence the modeling result in LULC impact assessment?**
For answering research question (iii), soil hydraulic properties did not vary with land use which may create a bias as it was shown that land use has an effect on soil infiltration (research question (i)). Therefore, the consequences of integrating land use related effects on soil infiltration rate in LULC change impact assessment were evaluated using WaSiM and two soil parameterization approaches. A model setup with a refined soil, integrating LULC related effects on soil infiltration rate, was compared to a model with a classic soil parameterization. Application of the two models in LULC change impact assessment led to very similar trends in the change of water balance components. This result supports the validity of both soil parameterization approaches in LULC change impact assessment. However, differences in water balance components were found between the two parameterizations approaches. The difference in water balance components due to soil parameterization was often found to be higher than LULC change effects. Model time steps further proved to considerably influence the modelling outcome while integrating LULC related effect in LULC impact assessment. As field measurements confirmed significant differences in infiltration rates between LULC classes, it can be concluded that the plausibility of LULC change scenarios is improved with the integration of land use change related effect on soil hydraulic properties;

(v) **what is the likely trend in precipitation and temperature for the future period 2021-2050 compared to the historical period 1971-2000 and how is this trend likely to impact water resources in the catchment?**
The historical simulations of precipitation and temperature of six regional climate products were compared with observations for the catchment over the period 1971-2000. This evaluation showed in general a good ability of the climate models to reproduce the observed temperatures. However, considerable biases such as the misrepresentation of annual rainfall pattern were exhibited by the climate model ensemble. Bias correction of precipitation was applied and the agreement between simulated and observed precipitations was considerably increased. This historical comparison showed that bias correction is necessary to achieve a good agreement between climate model outputs and observations.
Compared to the reference period 1971-2000, consistent temperature increase of 0.1 to 2.6 °C over the period 2021-2050 was shown for both RCP4.5 and RCP8.5. However, projected precipitation showed comparable increase and decrease for the same period depending on the considered climate

model. It was concluded that considering a large ensemble of climate models is necessary to properly assess future climate projection in the catchment. However, the commonly acknowledged warming signal for the region was clearly confirmed.

Temperature and bias corrected precipitation of the climate model ensemble were used as input for WaSiM to simulate future discharge for the catchment. Consistently with the projected precipitation signal, both increase and decrease in discharge are similarly projected over the period 2021-2050. It was found that having a clear future signal for temperature alone does not permit drawing any conclusion with regards to future discharge within the catchment. As the environmental system of the catchment is water limited, change in discharge regime is primarily dependant on precipitation, while temperature change as projected will have a minor effect. The uncertainty about how water resources in the catchment will evolve by 2050 due to climate change suggests adaptation strategies to consider both increase and decrease in discharge.

Although a clear future trend in water resources availability due to climate change was not demonstrated, it was clearly found that the catchment is undergoing cropland expansion. Infiltration rate within the catchment is decreasing and total discharge decreased with cropland expansion. Therefore, flood frequency and loss of soil fertility due to erosion are expected to increase. Implementation of soil and water conservation techniques like “stone lines” or “rock bunds”, rainwater harvesting, composting etc. which are well-known measures used to buffer runoff, improve water infiltration and reduce the removal of topsoil is crucial to cope with LULC change impact. These techniques are further effective under an uncertain climate as projected. However, experiences in the region demonstrated that adoption of soil and water conservation techniques depend on several determinants such as educational attainment and training level, perception of flood risk and soil erosion, level of organization etc. which requires time for effective implementation.

This study constitutes a contribution to water resources management in the region under land use and climate change. However, several challenges with regard to climate and land use change impact on water resources in the region remain; and could be investigated in future works. This includes:

(i) to integrate land use change into future climate change impact assessment. In line with other studies, one conclusion of the current study was a continuous degradation of savannah in the region. This implies that climate and land use change occurs simultaneously; and assessment of projected climate change impact on water resources will be more plausible if integrating future land use change;

(ii) to investigate the influence of different crop species on soil hydraulic properties. Several works in similar contexts ascertained that crop species differently affect soil hydraulic properties. Cotton production has increased threefold over the period 1990-2007 in the country. Other works support the idea that the increase in cotton was a driver to the production of maize. Therefore, LULC change should not only be seen in terms of change in cropped area, but in terms of crop species and their spatial pattern as well. The recent development of agricultural land use maps of the catchment (delivering the spatial distribution of crops and croplands) provides the opportunity to integrate this information in the hydrological modelling;

(iii) to investigate the impact of climate change on groundwater resources. Groundwater plays a crucial role for water supply in the region. However, many climate change impacts studies concentrated on surface water. Limited knowledge about the aquifers geometry and soil hydraulic properties are the main constraints often reported.

Finally, a major constraint in the region is data availability. Establishing a hydro-meteorological network for the catchment was a considerable achievement of the study. The maintenance of this network is crucial for long term and future investigations.

REFERENCES

Abbaspour, K.C., 2009. SWAT-CUP2. SWAT Calibration Uncertain. Programs User Man. http://swat.tamu.edu/media/114860/usermanual_swatcup.pdf

Agyare, W.A., 2004. Soil Characterization and Modeling of Spatial Distribution of Saturated Hydraulic Conductivity at Two Sites in the Volta Basin of Ghana. Cuvillier Verlag.

Ahmed, K.F., Wang, G., Silander, J., Wilson, A.M., Allen, J.M., Horton, R., Anyah, R., 2013. Statistical downscaling and bias correction of climate model outputs for climate change impact assessment in the U.S. northeast. Glob. Planet. Change 100, 320–332. doi:10.1016/j.gloplacha.2012.11.003

Aich, V., Liersch, S., Vetter, T., Huang, S., Tecklenburg, J., Hoffmann, P., Koch, H., Fournet, S., Krysanova, V., Müller, E.N., Hattermann, F.F., 2014. Comparing impacts of climate change on streamflow in four large African river basins. Hydrol Earth Syst Sci 18, 1305–1321. doi:10.5194/hess-18-1305-2014

Alletto, L., Coquet, Y., 2009. Temporal and spatial variability of soil bulk density and near-saturated hydraulic conductivity under two contrasted tillage management systems. Geoderma 152, 85–94. doi:10.1016/j.geoderma.2009.05.023

Amisigo, A.B., 2005. Modelling riverflow in the Volta Basin of West Africa: A data-driven framework (PhD Thesis). University of Bonn, Germany. http://www.zef.de/fileadmin/template/Glowa/Downloads/Amisigo_doc_thesis_2006.pdf.

Andréassian, V., Perrin, C., Michel, C., Usart-Sanchez, I., Lavabre, J., 2001. Impact of imperfect rainfall knowledge on the efficiency and the parameters of watershed models. J. Hydrol. 250, 206–223. doi:10.1016/S0022-1694(01)00437-1

Ardoin-Bardin, S., Dezetter, A., Servat, E., Paturel, J.E., Mahé, G., Niel, H., Dieulin, C., 2009. Using general circulation model outputs to assess impacts of climate change on runoff for large hydrological catchments in West Africa. Hydrol. Sci. J. 54, 77–89. doi:10.1623/hysj.54.1.77

Awotwi, A., Yeboah, F., Kumi, M., 2015. Assessing the impact of land cover changes on water balance components of White Volta Basin in West Africa. Water Environ. J. 29, 259–267. doi:10.1111/wej.12100

Azuka, V.C., M, I.A., B, D., A, I.C., 2015. Soil survey and soil classification of the Koupendri catchment in Benin, West Africa. Afr. J. Agric. Res. 10, 3938–3951. doi:10.5897/AJAR2015.9904

Beck, H.E., Bruijnzeel, L.A., Dijk, A.I.J.M. van, McVicar, T.R., Scatena, F.N., Schellekens, J., 2013. The impact of forest regeneration on streamflow in 12 mesoscale humid tropical catchments. Hydrol. Earth Syst. Sci. 17, 2613–2635. doi:10.5194/hess-17-2613-2013

Benjamin, J.G., 1993. Tillage effects on near-surface soil hydraulic properties. Soil Tillage Res. 26, 277–288. doi:10.1016/0167-1987(93)90001-6

Bennett, N.D., Croke, B.F.W., Guariso, G., Guillaume, J.H.A., Hamilton, S.H., Jakeman, A.J., Marsili-Libelli, S., Newham, L.T.H., Norton, J.P., Perrin, C., Pierce, S.A., Robson, B., Seppelt, R., Voinov, A.A., Fath, B.D., Andreassian, V., 2013. Characterising performance of environmental models. Environ. Model. Softw. 40, 1–20. doi:10.1016/j.envsoft.2012.09.011

Beven, K., Freer, J., 2001. Equifinality, data assimilation, and uncertainty estimation in mechanistic modelling of complex environmental systems using the GLUE methodology. J. Hydrol. 249, 11–29. doi:10.1016/S0022-1694(01)00421-8

Beven, K.J., 2012. Rainfall-Runoff Modelling: The Primer, 2nd Edition, 2nd ed. John Wiley & Sons, Ltd, Lancaster, England.

Beven, K.J., 2003. Rainfall - Runoff Modelling: The Primer. John Wiley & Sons.

Blin, J., Sidibe, S., 2012. Caractérisation et amélioration d'un foyer de cuisson de "dolo" équipé d'un brûleur à huile végétale (jatropha) [WWW Document]. Proceding CIFEM2 2012. URL http://agritrop.cirad.fr/577011/ (accessed 3.26.16).

Blöschl, G., Sivapalan, M., 1995. Scale issues in Hydrological Modelling: A review. Hydrol. Process. VOL 9 251-290 1995.

Bormann, H., 2005. Evaluation of hydrological models for scenario analyses: signal-to-noise-ratio between scenario effects and model uncertainty. Adv Geosci 5, 43–48. doi:10.5194/adgeo-5-43-2005

Bormann, H., Breuer, L., Gräff, T., Huisman, J.A., 2007. Analysing the effects of soil properties changes associated with land use changes on the simulated water balance: A comparison of three hydrological catchment models for scenario analysis. Ecol. Model., Recent Developments in Hydrological Modelling towards Sustainable Catchment Management 209, 29–40. doi:10.1016/j.ecolmodel.2007.07.004

Bormann, H., Breuer, L., Gräff, T., Huisman, J.A., Croke, B., 2009. Assessing the impact of land use change on hydrology by ensemble modelling (LUCHEM) IV: Model sensitivity to data aggregation and spatial (re-)distribution. Adv. Water Resour. 32, 171–192. doi:10.1016/j.advwatres.2008.01.002

Bormann, H., Faß, T., Giertz, S., Junge, B., Diekkrüger, B., Reichert, B., Skowronek, A., 2005. From local hydrological process analysis to regional hydrological model application in Benin: Concept, results and perspectives. Phys. Chem. Earth Parts ABC 30, 347–356. doi:10.1016/j.pce.2005.06.005

Bormann, H., Klaassen, K., 2008. Seasonal and land use dependent variability of soil hydraulic and soil hydrological properties of two Northern German soils. Geoderma 145, 295–302. doi:10.1016/j.geoderma.2008.03.017

Bossa, A.Y., 2012. Multi-scale modeling of sediment and nutrient flow dynamics in the Oueme catchment (Benin) - towards an assessment of global change effects on soil degradation and water quality (PhD Thesis). University of Bonn, Germany. http://hss.ulb.uni-bonn.de/2012/2983/2983.pdf.

Bossa, A.Y., Diekkrüger, B., Agbossou, E.K., 2014. Scenario-Based Impacts of Land Use and Climate Change on Land and Water Degradation from the Meso to Regional Scale. Water 6, 3152–3181. doi:10.3390/w6103152

Bossa, A.Y., Diekkrüger, B., Giertz, S., Steup, G., Sintondji, L.O., Agbossou, E.K., Hiepe, C., 2012a. Modeling the effects of crop patterns and management scenarios on N and P loads to surface water and groundwater in a semi-humid catchment (West Africa). Agric. Water Manag. 115, 20–37. doi:10.1016/j.agwat.2012.08.011

Bossa, A.Y., Diekkrüger, B., Igué, A.M., Gaiser, T., 2012. Analyzing the effects of different soil databases on modeling of hydrological processes and sediment yield in Benin (West Africa). Geoderma 173–174, 61–74. doi:10.1016/j.geoderma.2012.01.012

Boulain, N., Cappelaere, B., Séguis, L., Favreau, G., Gignoux, J., 2009. Water balance and vegetation change in the Sahel: A case study at the watershed scale with an eco-hydrological model. J. Arid Environ. 73, 1125–1135. doi:10.1016/j.jaridenv.2009.05.008

Boussim, J.I., 2010. Les territoires phytogéographiques. In Atlas de la Biodiversité de l'Afrique de l'Ouest. Thiobiano, A., Kampmann, D., (ed). Ouagadougou & Frankfurt/Main.

Brakensiek, D.L., Rawls, W.J., 1994. Soil containing rock fragments: effects on infiltration. CATENA 23, 99–110. doi:10.1016/0341-8162(94)90056-6

Bruneau, P., Gascuel-Odoux, C., Robin, P., Merot, P., Beven, K., 1995. Sensitivity to space and time resolution of a hydrological model using digital elevation data. Hydrol. Process. 9, 69–81. doi:10.1002/hyp.3360090107

Brutsaert, W., 1982. Energy Fluxes at the Earth's Surface, in: Evaporation into the Atmosphere, Environmental Fluid Mechanics. Springer Netherlands, pp. 128–153.

Buontempo, C., Mathison, C., Jones, R., Williams, K., Wang, C., McSweeney, C., 2014. An ensemble climate projection for Africa. Clim. Dyn. 44, 2097–2118. doi:10.1007/s00382-014-2286-2

Callo-Concha, D., Gaiser, T., Ewert, F., 2012. Farming and cropping systems in the West African Sudanian Savanna. WASCAL research area: Northern Ghana, Southwest Burkina Faso and Northern Benin (No. 100). ZEF Working Paper Series.

Cameira, M.R., Fernando, R.M., Pereira, L.S., 2003. Soil macropore dynamics affected by tillage and irrigation for a silty loam alluvial soil in southern Portugal. Soil Tillage Res. 70, 131–140. doi:10.1016/S0167-1987(02)00154-X

Cappelaere, B., Descroix, L., Lebel, T., Boulain, N., Ramier, D., Laurent, J.-P., Favreau, G., Boubkraoui, S., Boucher, M., Bouzou Moussa, I., Chaffard, V., Hiernaux, P., Issoufou, H.B.A., Le Breton, E., Mamadou, I., Nazoumou, Y., Oi, M., Ottlé, C., Quantin, G., 2009. The AMMA-CATCH experiment in the cultivated Sahelian area of south-west Niger – Investigating water cycle response to a fluctuating climate and changing environment. J. Hydrol. 375, 34–51. doi:10.1016/j.jhydrol.2009.06.021

Caylor, K.K., Scanlon, T.M., Rodriguez-Iturbe, I., 2009. Ecohydrological optimization of pattern and processes in water-limited ecosystems: A trade-off-based hypothesis. Water Resour. Res. 45, W08407. doi:10.1029/2008WR007230

Chen, J., Brissette, F.P., Chaumont, D., Braun, M., 2013. Performance and uncertainty evaluation of empirical downscaling methods in quantifying the climate change impacts on hydrology over two North American river basins. J. Hydrol. 479, 200–214. doi:10.1016/j.jhydrol.2012.11.062

Chow, T.L., Rees, H.W., Monteith, J.O., Toner, P., Lavoie, J., 2007. Effects of coarse fragment content on soil physical properties, soil erosion and potato production. Can. J. Soil Sci. 87, 565–577. doi:10.4141/CJSS07006

Christiaens, K., Feyen, J., 2002. Use of sensitivity and uncertainty measures in distributed hydrological modeling with an application to the MIKE SHE model. Water Resour. Res. 38, 1169. doi:10.1029/2001WR000478

Codjoe, S.N.A., 2004. Population and land use/cover dynamics in the Volta River Basin of Ghana, 1960-2010 (PhD Thesis). University of Bonn, Germany. http://www.zef.de/fileadmin/webfiles/downloads/zefc_ecology_development/ecol_dev_15_text.pdf .

Collins, D.B.G., Bras, R.L., 2007. Plant rooting strategies in water-limited ecosystems. Water Resour. Res. 43, W06407. doi:10.1029/2006WR005541

Cook, K.H., 2008. Climate science: The mysteries of Sahel droughts. Nat. Geosci. 1, 647–648. doi:10.1038/ngeo320

Cook, K.H., Vizy, E.K., 2006. Coupled Model Simulations of the West African Monsoon System: Twentieth- and Twenty-First-Century Simulations. J. Clim. 19, 3681–3703. doi:10.1175/JCLI3814.1

Cord, A., Conrad, C., Schmidt, M., Dech, S., 2010. Standardized FAO-LCCS land cover mapping in heterogeneous tree savannas of West Africa. J. Arid Environ. 74, 1083–1091. doi:10.1016/j.jaridenv.2010.03.012

Cornelissen, T., Diekkrüger, B., Giertz, S., 2013. A comparison of hydrological models for assessing the impact of land use and climate change on discharge in a tropical catchment. J. Hydrol. 498, 221–236. doi:10.1016/j.jhydrol.2013.06.016

Cosby, B.J., Hornberger, G.M., Clapp, R.B., Ginn, T.R., 1984. A Statistical Exploration of the Relationships of Soil Moisture Characteristics to the Physical Properties of Soils. Water Resour. Res. 20, 682–690. doi:10.1029/WR020i006p00682

Cullmann, J., Krausse, T., Saile, P., 2011. Parameterising hydrological models – Comparing optimisation and robust parameter estimation. J. Hydrol. 404, 323–331. doi:10.1016/j.jhydrol.2011.05.003

Cullmann, J., Mishra, V., Peters, R., 2006. Flow analysis with WaSiM-ETH – model parameter sensitivity at different scales. Adv Geosci 9, 73–77. doi:10.5194/adgeo-9-73-2006

D. N. Moriasi, J. G. Arnold, M. W. Van Liew, R. L. Bingner, R. D. Harmel, T. L. Veith, 2007. Model Evaluation Guidelines for Systematic Quantification of Accuracy in Watershed Simulations. Trans. ASABE 50, 885–900. doi:10.13031/2013.23153

Debat, P., Nikiéma, S., Mercier, A., Lompo, M., Béziat, D., Bourges, F., Roddaz, M., Salvi, S., Tollon, F., Wenmenga, U., 2003. A new metamorphic constraint for the Eburnean orogeny from Paleoproterozoic formations of the Man shield (Aribinda and Tampelga countries, Burkina Faso). Precambrian Res. 123, 47–65. doi:10.1016/S0301-9268(03)00046-9

Descroix, L., Mahé, G., Lebel, T., Favreau, G., Galle, S., Gautier, E., Olivry, J.-C., Albergel, J., Amogu, O., Cappelaere, B., Dessouassi, R., Diedhiou, A., Le Breton, E., Mamadou, I., Sighomnou, D., 2009. Spatio-temporal variability of hydrological regimes around the boundaries between Sahelian and Sudanian areas of West Africa: A synthesis. J. Hydrol., Surface processes and water cycle in West Africa, studied from the AMMA-CATCH observing system 375, 90–102. doi:10.1016/j.jhydrol.2008.12.012

Diallo, M.A., 2001. Statistical analysis of agroclimatic parameters based on regional meteorological databas (Technical Report). AGRHYMET, Niamey, Niger.

Diekkrüger, B., 2003. Upscaling of Hydrological Models by Means of Parameter Aggregation Technique, in: Neugebauer, P.H.J., Simmer, C. (Eds.), Dynamics of Multiscale Earth Systems, Lecture Notes in Earth Sciences. Springer Berlin Heidelberg, pp. 145–165.

Diekkrüger, B., Giertz, S., Hiepe, C., Steup, G., Sintondji, L.O., 2010. Hydrological processes and soil degradation in Benin. In: Speth, P., Christoph, M., Diekkrüger, B. (Eds.), Impacts of Global Change on the Hydrological Cycle in West and Northwest Africa. pp. 161–197.

Dipama, M.A., 2010. Climate. In Atlas de la Biodiversité de l'Afrique de l'Ouest. Thiobiano, A., Kampmann, D., (ed). Ouagadougou & Frankfurt/Main.

Donohue, R.J., Roderick, M.L., McVicar, T.R., 2007. On the importance of including vegetation dynamics in Budyko's hydrological model. Hydrol Earth Syst Sci 11, 983–995. doi:10.5194/hess-11-983-2007

Dosio, A., Panitz, H.-J., Schubert-Frisius, M., Lüthi, D., 2015. Dynamical downscaling of CMIP5 global circulation models over CORDEX-Africa with COSMO-CLM: evaluation over the present climate and analysis of the added value. Clim. Dyn. 44, 2637–2661. doi:10.1007/s00382-014-2262-x

Druyan, L.M., Feng, J., Cook, K.H., Xue, Y., Fulakeza, M., Hagos, S.M., Konaré, A., Moufouma-Okia, W., Rowell, D.P., Vizy, E.K., Ibrah, S.S., 2009. The WAMME regional model intercomparison study. Clim. Dyn. 35, 175–192. doi:10.1007/s00382-009-0676-7

Ehret, U., Zehe, E., Wulfmeyer, V., Warrach-Sagi, K., Liebert, J., 2012. HESS Opinions "Should we apply bias correction to global and regional climate model data?" Hydrol Earth Syst Sci 16, 3391–3404. doi:10.5194/hess-16-3391-2012

Eriksen-Hamel, N.S., Speratti, A.B., Whalen, J.K., Légère, A., Madramootoo, C.A., 2009. Earthworm populations and growth rates related to long-term crop residue and tillage management. Soil Tillage Res. 104, 311–316. doi:10.1016/j.still.2009.04.006

Falkenmark, M., Andersson, L., Castensson, R., Sundblad, K., Batchelor, C., Gardiner, J., Lyle, C., Peters, N., Pettersen, B., Quinn, P., Rckström, J., Yapijakis, C., 1999. Water, a reflection of land use: options for counteracting land and water mismanagement. Swedish Natural Science Research Council, Stockholm, Sweden.

Falkenmark, M., Rockström, J., 2004. Balancing Water for Humans and Nature: The New Approach in Ecohydrology. Earthscan.

FAOSTAT of the U.N., 2015. Statistical Databases. Food Agric. Organ. U. N. URL http://faostat.fao.org/site/339/default.aspx

Feddes, R.A., Kowalik, P.J., Zaradny, H., 1978. Simulation of field water use and crop yield. Centre for Agricultural Publishing and Documentation.

Federer, C.A., Lash, D., 1983. BROOK - a hydrologic simulation model for eastern forests. Resources Research Center, University of New Hampshire.

Finnerty, B.D., Smith, M.B., Seo, D.-J., Koren, V., Moglen, G.E., 1997. Space-time scale sensitivity of the Sacramento model to radar-gage precipitation inputs. J. Hydrol. 203, 21–38. doi:10.1016/S0022-1694(97)00083-8

Fodor, N., Sándor, R., Orfanus, T., Lichner, L., Rajkai, K., 2011. Evaluation method dependency of measured saturated hydraulic conductivity. Geoderma 165, 60–68. doi:10.1016/j.geoderma.2011.07.004

Foley, A.M., 2010. Uncertainty in regional climate modelling: A review. Prog. Phys. Geogr. doi:10.1177/0309133310375654

Fontès, J., Guinko, S., 1995. Carte de la végétation et de l'occupation du sol du Burkina Faso: Notice explicative. Toulouse Ministère Coop. Fr. 66p 1.

Forkour, G., 2014. Agricultural Land Use Mapping in West Africa Using Multi-sensor Satellite Imagery (PhD Thesis). Julius-Maximilians-Universität Würzburg, Germany. http://opus.uni-wuerzburg.de/files/10868/Thesis_Gerald_Forkuor_2014.pdf.

Foufoula-Georgiou, E., Georgakakos, K.P., 1991. Hydrologic Advances in Space-Time Precipitation Modeling and Forecasting, in: Bowles, D.S., O'Connell, P.E. (Eds.), Recent Advances in the Modeling of Hydrologic Systems, NATO ASI Series. Springer Netherlands, pp. 47–65.

Gardner, W.R., 1958. Some steady-state solutions of the unsaturated moisture flow equation with applications to evaporation from a water table. Soil Sci. 228–232.

Gbobaniyi, E., Sarr, A., Sylla, M.B., Diallo, I., Lennard, C., Dosio, A., Dhiédiou, A., Kamga, A., Klutse, N.A.B., Hewitson, B., Nikulin, G., Lamptey, B., 2014. Climatology, annual cycle and interannual variability of precipitation and temperature in CORDEX simulations over West Africa. Int. J. Climatol. 34, 2241–2257. doi:10.1002/joc.3834

Ghaffari, G., Keesstra, S., Ghodousi, J., Ahmadi, H., 2010. SWAT-simulated hydrological impact of land-use change in the Zanjanrood basin, Northwest Iran. Hydrol. Process. 24, 892–903. doi:10.1002/hyp.7530

Giertz, S., 2004. Analyse der hydrologischen Prozesse in den sub-humiden Tropen Westafrikas unter besonderer Berücksichtigung der Landnutzung am Beispiel des Aguima-Einzugsgebietes in Benin (PhD Thesis). University of Bonn, Germany. http://hss.ulb.uni-bonn.de/2004/0406/0406.pdf.

Giertz, S., Diekkrüger, B., 2003. Analysis of the hydrological processes in a small headwater catchment in Benin (West Africa). Phys. Chem. Earth Parts ABC 28, 1333–1341. doi:10.1016/j.pce.2003.09.009

Giertz, S., Diekkrüger, B., Steup, G., 2006. Physically-based modelling of hydrological processes in a tropical headwater catchment (West Africa) – process representation and multi-criteria validation. Hydrol Earth Syst Sci 10, 829–847. doi:10.5194/hess-10-829-2006

Giertz, S., Junge, B., Diekkrüger, B., 2005. Assessing the effects of land use change on soil physical properties and hydrological processes in the sub-humid tropical environment of West Africa. Phys. Chem. Earth Parts ABC, Assessment of Anthropogenic Impacts on Water Quality 30, 485–496. doi:10.1016/j.pce.2005.07.003

Gray, L.C., 1999. Is land being degraded? A multi-scale investigation of landscape change in southwestern Burkina Faso. Land Degrad. Dev. 10, 329–343. doi:10.1002/(SICI)1099-145X(199907/08)10:4<329::AID-LDR361>3.0.CO;2-I

Green, T.R., Ahuja, L.R., Benjamin, J.G., 2003. Advances and challenges in predicting agricultural management effects on soil hydraulic properties. Geoderma 116, 3–27. doi:10.1016/S0016-7061(03)00091-0

Gudmundsson, L., Bremnes, J.B., Haugen, J.E., Engen-Skaugen, T., 2012. Technical Note: Downscaling RCM precipitation to the station scale using statistical transformations - a comparison of methods. Hydrol. Earth Syst. Sci. 16, 3383–3390. doi:10.5194/hess-16-3383-2012

Gupta, H.V., Kling, H., Yilmaz, K.K., Martinez, G.F., 2009. Decomposition of the mean squared error and NSE performance criteria: Implications for improving hydrological modelling. J. Hydrol. 377, 80–91. doi:10.1016/j.jhydrol.2009.08.003

Guswa, A.J., 2005. Soil-moisture limits on plant uptake: An upscaled relationship for water-limited ecosystems. Adv. Water Resour. 28, 543–552. doi:10.1016/j.advwatres.2004.08.016

Gwenzi, W., Hinz, C., Holmes, K., Phillips, I.R., Mullins, I.J., 2011. Field-scale spatial variability of saturated hydraulic conductivity on a recently constructed artificial ecosystem. Geoderma 166, 43–56. doi:10.1016/j.geoderma.2011.06.010

Hagemann, S., Chen, C., Haerter, J.O., Heinke, J., Gerten, D., Piani, C., 2011. Impact of a Statistical Bias Correction on the Projected Hydrological Changes Obtained from Three GCMs and Two Hydrology Models. J. Hydrometeorol. 12, 556–578. doi:10.1175/2011JHM1336.1

Hauser, S., Norgrove, L., Asawalam, D., Schulz, S., 2012. Effect of land use change, cropping systems and soil type on earthworm cast production in West and Central Africa. Eur. J. Soil Biol., Bioindication in Soil Ecosystems 49, 47–54. doi:10.1016/j.ejsobi.2012.01.006

Helsel, D.R., Helsel, Helsel, D.R., 1993. Statistical Methods in Water Resources, Pap/Dskt edition. ed. Elsevier Science Pub Co, Amsterdam; New York.

Hiepe, C., 2008. Soil degradation by water erosion in a sub-humid West-African catchment: a modelling approach considering land use and climate change in Benin (PhD Thesis). University of Bonn, Germany. http://hss.ulb.uni-bonn.de/2008/1628/1628.pdf.

Holden, J., 2009. Flow through macropores of different size classes in blanket peat. J. Hydrol. 364, 342–348. doi:10.1016/j.jhydrol.2008.11.010

Hölzel, H., Diekkrüger, B., 2010. Hydrological Analyses as a Prerequisite for Soil Erosion Modeling – Landscape Related Studies in a Mesoscale Hydrological Catchment, in: Otto, J.-C., Dikau, R. (Eds.), Landform - Structure, Evolution, Process Control, Lecture Notes in Earth Sciences. Springer Berlin Heidelberg, pp. 127–149.

Hottin, G., Ouédraogo, O.F., 1992. Carte Géologique du Burkina Faso. - 2. édition, (Bureau des Mines et de la Gélogie du Burkina). Echelle 1:1 000 000.

Huang, P.-T., Patel, M., Santagata, M., Bobet, A., 2009. Classification of Organic Soils. JTRP Tech. Rep. doi:10.5703/1288284314328

Igué, A.M., Gaiser, T., Stahr, K., 2004. A soil and terrain digital database (SOTER) for improved land use planning in Central Benin. Eur. J. Agron. 21, 41–52. doi:10.1016/S1161-0301(03)00062-5

INSD, 2006. Recensement Général de la Population et de l'Habitation. Ministère de l'Economie et des Finances, Ouagadougou, Burkina Faso.

IPCC, 2014. Climate change 2014: impacts, adaptation, and vulnerability. Part B: regional aspects. Contribution of Working Group II to the Fifth Assessment Report of the Intergovernmental Panel on Climate Change (Barros, V.R., C.B. Field, D.J. Dokken, M.D. Mastrandrea, K.J. Mach, T.E. Bilir, M. Chatterjee, K.L. Ebi, Y.O. Estrada, R.C. Genova, B. Girma, E.S. Kissel, A.N. Levy, S. MacCracken, P.R. Mastrandrea, and L.L. White, Cambridge University Press, Cambridge, United Kingdom and New York, NY, USA, 688. ed.

ISO 1100-2, 2010. Hydrometry -- Measurement of liquid flow in open channels -- Part 2: Determination of the stage-discharge relationship.

ISO 10694, 1995. Soil quality - Determination of organic and total carbon after dry combustion (elementary analysis).

ISO 11272, 1998. Soil quality - Determination of dry bulk density.

ISO 11277, 2002. Soil quality - Determination of particle size distribution in mineral soil material - Method by sieving and sedimentation.

ISO 13878, 1998. Soil quality - Determination of total nitrogen content by dry combustion ("elemental analysis").

ISO 17892, 2014. Geotechnical investigation and testing — Laboratory testing of soil — Part 1: Determination of water content.

Janssen, P.H.M., Heuberger, P.S.C., Sanders, R., 1994. UNCSAM: a tool for automating sensitivity and uncertainty analysis. Environ. Softw. 9, 1–11. doi:10.1016/0266-9838(94)90010-8

Jarvis, A., Reuter, H.I., Nelson, A., Guevara, E., 2008. Hole-filled SRTM for the globe Version 4. Available CGIAR-CSI SRTM 90m Database Httpsrtm Csi Cgiar Org.

Jobbágy, E.G., Jackson, R.B., 2000. The Vertical Distribution of Soil Organic Carbon and Its Relation to Climate and Vegetation. Ecol. Appl. 10, 423–436. doi:10.1890/1051-0761(2000)010[0423:TVDOSO]2.0.CO;2

Johnson, F., Sharma, A., 2015. What are the impacts of bias correction on future drought projections? J. Hydrol. 525, 472–485. doi:10.1016/j.jhydrol.2015.04.002

Jouquet, P., Janeau, J.-L., Pisano, A., Sy, H.T., Orange, D., Minh, L.T.N., Valentin, C., 2012. Influence of earthworms and termites on runoff and erosion in a tropical steep slope fallow in Vietnam: A rainfall simulation experiment. Appl. Soil Ecol., Microorganisms and the Sustainable Management of Soil 61, 161–168. doi:10.1016/j.apsoil.2012.04.004

Kaloga, B., Boulet, R., Leprun, J.C., Alboucq, G., Pottier, J.C., 1973. Carte pédologique de reconnaissance de la République de Haute-Volta. Office de la recherche scientifique et technique outre-mer, Centre ORSTOM de Dakar.

Kanitpong, K., Benson, C., Bahia, H., 2001. Hydraulic Conductivity (Permeability) of Laboratory-Compacted Asphalt Mixtures. Transp. Res. Rec. J. Transp. Res. Board 1767, 25–32. doi:10.3141/1767-04

Karambiri, H., García Galiano, S.G., Giraldo, J.D., Yacouba, H., Ibrahim, B., Barbier, B., Polcher, J., 2011. Assessing the impact of climate variability and climate change on runoff in West Africa: the case of Senegal and Nakambe River basins. Atmospheric Sci. Lett. 12, 109–115. doi:10.1002/asl.317

Kasei, R.A., 2009. Modelling impacts of climate change on water resources in the Volta Basin, West Africa. (PhD Thesis) University of Bonn, Germany. http://hss.ulb.uni-bonn.de/2010/1977/1977.pdf.

Kasei, R., Diekkrüger, B., Leemhuis, C., 2009. Drought frequency in the Volta Basin of West Africa. Sustain. Sci. 5, 89–97. doi:10.1007/s11625-009-0101-5

Kassa, A.K., 2013. Downscaling Climate Model Outputs for Estimating the Impact of Climate Change on Water Availability over the Baro-Akobo River Basin, Ethiopia. Universitäts-und Landesbibliothek Bonn.

Katul, G.G., Parlange, M.B., 1992. A Penman-Brutsaert Model for wet surface evaporation. Water Resour. Res. 28, 121–126. doi:10.1029/91WR02324

Kelishadi, H., Mosaddeghi, M.R., Hajabbasi, M.A., Ayoubi, S., 2014. Near-saturated soil hydraulic properties as influenced by land use management systems in Koohrang region of central Zagros, Iran. Geoderma 213, 426–434. doi:10.1016/j.geoderma.2013.08.008

Klein, C., Heinzeller, D., Bliefernicht, J., Kunstmann, H., 2015. Variability of West African monsoon patterns generated by a WRF multi-physics ensemble. Clim. Dyn. 45, 2733–2755. doi:10.1007/s00382-015-2505-5

Kling, H., Fuchs, M., Paulin, M., 2012. Runoff conditions in the upper Danube basin under an ensemble of climate change scenarios. J. Hydrol. 424–425, 264–277. doi:10.1016/j.jhydrol.2012.01.011

Korck, J., Danneberg, J., Willems, W., 2012. Impacts of climate change on the water regime of the Inn River basin – extracting adaptation-relevant information from climate model ensembles and impact modelling. Adv Geosci 32, 99–107. doi:10.5194/adgeo-32-99-2012

Krajewski, W.F., Lakshmi, V., Georgakakos, K.P., Jain, S.C., 1991. A Monte Carlo Study of rainfall sampling effect on a distributed catchment model. Water Resour. Res. 27, 119–128. doi:10.1029/90WR01977

Kunstmann, H., Jung, G., Wagner, S., Clottey, H., 2008. Integration of atmospheric sciences and hydrology for the development of decision support systems in sustainable water management. Phys. Chem. Earth Parts ABC, Hydrological Assessment and Integrated Water Resources Management with Special Focus on Developing Countries 33, 165–174. doi:10.1016/j.pce.2007.04.010

Kusumandari, A., Nugroho, P., 2015. Land Capability Analysis Based on Hydrology and Soil Characteristics for Watershed Rehabilitation. Procedia Environ. Sci., The 5th Sustainable Future for Human Security (SustaiN 2014) 28, 142–147. doi:10.1016/j.proenv.2015.07.020

Landmann, T., Herty, C., Dech, S., Schmidt, M., 2007. Land cover change analysis within the GLOWA Volta basin in West Africa using 30-meter Landsat data snapshots, in: Geoscience and Remote Sensing Symposium, 2007. IGARSS 2007. IEEE International. Presented at the Geoscience and Remote Sensing Symposium, 2007. IGARSS 2007. IEEE International, pp. 5298–5301. doi:10.1109/IGARSS.2007.4424058

Leemhuis, C., 2006. The Impact of El Niño Southern Oscillation Events on Water Resource Availability in Central Sulawesi, Indonesia. A hydrological modelling approach.

Leemhuis, C., Erasmi, S., Twele, A., Kreilein, H., Oltchev, A., Gerold, G., 2007. Rainforest conversion in Central Sulawesi, Indonesia: recent development and consequences for river discharge and water resources. Erdkunde 61, 284–293. doi:10.3112/erdkunde.2007.03.06

Leemhuis, C., Jung, G., Kasei, R., Liebe, J., 2009. The Volta Basin Water Allocation System: assessing the impact of small-scale reservoir development on the water resources of the Volta basin, West Africa. Adv Geosci 21, 57–62. doi:10.5194/adgeo-21-57-2009

Lendres, P., Faure, G., Belem, P.C., 1992. Pratiques paysannes et utilisation des intrants en culture cotonnière au Burkina Faso. Campagne 91/92. Rev. Sci. Tchad 2, 169–180.

Leonard, J., Mietton, M., Najib, H., Gourbesville, P., 2000. Rating curve modelling with Manning's equation to manage instability and improve extrapolation. Hydrol. Sci. J. 45, 739–750. doi:10.1080/02626660009492374

Logemann, K., Ólafsson, J., Snorrason, Á., Valdimarsson, H., Marteinsdóttir, G., 2013. The circulation of Icelandic waters–a modelling study. Ocean Sci. 9, 931–955.

MA, 2005. Ecosystems and Human Well-being: Current State and Trends.

Mahé, G., Diello, P., Paturel, J.-E., Barbier, B., Karambiri, H., Dezetter, A., Dieulin, C., Rouche, N., 2010. Baisse des pluies et augmentation des écoulements au Sahel : impact climatique et anthropique sur les écoulements du Nakambe au Burkina Faso. Sci. Chang. Planétaires Sécher. 21, 330–332. doi:10.1684/sec.2010.0268

Mahé, G., Paturel, J.-E., Servat, E., Conway, D., Dezetter, A., 2005. The impact of land use change on soil water holding capacity and river flow modelling in the Nakambe River, Burkina-Faso. J. Hydrol. 300, 33–43. doi:10.1016/j.jhydrol.2004.04.028

Marascuilo, L.A., McSweeney, M., 1977. Nonparametric and distribution-free methods for the social sciences. Brooks/Cole Monterey, CA.

Martin, N., 2005. Development of a water balance for the Atankwidi catchment, West Africa – A case study of groundwater recharge in a semi-arid climate (PhD Thesis). University of Bonn, Germany. http://www.zef.de/fileadmin/template/Glowa/Downloads/thesis_martin.pdf.

Mbaye, M.L., Hagemann, S., Haensler, A., Stacke, T., Gaye, A.T., Afouda, A., 2015. Assessment of Climate Change Impact on Water Resources in the Upper Senegal Basin (West Africa). Am. J. Clim. Change 4, 77. doi:10.4236/ajcc.2015.41008

McClean, C.J., Lovett, J.C., Küper, W., Hannah, L., Sommer, J.H., Barthlott, W., Termansen, M., Smith, G.F., Tokumine, S., Taplin, J.R.D., 2005. African Plant Diversity and Climate Change. Ann. Mo. Bot. Gard. 92, 139–152.

McKay, M.D., Beckman, R.J., Conover, W.J., 1979. A Comparison of Three Methods for Selecting Values of Input Variables in the Analysis of Output from a Computer Code. Technometrics 21, 239–245. doi:10.2307/1268522

McKee, T.B., Doesken, N.J., Kleist, J., 1993. The relationship of drought frequency and duration to time scales, in: Proceedings of the 8th Conference on Applied Climatology. American Meteorological Society Boston, MA, USA, pp. 179–183.

MEAHA, 2013. Annuaire statistique de l'eau potable et de l'assainissement des eaux usées et excreta. Ministère de l'Eau, des Aménagements Hydrauliques et de l'Assainissemnt. Ouagadougou, Burkina Faso.

Mettrop, I.S., Cammeraat, L.H., Verbeeten, E., 2013. The impact of subterranean termite activity on water infiltration and topsoil properties in Burkina Faso. Ecohydrology 6, 324–331. doi:10.1002/eco.1271

Miller, S.N., Kepner, W.G., Mehaffey, M.H., Hernandez, M., Miller, R.C., Goodrich, D.C., Kim Devonald, K., Heggem, D.T., Miller, W.P., 2002. Integrating Landscape Assessment and Hydrologic Modeling for Land Cover Change Analysis1. JAWRA J. Am. Water Resour. Assoc. 38, 915–929. doi:10.1111/j.1752-1688.2002.tb05534.x

Milne, B.T., Gupta, V.K., Restrepo, C., 2002. A scale invariant coupling of plants, water, energy, and terrain. Écoscience 9, 191–199.

Minasny, B., Hartemink, A.E., 2011. Predicting soil properties in the tropics. Earth-Sci. Rev. 106, 52–62. doi:10.1016/j.earscirev.2011.01.005

Miranda, J.P., Silva, L.M., Lima, R.L., Donagemma, G.K., Bertolino, A.V.A., Fernandes, N.F., Correa, F.M., Polidoro, J.C., Tato, G., 2009. Fallow Effects on Improving Soil Properties and Decreasing Erosion: Atlantic Forest, Southeastern Brazil, in: EGU General Assembly Conference Abstracts. Presented at the EGU General Assembly Conference Abstracts, p. 12276.

Mohanty, B.P., Kanwar, R.S., Everts, C.J., 1994. Comparison of Saturated Hydraulic Conductivity Measurement Methods for a Glacial-Till Soil. Soil Sci. 58.

Monteith, J.L., 1975. Vegetation and the atmosphere. Vol. 1. Principles. Vol. 2. Case studies. 298 ; 458 pp.

Monteith, J.L., 1975. Vegetation and the atmosphere. Vol. 1. Principles. Vol. 2. Case studies. Veg. Atmosphere Vol 1 Princ. Vol 2 Case Stud.

Moret, D., Arrúe, J.L., 2007. Dynamics of soil hydraulic properties during fallow as affected by tillage. Soil Tillage Res. 96, 103–113. doi:10.1016/j.still.2007.04.003

Moss, R.H., Edmonds, J.A., Hibbard, K.A., Manning, M.R., Rose, S.K., van Vuuren, D.P., Carter, T.R., Emori, S., Kainuma, M., Kram, T., Meehl, G.A., Mitchell, J.F.B., Nakicenovic, N., Riahi, K., Smith, S.J., Stouffer, R.J., Thomson, A.M., Weyant, J.P., Wilbanks, T.J., 2010. The next generation of scenarios for climate change research and assessment. Nature 463, 747–756. doi:10.1038/nature08823

Mounirou, L.A., 2012. Etude du ruissellement et de l'érosion à différentes échelles spatiales sur le bassin versant de Tougou en zone sahélienne du Burkina Faso : Quantification et transposition des données (PhD Thesis). Université de Montpellier II; Fondation 2iE, France, Burkina Faso. http://www.2ie-edu.org/assets/2iERapport-de-th%C3%A8se-Lawani-A.-Mounirou2012.pdf.

Muerth, M.J., Gauvin St-Denis, B., Ricard, S., Velázquez, J.A., Schmid, J., Minville, M., Caya, D., Chaumont, D., Ludwig, R., Turcotte, R., 2013. On the need for bias correction in regional climate scenarios to assess climate change impacts on river runoff. Hydrol Earth Syst Sci 17, 1189–1204. doi:10.5194/hess-17-1189-2013

Murphy, A.H., 1988. Skill Scores Based on the Mean Square Error and Their Relationships to the Correlation Coefficient. Mon. Weather Rev. 116, 2417–2424. doi:10.1175/1520-0493(1988)116<2417:SSBOTM>2.0.CO;2

Nash, J.E., Sutcliffe, J.V., 1970. River flow forecasting through conceptual models part I — A discussion of principles. J. Hydrol. 10, 282–290. doi:10.1016/0022-1694(70)90255-6

Neris, J., Jiménez, C., Fuentes, J., Morillas, G., Tejedor, M., 2012. Vegetation and land-use effects on soil properties and water infiltration of Andisols in Tenerife (Canary Islands, Spain). CATENA 98, 55–62. doi:10.1016/j.catena.2012.06.006

Newman, B.D., Wilcox, B.P., Archer, S.R., Breshears, D.D., Dahm, C.N., Duffy, C.J., McDowell, N.G., Phillips, F.M., Scanlon, B.R., Vivoni, E.R., 2006. Ecohydrology of water-limited environments: A scientific vision. Water Resour. Res. 42, W06302. doi:10.1029/2005WR004141

Niehoff, D., Fritsch, U., Bronstert, A., 2002. Land-use impacts on storm-runoff generation: scenarios of land-use change and simulation of hydrological response in a meso-scale catchment in SW-Germany. J. Hydrol., Advances in Flood Research 267, 80–93. doi:10.1016/S0022-1694(02)00142-7

Nikulin, G., Jones, C., Giorgi, F., Asrar, G., Büchner, M., Cerezo-Mota, R., Christensen, O.B., Déqué, M., Fernandez, J., Hänsler, A., van Meijgaard, E., Samuelsson, P., Sylla, M.B., Sushama, L., 2012. Precipitation Climatology in an Ensemble of CORDEX-Africa Regional Climate Simulations. J. Clim. 25, 6057–6078. doi:10.1175/JCLI-D-11-00375.1

Novák, V., Kňava, K., Šimůnek, J., 2011. Determining the influence of stones on hydraulic conductivity of saturated soils using numerical method. Geoderma 161, 177–181. doi:10.1016/j.geoderma.2010.12.016

Oguntunde, P.G., Abiodun, B.J., 2012. The impact of climate change on the Niger River Basin hydroclimatology, West Africa. Clim. Dyn. 40, 81–94. doi:10.1007/s00382-012-1498-6

Op de Hipt, F., 2013. Soil organic carbon and its determinants in a small watershed in south-western Burkina Faso (MsC Thesis). University of Köln, Germany, Köln.

Osunbitan, J.A., Oyedele, D.J., Adekalu, K.O., 2005. Tillage effects on bulk density, hydraulic conductivity and strength of a loamy sand soil in southwestern Nigeria. Soil Tillage Res. 82, 57–64. doi:10.1016/j.still.2004.05.007

Ott, I., Duethmann, D., Liebert, J., Berg, P., Feldmann, H., Ihringer, J., Kunstmann, H., Merz, B., Schaedler, G., Wagner, S., 2013. High-Resolution Climate Change Impact Analysis on Medium-Sized River Catchments in Germany: An Ensemble Assessment. J. Hydrometeorol. 14, 1175–1193. doi:10.1175/JHM-D-12-091.1

Ouattara, B., Ouattara, K., Serpantieé, G., Mando, A., Seédogo, M.P., Bationo, A., 2007. Intensity cultivation induced effects on soil organic carbon dynamic in the western cotton area of Burkina Faso, in: Bationo, A., Waswa, B., Kihara, J., Kimetu, J. (Eds.), Advances in Integrated Soil Fertility Management in Sub-Saharan Africa: Challenges and Opportunities. Springer Netherlands, pp. 749–758.

Ouédraogo, O.F., Equipe Projet SYSMIN, BRGM, 2003. Notice explicative de la carte géologique du Burkina Faso au 1/200 000.

Oyerinde, G.T., Hountondji, F.C.C., Wisser, D., Diekkrüger, B., Lawin, A.E., Odofin, A.J., Afouda, A., 2014. Hydro-climatic changes in the Niger basin and consistency of local perceptions. Reg. Environ. Change 15, 1627–1637. doi:10.1007/s10113-014-0716-7

Paeth, H., Hall, N.M.J., Gaertner, M.A., Alonso, M.D., Moumouni, S., Polcher, J., Ruti, P.M., Fink, A.H., Gosset, M., Lebel, T., Gaye, A.T., Rowell, D.P., Moufouma-Okia, W., Jacob, D., Rockel, B., Giorgi, F., Rummukainen, M., 2011. Progress in regional downscaling of west African precipitation. Atmospheric Sci. Lett. 12, 75–82. doi:10.1002/asl.306

Pappenberger, F., Beven, K.J., 2006. Ignorance is bliss: Or seven reasons not to use uncertainty analysis. Water Resour. Res. 42, W05302. doi:10.1029/2005WR004820

Paré, S., Söderberg, U., Sandewall, M., Ouadba, J.M., 2008. Land use analysis from spatial and field data capture in southern Burkina Faso, West Africa. Agric. Ecosyst. Environ. 127, 277–285. doi:10.1016/j.agee.2008.04.009

Patricola, C.M., Cook, K.H., 2009. Northern African climate at the end of the twenty-first century: an integrated application of regional and global climate models. Clim. Dyn. 35, 193–212. doi:10.1007/s00382-009-0623-7

PDIC/D, 2010. Programme de Développement intégré de la Commune de Dano. Commune urbaine de Dano & Dreyer Foundation. Dano, Burkina Faso.

Peigné, J., Cannavaciuolo, M., Gautronneau, Y., Aveline, A., Giteau, J.L., Cluzeau, D., 2009. Earthworm populations under different tillage systems in organic farming. Soil Tillage Res. 104, 207–214. doi:10.1016/j.still.2009.02.011

Piani, C., Weedon, G.P., Best, M., Gomes, S.M., Viterbo, P., Hagemann, S., Haerter, J.O., 2010. Statistical bias correction of global simulated daily precipitation and temperature for the application of hydrological models. J. Hydrol. 395, 199–215. doi:10.1016/j.jhydrol.2010.10.024

Pirastru, M., Castellini, M., Giadrossich, F., Niedda, M., 2013. Comparing the Hydraulic Properties of Forested and Grassed Soils on an Experimental Hillslope in a Mediterranean Environment. Procedia Environ. Sci. 19, 341–350. doi:10.1016/j.proenv.2013.06.039

Ramos, T.B., Gonçalves, M.C., Martins, J.C., van Genuchten, M.T., Pires, F.P., 2006. Estimation of Soil Hydraulic Properties from Numerical Inversion of Tension Disk Infiltrometer Data. Vadose Zone J. 5, 684. doi:10.2136/vzj2005.0076

Rawls, W.J., Brakensiek, D.L., 1989. Estimation of Soil Water Retention and Hydraulic Properties, in: Morel-Seytoux, H.J. (Ed.), Unsaturated Flow in Hydrologic Modeling, NATO ASI Series. Springer Netherlands, pp. 275–300.

Rawls, W.J., Nemes, A., Pachepsky, Y., 2004. Effect of soil organic carbon on soil hydraulic properties, in: Science, B.-D. in S. (Ed.), Development of Pedotransfer Functions in Soil Hydrology. Elsevier, pp. 95–114.

Rawls, W.J., Pachepsky, Y.A., Ritchie, J.C., Sobecki, T.M., Bloodworth, H., 2003. Effect of soil organic carbon on soil water retention. Geoderma, Quantifying agricultural management effects on soil properties and processes 116, 61–76. doi:10.1016/S0016-7061(03)00094-6

Reusser, D.E., Zehe, E., 2011. Inferring model structural deficits by analyzing temporal dynamics of model performance and parameter sensitivity. Water Resour. Res. 47, W07550. doi:10.1029/2010WR009946

Reynolds, W.D., Bowman, B.T., Brunke, R.R., Drury, C.F., Tan, C.S., 2000. Comparison of Tension Infiltrometer, Pressure Infiltrometer, and Soil Core Estimates of Saturated Hydraulic Conductivity. Soil Sci. Soc. Am. J. 64, 478. doi:10.2136/sssaj2000.642478x

Richter, O., Diekkrüger, B., Nörtersheuser, P., 1996. Environmental Fate Modelling of Pesticides. John Wiley & Sons.

Rienzner, M., Gandolfi, C., 2014. Investigation of spatial and temporal variability of saturated soil hydraulic conductivity at the field-scale. Soil Tillage Res. 135, 28–40. doi:10.1016/j.still.2013.08.012

Ruelland, D., Ardoin-Bardin, S., Collet, L., Roucou, P., 2012. Simulating future trends in hydrological regime of a large Sudano-Sahelian catchment under climate change. J. Hydrol. 424–425, 207–216. doi:10.1016/j.jhydrol.2012.01.002

Ruti, P.M., Williams, J.E., Hourdin, F., Guichard, F., Boone, A., Van Velthoven, P., Favot, F., Musat, I., Rummukainen, M., Domínguez, M., Gaertner, M.Á., Lafore, J.P., Losada, T., Rodriguez de Fonseca, M.B., Polcher, J., Giorgi, F., Xue, Y., Bouarar, I., Law, K., Josse, B., Barret, B., Yang, X., Mari, C., Traore, A.K., 2011. The West African climate system: a review of the AMMA model inter-comparison initiatives. Atmospheric Sci. Lett. 12, 116–122. doi:10.1002/asl.305

Salack, S., Sarr, B., Sangare, S.K., Ly, M., Sanda, I.S., Kunstmann, H., 2015. Crop-climate ensemble scenarios to improve risk assessment and resilience in the semi-arid regions of West Africa. Clim. Res. 65, 107–121. doi:10.3354/cr01282

Sandwidi, W.J.P., 2007. Groundwater potential to supply population demand within the Kompienga dam basin in Burkina Faso (Text.PhDThesis). University of Bonn, Germany.

Sarr, B., Sanoussi, A., Mohamed, L., Seyni, S., David, A.G., 2015. Adapting to climate variability and change in smallholder farming communities: A case study from Burkina Faso, Chad and Niger. J. Agric. Ext. Rural Dev. 7, 16–27. doi:10.5897/JAERD14.0595

Saxton, K.E., Rawls, W.J., 2006. Soil water characteristic estimates by texture and organic matter for hydrologic solutions. Soil Sci. Soc. Am. J. 70, 1569–1578.

Saxton, K.E., Rawls, W.J., Romberger, J.S., Papendick, R.I., 1986. Estimating Generalized Soil-water Characteristics from Texture1. Soil Sci. Soc. Am. J. 50, 1031. doi:10.2136/sssaj1986.03615995005000040039x

Schaap, M.G., Leij, F.J., van Genuchten, M.T., 2001. rosetta: a computer program for estimating soil hydraulic parameters with hierarchical pedotransfer functions. J. Hydrol. 251, 163–176. doi:10.1016/S0022-1694(01)00466-8

Scheffler, R., Neill, C., Krusche, A.V., Elsenbeer, H., 2011. Soil hydraulic response to land-use change associated with the recent soybean expansion at the Amazon agricultural frontier. Agric. Ecosyst. Environ. 144, 281–289. doi:10.1016/j.agee.2011.08.016

Schenk, H.J., Jackson, R.B., 2002. Rooting depths, lateral root spreads and below-ground/above-ground allometries of plants in water-limited ecosystems. J. Ecol. 90, 480–494. doi:10.1046/j.1365-2745.2002.00682.x

Schmengler, A.C., 2011. Modeling Soil Erosion and Reservoir Sedimentation at Hillslope and Catchment Scale in Semi-Arid Burkina Faso (PhDThesis). University of Bonn, Germany. http://hss.ulb.uni-bonn.de/2011/2483/2483.htm.

Schulla, J., 2015. Model Description WaSiM. http://wasim.ch/downloads/doku/wasim/wasim_2015_en.pdf.

Schulla, J., 2014. Model Description WaSiM. http://www.wasim.ch/downloads/doku/wasim/wasim_2013_en.pdf.

Schulla, J., 1997. Hydrologische Modellierung von Flussgebieten zur Abschätzung der Folgen von Klimaänderungen. Diss. Naturwiss. ETH Zürich, Nr. 12018, 1997. Ref.: H. Lang; Korref.: W. Kinzelbach; Korref.: R. Schulze, ZÜRICH.

Schulze-Makuch, D., Carlson, D.A., Cherkauer, D.S., Malik, P., 1999. Scale Dependency of Hydraulic Conductivity in Heterogeneous Media. Ground Water 37, 904–919. doi:10.1111/j.1745-6584.1999.tb01190.x

Schwartz, R.C., Evett, S.R., Unger, P.W., 2003. Soil hydraulic properties of cropland compared with reestablished and native grassland. Geoderma 116, 47–60. doi:10.1016/S0016-7061(03)00093-4

Schwärzel, K., Punzel, J., 2007. Hood Infiltrometer—A New Type of Tension Infiltrometer. Soil Sci. Soc. Am. J. 71, 1438. doi:10.2136/sssaj2006.0104

Schwen, A., Bodner, G., Scholl, P., Buchan, G.D., Loiskandl, W., 2011. Temporal dynamics of soil hydraulic properties and the water-conducting porosity under different tillage. Soil Tillage Res. 113, 89–98. doi:10.1016/j.still.2011.02.005

SCS, 1993. Soil survey manual. Soil Conservation Service. U.S. Department of Agriculture Handbook 18.

Shabtai, I.A., Shenker, M., Edeto, W.L., Warburg, A., Ben-Hur, M., 2014. Effects of land use on structure and hydraulic properties of Vertisols containing a sodic horizon in northern Ethiopia. Soil Tillage Res. 136, 19–27. doi:10.1016/j.still.2013.09.007

Sileshi, G., Mafongoya, P.L., 2003. Effect of rotational fallows on abundance of soil insects and weeds in maize crops in eastern Zambia. Appl. Soil Ecol. 23, 211–222. doi:10.1016/S0929-1393(03)00049-0

Singh, S.K., Liang, J., Bárdossy, A., 2012. Improving the calibration strategy of the physically-based model WaSiM-ETH using critical events. Hydrol. Sci. J. 57, 1487–1505. doi:10.1080/02626667.2012.727091

Sivakumar, M.V.K., Gnoumou, F., 1987. Agroclimatology of West Africa: Burkina Faso [WWW Document]. URL http://oar.icrisat.org/864/ (accessed 3.24.16).

Speth, P., Christoph, M., Diekkrüger, B., 2010. Impacts of Global Change on the Hydrological Cycle in West and Northwest Africa. Springer, Germany.

Stephenne, N., Lambin, E.F., 2001. A dynamic simulation model of land-use changes in Sudano-sahelian countries of Africa (SALU). Agric. Ecosyst. Environ. 85, 145–161.

Strudley, M.W., Green, T.R., Ascough II, J.C., 2008. Tillage effects on soil hydraulic properties in space and time: State of the science. Soil Tillage Res. 99, 4–48. doi:10.1016/j.still.2008.01.007

Sylla, M.B., Elguindi, N., Giorgi, F., Wisser, D., 2015. Projected robust shift of climate zones over West Africa in response to anthropogenic climate change for the late 21st century. Clim. Change 134, 241–253. doi:10.1007/s10584-015-1522-z

Teutschbein, C., Seibert, J., 2012. Bias correction of regional climate model simulations for hydrological climate-change impact studies: Review and evaluation of different methods. J. Hydrol. 456–457, 12–29. doi:10.1016/j.jhydrol.2012.05.052

Thiombiano, A., Kampmann, D., 2010. Atlas de la Biodiversité de l'Afrique de l'Ouest. Ouagadougou & Frankfurt/Main.

Tietje, O., Hennings, V., 1996. Accuracy of the saturated hydraulic conductivity prediction by pedo-transfer functions compared to the variability within FAO textural classes. Geoderma 69, 71–84. doi:10.1016/0016-7061(95)00050-X

Tomer, M.D., Schilling, K.E., 2009. A simple approach to distinguish land-use and climate-change effects on watershed hydrology. J. Hydrol. 376, 24–33. doi:10.1016/j.jhydrol.2009.07.029

Tomkins, K.M., 2014. Uncertainty in streamflow rating curves: methods, controls and consequences. Hydrol. Process. 28, 464–481. doi:10.1002/hyp.9567

UGT, U.-G.-T.G., 2012. Hood infiltrometer IL-2700. http://www.ugt-online.de/fileadmin/media/products/01%20bodenkunde/downloads/Hauben_etc/Hood-Infiltrometer_-_IL_2700.pdf.

Van Engelen, V., Wen, T., 1995. Global and National Soils and Terrain Digital Databases (SOTER). Procedures Manual (revised edition). ISSS-UNEP-FAO-ISRIC, Wagenigen, Netherlands.

Van der Sluijs, J.P., Janssen, P.H.M., Petersen, A.C., Kloprogge, P., Risbey, J.S., Tuinstra, W., Ravetz, J.R., 2004. RIVM/MNP guidance for uncertainty assessment and communication: tool catalogue for uncertainty assessment. Utrecht Univ. Downloadable Httpwww Nusap Netsections Php.

van Genuchten, M.T., 1980. A Closed-form Equation for Predicting the Hydraulic Conductivity of Unsaturated Soils1. Soil Sci. Soc. Am. J. 44, 892. doi:10.2136/sssaj1980.03615995004400050002x

van Genuchten, M.T., 1976. A Closed-form Equation for Predicting the Hydraulic Conductivity of Unsaturated Soils1. Soil Sci. Soc. Am. J. 44, 892–898. doi:10.2136/sssaj1980.03615995004400050002x

Vereecken, H., Maes, J., Feyen, J., 1990. Estimating unsaturated hydraulic conductivity from easily measured soil properties. Soil Sci. 149, 1–12. doi:10.1097/00010694-199001000-00001

Vicente-Serrano, S.M., Beguería, S., López-Moreno, J.I., 2009. A Multiscalar Drought Index Sensitive to Global Warming: The Standardized Precipitation Evapotranspiration Index. J. Clim. 23, 1696–1718. doi:10.1175/2009JCLI2909.1

Villeneuve, M., Cornée, J.J., 1994. Structure, evolution and palaeogeography of the West African craton and bordering belts during the Neoproterozoic. Precambrian Res. 69, 307–326. doi:10.1016/0301-9268(94)90094-9

Vogeler, I., Rogasik, J., Funder, U., Panten, K., Schnug, E., 2009. Effect of tillage systems and P-fertilization on soil physical and chemical properties, crop yield and nutrient uptake. Soil Tillage Res. 103, 137–143. doi:10.1016/j.still.2008.10.004

Wagner, P.D., Kumar, S., Schneider, K., 2013. An assessment of land use change impacts on the water resources of the Mula and Mutha Rivers catchment upstream of Pune, India. Hydrol Earth Syst Sci 17, 2233–2246. doi:10.5194/hess-17-2233-2013

Wang, D., Yates, S.R., Lowery, B., Th. van Genuchten, M., 1998. Estimating soil hydraulic properties using tension infiltrometer with varying disk diameter. Soil Sci. 163.

Wang, Y., Shao, M., Liu, Z., Horton, R., 2013. Regional-scale variation and distribution patterns of soil saturated hydraulic conductivities in surface and subsurface layers in the loessial soils of China. J. Hydrol. 487, 13–23. doi:10.1016/j.jhydrol.2013.02.006

Waongo, M., 2015. Optimizing Planting Dates for Agricultural Decision-Making under Climate Change over Burkina Faso/West Africa (PhD Thesis). Augsburg, Augsburg, Germany.

Waongo, M., Laux, P., Kunstmann, H., 2015. Adaptation to climate change: The impacts of optimized planting dates on attainable maize yields under rainfed conditions in Burkina Faso. Agric. For. Meteorol. 205, 23–39. doi:10.1016/j.agrformet.2015.02.006

Warburton, M.L., Schulze, R.E., Jewitt, G.P.W., 2012. Hydrological impacts of land use change in three diverse South African catchments. J. Hydrol. 414–415, 118–135. doi:10.1016/j.jhydrol.2011.10.028

Węglarczyk, S., 1998. The interdependence and applicability of some statistical quality measures for hydrological models. J. Hydrol. 206, 98–103. doi:10.1016/S0022-1694(98)00094-8

Wendling, U., 1975. Zur Messung und Schätzung der potentiellen Verdunstung. Zeitschrift für Meteorologie. Nr. 25 (1975),S. 103-111.

WHO, U., 2015. Progress on Sanitation and Drinking Water: 2015 Update and MDG Assessment. Geneva World Health Organ.

Wilcoxon, F., 1945. Individual Comparisons by Ranking Methods. Biom. Bull. 1, 80–83. doi:10.2307/3001968

WMO (Ed.), 2010. Manual on Stream Gauging Volume 1 - Fieldwork WMO-No. 1044. World Meterorological Organization, Geneva , Switzerland.

WMO, 1993. SITING EXPOSURE OF METEOROLOGICAL INSTRUMENTS (SEMI) WMO-No. 55 (No. 55). World Meteorological Organization, Lausanne.

Wooding, R.A., 1968. Steady Infiltration from a Shallow Circular Pond. Water Resour. Res. 4, 1259–1273. doi:10.1029/WR004i006p01259

WRB, I.U.S.S.W.G., 2006. World reference base for soil resources, World Soil Resources Reports No. 103. ed. Food & Agriculture Org. ftp://ftp.fao.org/docrep/fao/009/a0510e/a0510e00.pdf, Rom.

WWDR, U.N.W.W.A.P., 2015. The United Nations World Water Development Report: Water in a Sustainable World. UNESCO, Paris.

Young, M.D.B., Gowing, J.W., Hatibu, N., Mahoo, H.M.F., Payton, R.W., 1999. Assessment and development of pedotransfer functions for semi-arid sub-Saharan Africa. Phys. Chem. Earth Part B Hydrol. Oceans Atmosphere 24, 845–849. doi:10.1016/S1464-1909(99)00091-X

Zeng, C., Wang, Q., Zhang, F., Zhang, J., 2013. Temporal changes in soil hydraulic conductivity with different soil types and irrigation methods. Geoderma 193–194, 290–299. doi:10.1016/j.geoderma.2012.10.013

Zhang, H., Huang, G.H., Wang, D., Zhang, X., 2011. Uncertainty assessment of climate change impacts on the hydrology of small prairie wetlands. J. Hydrol. 396, 94–103. doi:10.1016/j.jhydrol.2010.10.037

Zhao, C., Shao, M., Jia, X., Nasir, M., Zhang, C., 2016. Using pedotransfer functions to estimate soil hydraulic conductivity in the Loess Plateau of China. CATENA 143, 1–6. doi:10.1016/j.catena.2016.03.037

Zimmermann, B., Elsenbeer, H., De Moraes, J.M., 2006. The influence of land-use changes on soil hydraulic properties: Implications for runoff generation. For. Ecol. Manag. 222, 29–38. doi:10.1016/j.foreco.2005.10.070

Zinn, Y.L., Lal, R., Resck, D.V.S., 2005. Texture and organic carbon relations described by a profile pedotransfer function for Brazilian Cerrado soils. Geoderma 127, 168–173. doi:10.1016/j.geoderma.2005.02.010

Zoungrana, B.J.-B., Conrad, C., Amekudzi, L.K., Thiel, M., Da, E.D., Forkuor, G., Löw, F., 2015. Multi-Temporal Landsat Images and Ancillary Data for Land Use/Cover Change (LULCC) Detection in the Southwest of Burkina Faso, West Africa. Remote Sens. 7, 12076–12102. doi:10.3390/rs70912076

Appendix 1 Soil depth, texture and coarse particle content

Soil component		Depth [cm]				Sand [%]				Clay [%]				Silt [%]				Coarse P [%]			
	Horizon N	1	2	3	4	1	2	3	4	1	2	3	4	1	2	3	4	1	2	3	4
Endopetric_Plinthosol	n	24	15	9	0	11	16	2	0	11	16	2	0	11	16	2	0	11	16	4	1
	Mean	13.4	36	66.7		35.1	26.6	25.4		19.9	30.3	34.5		45.9	43.7	37.8		51.8	61.7	71.5	90
	Sd.	4.51	2.62	10		8.28	7.26	12.5		9.52	8.36	0.57		9.94	7.95	6.61		19	19.9	14.2	
	Min	8	34	60		21	15.2	16.6		10.2	12.2	34.1		36.7	33.8	33.2		1	12.5	56.5	90
	Max	22	40	80		46.7	40.5	34.2		42	42	34.9		68.9	62.4	42.5		68.6	79.9	90	90
Epipetric_Plinthosol	n	15	3	0	0	16	16	0	0	16	16	0	0	16	16	0	0	16	16	2	0
	Mean	12	45			40.3	29.4			16.5	25.4			43.2	45.4			62.2	65.2	90	
	Sd.	2.54	0			7.94	8.07			3.35	7.12			8.24	8.79			19.8	17.2	0	
	Min	10	45			23.6	15.9			12.2	13.3			30.1	35.4			14	19.9	90	
	Max	15	45			52.5	43.8			22.8	38.5			63.6	63			85	85	90	
Gleyic_Lixisol	n	3	9	9	0	1	3	0	0	1	3	0	0	1	3	0	0	1	3	0	0
	Mean	17	37	74		32.1	14.4			18.2	31.5			47	51.1			40	37.1		
	Sd.	0	0	0		2.16				3.14				0.7				29.4			
	Min	17	37	74		32.1	12.9			18.2	27.9			47	50.5			40	10.6		
	Max	17	37	74		32.1	16.9			18.2	33.4			47	51.9			40	68.7		
Gleyic_Plinthosol	n	3	9	0	0	1	1	1	0	1	1	1	0	1	1	1	0	1	1	1	0
	Mean	40	100			27.3	17.1	15.1		26.2	60.1	60.4		49.8	35	37.9		72.2	72.4	53.6	
	Sd.	0	0																		
	Min	40	100			27.3	17.1	15.1		26.2	60.1	60.4		49.8	35	37.9		72.2	72.4	53.6	
	Max	40	100			27.3	17.1	15.1		26.2	60.1	60.4		49.8	35	37.9		72.2	72.4	53.6	
Haplic_Cambisol	n	41	45	42	9	6	10	1	1	6	10	1	1	6	10	1	1	6	10	1	1
	Mean	13.6	43.8	89.7	100	26.7	31.6	15.7	8.76	31.3	30.6	27.4	20.6	43	38.7	56.6	60.5	36.6	43.4	0	20
	Sd.	6.2	21.7	19.5	0	7.66	13.4			13.3	14.2			6.66	6.94			17.9	23.9		
	Min	5	13	43	100	14.8	16.6	15.7	8.76	10.7	12	27.4	20.6	36.8	29.3	56.6	60.5	13.5	3.09	0	20
	Max	24	70	100	100	34	50.5	15.7	8.76	46.9	50	27.4	20.6	55.3	51.7	56.6	60.5	58.5	76.9	0	20
Haplic_Gleysol	n	66	60	27	0	10	20	3	0	10	20	3		10	20	3	0	10	20	3	0
	Mean	22.5	49.7	77		20.4	14	17.6		29.8	37.1	43.1		53.8	51	49.7		10.5	9.55	24	
	Sd.	9.74	16.9	20.5		10.3	7.42	8.74		11.3	10.7	17.1		11.3	7.3	8.76		15.5	10.5	19.5	
	Min	8	28	51		3.7	2.2	11.5		16.5	22.8	24		34.5	36.9	41.7		0	0	1.79	
	Max	40	77	100		37.4	36.4	27.6		53.2	60.4	57.1		65.4	66	59.1		46.5	38.1	38.9	
Haplic_Lixisol	n	18	18	0	0	2	1	1	0	2	1	1	0	2	1	1		2	1	1	0
	Mean	26.5	62.5			21.5	14.3	14.6		22.5	38.3	37.4		60.3	55.7	55.5		14	19.9	19.9	
	Sd.	3.6	2.57			2.63				12.7				4.03				0			

		Depth [cm]				Sand [%]				Clay [%]				Silt [%]				Coarse P [%]			
	Horizon N	**1**	**2**	**3**	**4**	**1**	**2**	**3**	**4**	**1**	**2**	**3**	**4**	**1**	**2**	**3**	**4**	**1**	**2**	**3**	**4**
	Min	23	60			19.6	14.3	14.6		13.6	38.3	37.4		57.4	55.7	55.5		14	19.9	19.9	
	Max	30	65			23.4	14.3	14.6		31.5	38.3	37.4		63.1	55.7	55.5		14	19.9	19.9	
Haplic_Plinthosol	n	42	57	39	0	25	41	6	0	25	41	6	0	25	41	6	0	25	41	6	0
	Mean	16.7	50.8	98.2		32.9	22.4	24.4		22.4	37.4	37.3		45.6	40.4	40.1		52.3	56	56.2	
	Sd.	5.97	10.5	8.6		11.2	8.08	6.78		10	11.9	10.7		10.2	8.62	8.35		18.7	21.8	17.1	
	Min	7	30	69		10.7	2.83	15.6		7.82	15.6	20.6		24.3	20.7	28.8		2.75	0	33.5	
	Max	23	63	102		51.7	38.1	36.5		45.4	62.9	48		69.9	58.1	51.1		75.3	83.6	82.6	
Haplic_Stagnosol	n	18	18	15	0	1	5	0	0	1	5	0	0	1	5	0	0	1	5	0	0
	Mean	17	31	100		43.9	14.5			20.9	38.3			36.2	46.4			57	26.9		
	Sd.	3.09	11.3			5.83				2.97				3.85				18.3			
	Min	14	20	100		43.9	4.48			20.9	33.2			36.2	42.7			57	10.2		
	Max	20	42	100		43.9	18.6			20.9	40.5			36.2	50.7			57	56.9		
Lixic_Gleysol	n	15	27	15	0	2	3			2	3	0	0	2	3	0	0	2	3	0	0
	Mean	14.8	56.7	86		25.1	16.1			16.7	27.8			58.3	56.4			21.6	22		
	Sd.	6.59	20.9	17.7		0.65	7.25			1.24	8.74			2.05	3.54			6.29	2.56		
	Min	7	28	65		24.7	10.4			15.8	20.2			56.9	52.3			17.2	19.2		
	Max	20	75	100		25.6	24.2			17.6	37.4			59.7	58.6			26.1	24.1		
Lixic_Plinthosol	n	26	30	42	9	8	15	0	0	8	15	0	0	8	15	0	0	8	15	2	0
	Mean	19.1	43.7	95.1	100	37.2	25.7			18.2	31.4			45.9	43.1			54.3	56.7	38.2	
	Sd.	6.62	13.4	15.5	0	11.1	7.91			7.79	9.68			14.3	8.53			17.3	20.3	26	
	Min	12	30	40	100	19.6	11.8			10.7	19.6			21.6	29.6			14	12.3	19.9	
	Max	27	60	101	100	54.4	41			34.3	57.6			65	59.6			71.8	82.6	56.6	
Lixic_Stagnosol	n	9	12	9	0	1	1	1	0	1	1	1	0	1	1	1	0	1	1	1	
	Mean	23	50.3	100		32.1	21.6	28.8		31.7	46.4	39.6		45.5	41.1	40.7		14.1	10.8	35.6	
	Sd.	0	17.6	0																	
	Min	23	21	100		32.1	21.6	28.8		31.7	46.4	39.6		45.5	41.1	40.7		14.1	10.8	35.6	
	Max	23	60	100		32.1	21.6	28.8		31.7	46.4	39.6		45.5	41.1	40.7		14.1	10.8	35.6	
Plinthic_Cambisol	n	9	9	6	0	1	2	0	0	1	2	0	0	1	2	0	0	1	2	0	0
	Mean	10	49	100		26.5	26.5			29	29			39.4	39.4			22	26.1		
	Sd.	0	0	0		3.5				5.44				4.15				21.3			
	Min	10	49	100		26.5	24			29	25.2			39.4	36.4			22	11.1		
	Max	10	49	100		26.5	29			29	32.9			39.4	42.3			22	41.2		
Plinthic_Gleysol	n	16	18	15	0	3	6	0	0	3	6	0	0	3	6	0	0	3	6	0	0
	Mean	14.2	27	50.6		32.6	23.1			17.7	31.1			51.8	44.3			39.1	45.6		
	Sd.	2.56	7.84	12.2		15.6	11.4			2.85	8.74			16.2	5.85			29.5	17.9		
	Min	12	17	41		15.6	7.9			14.5	20.8			38.8	37.1			12.3	22.3		
	Max	17	34	65		46.1	33.1			19.6	42.3			70	49.8			70.7	66.4		

		Depth [cm]				Sand [%]				Clay [%]				Silt [%]				Coarse P [%]			
	Horizon N	**1**	**2**	**3**	**4**	**1**	**2**	**3**	**4**	**1**	**2**	**3**	**4**	**1**	**2**	**3**	**4**	**1**	**2**	**3**	**4**
Plinthic_Lixisol	n	6	0	0	0	2	2	2	0	2	2	2	0	2	2	2	0	2	2	2	0
	Mean	24				20.8	10.7	14.9		22	31.4	34.6		56.3	54.9	46.8		40	37.1	68.7	
	Sd.	0				7.17	4.64	8.84		4.54	3.14	7.27		0.45	1.68	1.44		0	0	0	
	Min	24				15.7	7.39	8.7		18.8	29.2	29.4		56	53.7	45.8		40	37.1	68.7	
	Max	24				25.9	13.9	21.2		25.2	33.6	39.7		56.7	56.1	47.8		40	37.1	68.7	
Plinthic_Stagnosol	n	15	18	15	0	2	4	0	0	2	4	0	0	2	4	0	0	2	4	0	0
	Mean	14.8	33	101		32.9	24.9			18.6	34.1			48.8	40.9			7.34	24.3		
	Sd.	4.06	1.03	0.51		7.71	5.57			6.39	9.49			14.5	10.4			10.4	29.2		
	Min	10	32	100		27.4	18.9			14.1	23.5			38.5	30.2			0	1.09		
	Max	18	34	101		38.4	31.1			23.2	44.9			59	54.4			14.7	67		
Stagnic_Cambisol	n	18	21	9	6	2	6	1	0	2	6	1	0	2	6	1	0	2	6	1	0
	Mean	25	38.6	69	100	26.7	18.6	24.7		28.9	37.5	31.3		53.1	48	63.5		45.3	33.5	12.5	
	Sd.	5.14	3.59	0	0	7.59	5.71			4.41	8.86			14.3	7.8			26.2	19.7		
	Min	20	30	69	100	21.3	10.7	24.7		25.8	29.4	31.3		42.9	40.4	63.5		26.8	7.81	12.5	
	Max	30	40	69	100	32	23.8	24.7		32	51.2	31.3		63.2	62.4	63.5		63.8	62.6	12.5	
Stagnic_Plinthosol	n	18	27	27	18	3	6	1	1	3	6	1	1	3	6	1	1	3	6	1	1
	Mean	12.5	54	83	100	30.5	17.1	15.9	16.5	31.4	45.3	60.3	62.6	46.8	41.5	29.5	33.1	36.8	57.8	81.4	78.4
	Sd.	2.57	17.3	26.9	0	10.3	7.98			8.67	11.8			8.67	9.28			34.1	19.8		
	Min	10	38	60	100	23.7	8.21	15.9	16.5	25.2	31.4	60.3	62.6	40.6	29.3	29.5	33.1	0.88	22.9	81.4	78.4
	Max	15	73	120	100	42.4	27.2	15.9	16.5	41.3	59.8	60.3	62.6	56.7	55	29.5	33.1	68.6	77.7	81.4	78.4
Gleyic cambisol	n	1	3	0	0	1	3	0	0	1	3	0	0	1	3	0	0	1	3	0	0
	Mean	20	26.7			21	21.3			32	32			43	42.9			26.8	43.4		
	Sd.	0	5.86			0	3.49			0	3.44			0	2.59			0	16.6		
	Min	20	20			21	17.3			32	29.4			43	40.4			26.8	33.2		
	Max	20	26.7			21	21.3			32	32			43	42.9			26.8	43.4		
Haplic leptosol	n																				
	Mean	26.5	62.5			21.5	14.3	14.6		22.5	38.3	37.4		60.3	55.7	55.5		14	19.9	19.9	
	Sd.																				
	Min																				
	Max																				
Stagnic lixisol	n	1				1				1				1				1			
	Mean	7				47.2				23.5				30.9				71			
	Sd.																				
	Min																				
	Max																				

Appendix 2 Bulk density, *SOC*, *θs* and measured *Ks*.

		BD [g/cm³]				C org [%]				θs [Vol.%]				Ks [cm/day]			
Horizon N		**1**	**2**	**3**	**4**	**1**	**2**	**3**	**4**	**1**	**2**	**3**	**4**	**1**	**2**	**3**	**4**
Soil component																	
Endopetric_Plinthosol	n	11	16	4	1	11	16	2	0	24	15	9	0	24	15	9	0
	Mean	1.49	1.52	1.66	1.9	1.158	0.801	0.968		36.34	36.26	34.42		1669	820.1	909.1	
	Sd.	0.07	0.08	0.17		0.412	0.579	0.135		3.437	2.584	5.737		617.3	328	661.2	
	Min	1.34	1.39	1.5	1.9	0.485	0.28	0.872		31.25	31.71	29.14		303.4	283.6	450.2	
	Max	1.6	1.7	1.9	1.9	1.815	2.258	1.064		40.87	39.3	41.85		2482	1172	1790	
Epipetric_Plinthosol	n	16	16	2	0	16	16	0	0	15	3	0	0	15	3	0	0
	Mean	1.52	1.48	1.9		1.786	0.947			36.7	44.29			1005	1731		
	Sd.	0.09	0.12	0		0.56	0.391			5.021	0			549.6	42.82		
	Min	1.35	1.15	1.9		0.451	0.066			27.48	44.29			0.314	1706		
	Max	1.7	1.68	1.9		2.619	1.522			41.36	44.29			1485	1780		
Gleyic_Lixisol	n					1	3	0	0	3	9	9		3	9	9	0
	Mean	1.4	1.5		0	0.921	0.349			41.25	35.58	33.59		389.3	704.3	1037	
	Sd.	0.26				0.134				0	1.601	1.105		9.917	1032	604.2	
	Min	1.4	1.24			0.921	0.22			41.25	33.5	32.15		377.9	7.252	362.6	
	Max	1.4	1.75			0.921	0.488			41.25	37.03	34.57		395.1	2108	1762	
Gleyic_Plinthosol	n	1	1	1	0	1	1	1	0	3	9	0	0	3	9	0	0
	Mean	1.64	1.61	1.42		1.177	0.634	0.64		42.27	48.21			954.9	0.047		
	Sd.									0	1.614			0	0.002		
	Min	1.64	1.61	1.42		1.177	0.634	0.64		42.27	46.08			954.9	0.044		
	Max	1.64	1.61	1.42		1.177	0.634	0.64		42.27	49.52			954.9	0.048		
Haplic_Cambisol	n	6	10	1	1	6	10	1	1	41	45	42	9	41	45	42	9
	Mean	1.32	1.47	1.41	1.07	1.223	0.657	0.446	0.952	45.85	42.77	41.86	38.8	1172	401.1	318.8	10.95
	Sd.	0.2	0.14			0.345	0.453			4.059	5.232	5.448	0.983	785.3	606.6	497.3	9.555
	Min	1.04	1.31	1.41	1.07	0.895	0	0.446	0.952	36.67	35.02	33.08	37.79	8.815	0.551	0.512	1.133
	Max	1.62	1.77	1.41	1.07	1.884	1.47	0.446	0.952	51.5	51.16	49.95	40.03	2489	2117	1888	24.93
Haplic_Gleysol	n	10	20	3	0	10	20	3	0	66	69	33	0	66	69	33	0
	Mean	1.38	1.49	1.32		1.379	0.614	0.408		43.12	39.84	40.5		229.6	169.2	74	
	Sd.	0.15	0.1	0.23		0.563	0.297	0.126		6.724	5.998	4.069		348	367.8	216.2	
	Min	1.14	1.3	1.06		0.861	0	0.31		28.69	31.11	31.61		0.113	0.143	0.105	
	Max	1.59	1.73	1.46		2.581	1.197	0.55		50.95	49.06	44.5		1265	1632	803.3	
Haplic_Lixisol	n	2	1	1	0	2	1	1	0	18	18	0	0	18	18	0	0
	Mean	1.46	1.15	1.15		1.108	1.123	0.945		37.32	36.62			263.1	165		

		BD [g/cm³]				C org [%]				θs [Vol.%]				Ks [cm/day]			
	Horizon N	**1**	**2**	**3**	**4**	**1**	**2**	**3**	**4**	**1**	**2**	**3**	**4**	**1**	**2**	**3**	**4**
	Sd.	0.02				0.131				3.435	1.178			392.1	189.8		
	Min	1.45	1.15	1.15		1.015	1.123	0.945		32.51	34.33			23.87	6.267		
	Max	1.47	1.15	1.15		1.201	1.123	0.945		41.41	37.92			1753	477.5		
Haplic_Plinthosol	n	25	41	6	0	25	41	6	0	42	57	39	0	42	57	39	0
	Mean	1.48	1.54	1.59		1.598	0.641	0.49		39.8	42.43	39.27		1098	519	858.3	
	Sd.	0.13	0.13	0.11		0.717	0.305	0.357		7.785	8.743	5.425		786.3	751.3	664.9	
	Min	1.15	1.22	1.46		0.448	0	0.058		28.91	25.37	30.58		55.23	0.628	40.79	
	Max	1.7	1.75	1.76		3.175	1.276	1.122		53.33	54.25	51.42		2220	2251	2176	
Haplic_Stagnosol	n	1	5	0	0	1	5	0	0	18	18	15	0	18	18	15	0
	Mean	1.51	1.46			0.262	0.962			37.59	35.31	39.91		6.757	3.432	33.56	
	Sd.	0.23				0.468				0.654	4.761	2.039		6.412	3.192	64.55	
	Min	1.51	1.19			0.262	0.41			36.7	28.91	36.59		1.395	0.435	0.209	
	Max	1.51	1.66			0.262	1.633			38.43	39.9	42.68		26.11	10.04	160.7	
Lixic_Gleysol	n	2	3	0	0	2	3	0	0	15	27	15	0	15	27	15	0
	Mean	1.48	1.47			0.838	0.482			38.13	40.5	44.52		755.2	119.9	71.74	
	Sd.	0.04	0.16			0.131	0.1			6.117	8.687	8.511		988.1	133.5	145.3	
	Min	1.45	1.28			0.745	0.366			32.44	33.61	33.61		2.929	0.062	0.058	
	Max	1.51	1.57			0.93	0.548			45.83	59.49	51.91		2467	326.4	352.5	
Lixic_Plinthosol	n	8	15	2	0	8	15	0	0	26	30	42	9	26	30	42	9
	Mean	1.52	1.6	1.37		1.591	0.663			35.12	34.47	39.14	34.32	959.6	1085	537.8	127.4
	Sd.	0.09	0.23	0.31		0.564	0.408			4.664	5.391	7.048	1.356	842.8	635.6	725.7	171.5
	Min	1.35	1.15	1.15		0.721	0.141			28.42	29.34	24.37	32.52	52.52	5.828	0.105	13.05
	Max	1.62	1.96	1.59		2.574	1.732			45.92	44.78	48.19	35.37	1981	1918	2149	356
Lixic_Stagnosol	n	1	1	1	0	1	1	1	0	9	12	9	0	9	12	9	0
	Mean	1.4	1.52	1.67		2.003	0.792	1.118		45.45	41.46	36.07		1160	384.4	12.11	
	Sd.									0.786	2.695	0.703		213	658.2	0.259	
	Min	1.4	1.52	1.67		2.003	0.792	1.118		44.82	39.17	35.13		954.9	18.68	11.94	
	Max	1.4	1.52	1.67		2.003	0.792	1.118		46.49	45.84	36.6		1432	1498	12.46	
Plinthic_Cambisol	n	1	2	0	0	1	2	0	0	9	9	6	0	9	9	6	0
	Mean	1.24	1.1			1.596	1.209			54.73	50.07	47.57		1202	403.2	14.15	
	Sd.	0.14				0.022				1.359	1.326	0.756		903.4	264.4	8.93	
	Min	1.24	1			1.596	1.194			53.32	48.71	46.88		293.7	50.77	5.136	
	Max	1.24	1.2			1.596	1.225			56.42	51.73	48.26		2341	639.7	24.12	
Plinthic_Gleysol	n	3	6	0	0	3	6	0	0	16	18	15	0	16	18	15	0
	Mean	1.41	1.61			1.79	0.751			43.4	41.43	34.66		652.4	287.2	343.4	
	Sd.	0.15	0.15			0.366	0.316			2.035	2.323	1.72		613.5	441.3	553.1	
	Min	1.31	1.44			1.37	0.41			40.29	37.43	31.6		42.74	0.101	7.833	

		BD [g/cm³]				C org [%]				θs [Vol.%]				Ks [cm/day]			
	Horizon N	**1**	**2**	**3**	**4**	**1**	**2**	**3**	**4**	**1**	**2**	**3**	**4**	**1**	**2**	**3**	**4**
	Max	1.59	1.82			2.04	1.224			46.13	44.72	36.54		1697	1166	1432	
Plinthic_Lixisol	n	2	2	2	0	2	2	2	0	6	0	0	0	6	0	0	0
	Mean	1.4	1.5	1.75		0.645	0.515	0.371		29.29				23.98			
	Sd.	0	0	0		0.156	0.045	0.019		0.639				8.147			
	Min	1.4	1.5	1.75		0.535	0.483	0.358		28.7				13.3			
	Max	1.4	1.5	1.75		0.755	0.547	0.384		29.87				33.07			
Plinthic_Stagnosol	n	2	4	0	0	2	4	0	0	15	18	15	0	15	18	15	0
	Mean	1.35	1.6			0.807	0.442			40.89	39.91	37.96		475.3	76.25	9.983	
	Sd.	0.09	0.06			0.152	0.355			3.082	1.414	1.976		457.7	148	7.382	
	Min	1.28	1.56			0.699	0.043			37.27	37.5	34.59		9.964	0.072	1.641	
	Max	1.41	1.68			0.915	0.905			44.31	42.03	40.53		1313	397.2	19.1	
Stagnic_Cambisol	n	2	6	1	0	2	6	0	0	18	21	9	6	18	21	9	6
	Mean	1.28	1.38	1.4		1.119	0.721	0.7		45.87	46.48	50.88	47.53	774	209.5	503.2	977.3
	Sd.	0.13	0.06			1.15	0.454			5.511	4.258	1.111	0.269	633.1	211.4	286.9	1022
	Min	1.19	1.31	1.4		0.306	0.228			39.36	38.68	49.73	47.29	15.5	14.32	125.3	43.2
	Max	1.38	1.46	1.4		1.933	1.383			52.76	51.51	52.26	47.78	1779	549.1	775.2	1910
Stagnic_Plinthosol	n	3	6	1	1	3	6	1	1	18	27	27	18	18	27	27	18
	Mean	1.53	1.66	1.75	1.67	1.467	0.568	0.676	0.119	40.34	35.3	35.52	38.23	66.23	515.7	496.1	231.8
	Sd.	0.18	0.17			0.318	0.342			1.683	3.702	2.132	3.599	113	763.4	669.9	275.7
	Min	1.34	1.44	1.75	1.67	1.168	0.199	0.676	0.119	37.44	30.06	32.28	34.18	5.876	2.266	0.227	0.201
	Max	1.69	1.85	1.75	1.67	1.8	0.999	0.676	0.119	42.46	39.4	38.68	41.95	313.8	2381	2186	747.3
Gleyic cambisol	n	1	3	0	0	1	3	0	0	9	15	0	0	9	15	0	0
	Mean	1.19	1.4			1.93	1.082			50.09	50.43			666.5	669		
	Sd.	0	0.04				0.29			2.586	0.653			14.41	10.9		
	Min	1.19	1.37			1.93	0.803			44.78	49.73			650.7	653.4		
	Max	1.19	1.4			1.93	1.082			52.76	51.51			683.9	686.5		
Haplic leptosol	n																
	Mean	1.46	1.15	1.15		1.108	1.123	0.945		37.32	36.62			263.1	165		
	Sd.																
	Min																
	Max																
Stagnic lixisol	n	1				1											
	Mean	1.24				0.8											
	Sd.																
	Min																
	Max																

Appendix 3 van Genuchten parameters, *θr* and PTF based *Ks*

	Van Genuchten parameter												Saxton & Rawls				Saxton et al.				Schaap et al.				Vereecken et al.				Cosby et al.			
	α [1/cm]				θr [cm³/cm³]				n [-]				Ks [cm/d]				Ks [cm/d]				Ks [cm/d]				Ks [cm/d]				Ks [cm/d]			
	1	2	3	4	1	2	3	4	1	2	3	4	1	2	3	4	1	2	3	4	1	2	3	4	1	2	3	4	1	2	3	4
Soil component																																
Endopetric_Plinthosol	0.03	0.02	0.01	0.01	0	0	0	-0	1.3	1.3	1.2	1.4	12	3.9	2.8		22	10	8		16	12	9.9		16	12	3		31.6	21.2	19.2	
Epipetric_Plinthosol	0.04	0.03	0.01	-	0	0	-0	-	1.3	1.3	1.4	-	18	5.3			31	14			15	13			11	18			38.7	24.7		
Gleyic_Lixisol	0.04	0.01	-	-	0	0.1	-	-	1.3	1.2	-	-	15	5.7			28	12			11	13			44	28			29.7	14.6		
Gleyic_Plinthosol	0.01	0	0.01	-	0	0	0	-	1.3	1	1.1	-	5.4	0.6	0.8		14	5	5		14	13	13		4.1	4.2	23		23	10.4	9.75	
Haplic_Cambisol	0.03	0.03	-	0.03	0.1	0.1	-	0.1	1.3	1.2	-	1.3	6.6	5.1	7.3	9.3	9	9	15	31	12	9	12	13	51	18	61	151	21	24.4	16.1	15
Haplic_Gleysol	0.02	0.01	0.01		0.1	0.1	0		1.3	1.2	0.4		9.9	5	2.9		12	8	6		13	12	13		37	22	82		17.8	13.3	13.5	
Haplic_Lixisol	0.02	0.03	0.03	-	0.1	0.1	0.1	-	1.3	1.3	1.3	-	13	5.4	5.1		21	8	8		14	12	12		26	268	293		20.5	13.2	13.5	
Haplic_Plinthosol	0.03	0.01	0.01	-	0	0	0	-	1.3	1.2	1.2	-	8	2.5	2.4		18	7	7		14	12	12		14	10	6.9		28.6	16.9	17.9	
Haplic_Stagnosol	0.04	0.01	-	-	0	0.1	-	-	1.3	1.2	-	-	9.7	4.8			18	8			9.6	13			22	21			40.1	13.3		
Lixic_Gleysol	0.02	0.01	-	-	0.1	0.1	-	-	1.3	1.2	-	-	18	6.4			35	15			21	12			30	35			24.8	16.2		
Lixic_Plinthosol	0.03	0.01	0.02	-	0	0	-0	-	1.3	1.2	1.4	-	17	3.8			26	9			16	12			12	6.6			34.5	20.3		
Lixic_Stagnosol	0.03	0.01	0.01	-	0.1	0.1	0.1	-	1.3	1.1	1.1	-	10	2.8			8	5			12	13	10		18	9.2	2.2		24.4	14.5	19.7	
Plinthic_Cambisol	0.04	0.05	-	-	0.1	0.1	-	-	1.3	1.3	-	-	11	8.6			11	11			11	11			95	357			21.5	21.5		
Plinthic_Gleysol	0.04	0.01	-	-	0	0.1	-	-	1.3	1.2	-	-	21	4.5			29	10			20	12			29	6			30.3	18.9		
Plinthic_Lixisol	0.02	0.01	0.01	-	0	0.1	0	-	1.3	1.2	1.2	-	7.8	4.4			22	13	9		14	12	13		59	29	3.1		20.2	13.1	14.2	
Plinthic_Stagnosol	0.04	0.01	-	-	0.1	0.1	-	-	1.3	1.2	-	-	21	4.6			26	8			17	11			71	7.1			30.2	19.1		
Stagnic_Cambisol	0.04	0.03	0.02	-	0	0.1	0.1	-	1.3	1.3	1.3	-	6.4	3.8	6.9		11	7	10		13	13	14		77	40	36		21.7	15.1	19.8	
Stagnic_Plinthosol	0.02	0.01	0	0	0.1	0	0		1.2	1.1	1	1	7.2	1.7	0.9	0.7	9	6	5		12	14	23	24	7.1	3.8	1.3	5.4	23.4	12.9	9.98	
Gleyic cambisol	0.03	0.02			0.1	0.1			1.3	1.3			9	5.3			10	10			12	12			140	31			17.7	17.7		
Haplic leptosol	0.02	0.03	0.03	-	0.1	0.1	0.1	-	1.3	1.3	1.3	-	13	5.4			21	8			14	12	12		26	268	293		20.5	13.2	13.5	